

Rafael Ballagas

Bringing Iterative Design to Ubiquitous Computing



**Optimization of the Critical Content of Tramp Elements
in Ultra-High Strength Silicon Chromium Spring Steels
through Thermomechanical Treatment**

Von der Fakultät für Georessourcen und Materialtechnik
der Rheinisch-Westfälischen Technischen Hochschule Aachen

zur Erlangung des akademischen Grades eines
Doktors der Ingenieurwissenschaften
genehmigte Dissertation

vorgelegt von **Diplom-Ingenieur**

Araz Ardehali Barani

aus Teheran, Iran

Berichter: Professor Dr.-Ing. Dierk Raabe
Univ.-Prof. Dr.-Ing. Wolfgang Bleck

Tag der mündlichen Prüfung: 15. Juni 2007

Bibliografische Information der Deutschen Nationalbibliothek

Die Deutsche Nationalbibliothek verzeichnet diese Publikation in der Deutschen Nationalbibliografie; detaillierte bibliografische Daten sind im Internet über <http://dnb.ddb.de> abrufbar.

1. Aufl. - Göttingen : Cuvillier, 2008

Zugl.: (TH) Aachen, Univ., Diss., 2007

978-3-86727-570-5

© CUVILLIER VERLAG, Göttingen 2008

Nonnenstieg 8, 37075 Göttingen

Telefon: 0551-54724-0

Telefax: 0551-54724-21

www.cuvillier.de

Alle Rechte vorbehalten. Ohne ausdrückliche Genehmigung des Verlages ist es nicht gestattet, das Buch oder Teile daraus auf fotomechanischem Weg (Fotokopie, Mikrokopie) zu vervielfältigen.

1. Auflage, 2008

Gedruckt auf säurefreiem Papier

978-3-86727-570-5

ACKNOWLEDGEMENT

I am grateful to Professor Dierk Raabe for giving me the possibility of enjoying the research at the Max-Planck-Institute für Eisenforschung in Düsseldorf, for his advice and assistance throughout the project. The stimulating and refreshing discussions with him were the source for new ideas.

I am grateful to Professor Wolfgang Bleck, the head of the department for ferrous Metallurgy at the RWTH Aachen for revising the work and giving me the opportunity to graduate at the University in Aachen.

I am especially indebted to my supervisor at the Max-Planck-Institute Dr. Dirk Ponge for many fruitful discussions and for his rich knowledge of papers on steel research and physical metallurgy.

I would like to thank Gerd Goris and Frank Schlüter for helping me to perform the heat treatment and forming experiments. Thanks are also due to Katja Angenendt, Heidi Bögershauser, Hedwig Falkenberg, Dorothea Gläser, and Monika Nellesson for introducing me to new metallography techniques, for electron microscopy, and for the microstructure characterization they performed. I want to thank Herbert Faul and the apprentices for the mechanical testing, Michael Adamek for the dilatometry experiments, Benedikt Sander for his accurate sample preparation, and the metallurgy team Jürgen Wichert and Frank Rütters for preparing the laboratory melts, Mrs. Regner for the literature, and the entire workshop team for the mechanical preparation of the samples. Last but not least, the work could not have been performed without the strong support of the IT team Bertholt Beckschäfer and Achim Kuhl.

I thank as well Fei Li who spent one year at the Institute in Düsseldorf and performed the experiments on grain growth and recrystallization behaviour.

All the above mentioned persons contributed in one way or the other to the thesis that is presented here. Beside that I am grateful to all the other colleagues, friends and family who accompanied me in the years during the thesis.

Thank are due to the members of the accompanying project group from the association of the German Spring Manufacturers (Deutscher Verband der Federnindustrie) and for the financial funding. Parts of the results presented here are from the research project AiF 13409N. Funding for this project was provided by the German Federal Ministry of Economics and Labour (BMWA) via the German Federation of Industrial Cooperative Research Associations „Otto von Guericke“ (AiF) and the Steel Forming Research Society (FSV). The long version of the final report can be ordered from the FSV, Goldene Pforte 1, D-58093 Hagen.

Araz Ardehali Barani

Wuppertal, Febraury 2008

TABLE OF CONTENTS

1 Scope of thesis	1
2 Theoretical background	5
2.1 Ferrous martensite	5
2.1.1 Martensite transformation.....	6
2.1.1.1 Nucleation	9
2.1.1.2 Growth	9
2.1.1.3 Crystallography of martensitic transformation	10
2.1.2 Martensite morphologies	12
2.1.3 Strength of martensite	14
2.1.4 Embrittlement of martensite	16
2.1.4.1 Fundamentals of grain boundary segregation	17
2.1.4.2 Carbide precipitation.....	21
2.2 Processing martensitic high strength steels	23
2.2.1 Austenitization	23
2.2.2 Austenite conditioning	25
2.2.3 Tempering.....	28
2.3 Strategy for optimization of mechanical properties	30
3 Experimental approach and methods	35
3.1 Approach	35
3.2 Materials	35
3.3 Sample processing	38
3.4 Mechanical testing.....	39
3.5 Microstructure characterization.....	41

4 Results and discussion	43
4.1 Definition of parameter windows	43
4.1.1 Austenitization	43
4.1.1.1 Experiments	43
4.1.1.2 Results	44
4.1.1.3 Discussion	44
4.1.2 Time-Temperature-Transformation	49
4.1.2.1 Experiments	49
4.1.2.2 Results	50
4.1.2.3 Discussion	50
4.1.3 Recrystallization behaviour	53
4.1.3.1 Experiments	54
4.1.3.2 Results	55
4.1.3.3 Discussion	58
4.1.4 Conclusion	59
4.2 Conventional Heat Treatment.....	60
4.2.1 Objective	60
4.2.2 Experimental	60
4.2.3 Results.....	61
4.2.3.1 Tempering temperature	61
4.2.3.2 Microalloying with vanadium	68
4.2.3.3 Effect of phosphorous on tensile properties.....	72
4.2.3.4 Effect of copper and tin.....	75
4.2.4 Discussion.....	79
4.2.4.1 Tempering temperature	79
4.2.4.2 Microalloying with vanadium	80
4.2.4.3 Effect of phosphorous	81
4.2.4.4 Effect of copper and tin.....	83
4.3 Thermomechanical Treatment.....	86
4.3.1 Objective.....	86
4.3.2 Definition of deformation temperature	86
4.3.2.1 Experimental	86

4.3.2.2 Results	87
4.3.2.3 Discussion	100
4.3.3 Austenitization temperature and strategy for thermomechanical treatment	104
4.3.3.1 Experimental	104
4.3.3.2 Results	105
4.3.3.3 Discussion	108
4.3.3 Tensile property after austenite conditioning	110
4.3.3.1 Experimental	110
4.3.3.2 Results	111
4.3.3.3 Discussion	117
4.3.4 Fatigue Results.....	121
4.3.4.1 Experimental	121
4.3.4.2 Results	121
4.3.4.3 Discussion	124
4.3.5 Microalloying and thermomechanical treatment	127
4.3.5.1 Results	127
4.3.5.2 Discussion	130
5 Final discussion.....	135
5.1 Process and impurity element effect.....	136
5.2 Morphology of grain boundary carbides	140
5.3 Refinement of martensite microstructure	142
6 Summary and conclusion.....	149
7 References	152
Zusammenfassung (abstract in German)	159
Lebenslauf (Curriculum Vitae)	163

1 SCOPE OF THE THESIS

This work is concerned with improving the mechanical properties of quenched and tempered martensitic steel, that is the alloy 54SiCr6 and is used for automotive coil springs. Steels for light-weight applications as in the case of automotive springs have to fulfil contradictory requirements. Automotive springs have to be optimized for minimum weight, for optimum package, maximum robustness and minimum cost. From these criteria the material selection criteria for spring steels can be derived (Fig. 1). These are high yield strength to allow higher stress levels in the elastic range, high endurance limit for a long operation and a minimum toughness to avoid catastrophic failure due to load shocks. Furthermore, most manufacturers and most industrial standards require a good ductility level. High ductility level usually corresponds to a good toughness and apart from that is needed for cold forming of coil spring of small diameter.

In this work, special attention is paid to the role of the impurity elements phosphorous, copper and tin. Phosphorous is known to deteriorate the toughness and ductility, but the concentration limits are not known for 54SiCr6 and manufacturing processes to minimize the negative effect on the mechanical properties are absent. Copper and tin are elements that are introduced into steels due to the increased usage of scrap in steel production. Most investigators have concentrated on the effect of copper on the hot liquid embrittlement. In the present work the effect of copper and tin on the mechanical properties of tempered martensite was investigated.



Fig. 1 Material selection criteria for coil springs

The ductility and toughness of the final part are affected by the concentration and distribution of the impurity elements in the bulk material. The distribution of these elements is a result of the process parameters, i.e. of the history of the material from the melt to the final process step. In this work the composition and the key heat treatment parameters were varied systematically and the resulting mechanical properties and the microstructure were characterized. The composition was varied changing the concentration of phosphorous, copper and tin. For each phosphorous and copper and tin concentration two melts were compared, one without vanadium and one with addition of vanadium.

Because the existing heat treatment used to manufacture springs, namely austenitization, quenching and tempering does not exploit the full potential of the existing steel grade, an additional degree of freedom for material optimization was introduced by austenite deformation prior to quenching. Such treatments that combine deformation and heat treatment are called thermomechanical treatment or thermomechanical processing. Former research in this field has proven that superior properties can be achieved after deformation of austenite prior to quenching (Hensger and Bernstein 1984, Zouhar 1984, Peters and Kaspar 1997, Wettlaufer and Kaspar 2000b). In this work the specific boundary conditions for manufacturing coil springs were considered for the new thermomechanical routes. The main goal was to develop a concept for a thermomechanical treatment that produces improved final material properties independent of impurity level.

In brief, the objective of the project from an industrial point of view was

- 1) to determine the impurity level limits below which the required properties are produced,
- 2) and to develop a novel treatment to increase the strength level above the strength of springs used today (around 2000 MPa) and maintain the ductility and fatigue properties without additional cost for a higher purity level.

The scientific motivation of the work is to extend the knowledge about the embrittling mechanisms in martensitic steels and the dependence of tempered martensitic microstructure on the grain structure of the parent austenite phase. The authors cited above ascribed the improvements in mechanical properties observed after thermomechanical treatment mainly to the substructure of the austenite grains prior to quenching. In commercially used alloys, this substructure can not be investigated due to the transformation the steel undergoes upon cooling. Instead iron nickel model alloys (Hensger and Bernstein 1984) and the final martensite have been investigated. It has been shown qualitatively that thermomechanical

treatment refines the martensite and increases the fraction of lath martensite (Hensger and Bernstein 1984, Peters 1997). Additionally, carbides formed during tempering are finely dispersed (Hensger and Bernstein 1984) and the internal stresses generated during cooling are reduced (Peters 1997). Furthermore, the role of impurity elements has been discussed, but is controversial (Hensger and Bernstein 1984, Zouhar 1984, Peters et al. 1996, and Wettlaufer 2000). In the present work we used modern techniques to understand the martensitic microstructure and its relation to the mechanical properties. Martensitic structural units that define the mechanical properties were investigated by crystal orientation imaging techniques using electron diffraction. Special attention was paid to the influence of the austenite condition and the martensite morphology, size distribution of structural units and the distribution and morphology of carbides at prior austenite grain boundaries.

2 THEORETICAL BACKGROUND

2.1 FERROUS MARTENSITE

Martensite, named after the German metallurgist Adolf Martens, exhibits the highest hardness of the phases known in iron based alloys. Martensitic microstructures can only be produced if the transformation to mixtures of ferrite and cementite or other phases is avoided. The high hardness associated with high strength, fatigue resistance, and wear resistance are the main reasons for the technological importance of martensitic steels. The properties can be varied by further annealing steps to obtain a desirable combination of strength and ductility or toughness. These characteristics are responsible for the variety of alloys and applications for ferrous martensite. Today, martensitic steels are used for light-weight structures in automotive and aerospace industry as springs, shafts, landing gears. They are used as ball and roller bearings.

The specific strength of martensitic steels is higher than that of the strongest aluminium alloys used in the aerospace industry. Only in cases where the stiffness (ratio of elastic modulus to density) requirements dominate, aluminium and titanium alloys become superior.

In order to produce martensite the diffusional transformations from austenite to other phases must be suppressed. Therefore all the martensite is produced by “quenching” from the austenite to a temperature below which martensite forms (*martensite start temperature M_S*). Quenching is a commonly used terminology, and can include cooling in water (low carbon steel), in oil or in even in air (high alloyed tool steel). The critical cooling speed in a given steel to obtain a fully martensitic microstructure depends very strongly on the chemical composition, especially on the content of carbon, on the austenite grain size, and on the austenite substructure or defect structure.

In this chapter first the characteristics of austenite-martensite transformation together with the transformation microstructures is presented. Main focus is placed on those factors influencing the transformation and microstructure and thus changing the mechanical properties. In the subsequent section then the mechanical properties as a result of the microstructure are explained.

2.1.1 MARTENSITE TRANSFORMATION

The martensite transformation is diffusionless, athermal and is characterized by a shear mechanism, where many atoms move cooperatively and (almost) simultaneously. This type of transformation implies necessarily a fixed orientation relationship between the parent and the final phase. The orientation relationships between the parent phase and daughter phase have been found for different alloy systems and have been reviewed in different papers (Ray and Jonas 1990, Morito 2003, Nolze 2004, Guo et al. 2004). The crystallography of martensitic transformation is described further below. A second consequence of the cooperative movement of atoms is that the composition of the daughter martensite phase is exactly the same like the parent austenite phase.

For a particular steel, the athermal reaction takes place in a specific temperature range. The transformation is accompanied by abrupt change of physical properties such as volume and electrical resistance. The reaction initiates at the *martensitic start temperature* M_S and ceases at the *martensitic finish temperature* M_f . Ideally, at the latter temperature all the austenite should have transformed to martensite, but in practice, a small fraction of the austenite does not transform. This is called *retained austenite*. Alloying elements influence the M_S temperatures of steels. A number of equations have been generated which relate the martensitic start temperature with steel composition. A review of these equations is given in (Krauss 1990 and Ohtani 1992). If the M_f drops below room temperature significant fraction of retained austenite is present at room temperature. Alloying elements that stabilize the austenite increase the fraction of retained austenite.

The plane in the austenite on which the martensite forms and grows is the *habit plane*. It affects the initiation and progress of the transformation and it determines the microstructural arrangement of the martensite crystals within one prior austenite grain (Krauss and Marder 1971, Davies and Magee 1971).

The carbon atoms in martensite as well as in the parent austenite occupy octahedral interstices. The average unit cell of both lattices expands in a linear manner as a function of carbon content. In contrast to the austenitic solid solution of iron and carbon where the enlarged lattice remains face centred cubic, carbon atoms in martensite produce nonsymmetrical distortions and convert the body centred cubic into body centred tetragonal structure (Cohen 1962). Because the lattice distortion caused by interstitial carbon in bct-iron is non-symmetrical (Fig. 2) it has been referred to as “distortion dipole” (Cohen 1962). The

tetragonality, defined as the ratio between the c- and a-axis depends on the carbon concentration (given in mass %, after Roberts, in Cohen 1962):

$$\frac{c}{a} = 1.000 + 1.045 C \quad (\text{Equation 1})$$

In iron-carbon systems the solubility of carbon in a bcc system is greatly exceeded after martensite transformation. Because the partition of carbon between ferrite and cementite through diffusion has been suppressed, the martensite is a metastable phase. If the martensite is heated to temperatures, where the carbon atoms become mobile, the carbon atoms move out of the octahedral sites and form clusters of carbon atoms or carbides (2.1.4.2). As a consequence the tetragonality is successively lost and the martensite is replaced by a mixture of ferrite and cementite.

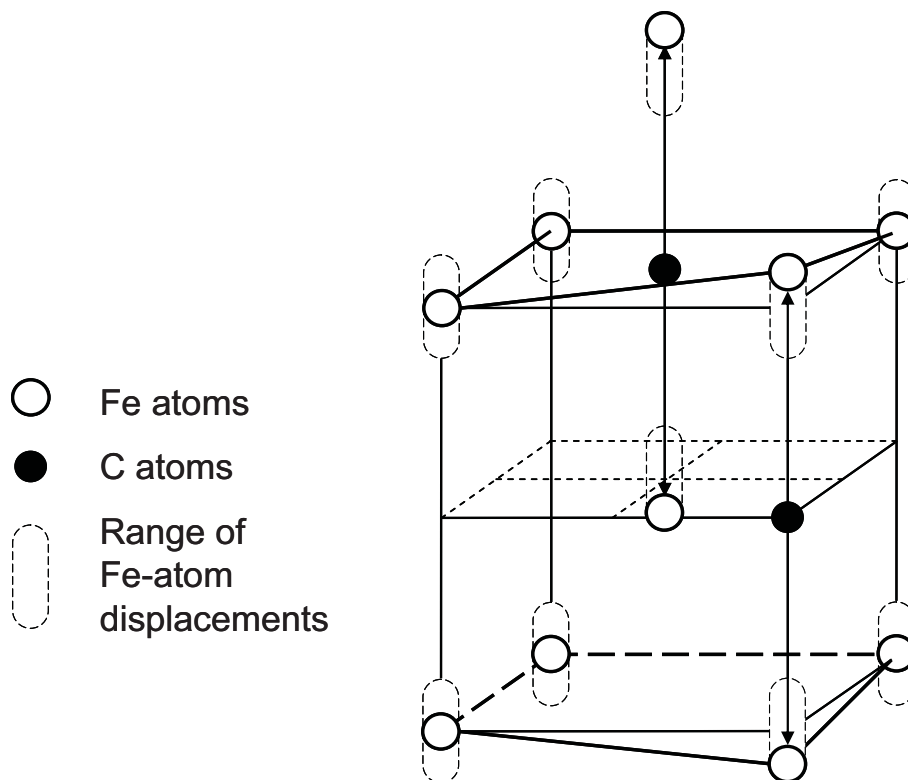


Fig. 2 Representation of iron-atom displacement due to the presence of carbon in body-centred tetragonal martensite lattice (after Lipson and Parker, Cohen 1962).

Generally the *lattice transformation* causes rotation of the final lattice from the habit plane. Fig. 3 shows how a number of cells of the parent crystal a) are transformed to a new lattice b). The grey vertical dashed lines represent the unrotated, undistorted habit plane. To satisfy the constraints of the surrounding matrix and maintain the shape, a *lattice invariant deformation* occurs that conserves the macroscopic shape of the phase. The lattice invariant deformation satisfies – on a macroscopic scale – the requirements of an unrotated, undistorted habit plane. It takes place by slip or by twinning as shown in Fig. 3 c) or d) respectively. When slip is the main mode of accommodation during lattice invariant deformation dislocations are introduced at the austenite-martensite interface. Additionally a high dislocation density is observed in the fine structure within the plates or lath (Swarr 1976). Does the transformation occurs at high temperatures (M_S around 450°C) as in the case of low- or medium-carbon steels then slip is the main lattice invariant deformation, while at lower M_S temperatures the main mechanism is twinning.

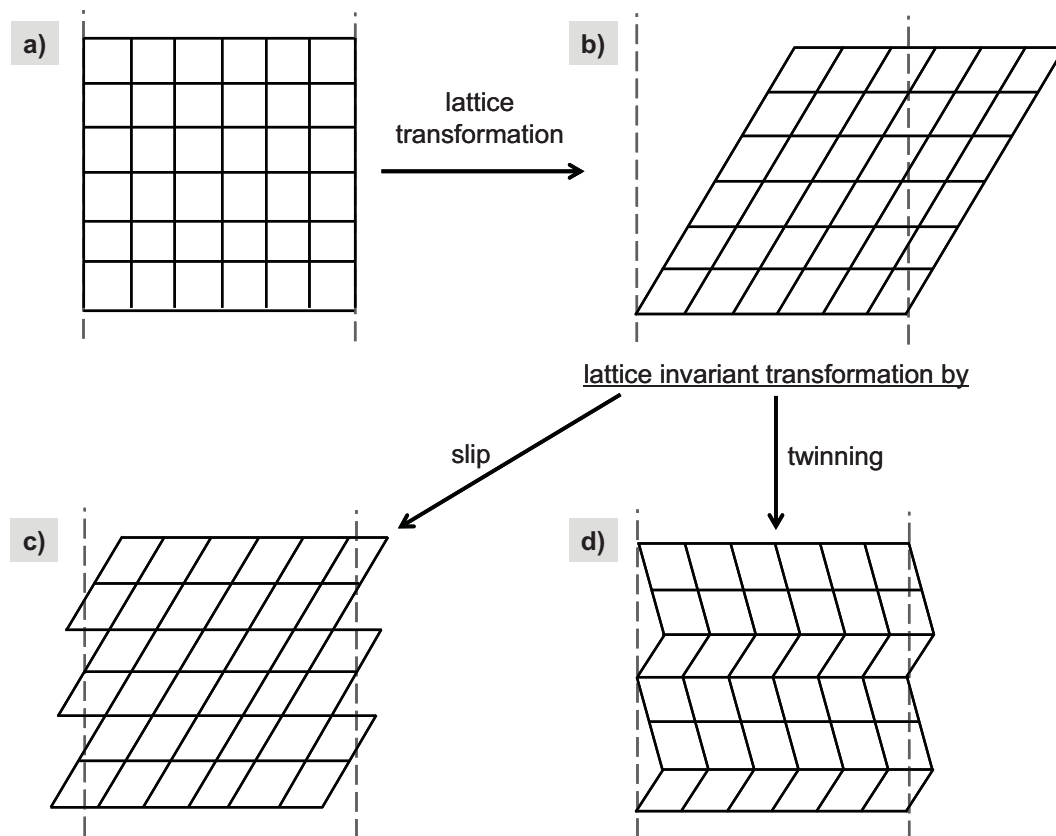


Fig. 3 Schematic diagram of martensitic transformation

2.1.1.1 NUCLEATION

It is commonly accepted that for bulk materials martensite nucleation is heterogeneous (Kaufmann and Cohen 1958, Olson 1992). Thus the transformation can take place at low driving forces where the fully coherent state is typically not stable, thus favouring semicoherent nucleation. Defect interaction leads to mobility controlled barrierless nucleation, where potency distributions of both initial and autocatalytically generated nucleation sites can dominate macroscopic transformation behaviour (Olson 1992).

Experimental evidence for heterogeneous nucleation has been provided by Cech and Turnbull (1956), and by Saburi and Nenno (1986). The first authors showed experimentally that nucleation at the martensite start temperature M_S occurs heterogeneously on sparsely distributed defects (Cech and Turnbull 1956). Saburi and Nenno (1986) directly observed a strong defect heterogeneous nucleation in Ti-Ni-Cu. It has been reported that dislocations do not act as favourable nucleation sites while certain types of grain boundaries would be potent nucleation sites (Olson 1992). Furthermore annealing twin boundaries act as potent nucleation sites for all types of ferrous martensite (ibid.). A detailed study of Tsuzaki et. al. showed that a polycrystalline sample of Fe-32%Ni (mass%) exhibits significantly higher M_S temperatures than a single crystal of the same material (Tsuzaki 1995). Bicrystalline experiments of the same authors showed that neither annealing twin boundaries nor high-angle grain boundaries (only four) have an effect on the M_S temperature. Petrov (1984) presented a mechanism of martensite nucleation at dislocations in austenite and shows the dominating role of dislocation arrangement of the austenite in the martensitic transformation of steel. The model was confirmed by experiments on Fe-13Cr-19Mn (mass%) steel.

2.1.1.2 GROWTH

Theoretical background of martensite growth was developed based on the energetic formulations of classical martensitic nucleation of Kaufmann and Cohen (1958). This model included the free energy change as function of shape and size. Later microscopic models were presented (Raghavan 1972). The models described the growth in the thickening direction as a result of interfacial dislocations normal to the interface, while radial growth occurred by dislocation expansion and the creation of new dislocations at the advancing tip of the particle. Integration of further ideas were introduced by Olson and Cohen (Olson 1975) taking an

elastic energy term for the elastic accommodation of the transformation shape change into account. According to this model the martensite growth is determined by the interfacial mobility and the accommodation of the transformation shape change (Grujicic 1992). The model presented by Petrov (1984) presents interfacial dislocation arrangements to maintain coherency between the parent austenite and the martensite phase and shows how the shape change can be accommodated by generating screw dislocations in the martensite phase.

2.1.1.3 CRYSTALLOGRAPHY OF MARTENSITIC TRANSFORMATION

The martensite forms by a displacive mechanism, where atoms cooperatively change the crystal structure from face-centred cubic crystal structure (austenite) to body-centred cubic, to body centred tetragonal (for Fe-C and Fe-Ni alloys), or to hexagonal closed packed (Fe-Cr-Ni or Fe- high Mn alloys). The cooperative movement of atoms in the same direction and of the same distance and the fact that the atomic neighbours are maintained before and after the transformation are proven experimentally by orientation relationships between the parent and the daughter phase. In ferrous systems the closed packed planes, i.e. the $\{111\}_\gamma$ and $\{110\}_\alpha$, are approximately parallel. The main orientation relationships observed are described additionally by the parallelism of lattice directions on these closed packed planes (Table 1).

Bain was the first proposing a model how a deformation of the austenite could lead to martensite (Bain 1924). According to Bain's model a bcc (α) lattice can be generated from a fcc (γ) lattice by compression along one principal axis (e.g. $[001]_{\text{fcc}}$) and a simultaneous uniform expansion along the other two axes perpendicular to it. Such a homogeneous

Table 1 orientation relationships overview

Orientation Relationship	Parallel Planes	Parallel Directions
Bain	$\{001\}_\gamma \parallel \{001\}_\alpha$	$\langle 001 \rangle_\gamma \parallel \langle 101 \rangle_\alpha$
Kurdjumov-Sachs (K-S)	$\{111\}_\gamma \parallel \{110\}_\alpha$	$\langle 1-10 \rangle_\gamma \parallel \langle 1-11 \rangle_\alpha$
Nishiyama-Wassermann (N-W)	$\{111\}_\gamma \parallel \{110\}_\alpha$	$\langle 112 \rangle_\gamma \parallel \langle 011 \rangle_\alpha$
Greninger-Troiano (G-T)	$\{111\}_\gamma \sim 1^\circ$ to $\{110\}_\alpha$	$\langle -12-1 \rangle_\gamma \sim 2^\circ$ to $\langle 1-10 \rangle_\alpha$
Pitsch	$\{001\}_\gamma \parallel \{-110\}_\alpha$	$\langle 110 \rangle_\gamma \parallel \langle 111 \rangle_\alpha$

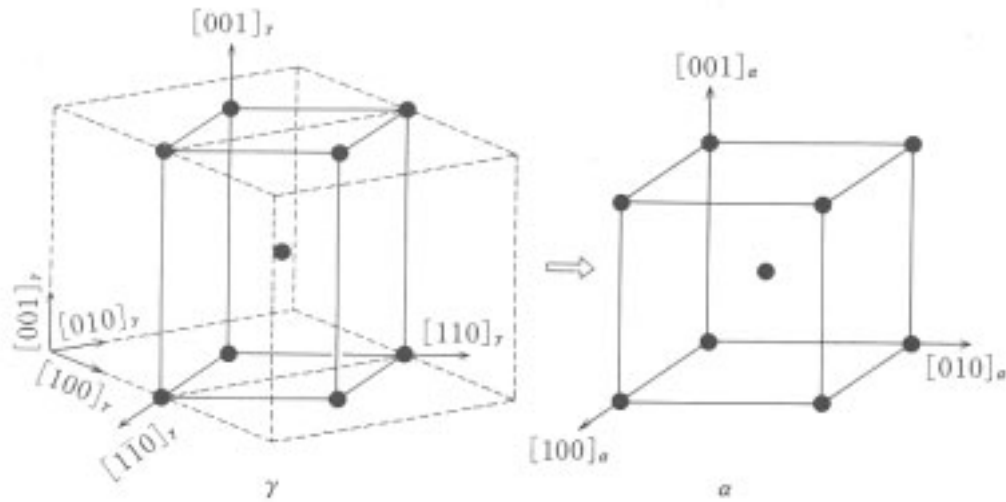


Fig. 4 Bain Model

distortion is called a lattice deformation, in the case of face to body centred cubic (or to body centred tetragonal) transformation, it is called the Bain distortion. The Bain correspondence describes the orientation relationship between the initial and final lattice. The martensite lattice is produced by a 45 degree rotation of the austenite lattice around the z-axis (Fig. 4). This correspondence does not imply a mechanism for phase transformation nor does it predict any orientation relationship or habit plane. Kurdjumov-Sachs (for Fe-1.4%C, Kurdjumov 1930) and Nishiyama-Wasserman (for Fe-30%Ni, Nishiyama 1978) showed experimentally the orientation relationships between actual crystals. The latter orientation relationship is presented schematically in Fig. 5.

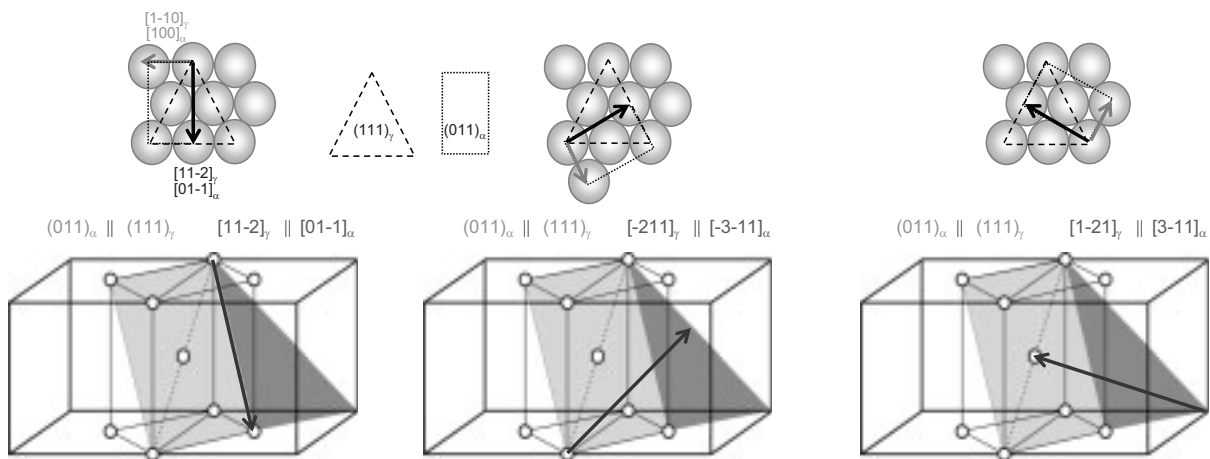


Fig. 5 Nishiyama-Wassermann Model

2.1.2 MARTENSITE MORPHOLOGIES

The microstructure of ferrous martensite has been the subject of intensive research (Krauss and 1971, Davies and Magee 1971, Nishiyama 1978, Maki 1990 and 1993, Morito et al. 2003a, only to name a few). In iron-carbon binary systems and in most heat treatable steels two major morphologies, lath or plate martensite, are observed. The terminologies for these and other morphologies observed in other alloys are based on the shape and alignment of the individual units of the martensite (martensite laths or needle). In lath martensite the lath are aligned parallel to each other while in plate martensite the adjacent plates do not form parallel to each other.

The morphology strongly depends on chemical composition, austenite grain size, and cooling temperature. Lath martensite forms at high M_S temperatures whereas plate martensite forms at M_S below 250°C (Krauss and Marder 1971, Nishiyama 1978). In iron-carbon binary systems the M_S temperature and the martensite morphology both depend on the carbon concentration. Below 0.6 mass% carbon only lath martensite is observed, whereas above 1.0 mass% carbon only plate martensite is observed. Between the two values both morphologies coexist. With increasing carbon content the fraction of plate martensite increases (Krauss 1990, Hougardy 2003, Morito et al. 2003a). In lath martensite the accommodation of the transformation shape change is carried out by formation and movement of dislocation, in plate martensite the shape change is accommodated by twinning within individual martensite laths (see Fig. 3). Beside the carbon content and the M_S temperature, the morphology and substructure of martensite is determined by the relative strength of austenite and martensite, the critical resolved shear stress for slip and twinning, and the stacking fault energy of austenite (Davies and Magee 1971, Thomas 1971, Krauss and Marder 1971), see Fig. 6.

The lath morphology is observed in Fe-C with low carbon content. It is characterized by well developed parallel blocks (Fig. 7). Each block is further divided into several laths. Several blocks together form a packet. Three blocks with different orientations exist in a packet. In a prior austenite grain several packets can exist. The size of the packets correlates with the prior austenite grain size (Roberts 1970, Marder and Krauss 1970, Swarr 1970, Maki 1993, Morito 2005). New automated characterizing techniques have further enabled us to understand the morphology and crystallography of lath martensite in Fe-C alloys in deeper details (Morito et al. 2003a, Shibata et al 2005).

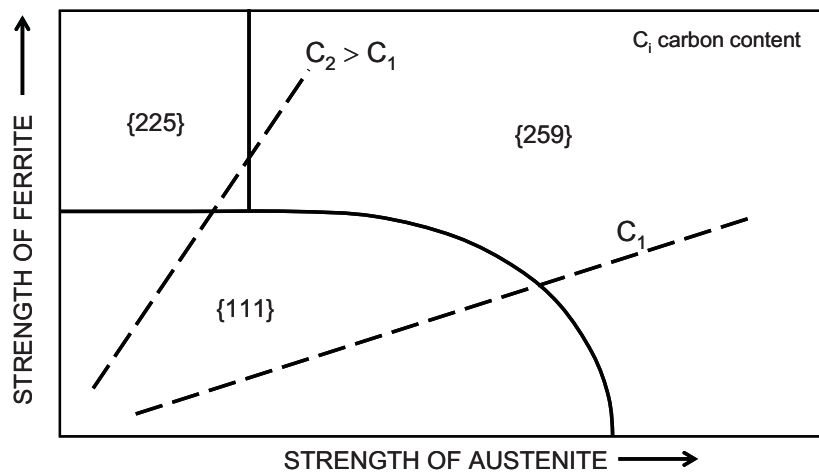


Fig. 6 Schematic representation of the effect of slip stress for dislocations in ferrite and austenite upon the martensite habit plane. Increasing the carbon concentration from C_1 to C_2 increases the strength of ferrite faster and results in a different habit plane and hence morphology (Davies and Magee 1971).

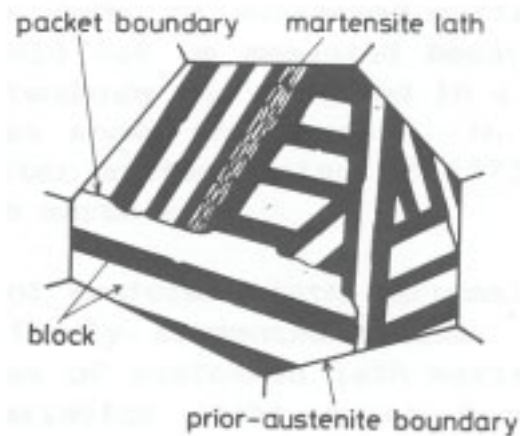


Fig. 7 The division of a prior austenite grain into packets, blocks and individual martensite lath (Tamura et al. 1982).

In lath martensite of low carbon alloys (0.0026 to 0.38 mass % carbon) each block consists of laths of two specific Kurdjumov-Sachs variants with the same habit plane (Morito et al. 2003a). The misorientation between the sub-blocks is about 10 degrees. According to Morito et al. (2003a) in iron carbon systems with more than 0.6% carbon blocks consist of lath with a single variant. Within one packet six blocks with different orientation relationships according to Kurdjumov-Sachs can exist.

Plate martensite is characterized by the various orientations of the martensite plates within one former austenite grain. This is directly related to the habit planes and the tendency of adjacent plates to adopt different variants of the habit plane. The habit planes are irrational. Grenninger and Troiano (1941) characterized the habit plane of two different alloys to be close to $\{259\}\gamma$ and $\{225\}\gamma$. Because plate martensite has not such a great technological importance, within this project focus is put on lath martensite. However, most of the commercial heat-treatable steels are not simple model alloys or binary Fe-C alloys. Due to the character of industrial related research work, for industrial alloys emphasis has not been put

on the microstructure analysis and therefore correlation between microstructural features and the desired properties have been rare.

In this work we investigate the effect of austenite deformation on the martensite morphology of industrially used silicon chromium steel and examine to which extent the terminology and definitions used for lath martensite in binary Fe-C systems can be applied to commercially employed low-alloy steels with medium carbon level. The nomenclature used by Ray and Jonas (1991) for the different Kurdjumov-Sachs variants was chosen by the present author to identify packets and blocks.

2.1.3 STRENGTH OF MARTENSITE

Various strengthening mechanisms contribute to the high strength of martensitic steels. These are carbon in solid solution, a high dislocation density, carbon clusters and precipitates (in tempered martensite), restriction of dislocation free path by twin boundaries, lath, packet and prior austenite grain boundaries. Due to the complex microstructures involved little progress has been made quantifying the different contributions to the overall strength of as quenched martensite or tempered martensite.

In as quenched martensite the highest contribution to the strength is from the carbon atoms in interstitial solid solution (Winchell and Cohen 1962 and 1963). The displacement of the iron atoms due to carbon atoms in the body-centred tetragonal lattice of martensite (Fig. 2) interacts strongly with dislocations and is considered as the major cause of the high strength of martensite (Krauss 1990, Nishiyama 1978, Pickering 1978, Owen 1992). The importance of carbon is reflected various equations, where the strength is either linearly dependent on the carbon concentration, or on its square or cube root (Pickering 1978, Krauss 1989).

Apart from the solid solution strengthening of the martensite by carbon, the substructure of the martensite plays an important role (Krauss 1990). During martensite deformation a high density of dislocations and or twins is introduced into a martensite lath or plate to accommodate the transformation shape change (Krauss 1990). Morito et. al. (2003b) studied the dislocation densities within lath martensite in Fe-C (0 to 0.8 mass% C) and Fe-Ni (0 to 23 mass% Ni) and showed, that the dislocation density increases with carbon concentration up to 0.61 mass% C. The dislocation density for 0.61 mass carbon is $32.1 \times 10^{14} \text{ m}^{-2}$. When the carbon content is further increased to 0.78 mass %, the dislocation density decreases. They found out, that there is a good correlation between the volume change due to transformation

and the dislocation density in lath martensite. It is important to note that the dislocation density is in the order of 10^{14} per square meter and much larger than that of heavily deformed metals. In some formulations beside the contribution of alloying elements like nickel (138 MPa for 20 mass% nickel) and the friction stress or stress to move dislocations in pure bcc iron (69 MPa) the contribution of the martensitic substructure (255 MPa) is taken into account (Krauss 1990).

A high grain boundary area, including lath boundaries, which are at the same time either block or packet boundaries and prior austenite grain boundaries is a characteristic of as quenched martensitic microstructure. Depending on the carbon and alloying content these interfaces are stable in the temperature ranges where commercial martensitic steels are tempered or used commercially. Ferrite grains can form by recovery of martensite at temperatures above 650°C in low-carbon steels (Maki 1999).

In as quenched martensite lath or packet boundaries act as grain boundaries and contribute to the overall strength. In tempered martensite the lath or packet boundaries and dislocation fine structure are preferential segregation sites for carbon atoms. At these interfaces carbides can form and act as barriers to dislocation movement. Consequently, a strong dependency of strength on morphological features of martensite has been observed and proposed (Smith 1971, Pickering 1980, Krauss 1990).

In some reports improved mechanical properties are referred to the finer martensite microstructure (Hensger 1984, Peters 1997), i.e. to a finer needle width. The effective grain size, i.e. the mean slip distance within a plate of martensite, is almost the same as the plate thickness rather than the length, since the chances of slip in an orientation parallel to the plate habit are very small (Naylor 1972). In the past years investigations with local orientation measurements of tempered martensite have given a clearer picture of the martensite morphology (Morito et al. 2003a, Shibata et al. 2005) and lead to a picture of an effective grain size (Guo et al. 2004) that is defined differently. An *effective grain size* in terms of area is equal to an area enclosed by high angle grain boundaries, i.e. defined by a misorientation larger than 15 degrees. Such an area is equivalent to the block area, because the possible variants in a block are separated by a low angle boundaries (Morito et al. 2003a). Morris et al. (2001) differentiate between an effective grain size for strength and another for toughness. The effective grain size for toughness is the coherence length on {100} planes, which determines the cleavage crack length. This length is limited by the packet or block size, if the packet is further divided by crystallographic units. The effective grain size for strength is defined by the length of the slip systems in body centred cubic systems. The slip planes are

the $\{110\}$ planes and thus the slip length on these planes and the misorientation change at the interfaces between adjacent lath, blocks, packets, prior austenite grains is decisive for the strength. Whiteman, Onel and Smith have taken the mean linear intercept of the packet size into consideration and integrated it into their formulations (Pickering 1978).

In most applications the martensite is not used in the as quenched condition but in the tempered condition. In this condition the carbon is rejected from the lattice and has precipitated as iron or metal carbides. Thus an additional term counting for the effect of precipitates on dislocation movement contributes to the strength. The precipitates in tempered ferrous martensite are mainly iron carbides. The shear stress to overcome two particles depends on the interparticle spacing and on the Burgers vector of the glissile dislocations. The formulations of Cox, Malik, Onel, and Smith consider this effect (Pickering 1978).

2.1.4 EMBRITTLEMENT OF MARTENSITE

Embrittlement of high-strength quenched and tempered martensitic steels occurs when thin carbide films form at the prior austenite grain boundaries (PAGB), that are enriched with impurities such as phosphorous (Capus 1963, Horn 1978, Briant 1979). The tempering temperatures, where the embrittlement is observed, overlaps with the lower range of the third stage of tempering, in which cementite precipitation takes place. During tempering in this range the PAGB are preferential nucleation sites for cementite (Honeycombe 1995). The thin plate-like carbides can act as slip barriers and can initiate intergranular cracks at the already impurity weakened PAGB (Krauss and McMahon 1992). Because cementite causes cleavage and voids, it should be eliminated from “strong” steels (Caballero et al. 2004). Banerji et. al. (1978) showed that enrichment of the PAGB occurs during the austenitization before quenching and not in the temperature range where tempered martensite embrittlement was observed. In order to avoid or minimize the embrittlement, plate-like cementite should be fragmented or avoided at the PAGB, especially when impurity elements are present. In this chapter we will first present briefly an overview of equilibrium grain boundary segregation and then the carbide precipitation behaviour during tempering and the situations leading to brittle fracture will be described.

2.1.4.1 FUNDAMENTALS OF GRAIN BOUNDARY SEGREGATION

In early years of material science a correlation between the amount of embrittlement, expressed as change in the ductile to brittle transition temperature, and the amount of phosphorous present in steels was observed (Briant 1999). The introduction of Auger Electron Spectroscopy enabled researchers to analyze the chemical compositions of grain boundaries. Since then it is commonly accepted that grain boundary enrichment of elements like phosphorous, antimony, tin, sulfur, arsenic, and others are the main reason for the observed embrittlement phenomena (Briant 1999, Grabke 1999). Phosphorous and tin are usually present in steels as impurities in low concentrations. Typical concentrations are 100 to 200 mass ppm for phosphorous and 20 to 30 ppm for tin. Tin is introduced into steels mainly by the use of scrap in steel melting. Due to the increased use of scrap the tin content in steels will increase in the future, if no measures are applied to select tinned materials from the scrap or to remove tin from the steel melt by metallurgical procedures.

The above mentioned elements affect the mechanical properties if they are enriched at grain boundaries. This enrichment is expected to happen by equilibrium segregation. The main driving forces for equilibrium segregation are the decrease in interface or surface energy by interactions between the segregating atom species and free bonds at surfaces or interfaces or release of elastic energy by rejection of the segregating elements from the bulk to interfaces or surfaces.

During the research years an inverse relationship between the degree of segregation and the bulk solubility was experimentally recognized (Sutton and Balluffi 1995). The same factors determining the solid solubility dictate the tendency towards grain boundary segregation. Each solute atom causes a lattice distortion in the matrix around itself. Therefore atoms prefer regions or sites where the lattice distortion energy is minimized. Such regions or sites are grain boundaries, dislocations cores and the stress field around them, stress fields around precipitates, or the interfaces between precipitates and matrix (McLean 1957, Grabke 1999). Based on this idea and considering only the positional entropy the free energy due to solute atoms F was derived by McLean (McLean 1957):

$$F = p \cdot e + P \cdot E - kT \cdot \{n n! N! - \ln(n - p)! p! (N - P)! P!\} \quad (\text{Equation 2})$$

N is the number of undistorted and n the number of distorted lattice sites. P and p are the numbers of solute atoms distributed among the undistorted and distorted lattice. The distortion energy caused by a solute atom in one of the N initially undistorted sites is E and that caused by a solute atom in one of the initially distorted sites is e . In the assumption made by McLean e was taken as constant. Resolving for the minimum of the free energy and replacing the difference between e and E by Q (J/mol), the concentration p/n in the distorted region by C_d (i.e. grain boundary concentration), the concentration P/N in the undistorted region by C (i.e. bulk concentration) lead to the well known McLean equation:

$$C_d = \frac{AC \exp\left\{\frac{Q}{R \cdot T}\right\}}{1 - C + AC \exp\left\{\frac{Q}{R \cdot T}\right\}} \quad (\text{Equation 3})$$

In dilute approximation the McLean equation is similar to that derived by Langmuir for surface segregation (Hondros and Seah 1977). Both approaches assume a fixed number of adsorbing sites of identical adsorption potential, and exclude any adsorption interaction, i.e. the occupation of any site does not affect the occupation of adjacent sites. The equilibrium grain boundary coverage thus is proportional to the bulk solute content and inversely to the temperature. In the Langmuir model, it was assumed that adsorption could only occur on the unoccupied substrate adsorption sites, or on unoccupied segregation sites at grain boundaries. If the initial adsorbed layer can act as a substrate for further adsorption then, instead of the isotherm leveling off to some saturated value at high pressures, it is expected to rise indefinitely. The most widely used isotherm dealing with multiplayer adsorption was derived by Stephen Brunauer, Paul Emmet and Edward Teller, and is called the BET isotherm. The truncated BET isotherm developed by Brunauer, Deming, Deming and Teller for surface segregation assumes saturation coverage. In its grain boundary analogue the solubility limit is introduced, which makes the development of the differential free energy for segregation possible (Hondros and Seah 1977). All the aforementioned authors assume saturation coverage. Seah and Hondros observed tin segregation in α -iron up to several monolayers and demonstrated that the observations could be described by the BET theory for surface adsorption. The grain boundary analogue of the BET theory is presented in table 2. In this equation the pressure and the adsorbed quantity are replaced by the bulk and grain boundary fractions. The pressure at which a gas condenses as a liquid is replaced by the solubility limit. If adsorbate interaction is considered then the Fowler-Guggenheim theory can be applied, as was done by Hondros and Seah (Hondros 1977). Another important theory developed by

Guttman for multi-component systems takes the interaction between solutes into account and is called the co-segregation theory (Guttman et al. 1982).

Erhart investigated binary Fe-P systems (Erhart 1980) and showed that phosphorous can be enriched up to one atomic monolayer at the grain boundaries. By decreasing the cohesive energy between adjacent grains (Rez and Alvarez 1999) phosphorous causes embrittlement. The grain boundary segregation of phosphorous to grain boundaries as a function of the bulk concentration and holding temperature could be described with the Langmuir-McLean equation. The free energy for segregation was found to be (Erhart 1980):

$$\Delta G_0(\text{P}) = - 34300 - 21.5 T \text{ (J / mol)} \quad (\text{Equation 4})$$

Table 2 Models and equations for equilibrium grain boundary segregation

Equation number	Authors and References	Formulas	Assumptions
5	Langmuir 1918, McLean 1957	$\frac{X_b}{X_{b0} - X_b} = X_c \exp\left\{\frac{Q_{mono}}{RT}\right\}$	fixed number of adsorbing sites, no adsorbate interaction
6	Grain boundary analogue of truncated BET theory	$\frac{X_b}{X_{b0} - X_b} = \frac{X_c}{X_{c0}} \exp\left\{\frac{Q}{RT}\right\}$	fixed number of adsorbing sites, no adsorbate interactions, solubility limit makes access to thermodynamic data possible
7	Fowler-Guggenheim	$\frac{X_b}{X_{b0} - X_b} = X_c \exp\left\{\frac{Q - z \omega \frac{X_b}{X_{b0}}}{RT}\right\}$	fixed number of adsorbing sites, adsorbate interactions
8	Seah 1976	$\beta_b = \frac{X_b}{X_{b0}} \cdot \frac{1}{X_c} = \frac{\exp\left\{\frac{Q}{RT}\right\}}{X_{c0}}$	

X_b grain boundary concentration, X_{b0} saturation level of X_b , X_c bulk concentration, Q_{mono} = (E-e) x Avogadro's number is the grain boundary adsorption energy, X_{c0} solubility limit, Q Difference of the free energy of the first layer and the free energy of condensing successive layer (corresponding to a precipitation reaction), z coordination number for adsorbate species, ω interaction energy between adjacent adatoms, β_b enrichment ratio.

Table 3 presents the data obtained by different researchers for binary systems and industrial alloys. In ternary Fe-P-C systems Erhardt observed a rejection of phosphorous from the grain boundaries with increasing carbon content. At the same time the fraction of intergranular fracture lowered in the fracture surface. The rejection of phosphorous through nitrogen was less pronounced. Investigations on ternary Fe-Cr-P and Fe-Ni-P systems showed that chromium does not segregate to the grain boundaries and therefore has no influence on the phosphorous level at the grain boundaries. Nickel was enriched at the grain boundaries and lowered the concentration of phosphorous. The results opposed the cosegregation theory, which predicts segregation of chromium or nickel and phosphorous due to positive interactions (Guttman et al. 1982). Comparison between Fe-Cr-C-P and Fe-C-P showed an increased grain boundary concentration for the first system. The strong interaction between chromium and carbon lead to carbide formation and less carbon was left to compete with phosphorous for the available vacant sites. In contrast to this observation the nickel enhances the carbon activity in iron and hence the grain boundary concentration of phosphorous was reduced in the Fe-Ni-C-P system.

For a series of medium carbon manganese steels Abe (1990) investigated the segregation of phosphorous in the austenite range. He observed increasing grain boundary concentration of phosphorous with increasing bulk content and with decreasing temperature. For a constant carbon bulk concentration the grain boundary concentration of carbon increases with increasing grain boundary concentration of phosphorous. The results imply that other mechanisms beside site competition operate in the austenite range.

Two equations are mainly used for investigation of segregation kinetics, the MacLean and the Crank equation. The subsequent equation derived by McLean (McLean 1957) describes the kinetic of grain boundary segregation:

$$\frac{X_b(t) - X_b(0)}{X_b(\infty) - X_b(0)} = 1 - \exp\left(\frac{4Dt}{\alpha^2 d^2}\right) \operatorname{erfc} \sqrt{\frac{4Dt}{\alpha^2 d^2}} \quad (\text{Equation 9})$$

$X_b(0)$, $X_b(t)$ and $X_b(\infty)$ are the grain boundary segregation levels at the start of an isothermal annealing directly after quenching from higher temperature, at time t and at infinite time (i.e. equilibrium level), respectively. D is the volume diffusivity of the solute, α is the ratio of the concentration of the solute in the grain boundary to that in the matrix. d is the grain boundary thickness enriched with solute atoms. The Crank equation is a simplified equation valid below coverage of 0.2 atomic layers (Seah 1977):

$$X_b(t) - X_b(0) = X_c \frac{4d^2}{a^3} \sqrt{\frac{Dt}{\pi}} \quad (\text{Equation 10})$$

X_c is the bulk mol fraction of solute; a^3 is the volume of matrix atoms. The latter equations have successfully been used to derive diffusivities for solutes, from that segregation enthalpies, and segregation kinetics (Seah 1977, Grabke 1999, Perhacova 2000, Christien 2003).

2.1.4.2 CARBIDE PRECIPITATION

As mentioned earlier most commercial martensitic steels are tempered after quenching in order to increase the toughness and ductility. Usually the tempering is carried out in the temperature range between 200°C and A_{c1} . Because the as quenched martensite is thermodynamically not stable, the atoms become mobile with increasing temperature and the diffusional phase transformations to ferrite and cementite can take place. However at lower temperatures intermediate reactions take place. The kinetics of these solid state reactions is controlled by the carbon diffusivity in the martensitic structure. The reactions can be

Table 3 Segregation and diffusion data for various alloys

Alloy	segregating element	segregation enthalpy (J/mol)	Diffusivity	authors
Fe-P (α -iron)	P	-34300-21,5T		Erhart 1980
Fe-P (α -iron)	P	-15000-33T		Ishida 1985
Fe-P (γ -iron)	P	-49000+/-4 at 1000°C		Paju 1984
Fe-Sn (α -iron)	Sn	-(22500+/-2800)-(26,1+/-0,9) T		Grabke 1989
Fe-0,1C-0,85Cr-0,3Mn-0,4Mo-0,2Si-0,25V	P	-21260-19,8 T	$7,7 \cdot 10^{-9} \exp \{-151/RT\}$	Perhacova
Fe-0,1C-2,5Cr-0,3Mn-0,4Mo-0,2Si-0,25V	P	-18870-27,1 T	$2,5 \cdot 10^{-7} \exp \{-168/RT\}$	Perhacova
17-4PH	P	-43100+/-4 @ 600°C	$0,183 \cdot 10^{-4} \exp \{-229/RT\}$	Christien
Fe-P	P		$7,1 \cdot 10^{-3} \times \exp (-20000/T)$ cm ² /s	Leslie
Fe-C	C		$0,02 \exp \{-20100/RT\}$	Wert 1950, McLean 1954
Fe-P	P		1,58 $\exp \{-52300/RT\}$ (cm ² /s)	Seah 1977 (Gruzin & Muddal)

classified in two categories (Krauss 1984, Honeycombe 1995), the precarbide precipitation reactions (as well called as ageing reactions) and into the carbide formation reactions (tempering stages). The ageing reactions include carbon clustering, formation of modulated structures on (102) martensite plates, and of superstructures. Formation of transition carbides, the transformation of the retained austenite, cementite formation and precipitation of alloy carbides in alloy steels are considered as different tempering stages. Fig. 8 summarizes the reactions and the temperature range.

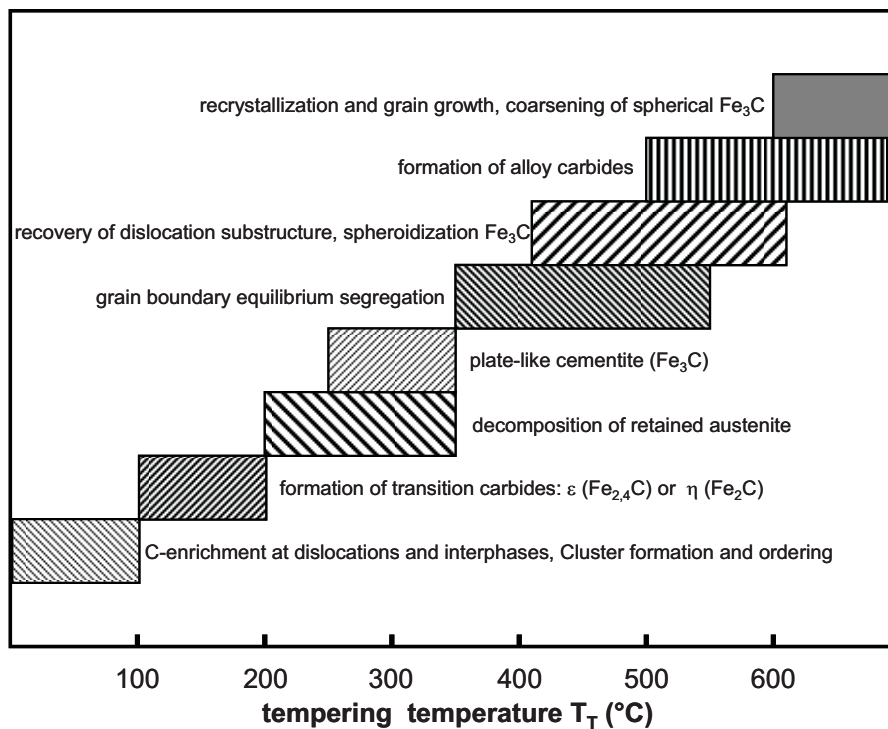


Fig 8 Schematical representation of the different ageing and tempering stages

As mentioned before, at the lower temperature range of the third tempering stage, where cementite precipitation starts, grain boundaries are preferential nucleation sites. It is known that defects such as grain boundaries can be heterogeneous nucleation sites, because the creation of a nucleus at such a site would lead to the destruction of a defect, thereby releasing some free energy and reducing or even removing the activation barrier (Easterling 1992). High angle grain boundaries are especially effective sites for incoherent precipitates with high interface energies between the matrix and the precipitate. If the adjacent grains and the precipitate allow the formation of lower energy facets then the critical nucleus size and the activation energy barrier for heterogeneous nucleation will further be reduced. The nucleus will then have an orientation relationship with one of the grains (Easterling 1992). The orientation relationship found experimentally between the martensite and cementite is the

Bagaryatski relationship (Honeycombe 1995). It has been reported by Furuhashi et al. (1996) that of the possible crystallographic variants only one single variant tends to precipitate on a flat grain boundary of titanium. A film along the grain boundary is then formed by further growth and coalescence of small individual precipitates of the same variant. The selection of the variant depends on the activation energy for the formation of the critical nucleus. It is assumed that similar assumptions must apply to the precipitation of cementite during tempering of martensite at prior austenite grain boundaries. The cementite films are usually very thin and hard to detect, but with increasing temperature they spheroidize and give rise to well-defined particles of cementite in the grain boundaries (Honeycombe 1995).

2.2 PROCESSING MARTENSITIC HIGH STRENGTH STEELS

The final properties of any specific material, i.e. an alloy with fixed composition, are defined by its microstructure or defect structure. The microstructure itself is the result of the process parameters used during production and the composition. In this chapter the main process steps of quenched and tempered martensitic steels and their effects on microstructure and thus on the properties are discussed. The conventional heat treatment for producing high strength martensitic steels consists of austenitization, followed by quenching and tempering. Control of the microstructure in a thermomechanical treatment is usually carried out by deformation of the austenite prior to quenching with the aim to improve the properties. Therefore the changes induced by thermomechanical treatment are explained within the section of austenite conditioning after discussion of austenitization.

2.2.1 AUSTENITIZATION

One objective of the austenitization is to obtain a homogeneous *solid solution of austenite*, where all the carbon and alloying elements are statistically distributed. A homogeneous distribution of carbon and alloying elements is necessary to obtain uniform properties. The amount of carbon in solid solution determines the hardness of the final martensite (see 2.1.3). If metal carbides other than iron carbides are present a minimum austenitization temperature or time is needed to dissolve all the carbides and distribute the carbon. Such metal carbides can be compounds of carbon with microalloying elements such as vanadium or with alloying

elements such as chromium. Their presence can lead to smaller grain size or to a bimodal grain size distribution (Lagneborg 1999, Hougardy 2003). Another process which can occur during austenitization is equilibrium segregation of impurity elements such as phosphorous to the grain boundary (refer to 2.1.4.1). Phosphorous enrichment at grain boundaries can lead to brittle failure of the final part (Banerji et al. 1978, Briant and Banerji 1979b, Briant 1999, and Krauss 1992). The higher the austenitization temperature the lower is the concentration of the impurity elements at the austenite grain boundaries (Abe 1990). Summarizing the above information it is necessary to use high austenitization temperature in order to obtain a uniform distribution of carbon and alloying elements and to minimize the enrichment of impurity elements at the grain boundaries. But as in most problems in material science, there is a contradiction to be solved. In contrast to the homogenization during austenitization the grain size refinement requires rapid heating to low temperatures in the austenite range and short holding times followed by rapid cooling, which is required anyhow for martensite formation. Such a treatment is called short cycle austenitizing (Cohen 1963).

The *austenite grain size* determines the toughness of high strength steels. Ohtani et. al. (1972) showed that the ductile to brittle transition temperature decreases with the average austenite grain size. Because the size of the packets and blocks depends on the prior austenite grain size, the effective grain size is influenced as well by the austenite grain size (see 2.1.2). Thus small austenite grain size is desirable to obtain high toughness for a specific strength level. Grain refinement further leads to increase of the grain boundary area. Thus for a given impurity concentration more segregation sites are offered to the same amount of atoms (for fixed impurity bulk concentration) leading to a lower grain boundary concentration of the atoms at the grain boundaries.

For the same initial microstructure and constant heating rate to the austenitization temperature the austenitization temperature and time are the main factors. They determine the austenite grain size prior to quenching. The higher the austenitization temperature and the longer the austenitization time the larger is the average austenite grain size after austenitization (Fig. 9). To obtain small average grain size usually the lowest austenitization temperature and time are selected. However, the selected austenitization temperature must be high enough to lead to a homogeneous solid solution of austenite as described above.

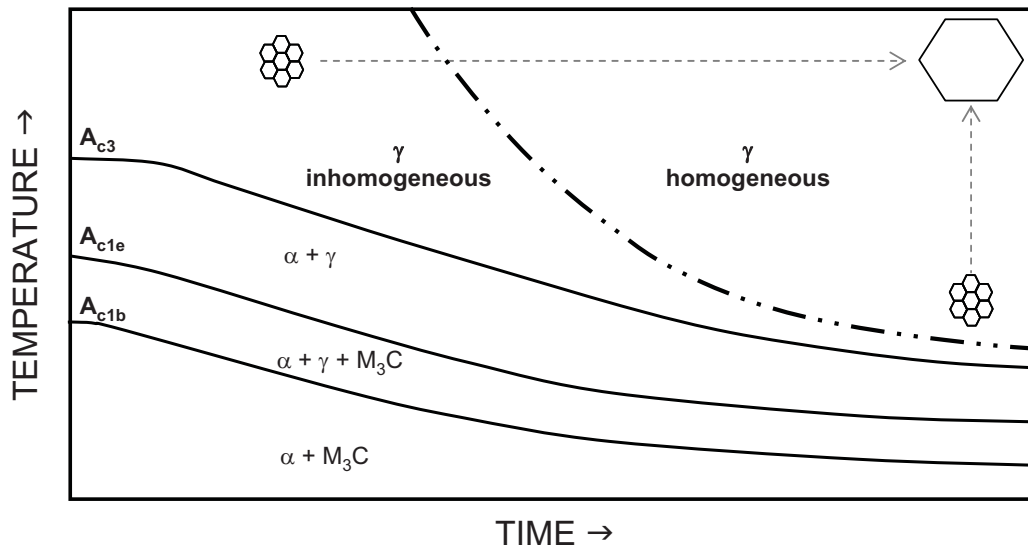


Fig. 9 Schematic presentation of a isothermal time temperature austenitization diagram for a low alloyed steel

2.2.2 AUSTENITE CONDITIONING

Because martensite forms by a displacive transformation from the parent austenite phase, and because the atoms do not change their neighbours, the grain and dislocation structure, or in general the defect structure is inherited to the product phase. Thus the microstructure of the austenite is very essential for the final properties of the martensite. It has been shown that austenite deformation prior to quenching can lead to an increase in strength without adverse effects on ductility or toughness (Zouhar 1984, Hensger and Bernstein 1984, Peters 1997, Wettlaufer 2000). The deformation and the subsequent solid state reactions prior to quenching lead either to austenite grain refinement or to a subgrain dislocation structure. These microstructures have a positive effect on the final properties (Hensger and Bernstein 1984). Therefore, it is important to understand how deformation within the austenite region controls the evolution of grain size and shape and generates a favorable dislocation substructure.

Fig. 10 presents hot-working flow curves. During hot working first the stress rises due to strengthening and later is compensated by softening. Depending on which mechanism is dominantly responsible for softening two different types of stress evolution with increasing strain are observed. If softening only takes place by dynamic recovery then curve 1 is observed. Flow curves of type 2 occur when softening at strains higher than the maximum stress is carried out by dynamic recrystallization. During dynamic recrystallization the

softening leads to a drastic decrease of the dislocation density, whereas during dynamic recovery a stable dislocation rearrangement is the main mechanism of softening. Therefore, the stress decrease observed during dynamic recrystallization is larger. The microstructure of metallic materials is determined significantly by the separation of dislocation and therefore depends strongly on the stacking fault energy. The larger the stacking fault energy the larger is the tendency for softening by dynamic recovery and polygonization during hot rolling. Values for commercial alloys can be found rarely. The stacking fault energy is strongly on carbon concentration (Adeev and Petrov 1975). The latter author additionally observed a dependency of the stacking fault energy on the austenite grain size and explained it by the segregation of carbon atoms to the grain boundaries.

Fig. 11 shows the microstructure evolution for a material that is deformed in compression and recrystallizes dynamically. Shortly before reaching the flow curve maximum the austenite grains are elongated and the primary grain boundaries are serrated (Hensger 1985). The serration is correlated to the accelerated polygonization in the vicinity of grain boundaries. Around the maximum of the flow curve a small volume fraction of small recrystallized grains is observed at the primary austenitic grain boundaries. With increasing strain the volume fraction of recrystallized grains increases.

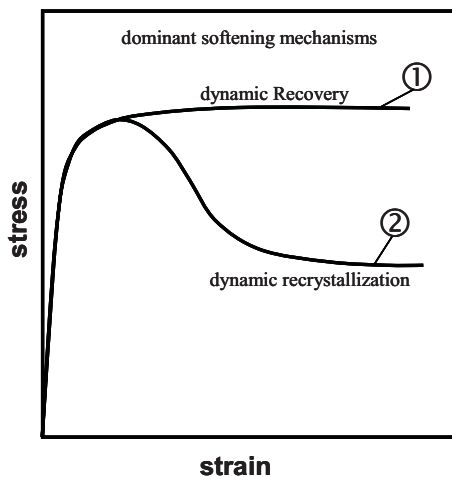


Fig. 10 Schematic presentation of hot-working flow curves for 1) metals undergoing dynamic recovery and 2) for metals undergoing dynamic recrystallization after initial period of dynamic recovery (Hensger et al. 1985)

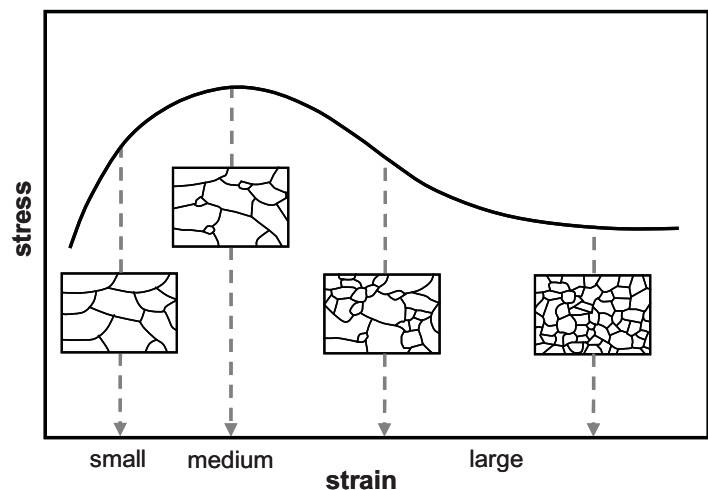


Fig. 11 Schematic presentation of hot-working flow curve and microstructure evolution for metallic materials that soften predominantly by dynamic recrystallization (Hensger et al. 1985)

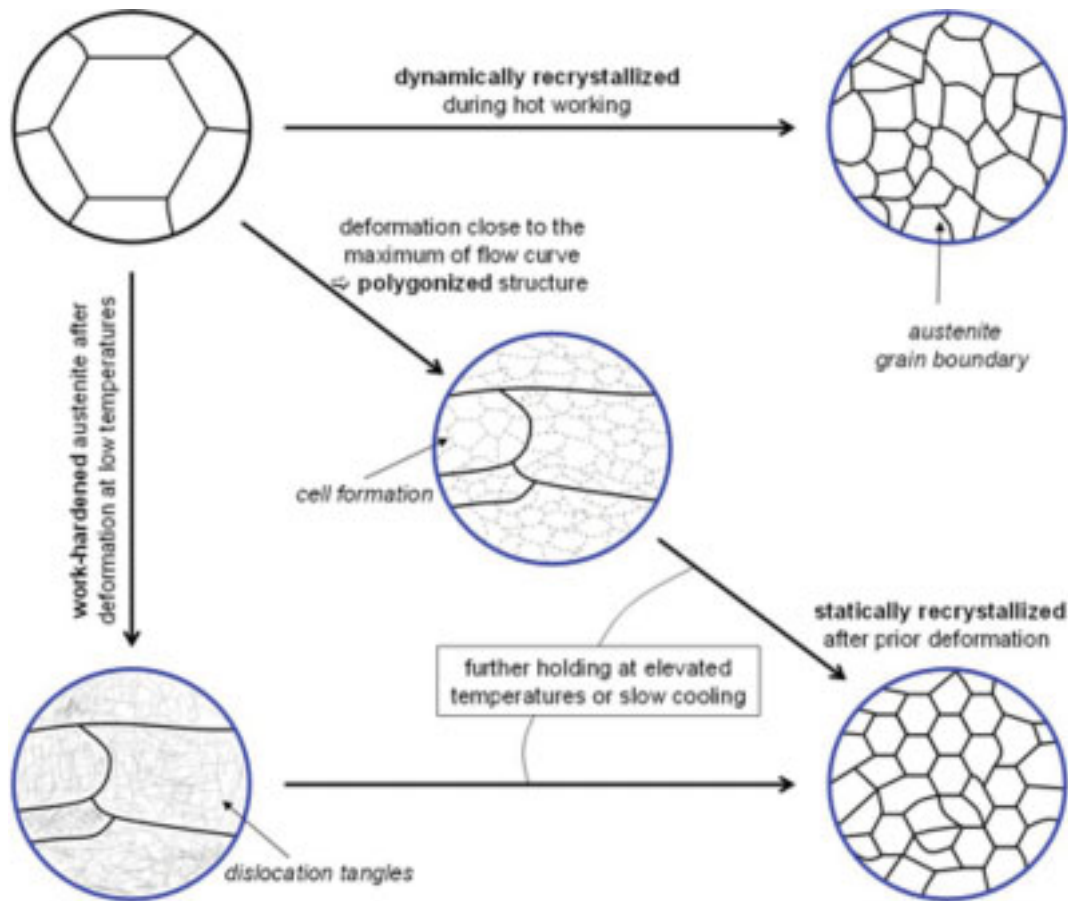


Fig. 12 Schematic presentation of possible austenite microstructures caused by a deformation after austenitization and prior to quenching.

Hot working offers a wide variety of microstructure control (Fig. 12). In case of thermomechanical treatment the aim is to optimize the mechanical properties. Therefore it is necessary to understand which austenitic condition results in optimized properties. It has been shown, that for low alloyed steel, deformation temperatures in the range of 900 to 950°C, strain rates of 3 to 20 s⁻¹ and strains between 25 and 40% the maximum of the flow curve is observed (Hensger and Bernstein 1984, Honeycombe 1995). With increasing strength of the austenite not only the strength of the resultant quenched and tempered martensite increases but as well the toughness and the reduction of area (Fig. 13). The authors ascribe the improved properties to a dynamically polygonized subgrain structure of the austenite, which was observed independently of strain rate (within the range of 1 to 20 s⁻¹) for strains leading to the maximum stress of the hot-working flow curve. The improvement in the fracture toughness was explained with the higher volume fraction of lath martensite, allowing larger energy absorption in the front of the crack tip, and due to pinning of the dislocation

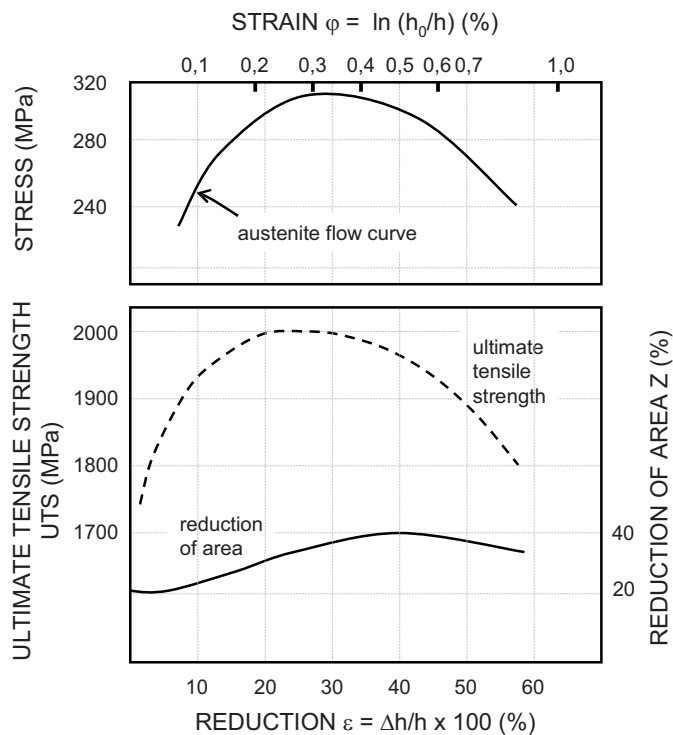


Fig. 13 Hot-working flow curve of austenite and mechanical properties after high-temperature thermomechanical treatment and tempering at 420°C for Fe-0.55C-1.6Si-0.6Mn (mass%) (Hensger and Bernstein 1984). Austenite deformation at 950°C with a strain rate of $20s^{-1}$.

substructure (that is inherited to the martensite) by finely dispersed precipitates. Additionally Bernstein (in: Hensger and Bernstein 1984) assumes that during the high-temperature thermomechanical treatment, the embrittling impurity elements are distributed to the subgrain boundaries of the austenite and minimize their “embrittling activity”, i.e. the concentration of the impurities at the prior austenite grain boundaries is lowered. According to Zouhar (1984) recrystallization of austenite can enrich impurities at the prior austenite grain boundaries. Abe et al. (1990) have shown that the enrichment of phosphorous and carbon at the austenite grain boundary depend on the one hand on the velocity of the moving boundaries during recrystallization and on the other hand on the diffusivity of the appropriate elements. According to their work grain boundary migration during recrystallization and grain growth of austenite leads to non-equilibrium segregation. A higher solute concentration than that of equilibrium segregation was observed. They proposed that the sweep effect during grain boundary migration is responsible for the higher solute concentration at the grain boundaries.

2.2.3 TEMPERING

Tempering at temperatures below A_{c1} after quenching is performed to set the desired combination of mechanical properties. The various solid state reactions taking place during

tempering have already been described earlier (2.1.4.2). It has been shown, that fracture toughness of spring steels is not dependent on the tempering time (below 2 hours) while it decreases with increasing strength, i.e. with decreasing tempering temperature (AiF 7966). Furuhara et al. (2004) have shown that high heating rates and short tempering times increase the hardness. The increase has been ascribed to smaller carbide particles that are dispersed more uniformly. The relationship between tempering temperature and mechanical properties is shown in Fig. 14. The ductility and toughness of quenched martensite decrease with increasing strength, i.e. with decreasing tempering temperature (Berns et al. 1984, Dziemballa and Manke 2005). Additions of impurity elements further reduce the ductility or toughness. A drastic loss in ductility or toughness is observed in the lower temperature range where cementite starts to precipitate (Krauss 1992, Briant 1979 & 1979c, Horn 1978, Capus 1963). As described earlier, in this range cementite preferentially precipitates in form of thin films at martensite lath or grain boundaries. In case of impurity loaded boundaries, during loading the metal fails in an intergranular way.

The deformation of austenite prior to quenching strongly affects the carbide precipitation during tempering. The austenite transforms without diffusion into martensite. Defect

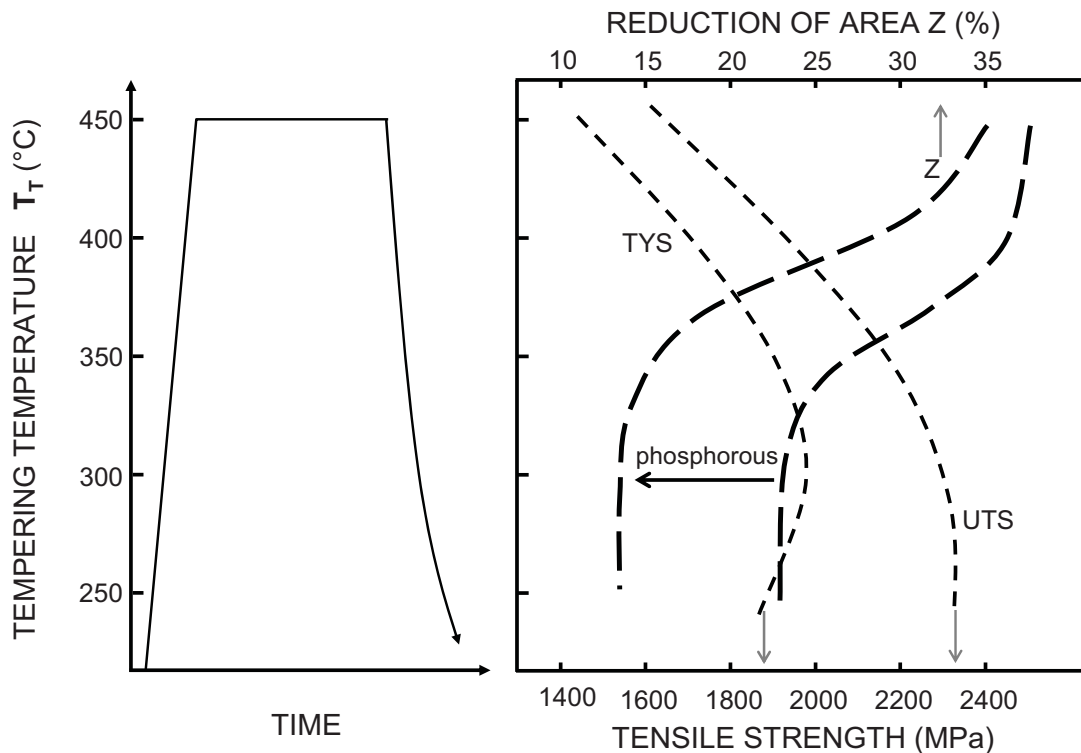


Fig. 14 Relationship between tempering temperature T_T and mechanical properties (tensile yield strength TYS , ultimate tensile strength UTS and reduction of area Z) for $Fe-0.55C-1.4Si-0.65Cr-0.65Mn$ (mass %)

structures generated during or after deformation like dislocations substructures are inherited during quenching to the martensite lattice. These inherited structures influence the carbide precipitation within the matrix, and at the former austenite grain boundaries (Zouhar et al. 1984, Yusa et al. 1999).

2.3 STRATEGY FOR OPTIMIZATION OF MECHANICAL PROPERTIES

After having discussed the basics principles of heat treatment and austenite deformation for high strength low alloy martensitic steels, a strategy for optimization of mechanical properties based on thermomechanical treatment will be presented. The necessary steps to be carried out during the optimization process are:

- 1) determination of CCT (Continuous-Cooling-Transformation) diagram with and without deformation
- 2) determination of optimum austenitization conditions with and without deformation
- 3) recrystallization behaviour and post deformation solid state reactions
- 4) defining the optimum deformation temperature for optimum mechanical properties
- 5) final optimization including optimization of tempering temperature and combination of deformation steps

CCT diagrams for most commercial steels are available and well known. The important information to be extracted from such diagrams is the critical time needed for quenching from austenitization temperature to obtain a fully martensitic microstructure. However, conventional CCT diagrams may become less important, when the austenite is deformed prior to transformation. The respective parameters of the thermomechanical treatment determine the state of austenite and hence influence the kinetics of the subsequent transformation and the microstructure of the product phase (Kaspar 1994). Deformation of austenite prior to quenching accelerates the transformation to ferrite and pearlite (Kaspar et al. 1994). Homogeneously distributed dislocations can depress the martensite start temperature (M_S), whereas localized shear bands will aid nucleation and raise the M_S (Kaspar et al. 1994).

Optimum *austenitization conditions* have been theoretically and experimentally determined and proven in practice for steels used commercially. The dependency of grain size with austenitization temperature is well known and reflects itself in lower toughness and ductility properties with increasing austenitization temperature (Ohtani 1972, Streißberger 1984). For microstructures that are produced by deformation, the ductility or toughness can be independent of austenitization temperature (Streißberger 1984). If recrystallization of austenite is involved in the thermomechanical treatment the effect of austenite grain size produced during austenitization is minimized, because the resultant grain size is the consequence of the recrystallization during or after deformation and does not vary strongly with the austenitization temperature prior to deformation. Streißberger's work shows that the thermomechanical treatment leads to an improvement of strength and toughness properties. It resulted in refined austenite grain size and a more homogeneous grain size distribution. As a consequence a refined martensite structure was observed after tempering.

The knowledge of *recrystallization behaviour* is essential in defining the deformation temperatures for an optimum thermomechanical treatment. Through recrystallization austenite grain refinement can be achieved leading to improved toughness and ductility properties. Nowadays, recrystallization behaviour can be investigated using dilatometers or similar devices. Theoretical approaches and mathematical models are available to define the critical strain for dynamic recrystallization for each deformation temperature (Poliak 2003). The determination of the recrystallization behaviour will accelerate the process definition for a thermomechanical treatment. Any solid state reaction after deformation like recovery, recrystallization or grain growth process will affect the mechanical properties. Because the direct investigation of the austenite grain substructure for commercial alloys is almost impossible, mechanical testing for different conditions can not be avoided. To retard any solid state reactions, which might negatively alter the mechanical properties microalloying elements such as niobium and vanadium can be used together with the thermomechanical treatment (Pickering 1978, Peters 1996, Peters and Kaspar 1997, Wettlaufer 2000, Ayada 1998).

The *deformation parameters*, i.e. deformation temperature and strain together with the strain rate and time between deformation and quenching determine the austenite state prior to quenching. During process development for a specific steel the effect of deformation on microstructure and mechanical properties can be investigated separately. To understand the

relationship between the developed microstructure and the mechanical properties, it is more convenient to combine the tests and relate the mechanical properties to the microstructure. Fig. 13 shows the variation of ultimate tensile strength and reduction of area for the steel Fe-0.55C-1.6Si-0.6Mn as a function of deformation strain. Streißlberger's investigation confirms the dependency of strength on deformation strain. For 50CrV4 (Fe-0.54C-1.09Cr-0.97Mn-0.32Si-0.12V (mass%)) Peters demonstrated that both a recrystallized (deformation temperature $T_D=860^\circ\text{C}$) and a non-recrystallized ($T_D=770^\circ\text{C}$) austenite grain structure lead to a significant increase of the ductility while maintaining the same level of strength (Peters and Kaspar 1997). Samples were subjected to logarithmic strains in the range of 0.3 to 1.0. After tempering at 280, 380, 420 or 460°C the ductility was constant for all deformation strains.

In Fig. 15 different thermomechanical treatments are compared with the conventional heat treatment. As already described above, the thermomechanical treatment can result in a recrystallized or non-recrystallized austenitic grain structure prior to quenching. Relative to the conventional treatment, both austenite grain structures might result in superior properties. Then the question arises, which treatment should be selected. The selection of variables depends on the production limitations and on the design requirements of the part for which the steel is used. A work-hardened, non-recrystallized grain structure (route number 3) can behave more anisotropic than a recrystallized variant (route number 2) and might not be used in applications, where load directions other than the rolling directions might be important. This anisotropy is due to the prior austenite grain structures that are inherited to the final martensitic structures. The degree of anisotropy depends as well on the austenite grain size before deformation. However, a sequence of deformations in some cases might be more beneficial for the properties (Zouhar 1984, Peters and Kaspar 1997). The thermomechanical treatment might consist of two or more deformations. All the successive deformations might be carried out in such a way to minimize the austenite grain size. It is possible as well to perform the final deformation in such a way to work-harden the austenite and generate an austenite substructure that is beneficial for the final properties.

In the present work, the aim is to systematically compare the final properties of the tempered martensite resulting from various austenite conditions with that resulting from conventional heat treatment. Microstructure investigation of the final martensite should help to better understand the relationship between austenite condition prior to quenching, martensite microstructure and final properties.

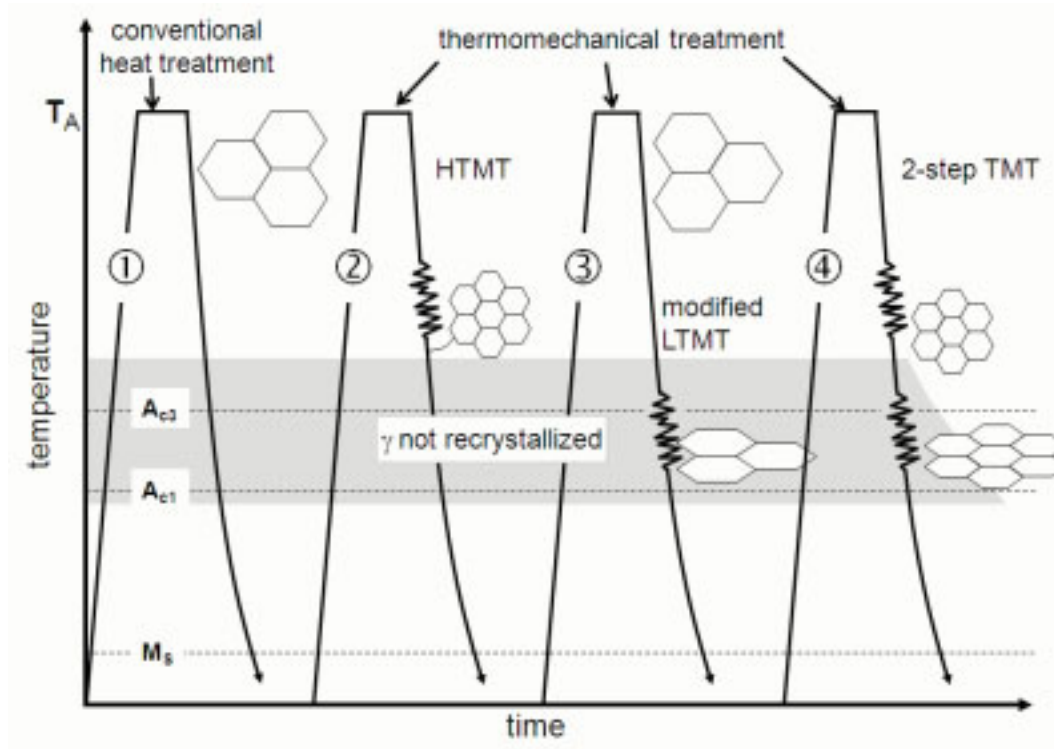


Fig. 15 Schematic presentation of various processing: 1) conventional heat treatment without any deformation of the austenite prior to quenching, 2) high temperature thermomechanical treatment HTMT with deformation and recrystallization of the austenite prior to quenching, 3) modified low temperature thermomechanical treatment LTMT resulting in work hardened austenite prior to quenching, 4) combination of 2 and 3.

In the present work, the aim is to systematically compare the final properties of the tempered martensite resulting from various austenite conditions with that resulting from conventional heat treatment. Microstructure investigation of the final martensite should help to better understand the relationship between austenite condition prior to quenching, martensite microstructure and final properties.

3 EXPERIMENTAL APPROACH AND METHODS

3.1 APPROACH

The first objective of the study is to determine the upper concentration limits of the impurity elements phosphorous, copper and tin below which the mechanical properties of 54SiCr6 fulfil the design requirements. The second objective is to improve the strength properties without any loss of ductility and fatigue limit. Thermomechanical treatment has proven to be effective in serving the latter objective (see 2.2.2). Because the final mechanical properties are the result of the composition and the material's history, i.e. the parameters used during processing, throughout the study always one parameter was varied while keeping the rest constant.

Melts with different compositions were produced with different levels of phosphorous, and copper and tin (Fig. 16). The parameter windows for conventional heat treatment and thermomechanical treatment were determined in small scale dilatometry tests. The mechanical properties after conventional heat treatment were determined as a function of impurity level and tempering temperature. The mechanical property improvements achieved through application of thermomechanical treatment are all evaluated with reference to the values obtained by conventional heat treatment. The comparison of mechanical properties is complemented with a detailed microstructure investigation. The aim was to identify the main microstructural features responsible for the changes in mechanical property, especially in the embrittlement of the tempered martensite. Within this chapter the materials tested and the experimental methods are described.

3.2 MATERIALS

To investigate the influence of the impurity elements and exclude all other parameters laboratory melts were produced on the basis of Fe-0.55C-1.4Si-0.65Cr-0.65Mn (all mass %) without and with vanadium (54SiCr6 and 54SiCrV6). Coil springs for automotive application produced in Europe are mainly made of silicon chromium alloys. In the beginning of the nineties, these alloys were introduced and a significant increase of the design stress of coil

springs was achieved (Dziemballa and Manke 2005). The addition of silicon reduces the carbon diffusivity in iron, inhibits the carbon depletion from the matrix, and retards the cementite precipitation during tempering (Alten 1953, Houdremont 1956, Altstetter et al. 1962, Nam 2000), thus higher strength levels could be achieved at the tempering temperatures used at that time. Miyamoto et al. (2005) have reported that silicon addition not only retards the conversion from epsilon carbide to cementite, but as well controls cementite growth and refines its dispersion by silicon partitioning between ferrite and cementite. The carbon contents of the silicon chromium steels used today lie between 0.55 and 0.68 mass %. This medium carbon level is a good compromise between strength and toughness. Chromium and manganese additions increase the hardenability and are present in almost all low-alloy heat-treatable steels.

For each base alloy the composition of phosphorous, copper and tin was varied systematically (Fig. 16). The ratio of copper and tin was kept constantly at 9:1. To ascertain the concentration limits for the worst case, the amount of sulphur was kept high. In addition to the laboratory melts, two industrial melts were included into the study to verify the results obtained for laboratory melts. The two melts were of different origin and from different metallurgical processes: one from the blast furnace route and the other from the electrical arc route.

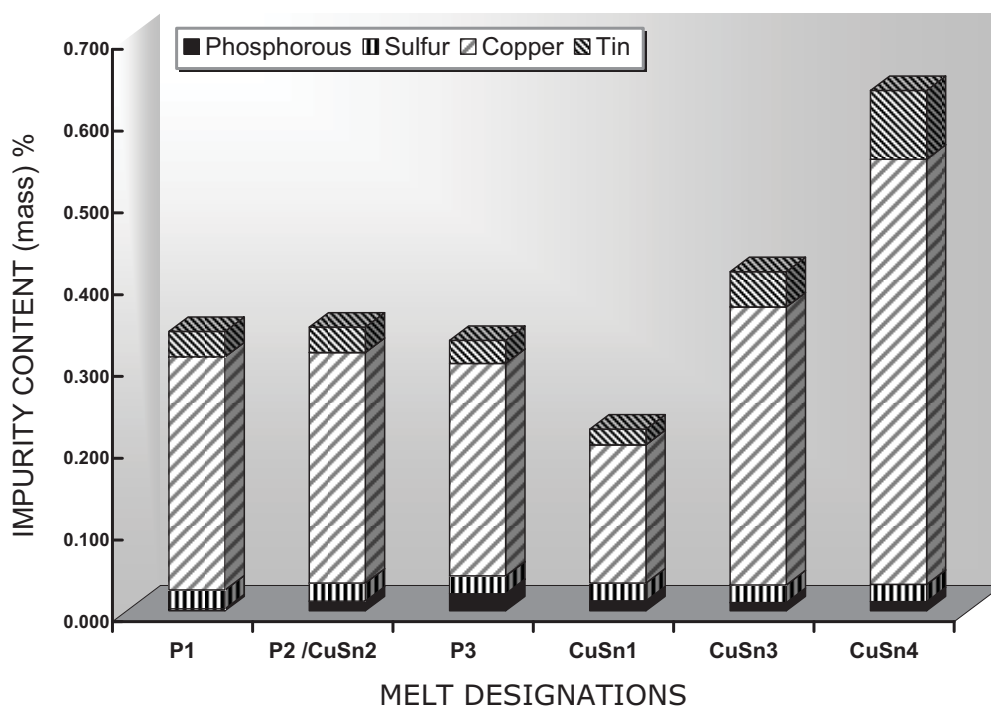


Fig. 16 Level of phosphorous, copper and tin in the base alloy without addition of Vanadium

The experimental alloys used were prepared from high-purity base materials as 70kg vacuum induction melts. The alloy compositions studied are presented in table 4.

The ingots with a cross section of 140 x 140 mm² were cut into pieces with a cross section of 70 x 70 mm². After homogenization at 1100°C for one hour the samples were rolled to 30 mm thickness and air cooled. After reheating to 1100°C and holding for one hour again the samples were then rolled to 21 or 15 mm thickness respectively and air cooled to room temperature. The depth of the decarburization during homogenization and rolling was checked for the bars with the longest soaking time at homogenization temperature and was determined to be around 500µm. At least one millimetre was machined from each surface to ensure that the entire decarburized surface fraction is removed. From the as-rolled bars samples were machined as shown in Fig. 17 for dilatometry, conventional heat treatment and thermomechanical treatment. Cylindrical samples of 5mm diameter and 10 mm height were used for dilatometer tests. The samples longitudinal direction was in the normal direction of the rolled bars made for conventional heat treatment.

Table 4 Chemical analysis of the investigated steels, melts indicated with a star were either supplied from industry (I1 from blast furnace route, and I2 from the electrical route) or produced later to investigate higher phosphorous contents.

Steel	Melt	Concentration (mass%)								
		C	Si	Mn	P	S	Cr	Cu	Sn	V
55SiCr6	P1	0.55	1.56	0.59	0.0023	0.0231	0.69	0.281	0.0304	<0.001
	P2 / CuSn2	0.55	1.57	0.6	0.012	0.0221	0.66	0.274	0.0298	<0.001
	P3	0.56	1.5	0.6	0.0213	0.0216	0.69	0.28	0.0311	<0.001
	CuSn1	0.55	1.37	0.58	0.0114	0.0218	0.68	0.188	0.0202	<0.001
	CuSn3	0.56	1.41	0.65	0.0115	0.0216	0.67	0.372	0.0377	<0.001
	CuSn4	0.56	1.50	0.59	0.0115	0.021	0.67	0.54	0.0538	<0.001
	P4*	0.51	1.43	0.63	0.0297	0.0042	0.68	0.280	0.027	0.0013
	P5*	0.52	1.47	0.61	0.0297	0.0092	0.70	0.018	<0.002	0.001
	I1*	0.55	1.44	0.70	0.0072	0.0056	0.66	0.026	0.002	0.002
	I2*	0.58	1.56	0.79	0.016	0.02	0.76	0.170	0.007	-
55SiCrV6	PV1	0.56	1.47	0.66	0.0025	0.0218	0.69	0.285	0.031	0.163
	PV2/CuSn2	0.56	1.38	0.54	0.0118	0.02	0.68	0.282	0.031	0.165
	PV3	0.55	1.34	0.61	0.021	0.0217	0.67	0.250	0.0240	0.1385
	CuSnV1	0.59	1.27	0.62	0.0123	0.0149	0.66	0.169	0.0193	0.152
	CuSnV3	0.58	1.50	0.64	0.0101	0.0255	0.66	0.340	0.0429	0.149
	CuSnV4	0.57	2.16	0.65	0.0113	0.0224	0.67	0.520	0.084	0.153

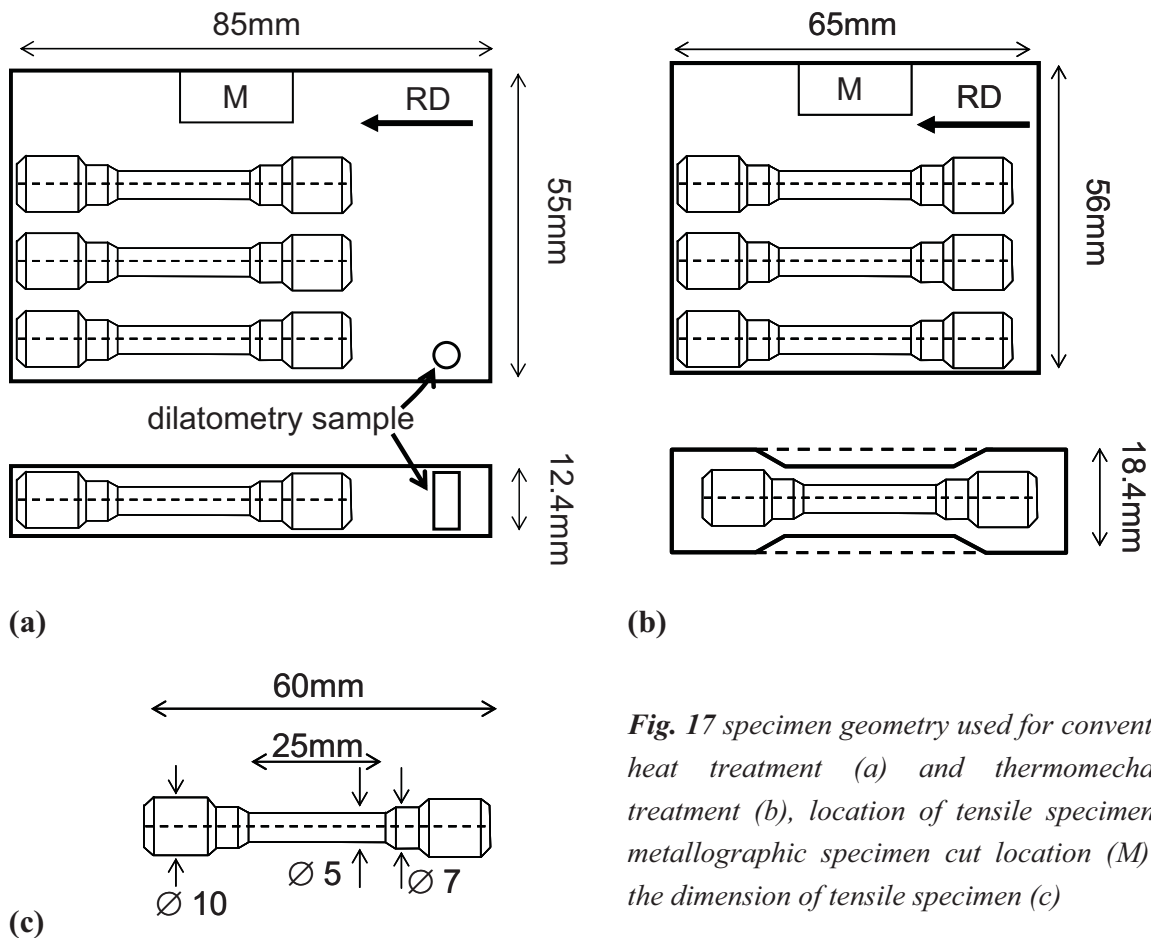


Fig. 17 specimen geometry used for conventional heat treatment (a) and thermomechanical treatment (b), location of tensile specimen and metallographic specimen cut location (M) plus the dimension of tensile specimen (c)

3.3 SAMPLE PROCESSING

The conventional heat treatment (CHT) and the thermomechanical treatment (TMT) were conducted using a large scale 2.5MN hot press at the Max-Planck-Institut für Eisenforschung (Pawelski et al. 1978). The treatments are presented schematically in Fig. 18. The temperature of the specimen was controlled in-situ at half thickness with a thermocouple inserted in a bore ($\varnothing 2\text{mm}$ and 12mm depth). Specimens were heated to austenitization temperature by induction heating. Today, modern production routes and machines for coil spring manufacturing are equipped with induction heating. Due to the short heating cycles the decarburization depth is minimized and rapid heating leads to finer austenitic grain size. The thermomechanically treated samples were air cooled to the deformation temperature T_D , deformed in a plane compression test (Fig. 17b and 18) and quenched after 15 s of quench delay. The quench delay is the time between the end of austenitization (for conventional heat

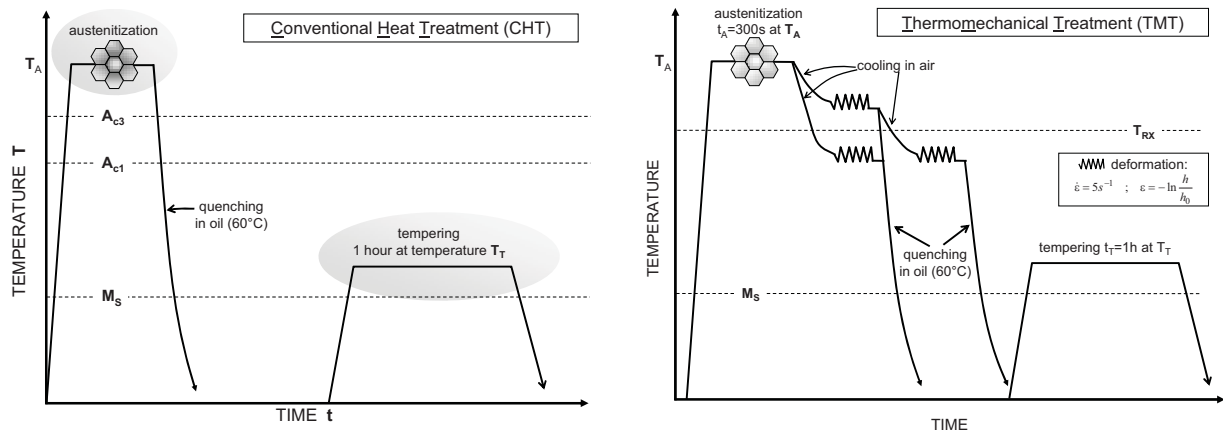


Fig 18 Schematic diagram for conventional heat treatment (left) and for thermomechanical treatment (right). t_A and T_A austenitization time and temperature, ϵ deformation strain, T_D deformation temperature, t_T and T_T tempering time and temperature. The quench delay between the deformation and quenching in oil was always 15s.

treatment) or the end of deformation (for thermomechanical treatment) and the start of quenching. The strain rate was 5 s^{-1} for all the tests and the total nominal logarithmic compressive strain ϵ_c was 0.4 or 0.8. The logarithmic strain is defined as the natural logarithm of initial thickness divided by the final thickness:

$$\epsilon_c = \ln\left(\frac{h_0}{h}\right) \quad (\text{equation 11})$$

The temperature of the oil bath for quenching was 60°C . Tempering was performed in a furnace for 1 hour at temperatures between 250°C and 450°C .

3.4 MECHANICAL TESTING

The mechanical properties were characterized in tensile tests or in rotary bending tests. Tensile testing was performed for each parameter combination, whereas fatigue testing was only performed for selected parameters. Round tensile specimen were machined from the tempered CHT or TMT samples in the RD direction as shown in Fig. 17. Three tensile tests were performed for each CHT or TMT sample at room temperature. The tensile tests were

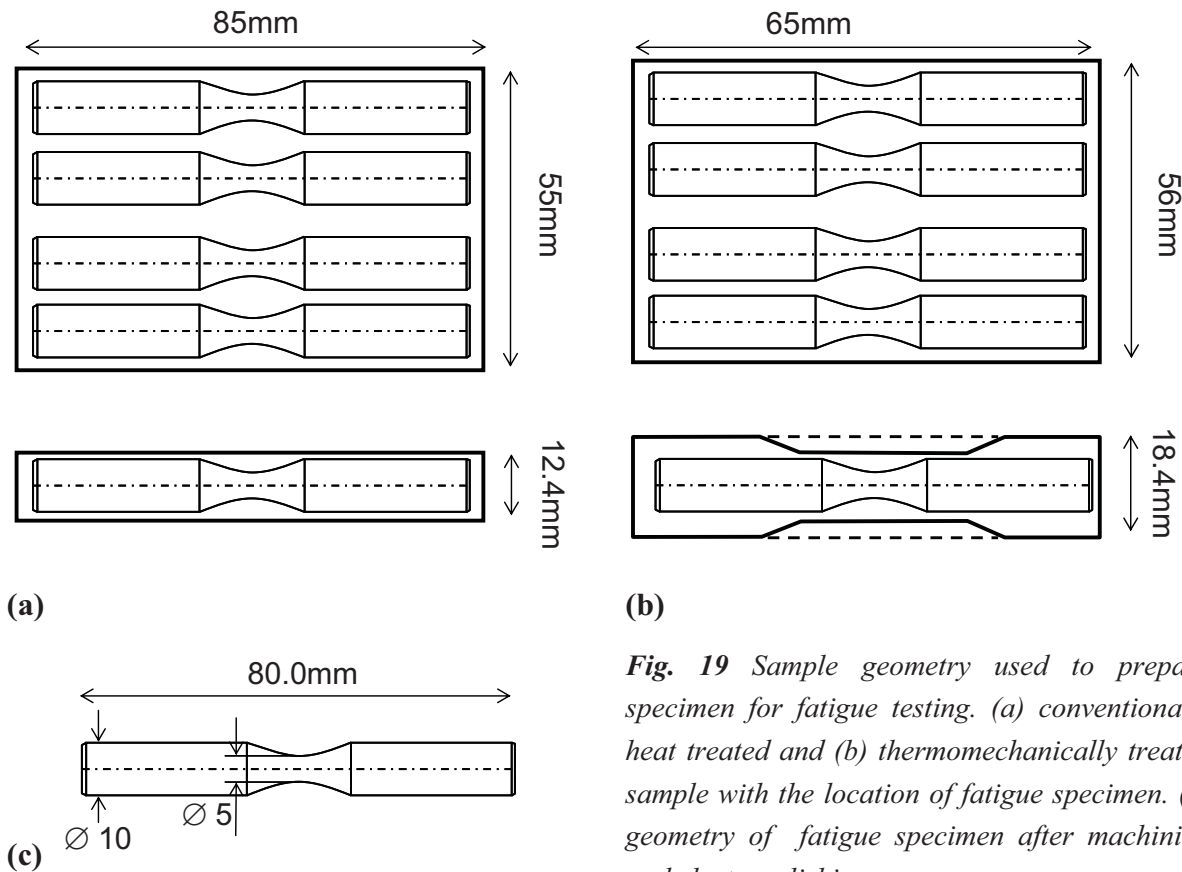


Fig. 19 Sample geometry used to prepare specimen for fatigue testing. (a) conventionally heat treated and (b) thermomechanically treated sample with the location of fatigue specimen. (c) geometry of fatigue specimen after machining and electropolishing.

performed according to the European standard EN 10002, part 2. The results presented in the next section are always average values from three tensile tests together with the standard deviation. For each parameter combination, i.e. composition and process, the tensile properties are presented. Thus the properties 0.2% offset yield strength $R_{p0.2}$, ultimate yield strength R_m , the engineering strain at fracture A_5 , and the reduction of area at fracture Z are directly connected to the parameters applied and indirectly to the composition when comparing the same parameter combination for different melts. Round specimen for rotary bending testing were taken in the longitudinal direction. Fig. 19 presents the specimen geometry for the rotary bending tests. The samples were machined and polished to 5.1 mm in the thinnest cross section. In order to minimize the internal stresses induced by machining, electrochemical polishing was used to remove 50 μm from the surface. The geometry of the samples shown in Fig. 19 is the final geometry after polishing. 12 samples were produced for each parameter combination. The stress level at which three specimens did not fail was considered as the endurance limit. Samples that did not fail were tested at higher (at least 400 MPa) stress levels. In the high cycle region the curves were fitted with the Basquin equation (Dieter 1988).

3.5 MICROSTRUCTURE CHARACTERIZATION

Microstructural observations, optical and scanning electron microscopy were performed on the TD plane after standard sample preparation and etching in nital (1%), in alkaline sodium picrate, or in picric acid.

Optical microscopy was mainly used to determine the austenite grain size and to evaluate austenite grain shape after deformation. For optical microscopy the nital and picric acid with copper chloride additions were used. High resolution scanning electron microscopy (JEOL JSM6500F) was used to characterize the carbide distribution within the martensitic lath and at the prior austenite grain boundaries. Equipped with a field emission gun of special construction, the JSM 6500F microscope allows high beam currents with high spatial resolutions. With a high precision, high-speed digital CCD camera *electron backscatter diffraction* (EBSD) patterns can be detected. These data are transferred to a personal computer and further processed to analyze the microstructure. The fundamentals of electron backscatter pattern technique is described in (Schwartz et al. 2000), in (Zaefferer 2004), and in a review by Dingley (2004). The orientation imaging microscopy of the final microstructure by automated EBSD measurements was applied with the aforementioned electron microscope on tempered specimens. In this work the step size for all orientation measurements was 0.1 μm , if not indicated otherwise. From the measurements inverse pole figure maps were generated and analyzed. Furthermore the grain size and shape was quantitatively calculated. The retained austenite fraction was determined at the same time and the grain boundary character examined.

The Camscan CS4 electron microscope was used for fractography. The fracture surfaces of the tensile and fatigue specimen were investigated after standard cleaning procedures.

4 RESULTS AND DISCUSSION

4.1 DEFINITION OF PARAMETER WINDOW

In this first section of chapter 4 results of the tests performed to define the parameter windows for conventional heat treatment and thermomechanical treatment are presented and discussed. Dilatometry was employed to define the austenitization conditions, to describe the transformation behaviour with and without prior deformation, and as a function of phosphorous, copper and tin bulk concentration.

4.1.1 AUSTENITIZATION

Tests were performed to investigate the influence of the austenitization time and temperature on the hardness and the austenite grain size. The hardness is an indirect measure for the dissolution of carbides during austenitization and the homogeneous distribution of carbon atoms (refer to 2.2.1). Maximum hardness after quenching is obtained, when at the end of austenitization all the carbon is in solid solution. The grain size plays a major role in optimizing the ductility (see 2.2.1).

4.1.1.1 Experiments

For the austenitization tests samples from the melts with the lowest phosphorous concentration, i.e. from P1 and PV1 (see 3.2), were used. Cylindrical dilatometer samples of 5 mm diameter (Fig. 17) were heated to austenitization temperatures between 800 and 1000°C and held between 300 and 3600 s. The heating and cooling rate were 130 K/s. The prior austenite grain size was determined by the linear interception method. For the melt without vanadium, the prior austenite grain boundaries were revealed with chemical etching after quenching and tempering at 450°C. Additionally the thermal etching method described elsewhere (Li 2006) was employed to determine the austenite grain size.

4.1.1.2 Results

Fig. 20 and 21 present the austenite grain sizes for various austenitization conditions. For the alloy without vanadium (Fig. 20) the austenite grain size increases with increasing austenitization temperature and time. The difference between the austenite grain sizes revealed by different methods, i.e. chemical and thermal etching, is not significant (Li 2006).

For the alloy with vanadium it was not possible to reveal the prior austenite grain boundaries with picric acid after tempering at various temperatures for one hour, therefore only the thermal etching method was used to determine the prior austenite grain size. Below 900°C the austenite grains are significantly finer for the steel with the addition of vanadium. The average austenite grain size is below 9µm and is reduced by more than 50% with respect to the alloy without vanadium. At 900°C a bimodal grain size distribution is observed for austenitization times between 900s and 3600s (Fig. 21 and 22). The average diameter of the large grains is still smaller than for the alloy without microalloying austenitized 900 s. Soaking for 300 s leads to a uniform grain size distribution and an average grain size of 7.5 µm. Austenitization times shorter than 900s at 950°C results in a duplex austenite grain size, whereas soaking times of 1800 and 3600 seconds result in uniform grain size distribution. Vanadium addition refines the austenite grain size over the entire tested temperature range. In Fig. 22 the grain size for the microalloyed steel PV1 is shown as a function of time and temperature.

The hardness of as quenched samples of vanadium free steel after austenitization at various temperatures and times are plotted in Fig. 23. Because there is no significant change in hardness with increasing austenitization temperature at 850°C, it is concluded that all the carbides are dissolved at this temperature for the holding times tested. Fig. 24 shows how the hardness and the average austenite grain size are inversely proportional for 54SiCr6.

4.1.1.3 Discussion

The kinetics of grain growth has been calculated for various types of steel with the following equation:

$$d^n = d_0^n + A \cdot t \cdot \exp(-Q_{gg} / RT), \quad (\text{Equation 22})$$

where d is the final grain diameter, d_0 is the initial grain diameter, t is the annealing time, A and n are constants that depend on material composition and processing conditions. Q_{gg} is the apparent activation energy for grain growth, R is the universal gas constant and T is the absolute temperature. The equation is derived considering that the grain boundary velocity is a function of the grain boundary mobility m and the force p acting on the grain boundary. This force is a function of the grain boundary energy and the curvature. For ideal conditions, i.e. for situations where the grain boundary is not affected by solute atoms or precipitates, n would be equal to 2 (Li 2006). But in commercially used alloy systems and for laboratory melts equation 12 describes the results best when n has a higher value. Manohar et al. (1996) have reviewed the values n , A and Q_{gg} for different steels and have shown that n can vary between 2 and 10.

Li (2006) has shown that the grain growth behaviour of the vanadium free steel with low phosphorous content (melt P1) is best described when n is equal to 10. Fig. 25 shows the regression performed for samples held one hour at different austenitization temperatures.

In the microalloyed steel PV1 (see table 4), a bimodal grain size distribution for certain austenitization temperature and times is observed. The dissolution of vanadium carbides can cause abnormal grain growth. The dissolution temperatures for vanadium carbides in a ternary Fe-C-V system with the same vanadium and carbon content as for 54SiCrV6-PV1 are shown in table 5. A mixed microstructure occurs a little below or close to the complete dissolution temperature of the particles. When the austenitization temperature is too low, e.g. 850 °C, both, particle coarsening and particle dissolution are drastically reduced. Therefore, fine grains persist because of the strong pinning forces in that regime. When the temperature is close to the complete dissolution temperature, i.e. 950°C, at least 900 s are required for all the vanadium to be dissolved. The existence of a mixed microstructure at 900 s indicates that vanadium is partly dissolved or that particle coarsening has occurred. It can be concluded that the grain-coarsening temperature is just below or near the particle complete dissolution temperature. However, because the dissolution requires time, kinetics must be considered as well.

The results indicate that for the vanadium free steel temperatures below 900°C have to be selected to obtain austenitic grain sizes around 20µm. If induction heating is used, an even finer austenite grain size can be achieved by short soaking times. In this lower temperature range for austenitization the dissolution of carbon takes place within the first 900 s. The hardness does not increase significantly with increasing time. Significant austenite grain

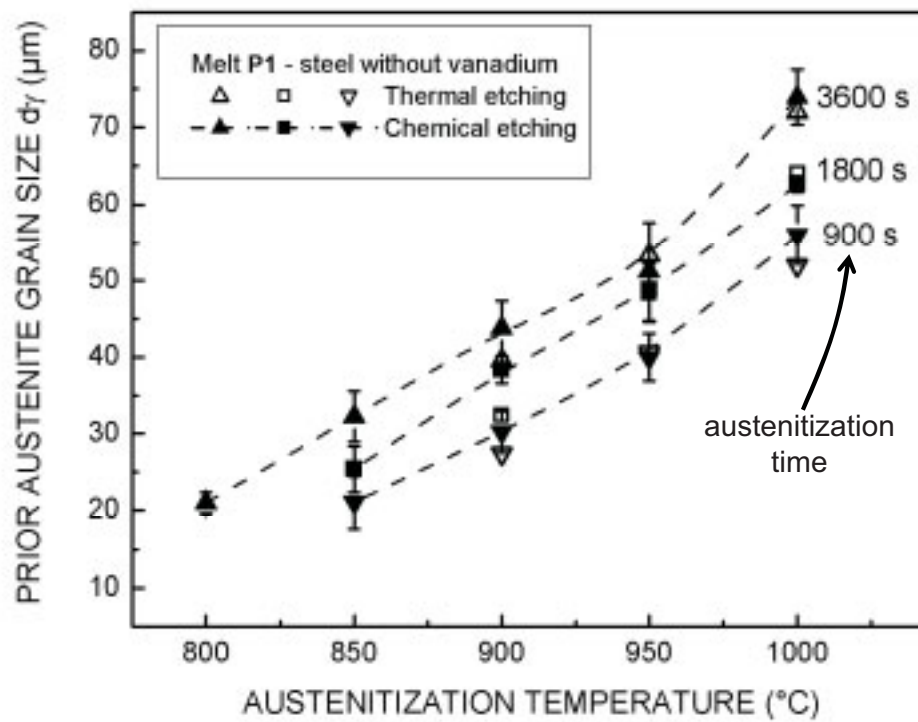


Fig. 20 Prior austenite grain size of steel without vanadium as a function of austenitization time and temperature

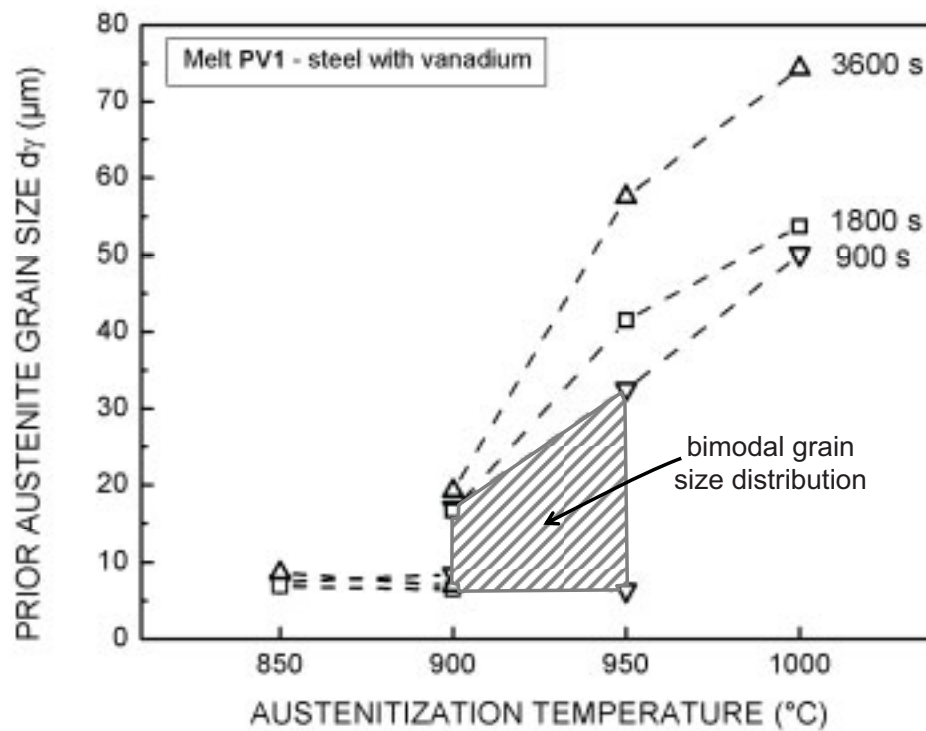


Fig. 21 Prior austenite grain size of steel with vanadium as a function of austenitization time and temperature.

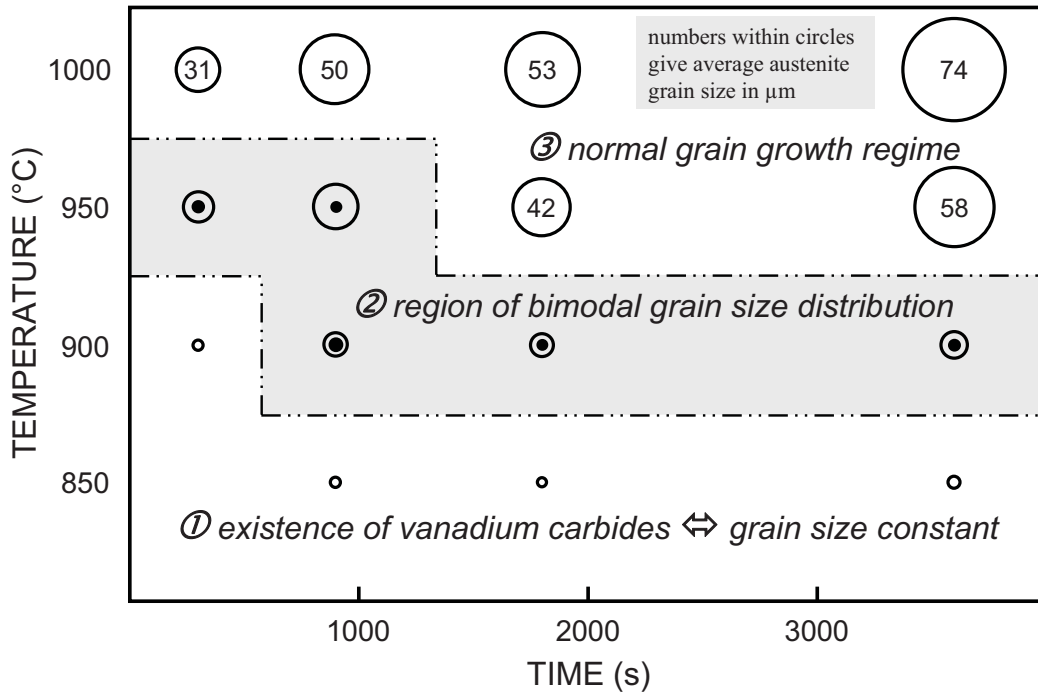


Fig. 22 The resultant austenite grain size (in μm) of microalloyed steel 54SiCrV6 for various austenitization conditions. Outer circle diameter represents the average diameter of larger grains while the average of smaller grain is represented by the inner circle.

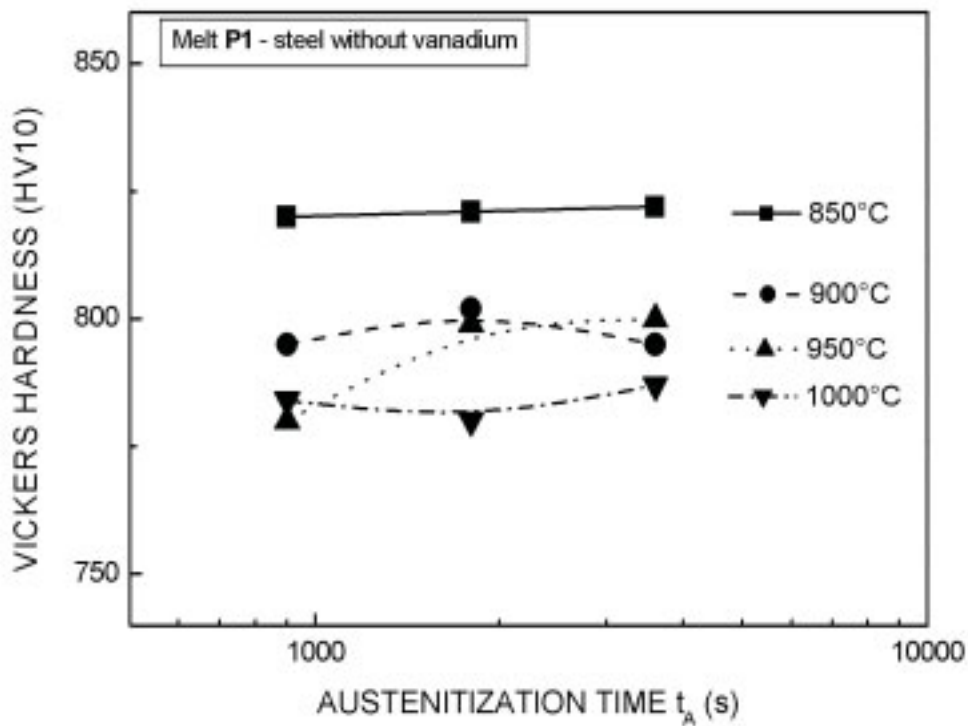


Fig. 23 Vickers hardness of as quenched samples of 54SiCr6 after austenitization at temperatures between 850 and 1000°C and austenitization times below 1 hour.

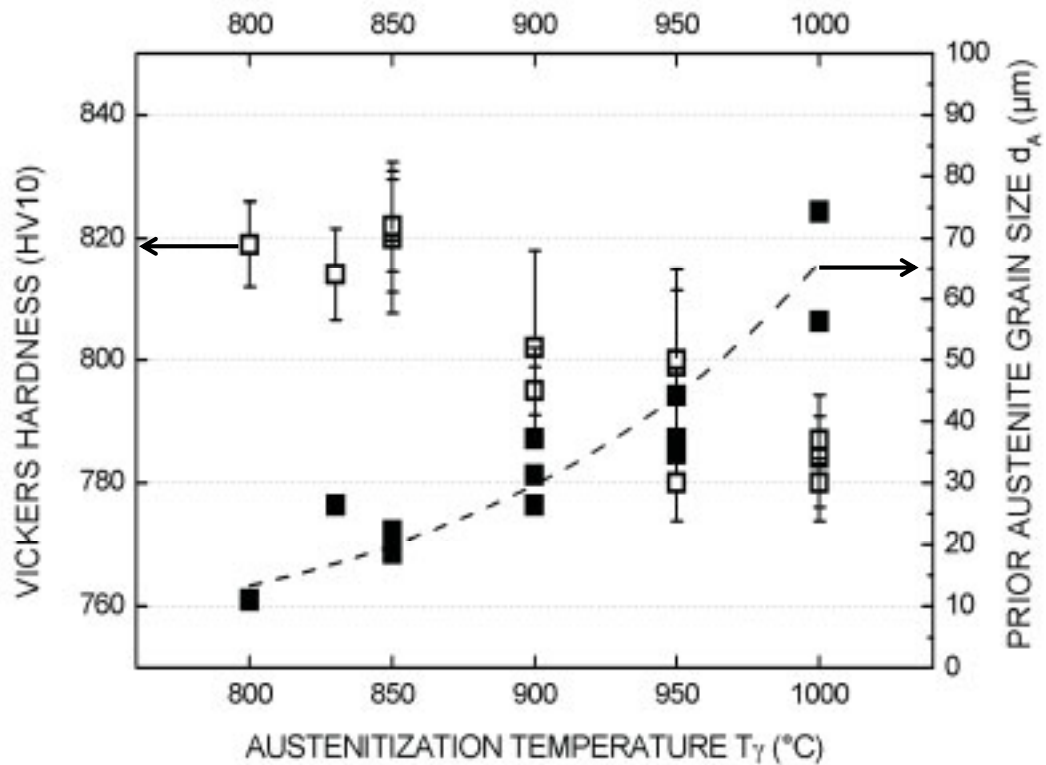


Fig. 24 Vickers hardness and prior austenite mean grain diameter of as quenched samples of 54SiCr6 after austenitization at temperatures between 800 and 1000°C and austenitization times below 1 hour.

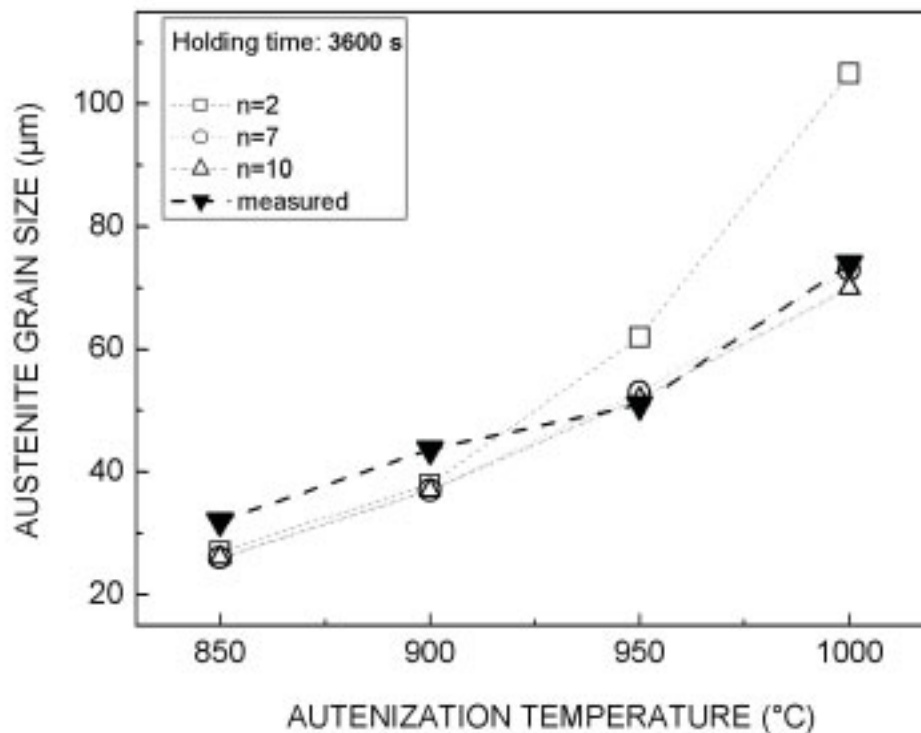


Fig. 25 Comparison of grain sizes between calculated values and experimental values for 54SiCr6, melt P1. Austenitization time $t_A=3600$ s.

refinement can be obtained by addition of vanadium. The advantage is that no change of production and process is then necessary. Applying short austenitization times at or below 900°C results in a uniform grain size distribution (Fig. 22). The average austenite grain size for the microalloyed system is less than half of the vanadium free steel.

Table 5 Temperature dependence of (equilibrium) solubility product of vanadium carbide in austenite (Li 2006).

Equation number	Carbide	Equations (T in K, concentration in mass %)	Complete dissolution temperature, °C
13	VC	$\lg[V] \times [C] = -9500/T + 6.72$	951
14	VC	$\lg[V] \times [C]^{0.75} = -6560/T + 4.45$	936

4.1.2 TIME-TEMPERATURE-TRANSFORMATION

The transformation characteristics of austenite to martensite are important for the definition of the cooling conditions to obtain a fully martensitic microstructure and to avoid the formation of other phases. Thus the critical cooling time to obtain 100% martensite has to be determined. Additionally, the effect of deformation and impurity elements phosphorous, copper and tin will be investigated.

4.1.2.1 Experiments

Cylindrical dilatometer samples of 5 mm diameter from the melts P1 and PV1 were heated to 900°C and held for 300 s. The heating rate was 130 K/s. The cooling rate was varied between 10 to 100 K/s to generate the Time-Temperature-Transformation diagram and to detect the critical cooling time to obtain 100% martensite. For the base alloy without vanadium, melts with different impurity element levels were austenitized as described above and quenched with 10 K/s. After austenitizing for five minutes at 900°C a conventional heat treatment sample as described in chapter 3 was quenched in an oil bath (bath temperature 60°C) to compare the cooling conditions of the large scale samples (sample of 12 mm thickness for conventional heat treatment, see Fig. 17a) with the small scale samples (dilatometer sample of 5 mm diameter).

Samples from all melts of 54SiCr6 were austenitized 300 s at 900°C and cooled to room temperature with a $t_{8/5}$ of 10 s. These tests were employed to ascertain the effect of impurity element content on the martensite start temperature. The $t_{8/5}$ time is the time needed to cool the sample or part from 800°C to 500°C. The evolution of temperature with time is simulated with an exponential function that describes best the cooling conditions observed in practice.

To detect any effect of deformation on the M_S temperature, dilatometer samples from the melt P1 were further subjected to deformation prior to quenching. The deformation strain was 0.4, the strain rate 5 s^{-1} . After deformation the samples were held 15 s (we define this time as quench delay) at the deformation temperature prior to quenching. Deformations were carried out between 750 and 850°C. The microstructure was observed by optical microscopy after etching with nital (1%). The hardness was determined after quenching.

4.1.2.2 Results

Fig. 26 shows the TTT diagram for the melt P1. The martensite start temperature is 276°C for the steel without vanadium and 284°C for the steel with vanadium. For both steels (with and without vanadium), $t_{8/5}$ times smaller than 30 s lead to a fully martensitic microstructure after quenching. In Fig. 26 the cooling curve of a sample used later for conventional heart treatment is presented as well. The sample had a thickness of 12.4 mm and was quenched in oil that was held at 60°C. The temperature was measured at half thickness. The temperature of this sample falls faster than that of dilatometer samples with a $t_{8/5}$ of 10 s.

No change of martensite start temperature M_S was observed with increasing copper and tin content. With increasing phosphorous concentration the M_S reduces to below 260°C (Fig. 27). Deformation of austenite prior to quenching reduces the M_S as well (Fig. 28). Samples deformed between 850 and 775°C have mainly equiaxial austenite grains prior to quenching, while the sample deformed at 750°C exhibits elongated pan-cake grains.

4.1.2.3 Discussion

The obtained martensite start temperature M_S for 54SiCr6 is close to the predictions of the formulas proposed by Steven and Kunitake (Table 6, Ohtani 1992). None of the formulae takes the effect of phosphorous, tin and vanadium into account. For the alloy investigated

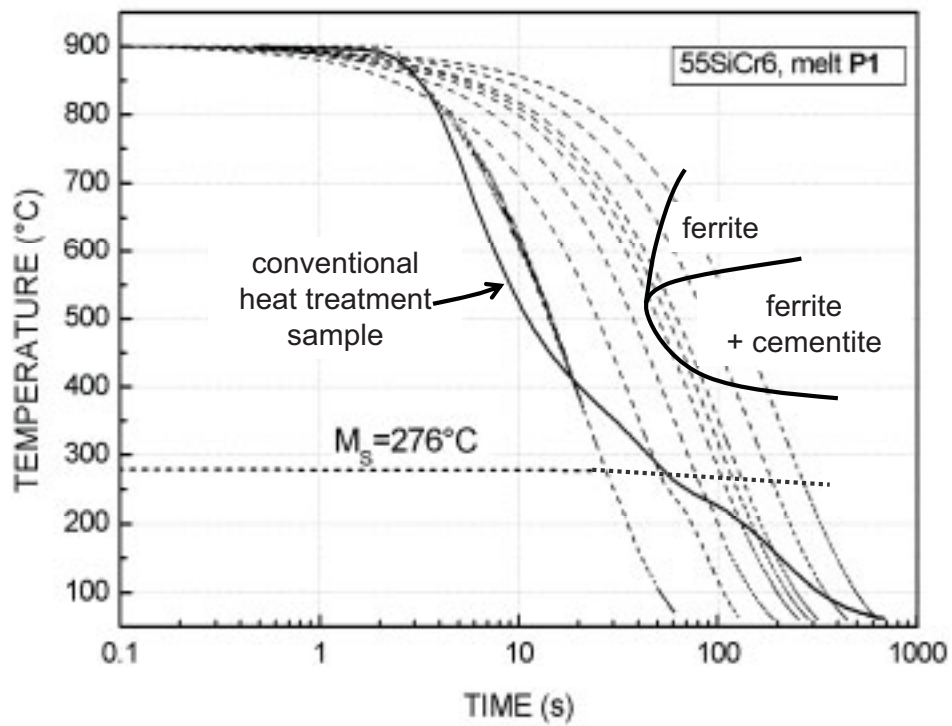


Fig. 26 Time-Temperature-Transformation Diagram for 54SiCr6-P1, and cooling curve for a conventional heat treated sample with a thickness of 12 mm.

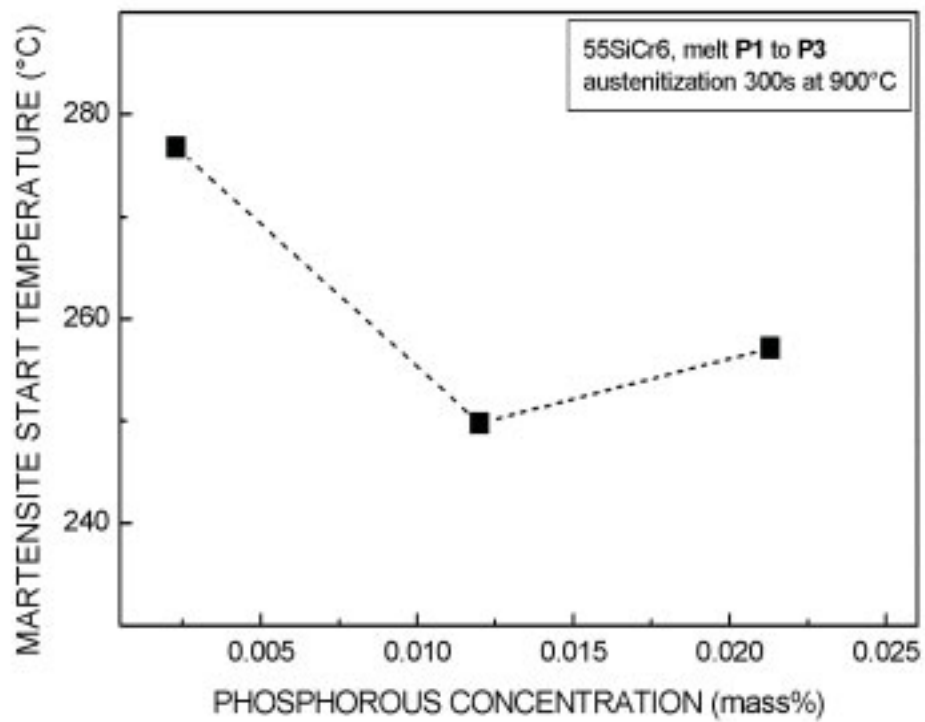


Fig. 27 Effect of phosphorous on martensite start temperature, austenitization 300 s at 900°C followed by cooling with a $t_{8/5}$ of 10s.

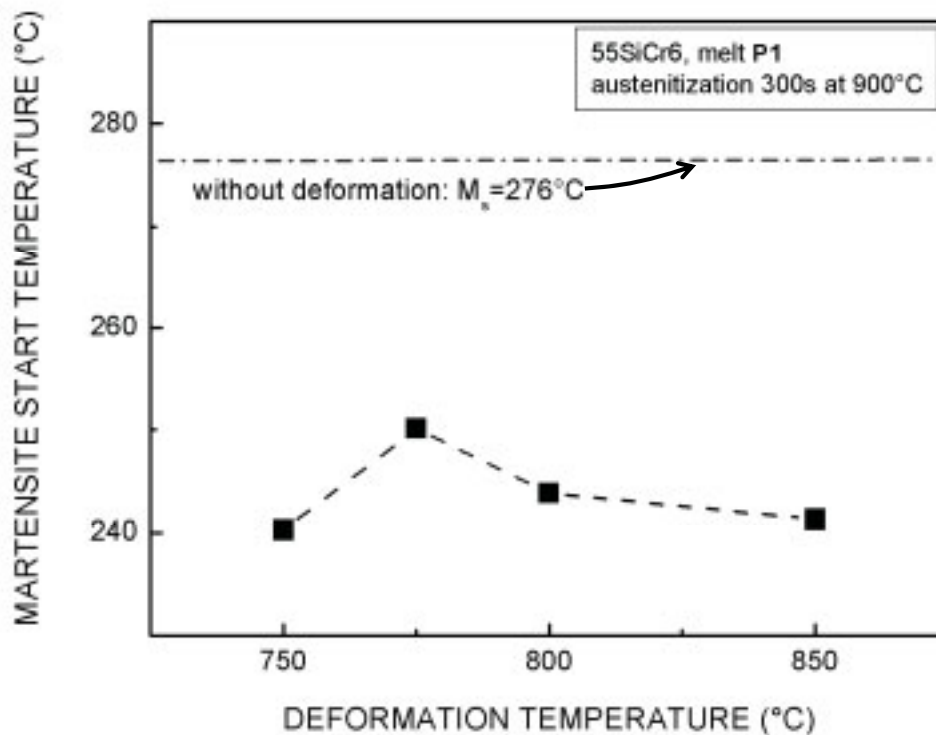


Fig. 28 Effect of deformation temperature on martensite start temperature, deformation strain $\varphi=0.4$, strain rate $d\varphi/dt=5\text{ s}^{-1}$, quench delay $t_D=15\text{ s}$.

here, the second formula is more reasonable, because the effect of the main alloying elements and copper is taken into account. Using Kunitake's formula to estimate the effect of copper on the martensite start temperature M_S for the composition range investigated in this study, we see that its effects can be neglected. If the copper content is increased by 0.36 mass % the M_S temperature decreases 2 K. This change is not significant and therefore it could not be detected experimentally.

Table 6 Empirical formulae for calculating the martensite start temperature M_S from the chemical composition and calculated M_S for 54SiCr6-P1

Equation number	Formula	M_S (°C)	Author & Reference
15	$M_S = -474C - 33Mn - 17Ni - 17Cr - 21Mo$	268	Steven (Ohtani 1992)
16	$M_S = -353C - 22.0Si - 24.3Mn - 7.7Cu - 17.3Ni - 17.7Cr - 25.8Mo$	267	Kunitake (Ohtani 1992)

Deformation of austenite prior to quenching lowers the M_S temperature. The reduction is smallest for deformation at 775°C, i.e. at this temperature the highest M_S temperature is observed after prior deformation of the austenite. Below 775°C the final microstructure after quenching constitutes of elongated prior austenitic grains and no recrystallization has taken place between the end of deformation and quenching. Above 775°C the microstructure consists of equiaxial prior austenite grains, thus recrystallization must have taken place after or during deformation. Both austenite modifications, the recrystallized (with a reduced grain size) and the work-hardened, exhibit approximately the same M_S temperature ($M_S \approx 240$ K, 36K below that without prior deformation). Peters (1996) demonstrated for 50CrV4 (Fe-0.5C-0.3Si-1.0Mn-1.1Cr all in mass %) that deformation of austenite lowers the M_S temperature. In his study, the austenitization temperature for deformed austenite was 920°C, whereas samples without deformation were austenitized at 840°C. The recrystallized austenite modification resulted in 5 K reduction of M_S , the work-hardened modification in 15 K. The dependence of the M_S temperature on the reduction of austenite, on the amount of work-hardening has been reported (Maki 1993) and is ascribed to mechanical stabilization of austenite.

The increased grain boundary area after recrystallization reduces the M_S temperature. The work-hardened austenite after deformation at 750°C stabilizes the austenite and hence suppresses the M_S temperature.

4.1.3 RECRYSTALLIZATION BEHAVIOUR

Through austenite deformation and temperature control various microstructures (Fig. 12) can be generated. Compared to a conventionally heat treated sample without austenite deformation, a thermomechanically treated sample, with a recrystallized austenite modification, exhibits an increased grain boundary area and different concentration of impurities at grain boundaries. If the austenite is work-hardened the concentration of defects in the austenite matrix is increased. Additionally the grain boundary area increases due to grain elongation (Kozasu 1992). These two microstructures could lead to different mechanical properties. In order to define different thermomechanical routes and to explore the aforementioned different effects on the final properties of the tempered martensite, the recrystallization temperature for specific deformation conditions, i.e. constant strain, constant strain rate at different temperatures for fixed holding times, need to be determined.

Special consideration is paid to the effect of the microalloying element vanadium on the recrystallization behaviour during and after austenite deformation, i.e. the role of vanadium on the dynamic and static recrystallization.

4.1.3.1 Experiments

Rectangular samples as described in 3.2 were subjected to austenitization in the hot-deformation simulator, deformed at different temperatures, and quenched. Samples of the two base alloys from the melts with the lowest phosphorous content (P1 and PV1) were used for these tests. The austenitization temperature was 950°C and the soaking time 300 s. After austenitization the samples were cooled in air to the deformation temperature, deformed, and then held 15 s at air before quenching in the oil bath. The compressive strain was $\varepsilon_c=0.4$, the strain rate $d\varepsilon/dt=5\text{ s}^{-1}$. The strain of 0.4 was taken according to the results reported in the literature (Hensger and Bernstein 1984, Streißlberger 1984). Deformation temperatures tested were 750, 800, 850, and 900°C. The cooling in air for the sample geometry used corresponds approximately to a cooling rate of 2.5 K s^{-1} at half thickness of the samples. After quenching the microstructure of the samples were examined by optical microscopy after etching with nital and picric acid for revealing the prior austenite grain boundaries. Samples that exhibit an equiaxial austenite grain shape were classified as recrystallized, while samples with a pan-cake shape were classified as non-recrystallized or work-hardened.

Dilatometry experiments were performed to analyse the static recrystallization behaviour of the steel with and without vanadium. As part of our studies, the critical strains ε_c for dynamic recrystallization of 54SiCr6 spring steel with and without vanadium have been determined based on changes in the strain hardening rate as a function of the flow stress (Li 2006). Either vanadium in solution at high austenitization temperature or vanadium carbides remaining undissolved at low austenitization temperature have little effect on the critical strain of DRX in the present steels. To ascertain the effect of vanadium on static recrystallization, interrupted compression tests were carried out (Fernandez et al. 1999). In this test, the material is deformed at the temperature of interest, and then held for a time t before a second deformation is applied. Assessment of the amount of softening is carried out by the analysis of the initial loading and reloading curve. In this work the 2% offset method as described in Fernandez et al. (1999) is used. Specimens were austenitized at 1000°C to dissolve all the carbides. In order to obtain a similar austenite grain sizes prior to deformation, different holding times were selected for 54SiCr6-P1 and 54SiCrV6-PV1. The soaking time was 300 s for 54SiCr6 and

900 s for 54SiCrV6. The austenite grain sizes determined after austenitization at 1000 °C are 51.9 μm for 54SiCr6 and 50.1 μm for 54SiCrV6, respectively. At first, the deformation temperature was varied between 750°C and 950°C and the holding time between the two deformations was kept constant (15s). In a second step the holding time was varied (1-100000s) while the deformation temperature was 850°C. The deformation strain was 0.2 for all the interrupted compression tests and is below the critical strain for dynamic recrystallization (Li 2006b).

4.1.3.2 Results

Fig. 29 shows flow curves for 54SiCr6 and 54SiCrV6 at deformation temperatures between 750 and 900°C measured in plane-strain compression with the hot-deformation simulator. The microalloyed steel with vanadium exhibits slightly higher flow stresses at deformation temperatures below 900°C. For the steel without vanadium only the sample deformed at 750°C showed a pan-cake austenite grain shape (Fig. 30). For the melt with vanadium a pan-cake structure was observed at 800°C as well. For the deformation conditions used, the vanadium addition increases the temperature range within which the austenite is not recrystallized prior to quenching. After recrystallization the average prior austenite grain size of samples without vanadium (i.e. from melt P1) is between ASTM 7 and ASTM 8 (31.2 to 22.1 μm average prior austenite grain diameter), for the vanadium microalloyed samples ASTM 10 (11.0 μm) was observed. Fig. 31 shows the influence of the microalloying element vanadium upon the softening after deformation between 750 and 950°C. For all deformation temperatures tested addition of vanadium slows the static softening kinetics.

The time between two deformation steps in Fig. 31 is 15 s and corresponds to the quench delay used for the conventional and thermomechanical tests in the hot deformation simulator, which will be described later. At all deformation temperatures tested the fractional softening of the microalloyed steel is at least 15 % less. Fig. 32 shows the static softening kinetics after austenite deformation at 850°C. Immediately after deformation at 850°C the softening is equivalent for both alloys. The softening of 54SiCr6 takes place a few seconds after deformation. After 100 s the fractional softening is over 90%. The addition of vanadium retards the softening after deformation significantly. After 10 s already an effect of the microalloying is observed. The difference enlarges until 100 s holding time and stays for

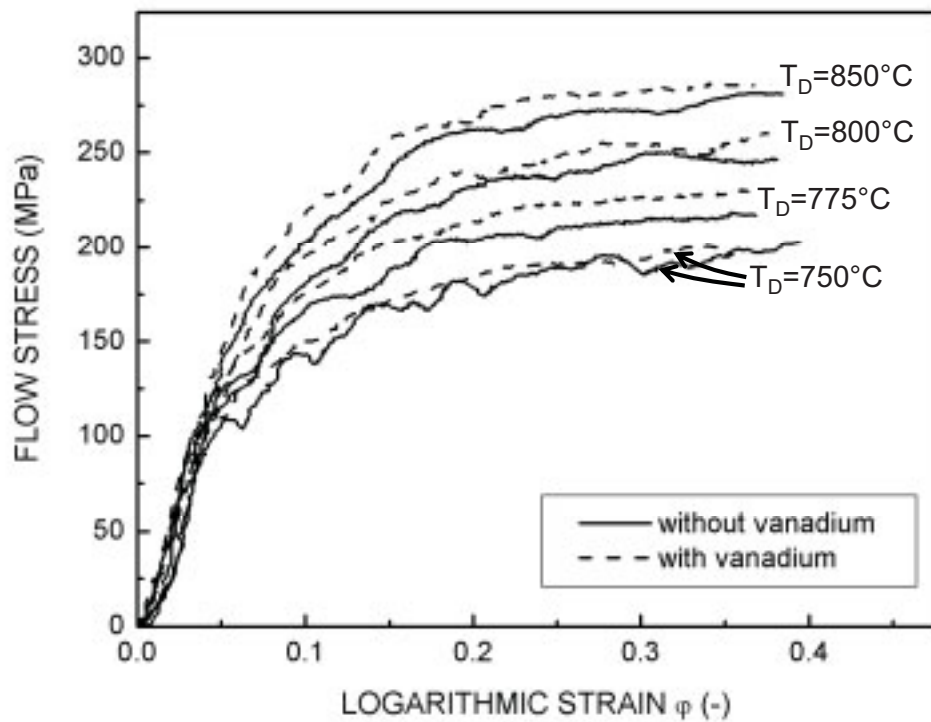


Fig. 29 Hot deformation flow curves for 54SiCr6-P1 and 54SiCrV6-PV1. Treatment: 300s at 950°C, followed by air cooling and deformation with a strain of 0.4 and strain rate of 5 s^{-1} at T_D .

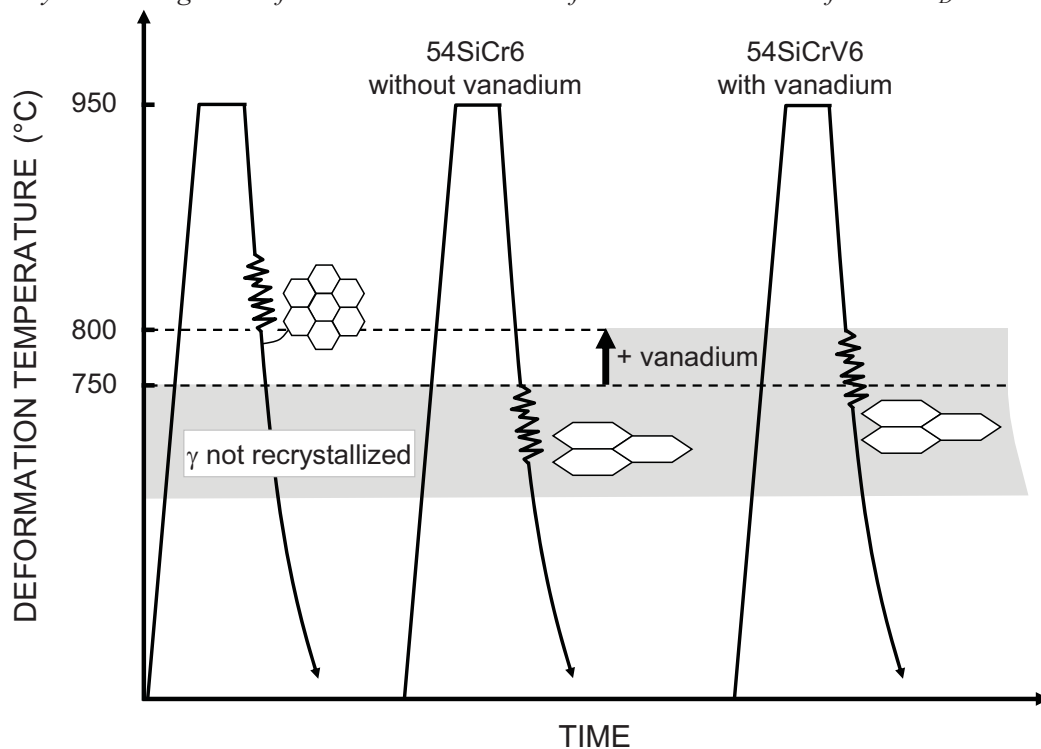


Fig. 30 Recrystallization temperature increase by vanadium addition. Flat compression test with TMT samples: 5min austenitization at 950°C, air cooling to deformation temperature T_D , deformation strain 0.4 with a strain rate of 5 s^{-1} , 15 s cooling in air, quenching in oil bath.

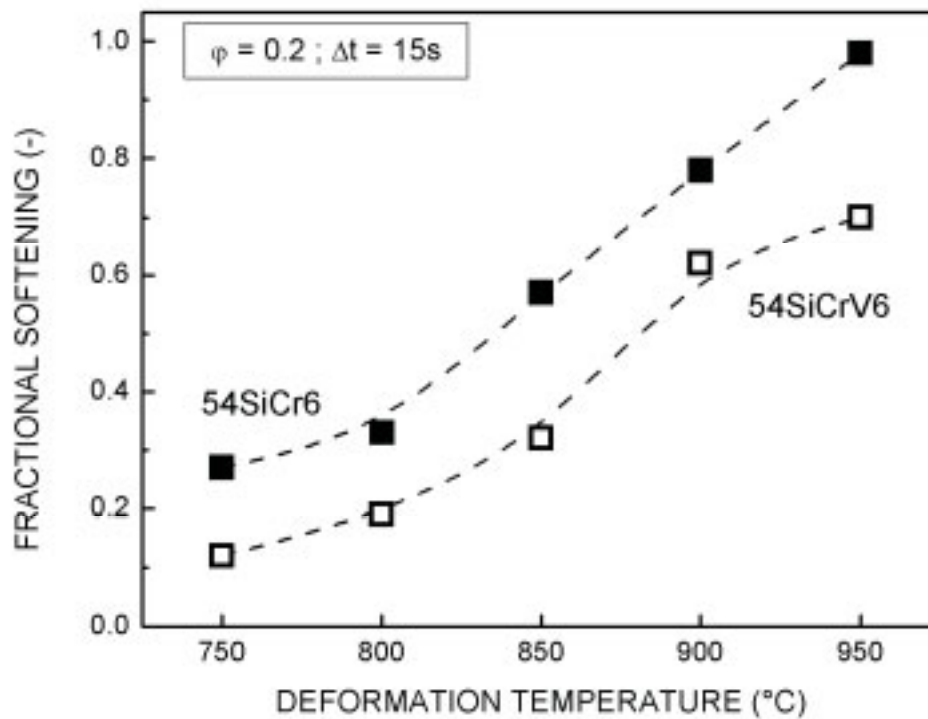


Fig. 31 Effect of vanadium on softening after deformation at different temperatures. Interrupted compression testing with cylindrical samples in a dilatometer. Austenitization: 300s at 1000°C for 54SiCr6 and 900s at 1000°C for 54SiCrV6.

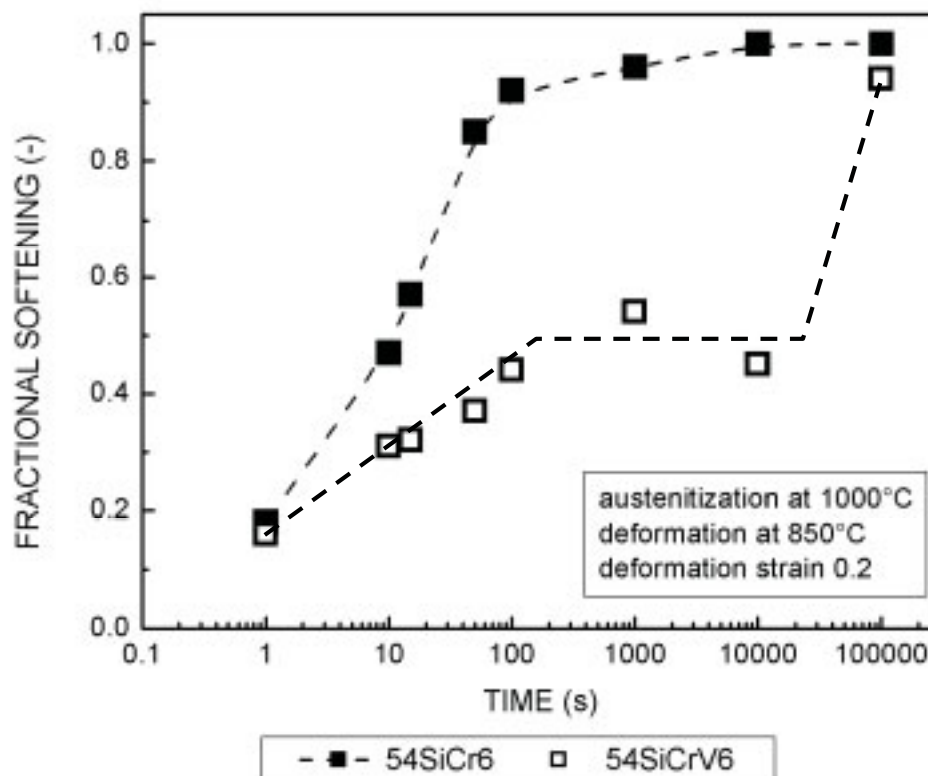


Fig. 32 Effect of vanadium on softening after deformation at 850°C.

times below 100000 s almost constant. The fractional softening increases slowly until 40% and remains constant around this value. The complete softening takes place between 10^4 and 10^5 s.

4.1.3.3 Discussion

For 54SiCr6 without vanadium the recrystallization of austenite results in austenite grain refinement. The average austenite grain diameter of P1 after conventional heat treatment at the same austenitization temperature is 37.5 μm . Thus a recrystallization at the conditions tested here reduces the grain diameter of the vanadium free steel by approximately 25 %. Recrystallization after austenite deformation leads to an average austenite diameter of 11.0 μm and the grain size distribution is uniform. For the tested deformation conditions and the constant quench delay the recrystallization temperature could be increased by 50°C through microalloying with vanadium.

Investigations of Li (2006b) showed that either vanadium in solution at high austenitization temperature or vanadium carbides remaining undissolved at low austenitization temperature have little effect on the kinetics of dynamic recrystallization in the present steels. The critical strains ε_c for dynamic recrystallization (DRX) in spring steel 54SiCr6 with and without vanadium have been determined based on changes in the strain hardening rate as a function of the flow stress. The ratio of critical strain ε_c to peak strain ε_p is 0.56 and the ratio of critical stress σ_c to peak stress σ_p is 0.94 for both steels at all the deformation conditions. The peak strain does not increase with decreasing deformation temperature or with increasing strain rate, which might result from the segregation of substitutional elements. The activation energy Q_{def} was derived as 537 kJ/mol for the steel with vanadium and 554 kJ/mol for the steel without vanadium, respectively. For mixed microstructures, the critical strain ε_c depends on the size of the smaller grains while for the peak strain ε_p the size of the large grains also play an important role. Either vanadium in solution at high austenitization temperature or vanadium carbides remaining undissolved at low austenitization temperature have little effect on the kinetics of dynamic recrystallization in the present steels.

However, vanadium microalloying retards the static recrystallization for deformation temperatures between 750 and 950°C (see Fig. 31 and 32). The austenitization of both steels, with and without vanadium was carried out at 1000°C to dissolve all the carbides. The dissolution temperatures for the vanadium carbide calculated according to the formulas listed in table 5 are 936 and 951°C. Thus, before the deformation all the vanadium carbides are

completely dissolved. The grain size study support these calculations as well. Uniform grain size distribution was observed after 900 s austenitization at 1000°C. According to the grain growth experiments and the solubility equations no vanadium carbides should be present after the austenitization at this temperature. It can therefore be concluded that vanadium carbides are formed after and with less probability during deformation and retard the recrystallization as reported by Ayada (1998).

4.1.4 CONCLUSION

The time transformation behaviour of the steel under investigation has been studied. Quenching of samples defined for conventional and thermomechanical treatment can be performed in an oil bath avoiding diffusional transformations. From the results obtained from dilatometry experiments the austenitization parameters were defined to be five minutes at 900°C. It was shown that addition of 0.163 mass % vanadium retards the grain growth for this austenitization condition, i.e. for the selected time and temperature. Furthermore, the austenite recrystallization temperature T_{RX} was determined using hot deformation simulator and dilatometry experiments. For deformation with a logarithmic strain of 0.4, strain rate of 5 s⁻¹ and 15 s quench delay a pan-cake austenite grain structure was only observed after deformation at 750°C. Addition of vanadium shifts the recrystallization temperature. A pan-caked grain structure can be obtained after deformation at 800°C and below. Vanadium retards the static recrystallization after the deformation and extends the process parameter windows for quench delay and for a deformation leading to a pan-cake structure.

4.2 CONVENTIONAL HEAT TREATMENT

4.2.1 OBJECTIVE

The main objective of investigating conventional heat treatment parameters was to ascertain the concentration limits for phosphorous, copper and tin below which acceptable ductility values for specified strength levels are obtained within industrial boundary conditions. Hence, the definition of heat treatment parameters is guided by the industrial practice. In this chapter we first describe for the base alloys 54SiCr6 (P1) the dependence of tensile properties and microstructure as a function of tempering temperature. Then the changes due to vanadium addition are presented thereafter. Finally, the influence of phosphorous content and copper and tin addition upon the tensile properties is presented.

In this chapter we start from the “simplest” system with low impurity concentration and present its mechanical properties together with the microstructural changes as a function of tempering temperature. Step by step then the effect of vanadium microalloying and the effect of impurity elements are presented.

On the one side the mechanical property values of conventionally heat treated sample with low impurity content serve as reference to quantify the effect of microalloying and that of impurities and on the other hand the effect of different thermomechanical routes can be evaluated for different impurity concentrations for the steels with and without microalloying.

4.2.2 EXPERIMENTAL

Up to the conventional heat treatment all the samples were subjected to the same processing, i.e. same rolling and annealing conditions up to the final sample preparation for heat treatment experiments. The chemical composition was different (see table 4). Industrially, silicon chromium spring steels for coil spring production are austenitized around 900°C. Increasing the austenitization temperature would on the one side lead to large austenite grains that are detrimental for the ductility and toughness and on the other side to excessive decarburization. After austenitization the annealed bars or wires are coiled before quenching in oil. Lowering the austenitization temperature would shorten the time window for coiling and bears the risk that the austenite partially transforms before quenching. Thus all the conventionally heat

treated samples were austenitized 5 minutes at 900°C, hold in air for 15 seconds before quenching in the oil bath. The quench delay, the time between the end of austenitization and quenching, was selected according to the time needed to coil the spring prior to quenching. The tempering temperature was varied for all the chemical compositions to explore the concentration levels for different strength levels. The tempering time was one hour. The tensile properties of quenched and tempered martensitic specimen together with the microstructure were investigated according to the procedures described in 3.4.

4.2.3 RESULTS

4.2.3.1 Tempering temperature

Fig. 33 presents strength values observed for composition P1 (see table 4) after conventional heat treatment. The ultimate tensile strength of melt P1 decreases gradually with increasing tempering temperature (Fig. 33). Below 350°C the 0.2% offset yield strength is almost constant, while decreasing rapidly above 350°C. Fig. 34 shows the ductility values measured in the tensile test for different tempering temperatures. A lower tempering temperature results in higher tensile strength values and lower ductility values, except at 350°C, where a minimum in ductility is observed. The reduction of area falls with decreasing tempering temperature to a minimum value at 350°C and then rises to values between 15 and 17 percent. The minimum in ductility observed for the steel with the lowest phosphorous concentration (P1) at 350°C is concurrent with an increase in the fraction of intergranular fracture. Samples below and above $T_T=350^\circ\text{C}$ exhibit significantly more ductile fracture. Fig. 35 presents the amount of intergranular fracture observed for P1 samples tempered at different temperatures. The highest fraction of intergranular fracture is observed after tempering at 350°C. Furthermore cracks separation of adjacent grain boundaries is observed (Fig. 36 c).

Fig. 37 and 38 show the carbide morphology at prior austenite grain boundaries and within its vicinity in the matrix. After tempering at 250°C very thin white films are found at the prior austenite grain boundary and at lath boundaries. Additionally not etched flat areas and deeply etched areas are visible. The deeply etched areas are always found close to the prior austenite grain boundaries and contain very small round carbides below 10nm. Up to 350°C carbide films exist at prior austenite grain boundaries and at lath boundaries. Beside carbide films a

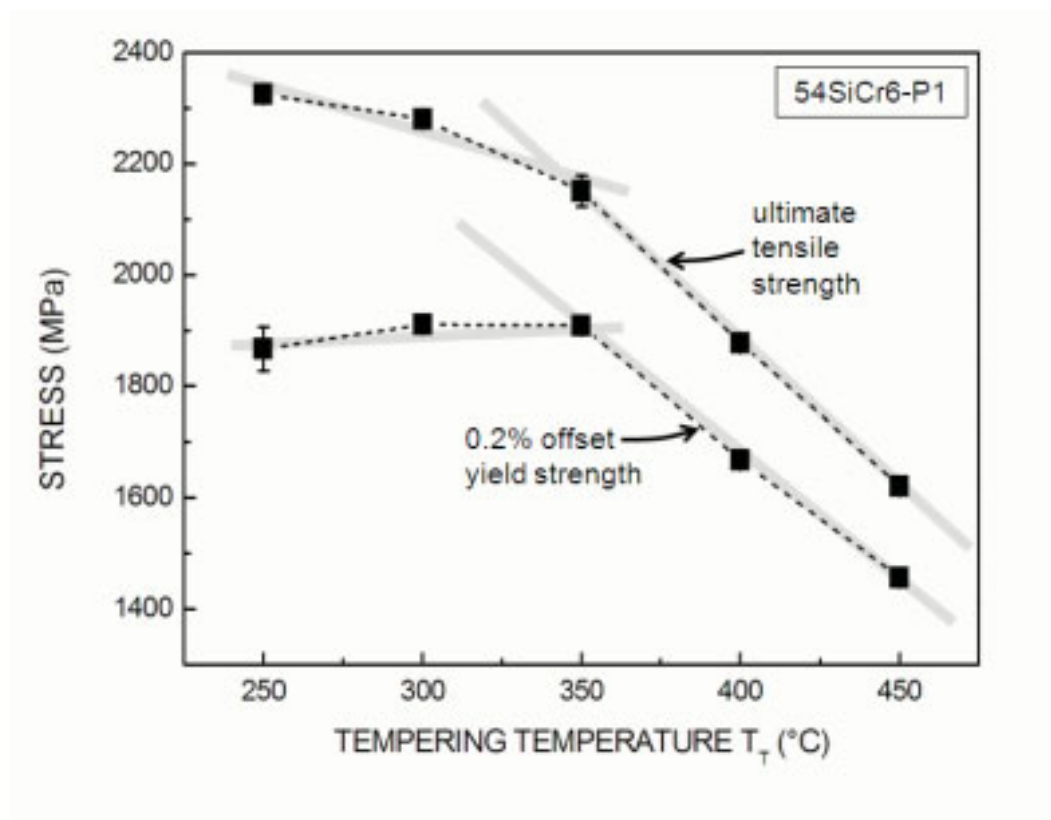


Fig. 33 Tensile strength values of conventionally heat treated samples of the alloy with low phosphorous bulk concentration. Melt P1, composition see table 1.

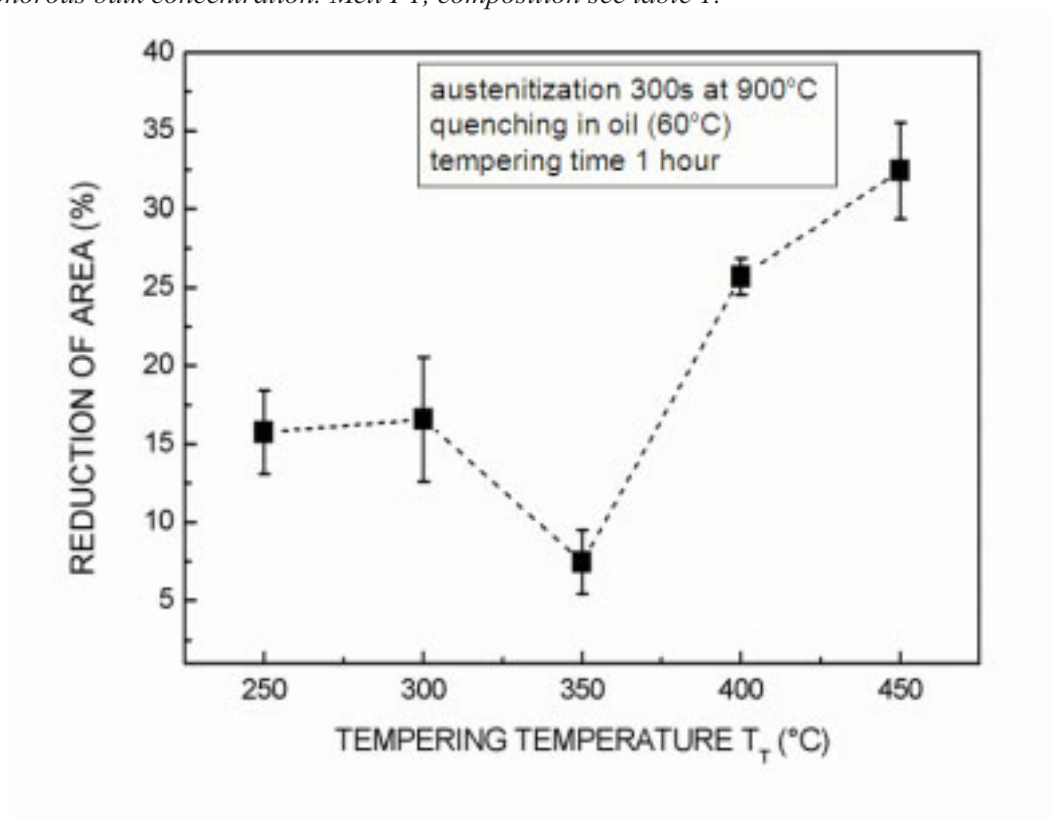


Fig. 34 Reduction of area values of conventionally heat treated samples of the alloy with low phosphorous bulk concentration. Melt P1, composition see table 4.

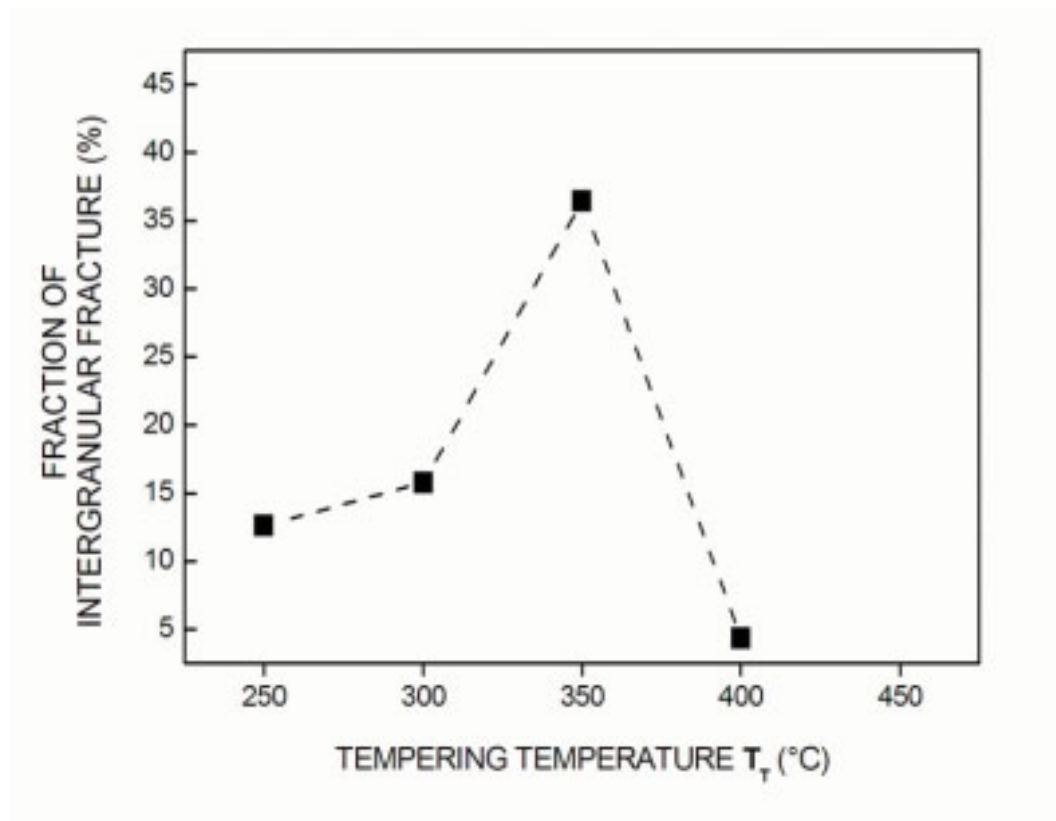


Fig 35 Fraction of intergranular fracture as a function of tempering temperature for conventionally heat treated samples of steel P1.

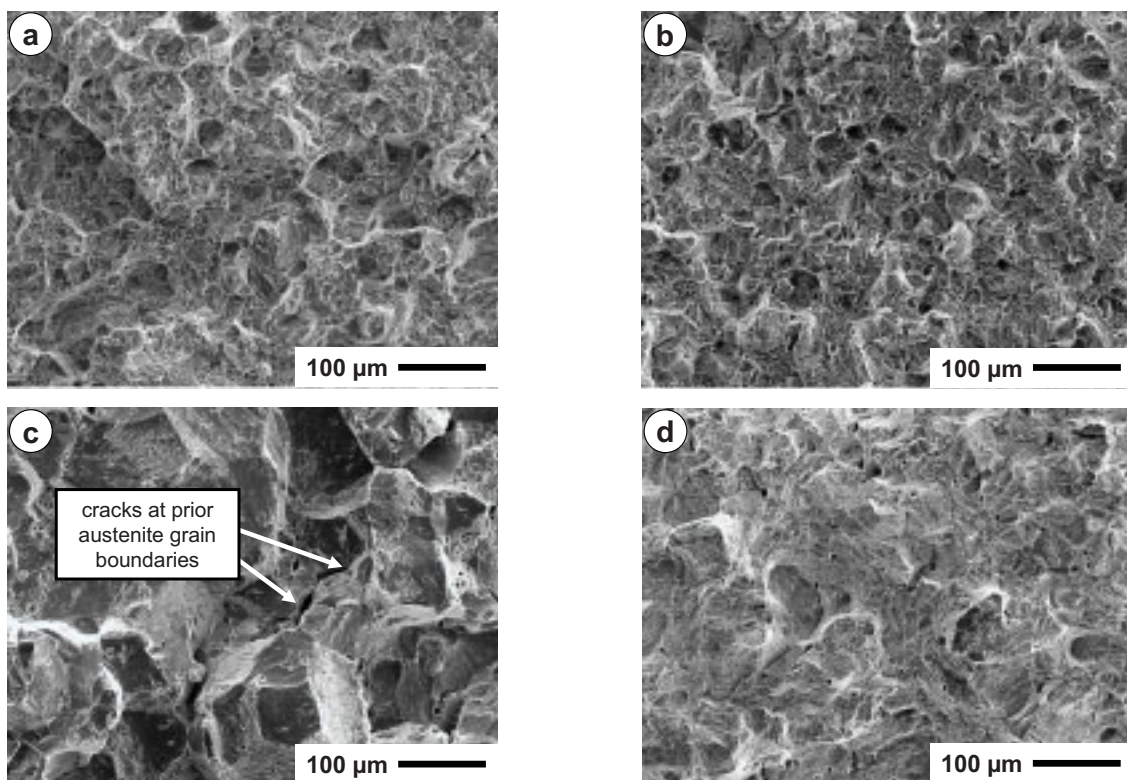


Fig 36 Fracture surfaces (after tensile test) of conventionally heat treated samples of steel P1 tempered at a) 250, b) 300, c) 350, and d) 400°C

small fraction of spherical carbides are present as well on the boundaries. Within the martensite lath platelet carbides and spherical carbides exist. At 400°C carbides start to spheroidize. Carbide films start to transform to small spherical or ellipsoidal carbides, which are still connected to each other. At 450°C the cementite particles are all spherical, within the matrix and at the grain boundary. The size of the cementite is smaller inside individual laths than at the interfaces, i.e. at grain or lath boundaries. Inside the laths the size of the spherical carbides is below 10 nm, whereas the size of the carbides at the interfaces is between 30 and 60 nm.

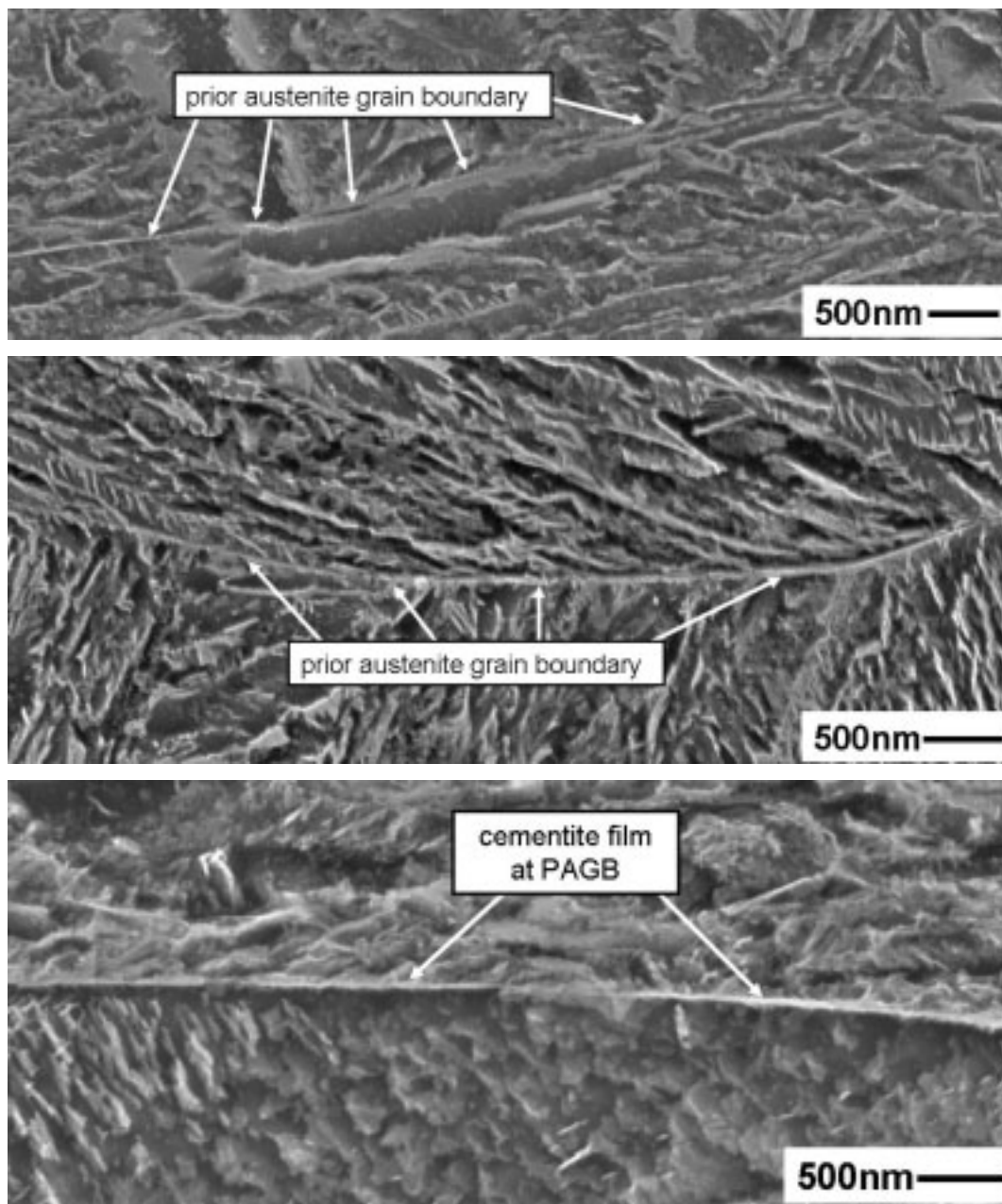


Fig 37 Conventionally heat treated samples from melt P1, austenitization 300s at 900°C, tempered at (from top to below) 250, 300, 350°C for 1 hour. Etched with 1% nital.

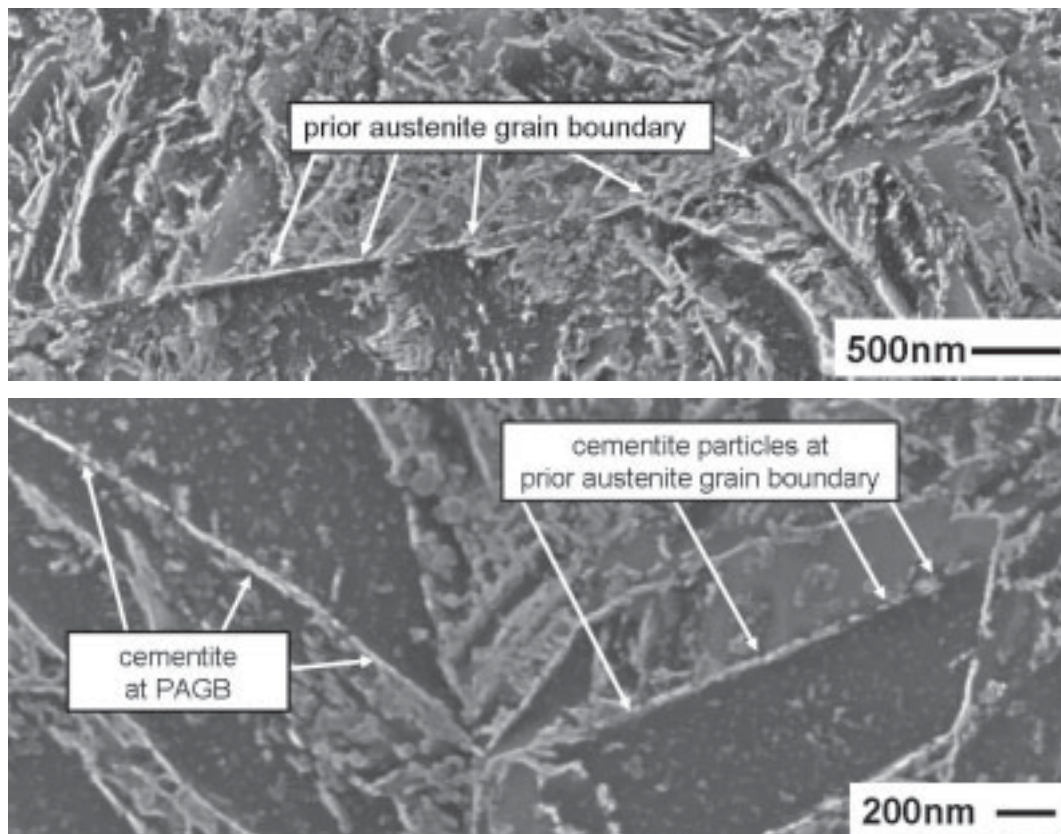


Fig. 38 Morphology of cementite at prior austenite grain boundaries of quenched and tempered martensite (melt P1). Austenitization 300s at 900°C, followed by quenching and tempering at 400°C (top) or 450°C (bottom). Etched in % nital.

Fig. 39 shows the microstructure of an as quenched and tempered sample. The analysis shows that each austenite grain transforms to a set of packets, each subdivided in laths of the same orientation relationship between the densest planes of the parent austenite and the final martensite. The size of the largest packet is limited by the size of the prior austenite grain. Each packet is further subdivided into parallel lath called blocks. Each block is further divided into parallel lath of maximum two variants. The two variants are always combinations of variant 1 and variant 4 (V1-V4), V2 and V5 or V3 and V6 (for nomenclature see Ray and Jonas 1990) and belong to the same group of lath with the same densest plane parallel to that of the parent austenite. The blocks are enclosed by high angle grain boundaries. These high angle grain boundaries have misorientation angles around that of the $\Sigma 3$ twin boundaries.

In Fig. 39 eight inverse pole figure maps of 85x85 μm^2 are put together. Many orientation maps were measured on one sample to explore the statistical sensitivity of the calculated values. From each map the fraction of phases (alpha and gamma), of low-, high-angle grain

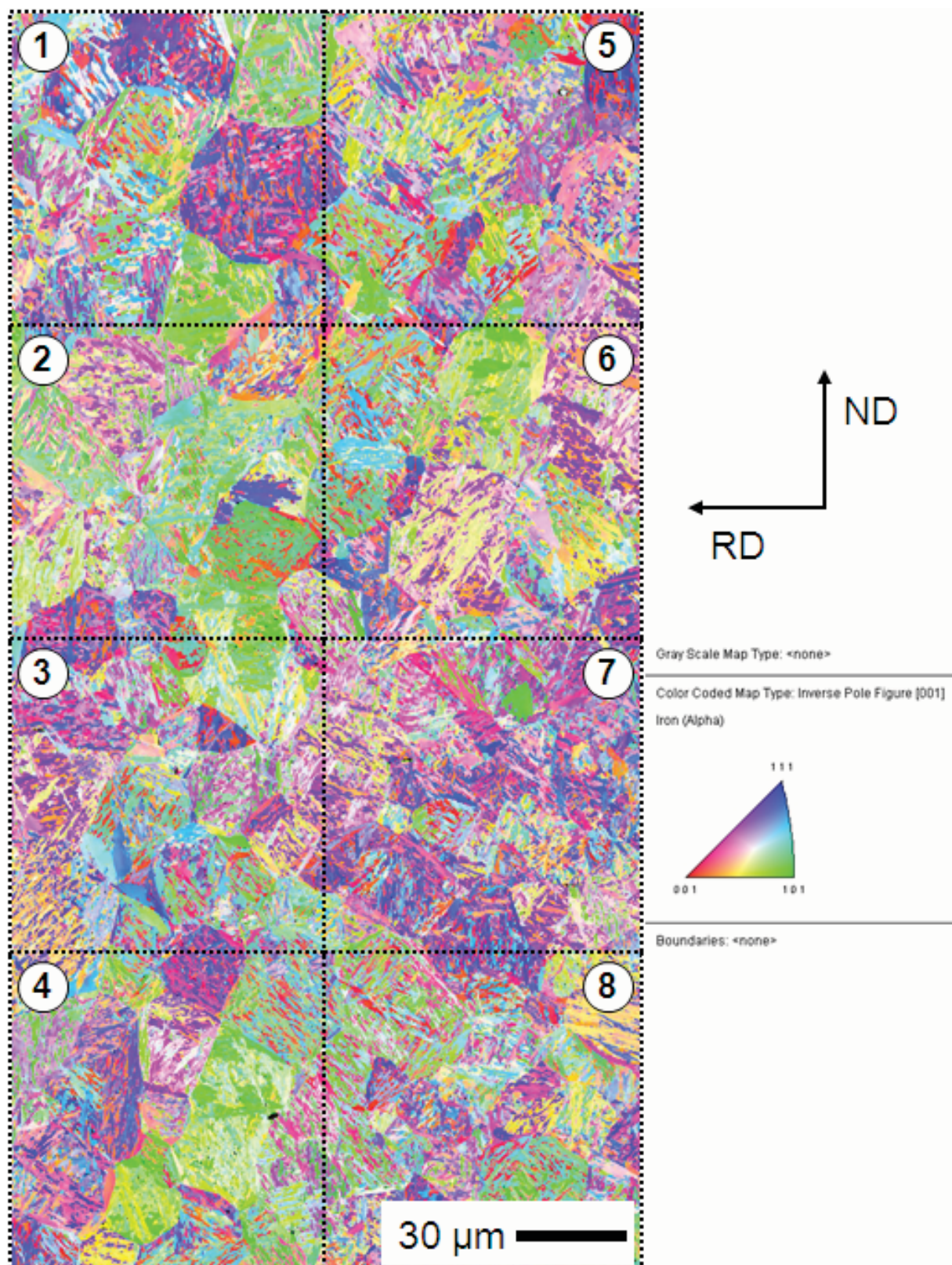


Fig. 39 8 inverse pole figure maps ($85 \times 85 \mu\text{m}^2$) of conventionally heat treated sample of melt P1. Austenitization 300 s at 900°C , tempering 1 h at 250°C . Crystallographic directions parallel to normal direction of sample. Step size for automatic orientation mapping $0.1 \mu\text{m}$.

and $\Sigma 3$ boundaries and the average effective grain size, as defined in chapter 2.1.3 were calculated. These results are presented in table 7. The total average for all values together with the standard deviation of all maps is presented in the last two lines of table 7. The fraction of retained austenite is around one percent. The fraction of low-angle grain boundaries is around one fourth of the total grain boundary length. One fourth of the total grain boundaries are approximately $\Sigma 3$ boundaries. The average effective grain area is $13.2 \mu\text{m}^2$. Depending on the austenite grain sizes in each map, the range of average effective grain size can vary almost 50%. The minimum value observed is 8.7 (map number 8), the maximum is 19.8 (map no. 6). After tempering between 250 and 350°C the amount of retained austenite is between 1 and 2 %. After tempering at 400°C almost all retained austenite is transformed. Only 0.1% is detected. The sample tempered at 450°C contains no retained austenite. Almost the entire retained austenite detected is within the prior austenite grains at lath boundaries.

Table 7 Quantitative analysis of the EBSD data of one conventionally heat treated sample of melt P1 tempered at 250°C. The fraction of gamma phase, low-angle, high-angle grain boundaries, $\Sigma 3$ twin boundaries and the average effective grain area corresponding to the martensite block area are given.

Map no.	Fraction of gamma phase (%)	Grain boundaries			Average effective grain area (μm^2)
		LAGB	HAGB (%)	$\Sigma 3$	
1	0.9	21.5	78.5	23.5	13.2
2	0.7	22.8	77.2	24.8	15.7
3	1.3	24.0	76.0	23.8	15.8
4	1.3	24.5	75.5	25.1	11.7
5	0.8	21.3	78.7	22.8	11.2
6	0.7	22.4	77.6	24.8	19.8
7	1.4	22.5	77.5	23.3	9.5
8	1.1	24.3	75.7	24.8	8.7
average	1.025	22.9	77.1	24.1	13.2
standard deviation	0.29	1.23	1.23	0.87	3.72

4.2.3.2 Microalloying with vanadium

As was shown in chapter 4.1.1 vanadium microalloying refines average austenite grain size for the conditions used here for austenitization, i.e. for 300 s at 900°C the average austenite grain diameter is reduced from approximately 30 μm to 8 μm . In this chapter we present the results gained from heat treatment experiments.

Fig. 40 compares the strength of the steel with and without microalloying of vanadium. The evolution of the 0.2% offset yield and ultimate tensile strength is comparable for both alloys. Above 400°C the ultimate tensile strength of the steel with vanadium (PV1) is higher. At 400°C the difference is around 50 MPa, at 450°C around 100 MPa. At 250°C the yield strength observed for the steel without vanadium is lower than that for the vanadium microalloyed steel and smaller than samples tempered at 300 and 350°C.

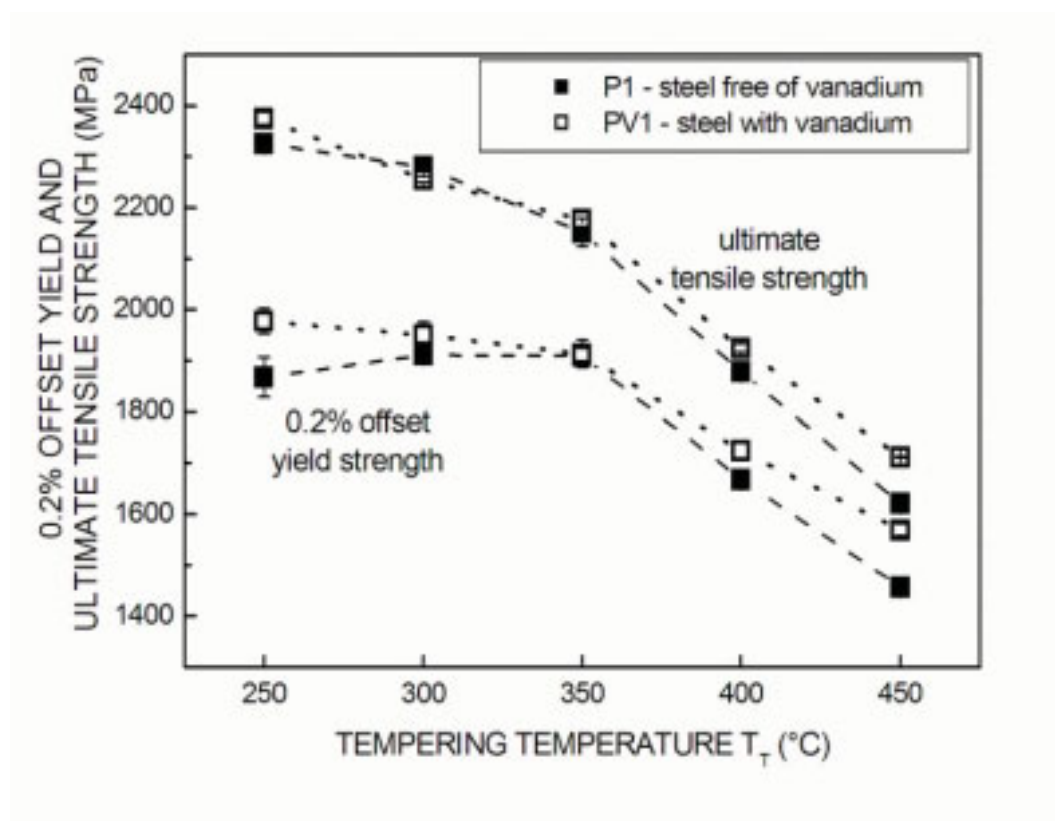


Fig. 40 Effect of vanadium addition on 0.2% offset yield strength and ultimate tensile strength for various tempering temperature, constant austenitization conditions ($t_\gamma=5\text{min}$, $T_\gamma=900^\circ\text{C}$) and constant tempering time (1h). Melts with low phosphorous content and with vanadium (PV1) or without vanadium (P1).

In contrast to the strength values that are not significantly affected by the vanadium addition, the ductility of the two melts differ strongly at tempering temperatures below 450°C (Fig. 41). Whereas for the steel without vanadium only tempering at 400°C or above results in reduction of area higher than 25 %, the microalloyed steel with the lowest phosphorous content (melt PV1) exhibits reduction of area values higher than 25 % over the entire tested tempering temperature range. The ductility of microalloyed samples increases continuously with increasing tempering temperature and reaches the maximum at 400°C, and then falls to the level of ductility measured after tempering at 450°C. In contrast to the steel without vanadium no minimum in ductility occurs at 350°. However, the ductility values of steel PV1 (table 4) tempered at the lower temperature range show a large scatter. At 300°C the three tensile specimens taken from one CHT sample exhibited values between 21.3 and 35.5%. At 350°C the vanadium microalloyed steel exhibits a reduction of area four times higher than without microalloying.

The stress-strain curves of samples tempered at 350°C are compared in Fig. 42. The uniform elongation and elongation to fracture of the vanadium-free steel is 2.7%, while the uniform elongation of the microalloyed steel is 4.2% and the elongation to fracture is 7.3%. For the austenitization condition selected (300 s at 900°C) the addition of vanadium reduces the austenite grain size significantly (chapter 4.1.1). In Fig. 43 the inverse pole figure maps of the samples discussed in Fig. 42 are presented. Black lines mark the prior austenite grain boundaries. From the inverse pole figure maps the effective grain size distributions and average grain sizes were extracted. The average effective grain area calculated in such a way for conventionally heat treated samples tempered at 350°C is refined by the vanadium addition from 30.5 to 7.5 μm^2 . The ratio of the average austenite grain size of the vanadium-free steel to the microalloyed steel is 3.75 and is close to the ratio of the effective grain area of both steels.

In the vanadium steel allotriomorphic ferrite films as shown in Fig. 44 were observed. At tempering temperatures below 400°C the allotriomorphic ferrite were observed at grain boundaries and at their triple points.

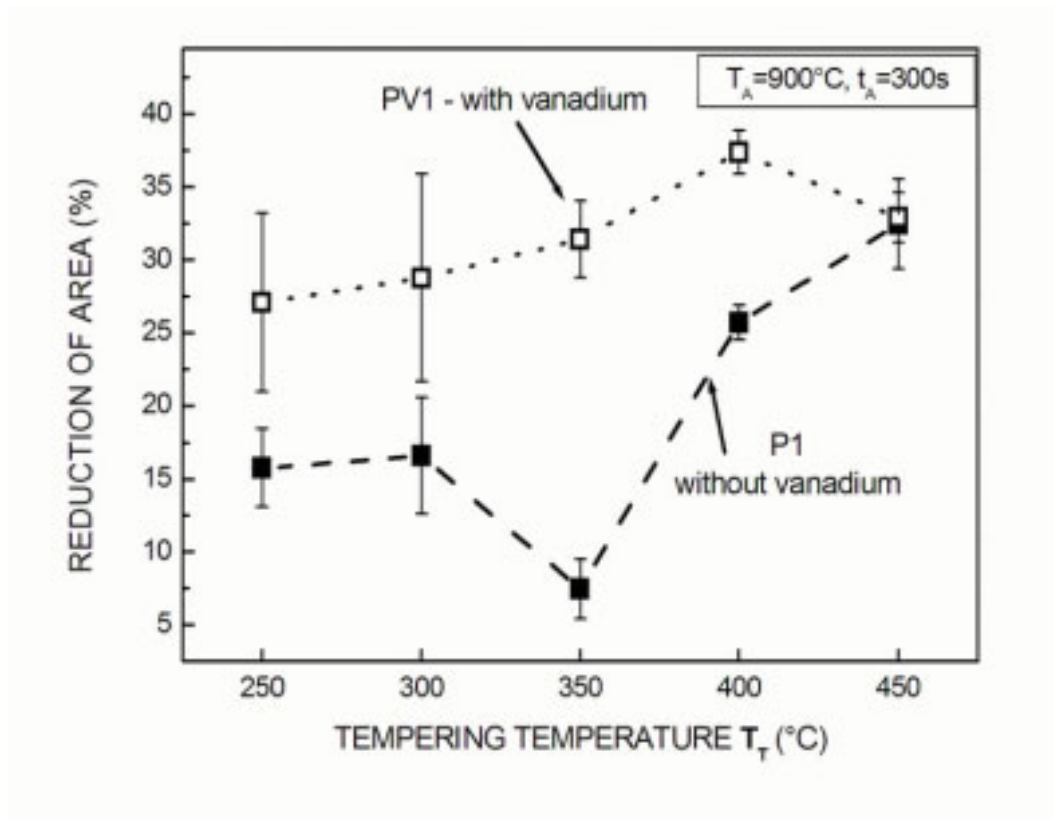


Fig. 41 Reduction of area over tempering temperature for the melts P1 and PV1. Austenitization: 300 s at 900°C. Tempering time: 1 hour.

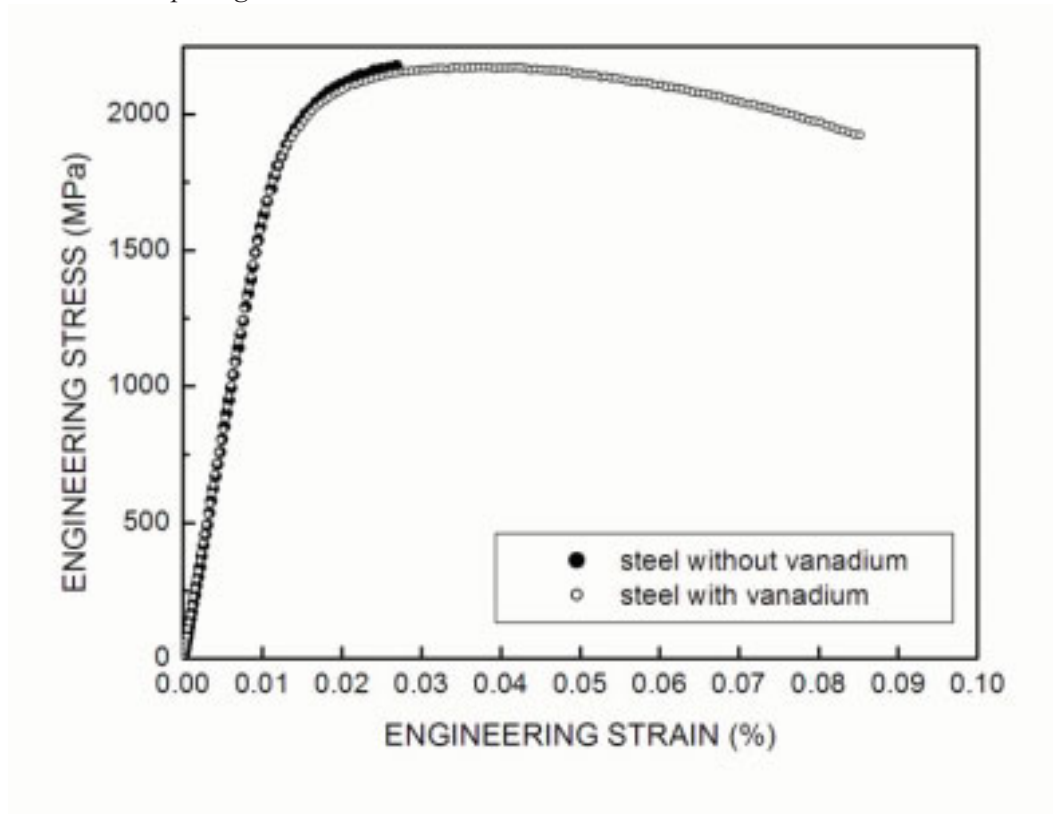


Fig. 42 Stress-strain curves for conventionally heat treated samples. Heat treatment: 300s at 900°C, oil quench, 1 hour at 350°C.

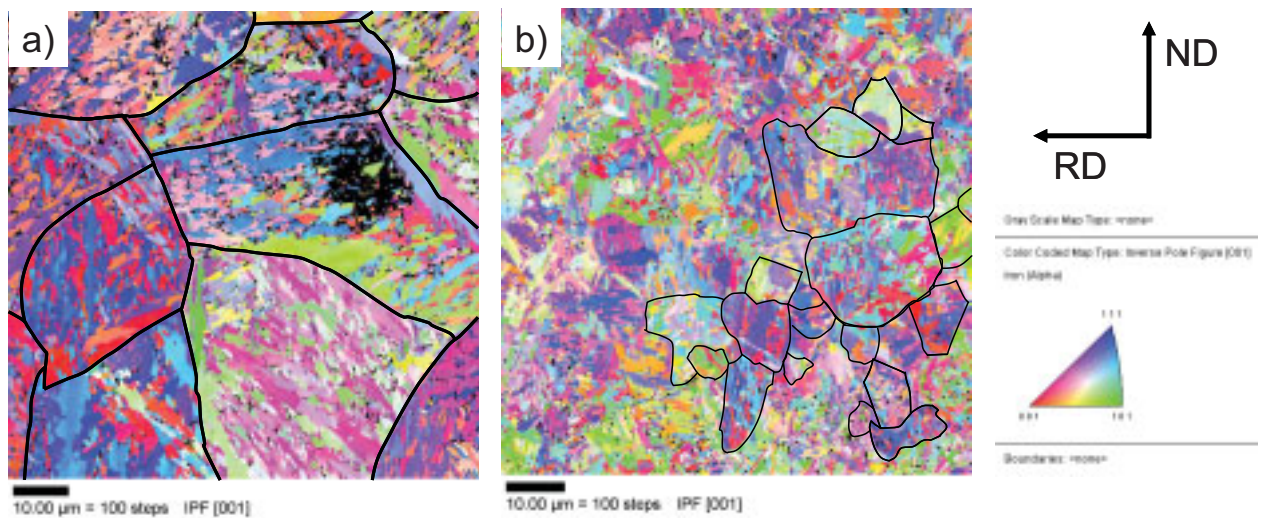


Fig. 43 Inverse pole figure maps of conventionally heat treated samples of 54SiCr6 (a) and 54SiCrV6 (b). Both samples were austenitized for 300 s at 900°C, quenched and tempered for one hour at 350°C. Some prior austenite grain boundaries marked with black lines.

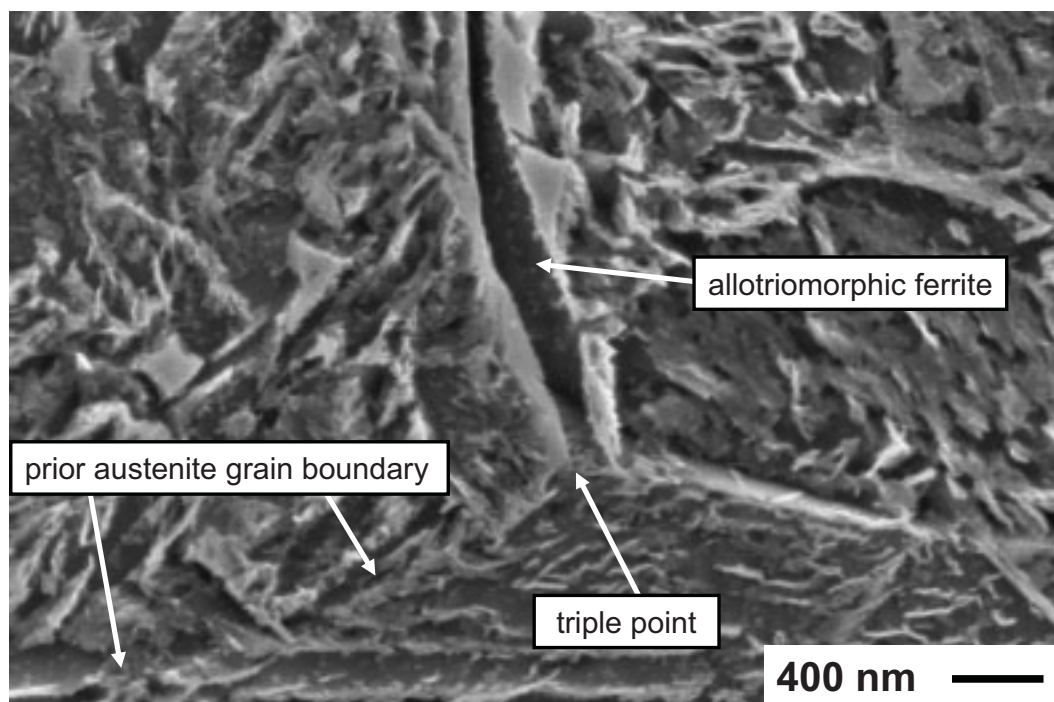


Fig.44 SEM micrograph of conventionally heat treated sample of 54SiCrV6 (melt PV1) tempered at 350°C. Etched in 1% nital.

4.2.3.3 Effect of phosphorous on tensile properties

In Fig. 45 the strength values determined in tensile test are presented for different phosphorous levels. The 0.2% offset yield strength $R_{p0.2}$ and the ultimate tensile strength R_m of the melts with higher phosphorous content fall with increasing tempering temperature in the same way as do the values for the melt with low phosphorous content (P1). Above $T_T=250^\circ\text{C}$, the $R_{p0.2}$ values increase with increasing phosphorous content. At $T_T=300^\circ\text{C}$ the change in $R_{p0.2}$ is 51 MPa for 190 ppm phosphorous, at $T_T=400^\circ\text{C}$ it is 44 MPa. The ultimate tensile strength shows a different tendency. Below $T_T=350^\circ\text{C}$ the ultimate tensile strength R_m falls with increasing phosphorous, at 350°C no tendency can be derived, and above 350°C it rises with increasing phosphorous content.

Fig. 46 shows the dependence of reduction of area for different tempering temperatures and phosphorous contents. Tempering at 250°C and 300°C leads to reduction of area values below 20%. The values for both tempering temperatures are comparable and do not differ much from each other. The reduction of area is strongly dependent on the phosphorous bulk concentration and reduces to values below 10% for phosphorous concentrations above 200 ppm. The amount of intergranular fracture increases with increasing phosphorous content (Fig. 47). The fraction of intergranular fracture increases with growing phosphorous content from 15% (P1, i.e. 0.0023 mass% P) to 30% (P3, i.e. 0.0231 mass% P). Independent of phosphorous concentration the values after tempering at 350°C are between 5% and 10%. At higher tempering temperature the matrix is softened due to rejection of carbon atoms and coarsening of carbides, and thus higher ductility values are observed. After tempering at 450°C the ductility decreases with increasing phosphorous content.

For the microalloyed steel the tempering temperatures of 350°C and 400°C were tested for all chemical compositions. Fig. 48 shows the effect of phosphorous concentration upon the ductility of the vanadium microalloyed steel. With increasing phosphorous content the reduction of area of samples tempered at 350 or 400°C decreases, while the scatter increases. No average could be calculated for specimen with high phosphorous content ($c(\text{P})=0.021$ mass%) tempered at 350°C because two out of three samples failed before reaching the 0.2% offset proof stress. The value shown in Fig. 48 for the high phosphorous sample from melt PV3 and $T_T=350^\circ\text{C}$ is higher than that of steel without microalloying, but it should be noted, that the point only represents a single value, because the others could not be determined.

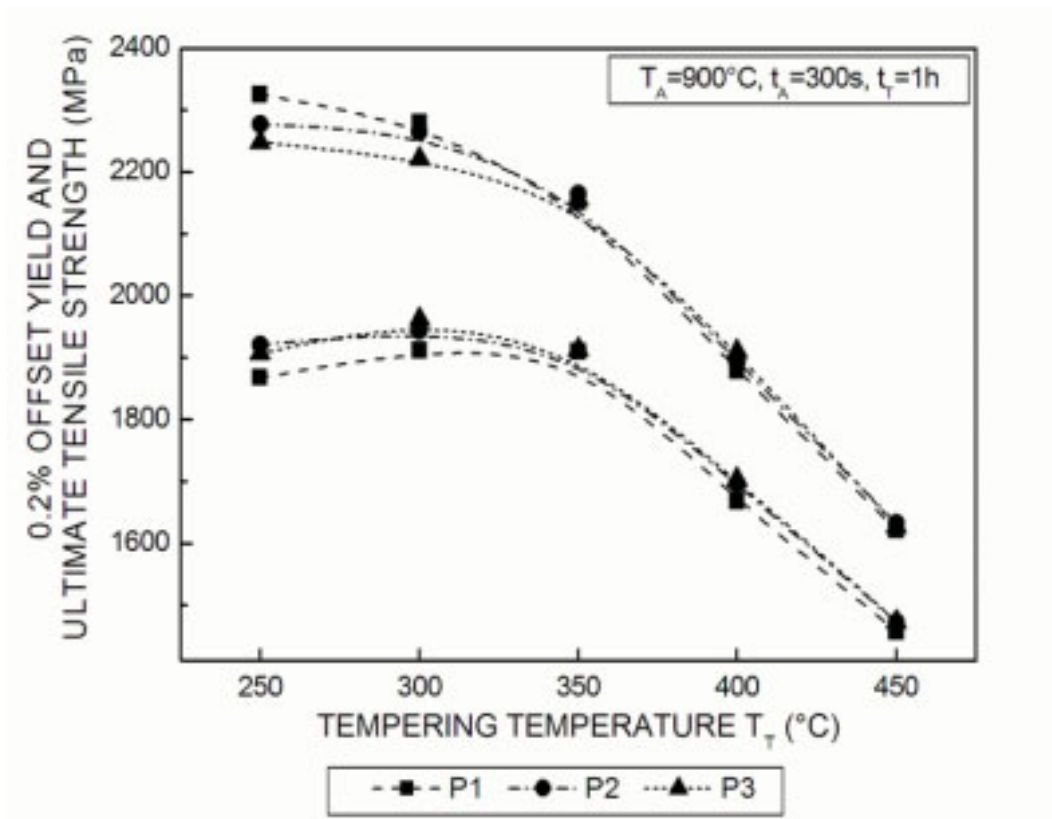


Fig 45 Tensile strength value for different phosphorous levels and tempering temperatures

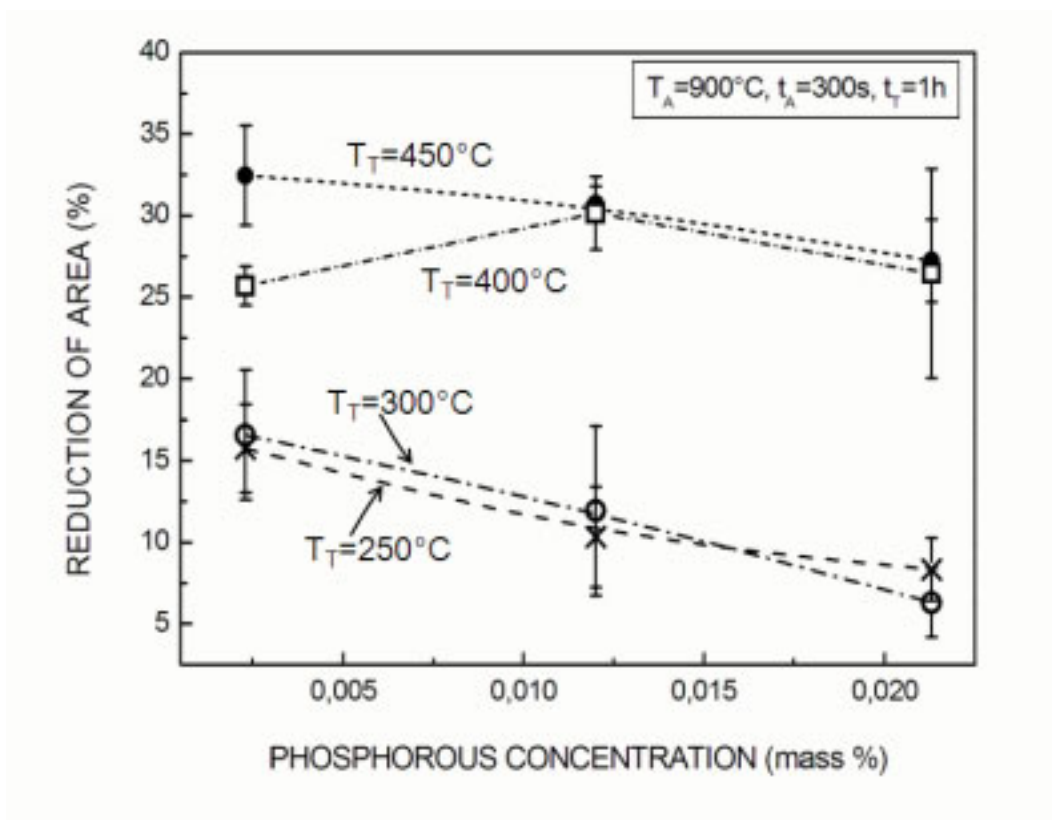


Fig. 46 Effect of phosphorous on the ductility of 54SiCr6 for different tempering temperatures TT

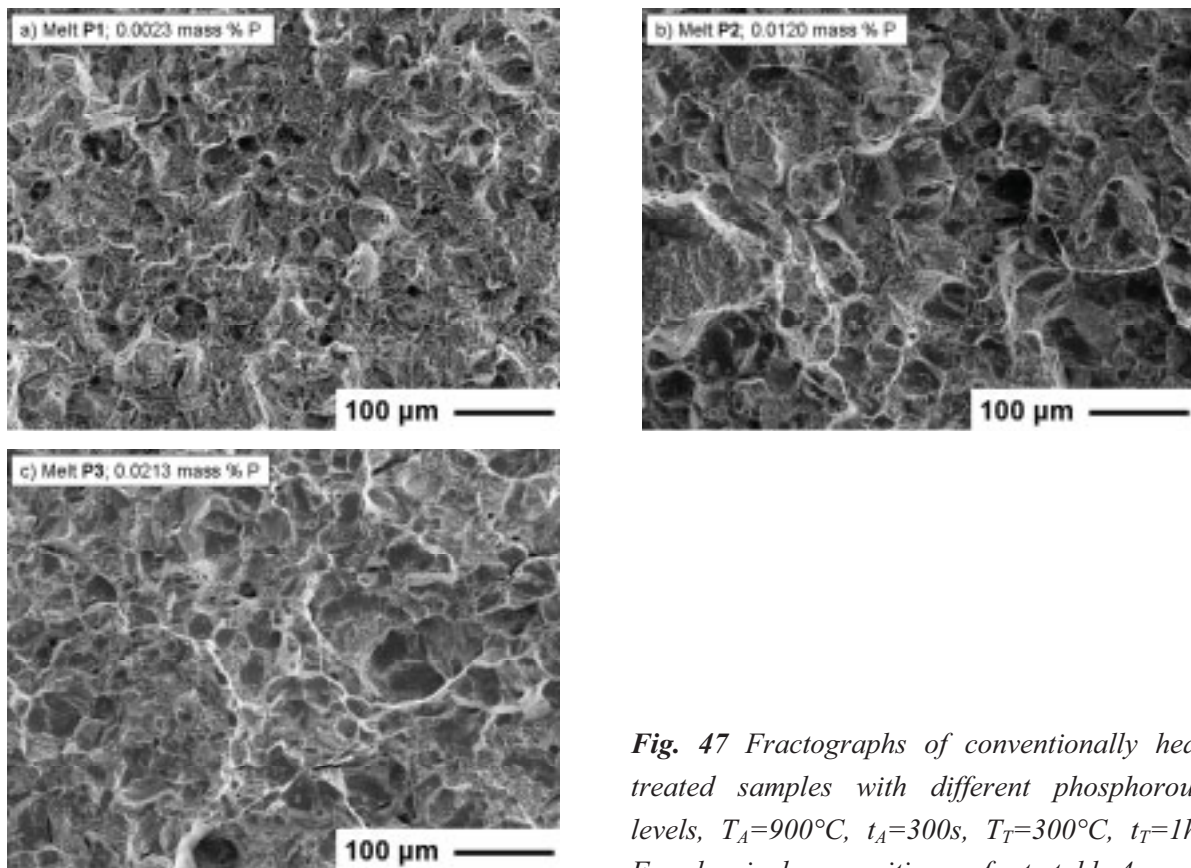


Fig. 47 Fractographs of conventionally heat treated samples with different phosphorous levels, $T_A=900^\circ\text{C}$, $t_A=300\text{s}$, $T_T=300^\circ\text{C}$, $t_T=1\text{h}$. For chemical compositions refer to table 4.

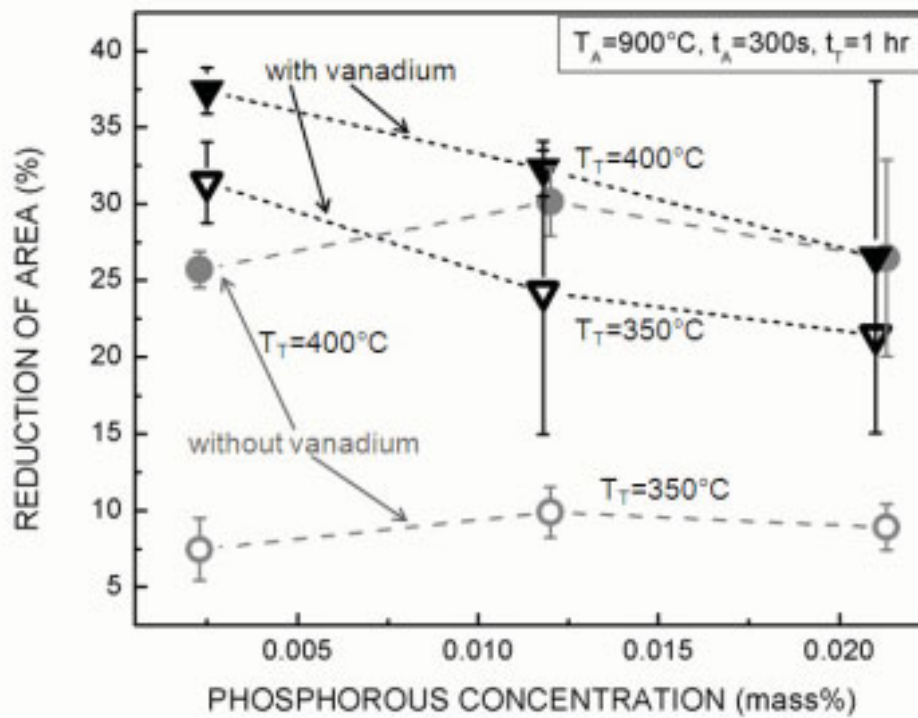


Fig 48 Reduction of area for different phosphorous levels for the vanadium microalloyed steel and for the steel without vanadium

Samples of microalloyed steel tempered at 400°C show a stronger dependency on phosphorous content than the steel without vanadium. The ductility of the sample with the lowest phosphorous bulk concentration of the microalloyed steel is 10% higher than that of the vanadium free steel. With increasing phosphorous content this difference diminishes. The reduction of area of samples with phosphorous levels above 200 mass ppm after tempering at 400°C is the same for steel with or without vanadium, whereas the scatter of the microalloyed variant is much higher.

4.2.3.4 Effect of copper and tin

In Fig. 49 the reduction of area is compared for the melts with highest (CuSn4) and second lowest (CuSn2) levels of copper and tin for the steel without vanadium within the entire tempering temperature range. Below the tempering temperature of 400°C the reduction of area values are below 15%. An increase in copper and tin to 0.6 mass percent leads to a significant loss of ductility at 400°C, and decreases the ductility at 450°C as well. Thus for the steel without vanadium, only the tempering temperatures of 400 and 450°C were selected to determine the limits of copper and tin. For the microalloyed case tempering temperatures of 350 and 400°C were investigated to ascertain whether an improvement of strength and ductility can be achieved by addition of vanadium.

For conventional heat treatment, the addition of copper and tin has a minor effect on strength (Fig. 50). A slight increase of the 0.2% offset yield strength and ultimate tensile strength is observed with increasing copper and tin content after tempering at 400°C. No effect with increasing content of these elements was observed after tempering at 450°C.

Fig. 51 shows the influence of copper and tin addition upon the elongation to fracture of conventionally heat treated samples. The elongation to fracture shows a strong dependency on the copper and tin concentration after tempering at 400°C. The elongation decreases from 8% to 3%, while the scatter increases at the same time. The loss in ductility is very rapid when the copper and tin level exceeds 0.3 mass% (Fig. 51). Increasing the copper and tin level from 0.3 to 0.4 reduces the reduction of area from 30.8 % to 21.5 %. For the tempering temperature of 450°C, the loss in ductility is below 1% in the composition range investigated.

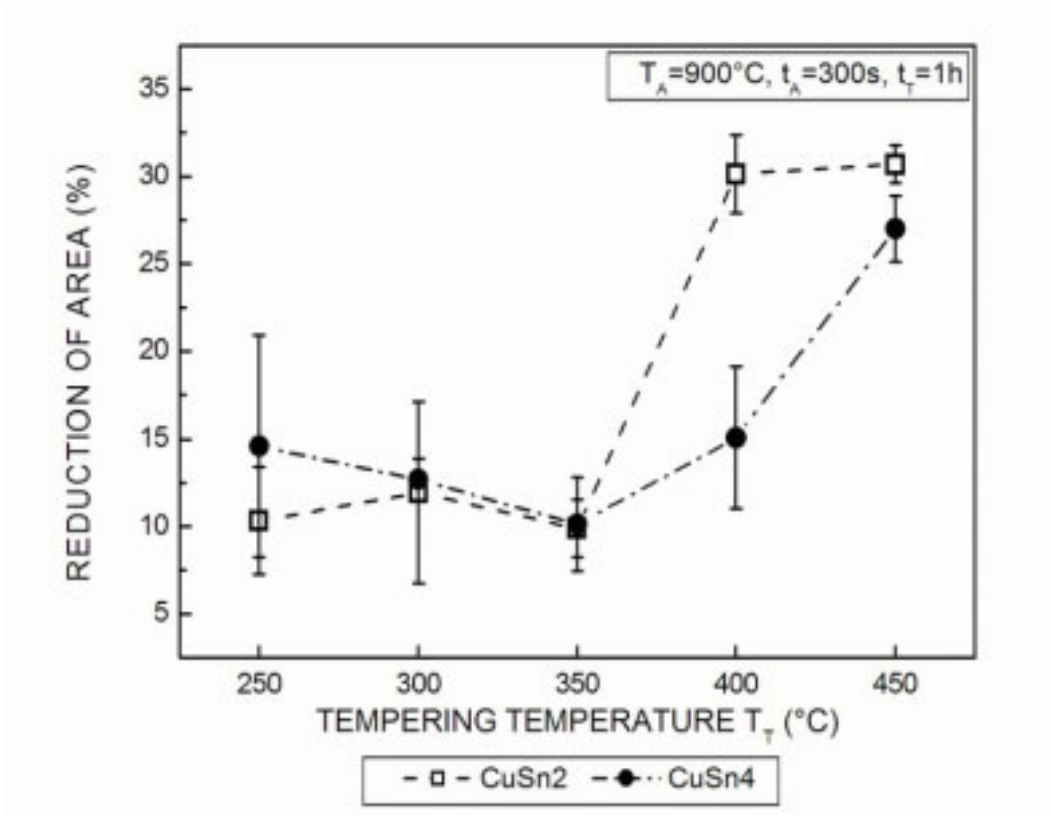


Fig. 49 Reduction of area for conventionally heat treated samples of 54SiCr6 with 0.3 and 0.6 mass % copper+ tin at different tempering temperatures.

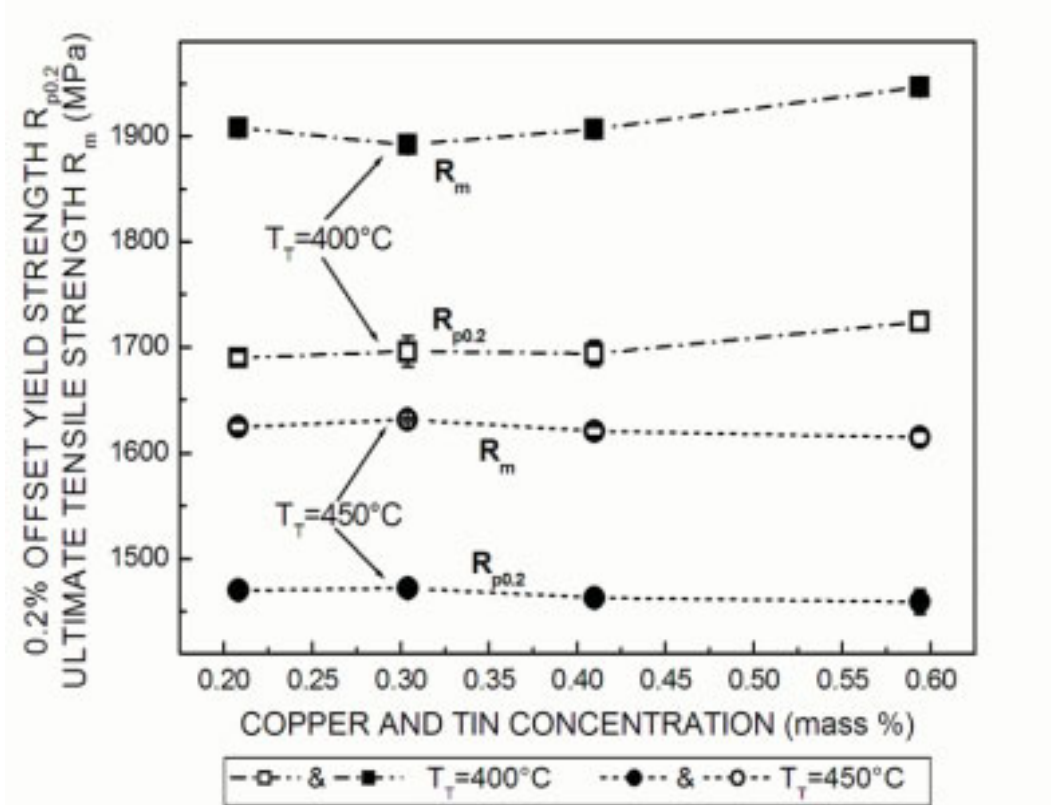


Fig 50 Influence of copper and tin concentration upon the tensile strength values of conventionally heat treated samples tempered at 400 and 450°C.

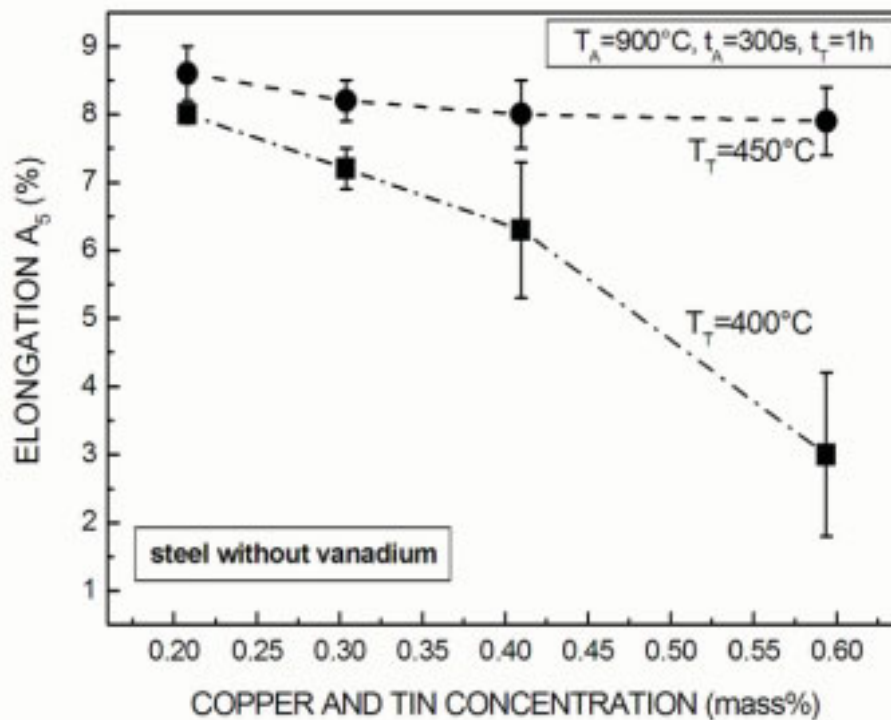


Fig. 51 Influence of copper and tin concentration upon elongation to fracture A_5 of conventionally heat treated samples tempered at 400 and 450°C.

For the microalloyed steel the average reduction of area after tempering at 400°C is higher within the entire copper and tin concentration range (Fig. 52 and 53). However, the loss in ductility with increasing copper and tin is more pronounced. Although the average values are larger for the microalloyed steel, the minimum values observed are comparable for both steels after tempering at 400°C and for copper and tin concentrations above 0.3 mass%. The average reduction of area after 350°C is larger for the steel with vanadium. Below 0.3 mass% the average is around 25 % and decreases with further increase of copper and tin to around 15%. However, after tempering at 350°C the scatter for all the conventionally heat treated samples of the steel with vanadium is very large.

The decrease in ductility with increasing copper and tin concentration is concurrent with an increase in intergranular fracture observed in the fracture surface of the tensile specimen.

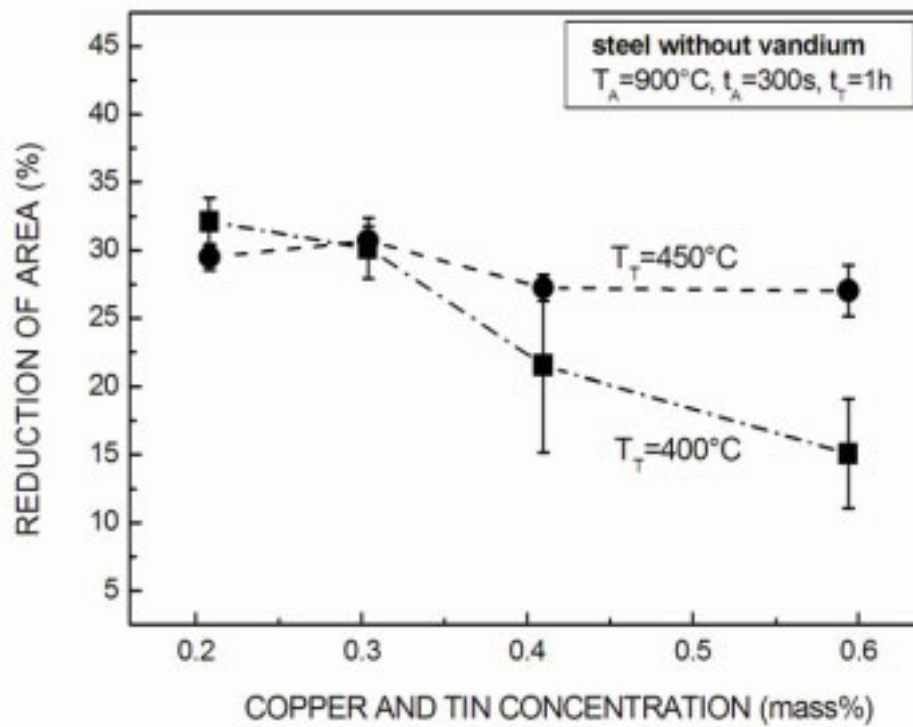


Fig. 52 Influence of copper and tin concentration upon reduction of area of conventionally heat treated samples of steel without vanadium tempered at 400 and 450°C.

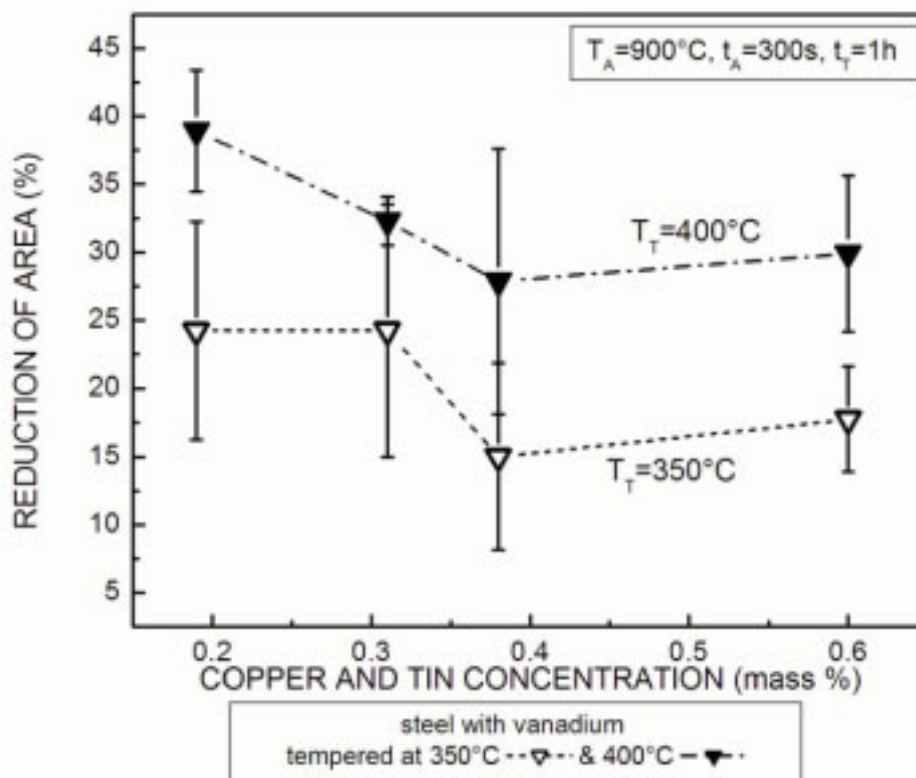


Fig. 53 Influence of copper and tin concentration upon reduction of area of conventionally heat treated samples of steel with vanadium tempered at 350 and 400°C.

4.2.4 DISCUSSION

4.2.4.1 Tempering temperature

The ultimate tensile strength of melt P1 decreases gradually with increasing tempering temperature (Fig. 33). Below 350°C the 0.2% offset yield strength is almost constant, while decreasing rapidly above 350°C. The slope of the both curves (stress vs. temperature) changes at 350°C. It is concluded, that the drop in strength commences at 350°C with stage III of tempering (Krauss 1990), in which transition carbides and low carbon martensite are replaced by cementite and ferrite. Silicon reduces the diffusivity of carbon in iron. The loss of carbon from the martensite lattice is therefore slowed down. Thus silicon shifts the start of stage III to higher temperatures (Altstetter 1962). For a similar alloy (Fe-0.59C-1.51Si-0.50Mn-0.50Cr mass %) Nam et al. (2000) observed ϵ -carbides up to 350°C. It is further known that formation of ϵ -carbide does not lead to a complete depletion of carbon from the martensite lattice (Cohen 1962) and that carbon in solid solution delivers the main contribution to strength. Hence, the onset of stage III and cementite formation will lead to a loss in strength as can be seen in Fig. 33.

The temperature threshold for cementite formation is reflected as well in loss of ductility at 350°C. Fig. 34 shows the ductility values measured in tensile test for different tempering temperatures. A lower tempering temperature results in higher tensile strength values and lower ductility values, except at 350°C, where a minimum in ductility is observed. The observed minimum in ductility or toughness after tempering at around 350°C is a well-known phenomenon related to the formation of carbide films at the prior austenite grain boundaries that are enriched with impurity elements such as phosphorous (Krauss 1990, Capus 1963, Horn 1978, Briant 1999, Reguly 2004). In the lower temperature regime of cementite formation during tempering, cementite forms at prior austenite grain boundaries, packet, block and lath boundaries, and at dislocations (Furuhara 2004). If the cohesion of adjacent austenite grain boundaries is weakened by segregation of impurity elements to these interfaces, brittle intergranular fracture of the final tempered martensite is observed. Fig. 54 shows such a cementite film observed at a prior austenite grain boundary in the conventionally heat treated sample of melt P1 (see table 4) tempered at 350°C. The increase in ductility observed at higher tempering temperatures above 350°C is a common observation

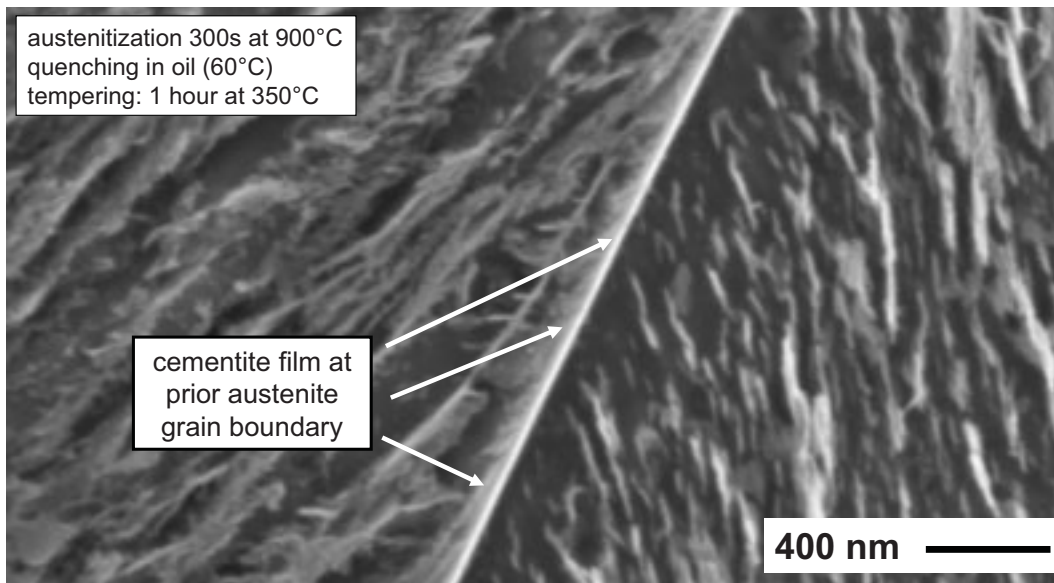


Fig. 54 SEM micrograph showing cementite at a prior austenite grain boundary of a conventionally heat treated sample of alloy P1 (see table 1). 1% alcoholic solution of HNO₃.

within the matrix and at the prior austenite grain boundaries start to spheroidize. The carbides within the matrix become coarser at higher temperatures and the matrix softening is manifested in the tensile strength values.

4.2.4.2 Microalloying with vanadium

The main effect of vanadium addition is the refinement of austenite grain size for the austenitization parameters used, i.e. for annealing 5 minutes at 900°C. The effective grain size of the martensite, i.e. the block size is significantly decreased by the austenite grain size refinement. Because not all the vanadium carbides are dissolved at 900, the concentration of carbon in solid solution decreases. Calculating the fraction of thermodynamically stable carbides at 900°C, the concentration of carbon can decrease maximally by 0.01 mass %. Thus the question is, which effect does the austenite grain refinement have on the transformation and the precipitation during tempering and how does all this reflect itself in the mechanical properties.

The cementite films that form either at prior austenite grain boundaries or at lath, block or packet boundaries are potential sources for crack initiation. Such cementite films were observed in the vanadium-free steel as was mentioned above, whereas in the microalloyed steel such films were absent (Fig. 44).

Additionally, in the vanadium steel allotriomorphic ferrite films were observed. The austenitization of the microalloyed steel was carried out at a temperature at which vanadium carbides were present. This means, that the amount of carbon in solid solution was lower in the steel with vanadium. Lower carbon concentration in solid solution results into a lower driving force for grain boundary segregation of carbon during austenitization and therefore the grain boundary concentration of carbon must be less in the austenite prior to quenching. Hence, for a constant austenite grain size the formation of cementite films at prior austenite grain boundaries is retarded during tempering. Since the diffusion of carbon is required to the prior austenite grain boundaries, less cementite films can be observed after constant tempering time. But because the vanadium carbides reduce the austenite grain size as well and enhance the grain boundary area, this effect is even more pronounced. At the same time the decrease of carbon in solid solution enhances the transformation temperature for the γ - α -transformation, which increases the formation of allotriomorphic ferrite during air cooling before quenching or even during quenching itself. Furthermore, the increase in the effective austenite grain boundary area, i.e. the austenite grain boundary area per unit volume promotes the γ - α -transformation, because austenite grain boundary areas are potential ferrite nucleation sites.

4.2.4.3 Effect of phosphorous

To enhance the strength it is necessary to decrease the tempering temperature. For the steel without vanadium it implies that the loss in ductility that is observed at around 350°C must be avoided. For the steel with vanadium a gradual decrease of ductility was observed with decreasing tempering temperature. Due to the high strength level below the tempering temperature of 350°C the cohesion of adjacent austenite grains and thus the concentration of phosphorous at the boundaries between them becomes very important. In the subsequent paragraph the influence of phosphorous on the ductility (measured in tensile test) of both steels with and without vanadium is presented.

The results show a clear dependency of ductility with phosphorous bulk concentration, even at lower tempering temperature. From the results we conclude that the decrease of ductility with increasing phosphorous concentration is due to phosphorous grain boundary segregation during austenitization. First, the fractographs show that the coherency between the prior austenite grain boundaries is weakened with increasing phosphorous levels (Fig. 47). The diffusion coefficient of phosphorous in ferrite is represented by (Leslie 1981):

$$D = 7.1 \times 10^{-3} \exp(-20000/T) \text{ cm}^2/\text{s} \quad (\text{Equation 17})$$

At 300°C the diffusion coefficient of phosphorous in alpha is calculated to be $4.97 \times 10^{-18} \text{ cm}^2/\text{s}$. The time required for a phosphorous atom to move a mean distance of 0.1 μm would require almost 139.6×10^6 hours. The average austenite grain size is around 30 μm . The tempering time was one hour. Thus the segregation of phosphorous must have taken place before the tempering stage, i.e. during austenitization (Banerji 1978, Briant 1979). The lower solubility of phosphorous in austenite (Fig. 55) leads to higher segregation driving force to grain boundaries as was explained in 2.1.4.1. Furthermore the diffusivity of phosphorous is higher in austenite. Abe et al. calculated the diffusion constant to be $1.99 \times 10^{-10} \text{ cm}^2/\text{s}$ at 1100°C. After quenching and prior to any tempering the prior austenite grain boundary are enriched with phosphorous atoms and the cohesion between the two neighbouring prior austenite grain areas is reduced. Cementite present at grain boundaries act as slip-barriers and promotes intergranular cracks at these weakened areas. We already mentioned that cementite start to form at temperatures above 350°C. Thus the question arises

why cementite is present at grain boundaries after tempering at 300°C. According to Krauss and others (Krauss 1995, Krauss 2001, Reguly 2004) in steels with carbon contents higher than 0.5 mass% the austenite grain structure consists of a combination of cementite and segregated phosphorous atoms. Thus the fraction of cementite present at 300°C has been most probably generated during austenitization and quenching.

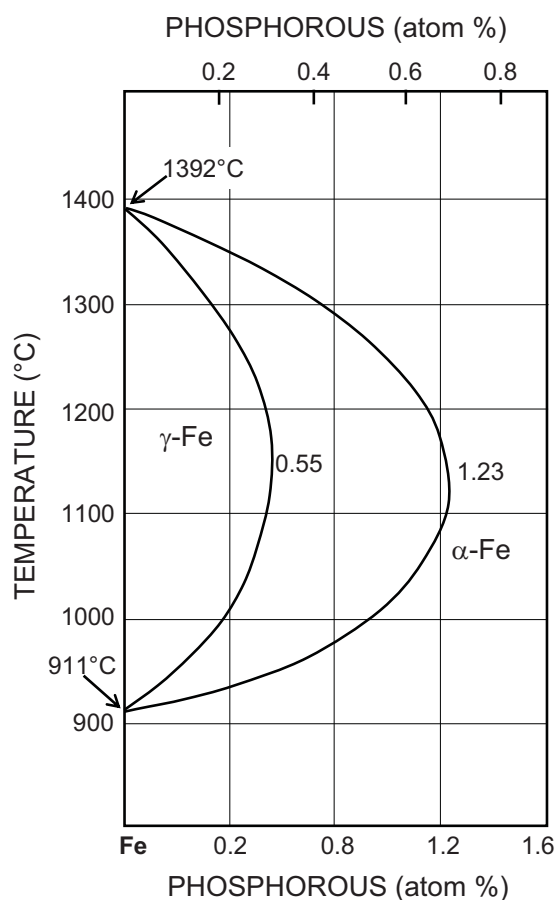


Fig. 55 Iron-phosphorous binary phase diagram (Kubaschewski 1982)

With increasing phosphorous concentration the cohesion between prior austenite grain boundaries becomes weaker and a reduction of ductility with increasing phosphorous content is observed (Figs. 46 and 48). Cementite films at prior austenite grain boundaries were observed after tempering at 300°C. However, their presence was rare. Carbide films found at the prior austenite grain boundary were in the order of 100 nm length.

4.2.4.4 Effect of copper and tin

Copper and tin were discussed in many papers due to their effect on the hot liquid embrittlement and the problems they cause during rolling of steels (Imai et al. 1997, Seo et al. 1997, Suzuki 1997, Shewmon 1998). Embrittlement of pressure vessel steels used in nuclear reactors has been correlated with the copper concentration in the α -iron. Copper-enriched clusters forming during neutron irradiation have been associated with solute atoms like Ni, Mn, Si and P and have been reported to be responsible for the embrittlement. Within this study the effect of copper and tin on hot liquid embrittlement was excluded and their effect on the mechanical properties was the centre of interest.

The results show that the ductility of the tempered martensite is dependent on the concentration of copper and tin. Strong decrease of the tensile ductility was observed with increasing copper and tin concentration for samples tempered at 400°C. Although the addition of vanadium shifts the level of ductility to higher values, concentrations exceeding 0.3 mass % copper and tin produce values, which are not reproducible and close to the tolerance limits acceptable for the industrial application of the material. Furthermore, fracture surface observations show that the decrease of ductility is correlated with an increase of intergranular fracture in tensile specimen.

In this study, the concentration of copper and tin have been varied together. Tin is known to have a strong embrittling effect (Briant 1999), while nothing is reported about the effect of grain boundary segregation of copper on the ductility of iron. The level of tin in the melt with the highest content of copper and tin is 840 mass ppm. This concentration is above the usual bulk concentrations, which are smaller than 0.02 mass %. According to Grabke (1989) tin has a low tendency towards grain boundary segregation in ferrite. With increasing carbon concentration in ternary Fe-Sn-C alloys the tin concentration decreases at the grain boundaries while that of carbon increases. Concurrently the fraction of intergranular fracture reduces. Furthermore the diffusivity of tin is relatively small in iron and during usual processing and heat treatment there will be no time for grain boundary segregation of tin to grain boundaries.

In the laboratory steels used here the copper and tin concentration exceeds the usual level observed in steels obtained from the electrical arc route. Typical concentration of commercial steels is about 0.3 mass%. The ratio of copper to tin is typically around 10. However, we see a strong decay of reduction of area or elongation to fracture after tempering at 400°C. Furthermore, Fig. 56 shows the loss in reduction of area by addition of 0.280 mass % copper and 0.027 mass % tin for different tempering temperatures. The results are obtained from two melts (P4 and P5, see table 4) with 297 mass ppm phosphorous and low sulphur content (below 100 mass ppm). The loss of reduction of area is larger after tempering at 400°C or above, at temperatures where significant solute element diffusion start to take place in iron and the secondary hardening regime starts. Tempering at 350°C produces generally low reduction of area values and therefore the difference is lowest at this temperature. From the results it is concluded that tin segregation to austenite grain boundaries is most probably the reason for the observed embrittlement. The embrittlement can be intensified by further precipitation of copper and further strengthening of the matrix. The higher the strength of the matrix, the more the cohesion of the grain boundary plays a role in the coherence of any structure, in this case the tensile specimen.

No significant increase of tensile strength was observed with increasing copper concentration after tempering at 400 and 450°C (Fig. 50). Again the comparison between the melts P4 and P5 shows that the addition of these elements has an effect on the tensile yield strength. The addition of 0.28 mass % copper and 0.027 mass % tin raises the yield strength for all tempering temperatures (Fig. 57). At 400°C and above the difference minimizes. From the results obtained here, it can be stated that copper and tin addition increases the tensile yield strength at low concentration for the process parameters used here. However, with increasing copper and tin content from 0.3 mass % no effect is seen after tempering at 400°C or above.

The investigation here shows that the role of copper with respect to embrittlement and strength of tempered martensite needs further research effort. Especially the interaction of copper with other elements in grain boundary segregation and precipitation processes should be thoroughly investigated. Whether copper is involved in promoting grain boundary segregation of carbon, phosphorous or tin in the austenite is not known. This question remains for future work and due to the increased use of scrap steel and the difficulty of removing copper and tin from the steel is of industrial importance.

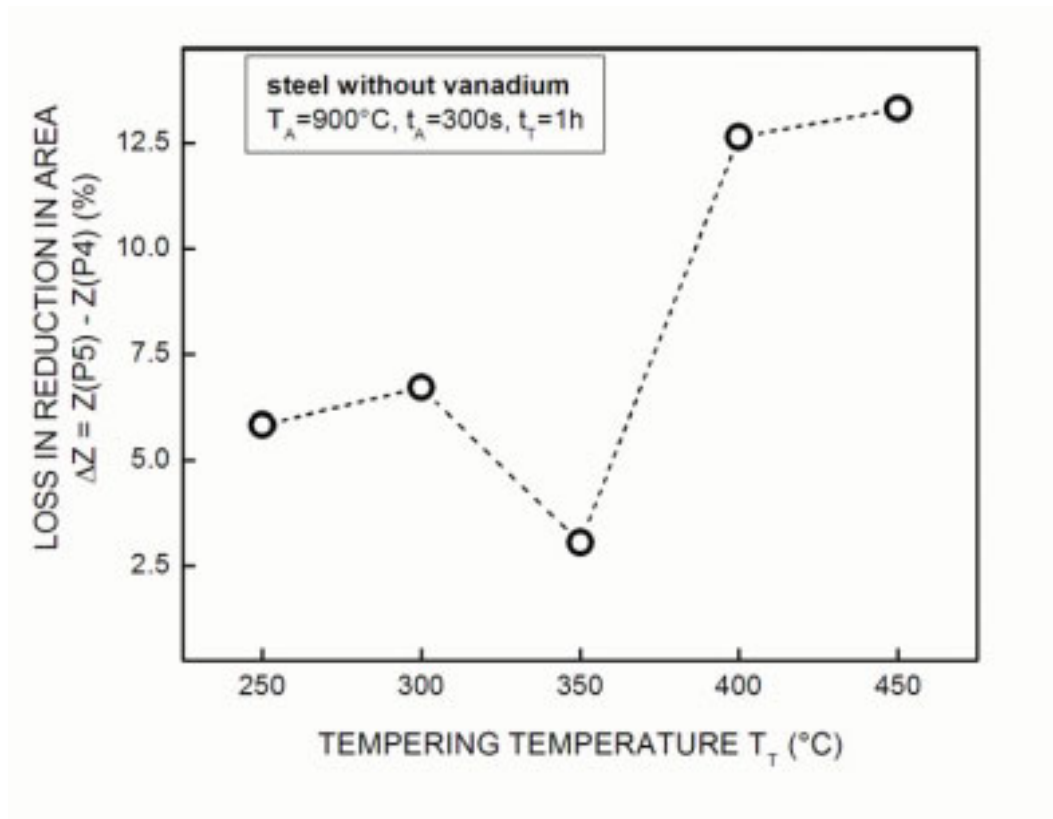


Fig. 56 Difference in reduction of area between conventionally heat treated samples of two melts with high phosphorous content (P4 and P5, refer to table 4) but different copper and tin content.

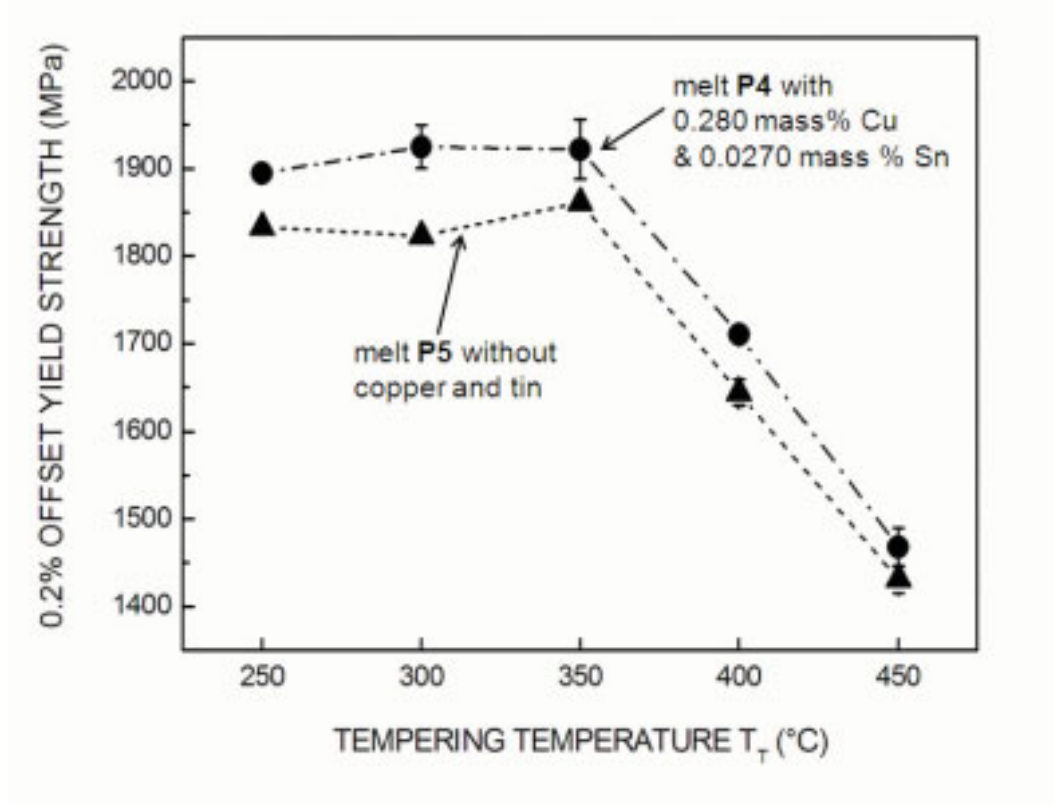


Fig. 57 0.2% offset tensile yield strength for two melts with and without copper and tin at different tempering temperatures.

4.3 THERMOMECHANICAL TREATMENT

4.3.1 OBJECTIVE

The aim of thermomechanical treatment is to modify the austenite condition by deformation in order to achieve the desired properties in the final product phase. The deformation of austenite allows obtaining various austenite grain structures and grain substructures. Refinement of the austenite grain can be achieved through recrystallization (either dynamic or static) by proper control of the deformation process and of the evolution of temperature-time. However in some cases a grain substructure with increased defect density (work-hardened austenite) or recovered structure might be beneficial. In the present study the specific aim was to improve the strength and ductility relative to the conventional heat treatment and to suppress the embrittling effect of the impurity elements phosphorous or copper and tin.

In chapter 4.1.3 the recrystallization behaviour of the austenite in the alloy system under investigation was studied and various austenite conditions could be produced in large laboratory scales with the hot deformation simulator. Because it is not possible to predict the mechanical properties of the different austenite conditions from the basic tests performed there, the optimum deformation temperature and austenitization temperature were determined in two series of tests. In the subsequent chapters first the results of these tests is presented.

On the basis of these latter results thermomechanical treatments with different austenite conditions were defined and their potential at different strength levels for various impurity or tramp element bulk content was explored. The systematic change of process parameters, chemical composition and at the same time microstructural characterization allows a deeper understanding of the interaction between process parameters, microstructure and the final properties.

4.3.2 DEFINITION OF DEFORMATION TEMPERATURE

4.3.2.1 Experimental

Because the vanadium free steel with the maximum content of copper and tin (melt CuSn4, see table 5) delivers the lowest ductility after conventional heat treatment, samples from this

melt were used for optimization of deformation temperature to achieve austenite conditions with maximum potential. Thermomechanical samples as described in 3.3 were heated to the austenitization temperature of 950°C by induction heating. The samples were air cooled to the deformation temperature, deformed in plane compression to a thickness of 13 mm (corresponding to a logarithmic strain of 0.4) and quenched after 15 s of quench delay. Deformation temperatures tested were 900, 850, 800 and 750°C. Tempering was performed in a furnace for 1 hour at 350 or 400°C. The samples were then characterized by mechanical testing, optical and electron microscopy and orientation imaging microscopy.

4.3.2.2 Results

Optical microscopy revealed that samples deformed above 800°C exhibited recrystallized austenite grains. The recrystallization reduced the average prior austenite grain size from 30 to 20 μm or below. The sample deformed at 750°C showed prolonged, pan-caked austenitic grains. The orientation imaging microscopy results were additionally used to obtain more information about the austenite state prior to quenching and hence prior to transformation. All the points identified as bcc alpha iron were removed and the remaining indexed austenite points or areas were dilated in all directions of the map until they met each other. These reconstructed inverse pole figures of the austenite confirms the findings made by optical microscopy. Apart from that, it indicates that after deformation at 800°C and subsequent recrystallization the austenite grains are much smaller than those produced after deformation at higher temperatures.

Figs. 58 to 60 present the tensile properties of deformed samples (thermomechanical treatment) with reference to the properties of conventionally heat treated samples. Average values together with the standard deviation are given for thermomechanically treated samples. The average values plus the standard deviation is drawn as reference line for not-deformed samples. The tensile yield strength of thermomechanically treated samples is comparable with values obtained without any deformation. Samples deformed above 850°C and tempered at 350°C exhibit the same level of yield strength. With decreasing deformation temperature from 850°C down to 750°C the yield strength increases. For samples tempered at 350°C, the austenite deformation increases the ultimate tensile strength for all deformation temperatures except for 850°C. After tempering at 400°C only the sample which was deformed at 750°C has an equivalent 0.2 offset yield strength and higher ultimate tensile strength. The rest exhibit slightly lower strength values, at maximum 2.5% less.

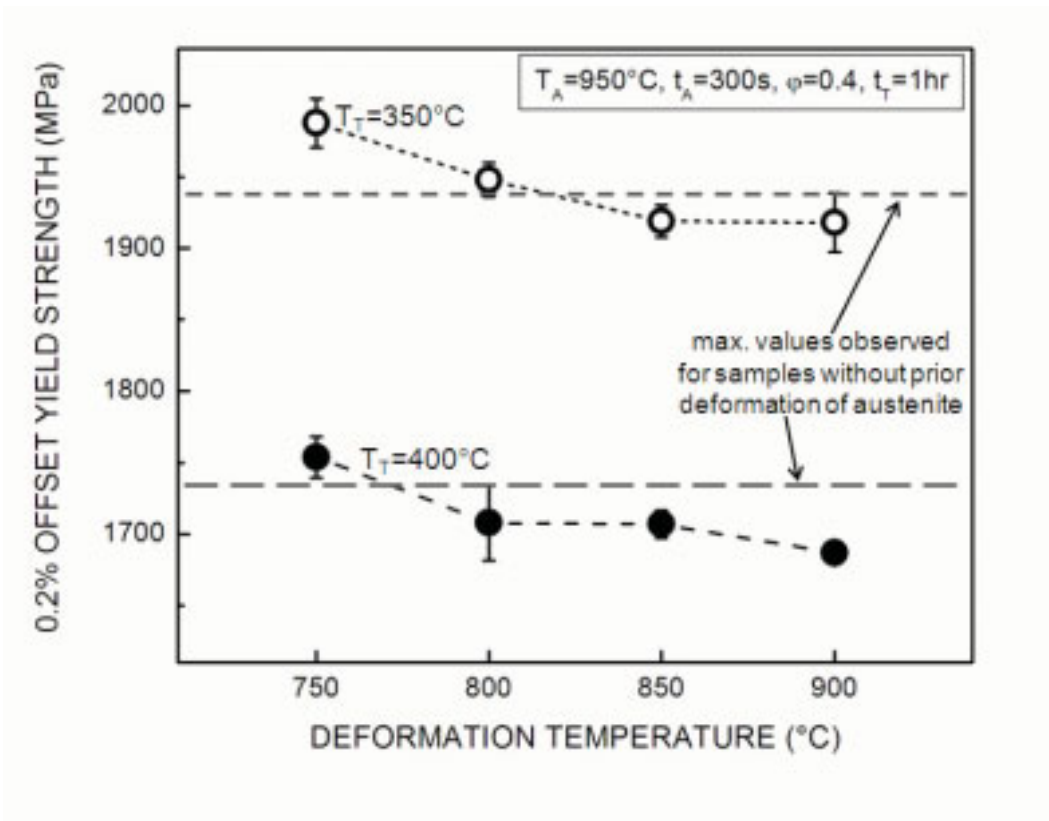


Fig. 58 0.2% offset yield strength of thermomechanically treated samples deformed at different temperatures. Melt CuSn4, austenitization 5 minutes at 950°C.

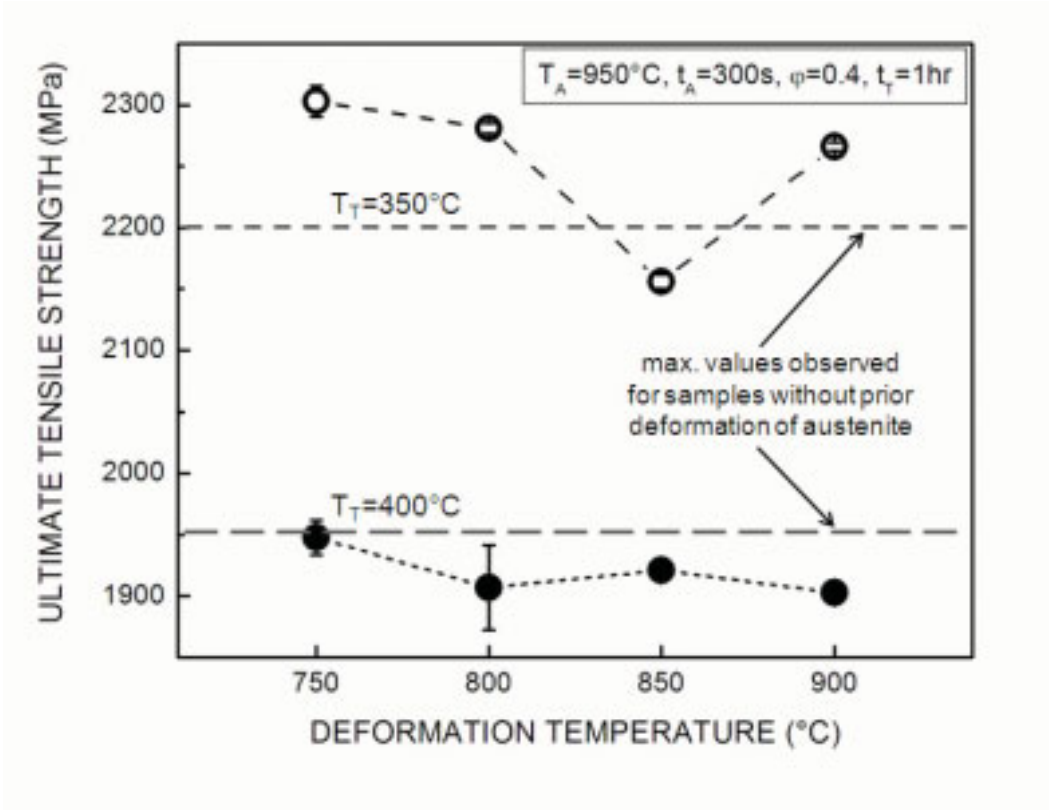


Fig. 59 Ultimate tensile strength of thermomechanically treated samples deformed at different temperatures. Melt CuSn4, austenitization 5 minutes at 950°C.

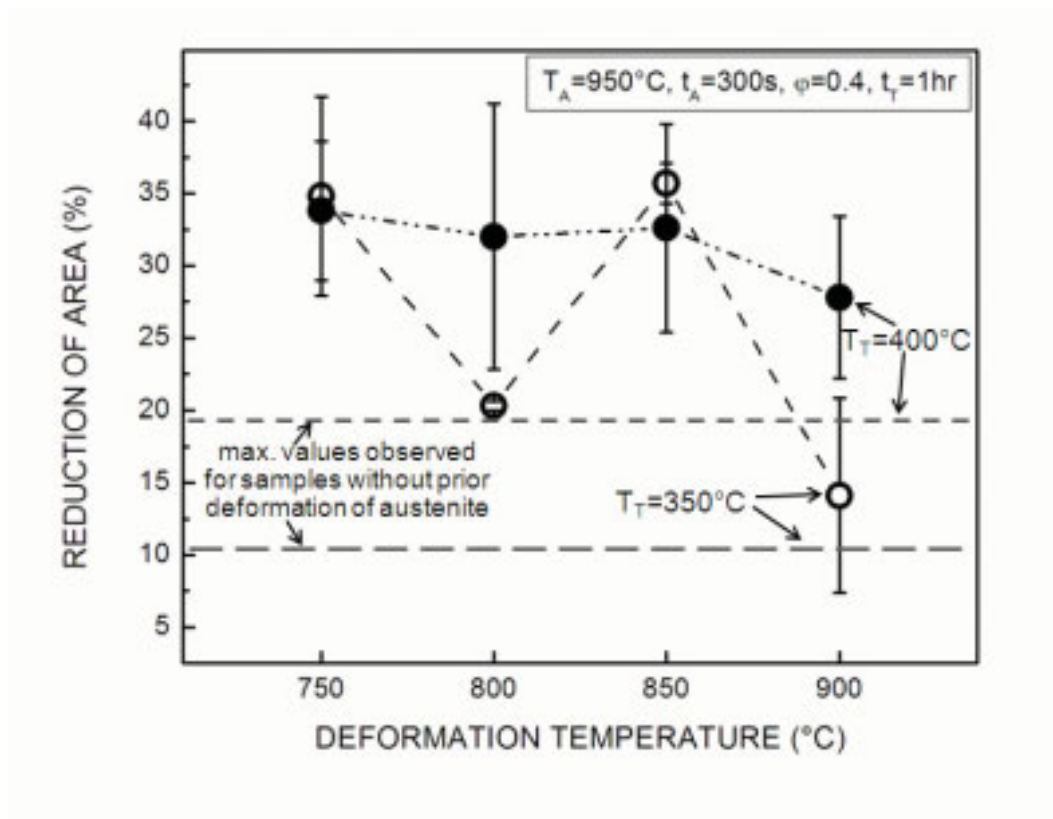


Fig. 60 Reduction of area of thermomechanically treated samples deformed at different temperatures. Melt CuSn4, austenitization 5 minutes at 950°C.

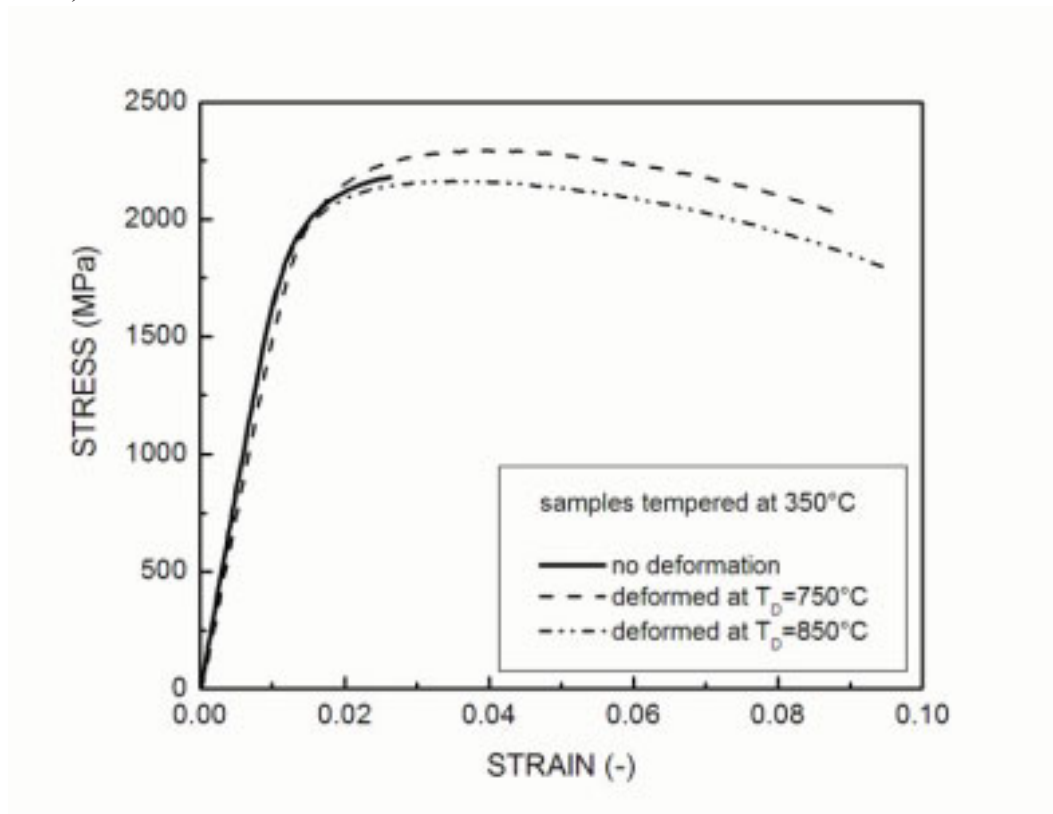


Fig. 61 Engineering stress-strain curves (tensile) for conventional heat treatment (no deformation), and for thermomechanically treated samples

In all cases the austenite deformation increases the reduction of area or the elongation to fracture. Significant increase is observed for deformation temperatures of 850°C and 750°C after tempering at 350°C. Conventionally heat treated samples that are tempered at 350°C fracture before necking starts (Fig. 61), after tempering at 400°C they fracture at strains slightly larger than the uniform strain. Deformation of austenite at 850 or at 750°C increase the uniform elongation of the steel after tempering at 350°C from 1.3 % for conventional heat treatment to 2.4 or 2.6 % respectively. The elongation to fracture is increased from 1.3 to 7.4 (deformation at $T_D=750^\circ\text{C}$) or to 8.3 % ($T_D=850^\circ\text{C}$) (Fig. 61).

The conventionally heat treated sample, tempered at 350 or 400°C and tested in tensile test exhibited a high fraction of intergranular fracture (Fig. 62 a). This corresponds to a low ductility (reduction in area $Z = 15\%$). Additionally, grain separation along the loading direction takes place between prior austenite grains. In contrast to conventionally heat treated samples the thermomechanically processed samples never failed by intergranular fracture. Thermomechanically treated samples always exhibited the higher ductility ($Z > 26\%$). Even after tempering at 350°C, where the conventionally heat treated samples revealed a minimum in ductility, the fracture surface of the thermomechanically processed sample shows a ductile fracture without intergranular fracture (Fig. 62 b).

Similar to the observations made for conventionally heat treated sample in chapter 4.2.3.1 scanning electron microscopy investigations revealed that continuous carbide films are present at flat prior austenite grain boundaries below the tempering temperature of 400°C. The cementite morphology of the conventionally heat treated sample tempered at 350°C is presented in Fig. 63. Cementite forms preferentially at prior austenite grain boundaries and at interfaces between neighbouring martensite laths. Cementite precipitation within individual lath is observed as well. After tempering at 350°C almost all former austenite grain boundaries are occupied with continuous cementite films.

Spheroidization of carbides within the matrix and at the prior austenite grain boundaries starts at 400°C. After tempering at 400°C carbide films consists of a chain of small spherical carbide particles that are still at some areas connected to each other (Fig. 64 a and b). For both tempering temperatures described above disc-like and spherical carbides were observed within individual laths. However, the tempering time and temperature is not sufficient enough to fragment the carbide films at this temperature.

At 450°C carbides at the former grain boundaries are isolated and their shape is spherical or ellipsoidal (Fig. 65). No disc-like or platelet carbides were observed after tempering at 450°C. The size of carbides is larger than those observed after tempering at lower temperatures.

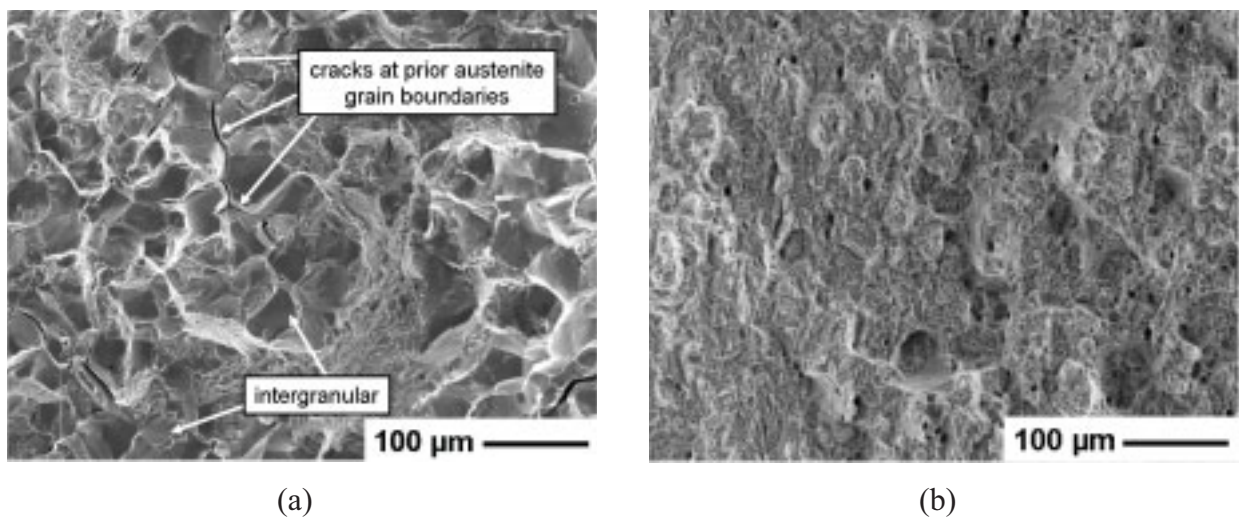


Fig. 62 Fractograph of conventionally heat treated sample (a) tempered at 400°C and exhibiting separation along prior austenite grain boundaries and fractograph of thermomechanically treated sample (b) deformed at $T_D=750^\circ\text{C}$ and tempered at $T_T=350^\circ\text{C}$

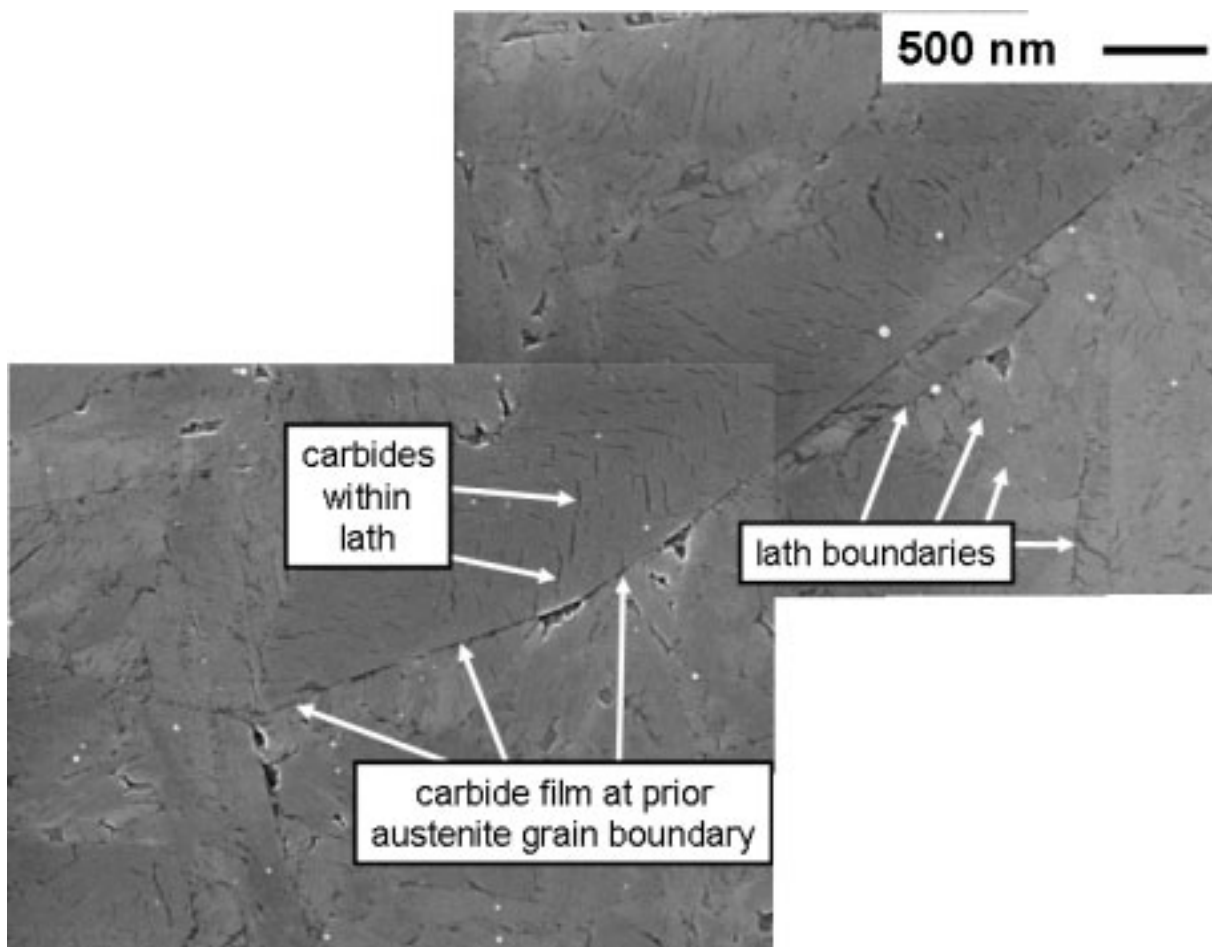


Fig. 63 SEM micrograph showing carbide morphology and distribution of conventionally heat treated specimen. Melt CuSn4 , austenitization 5 minutes at 900°C, tempered at 350°C. Etched in alkaline sodium picrate.

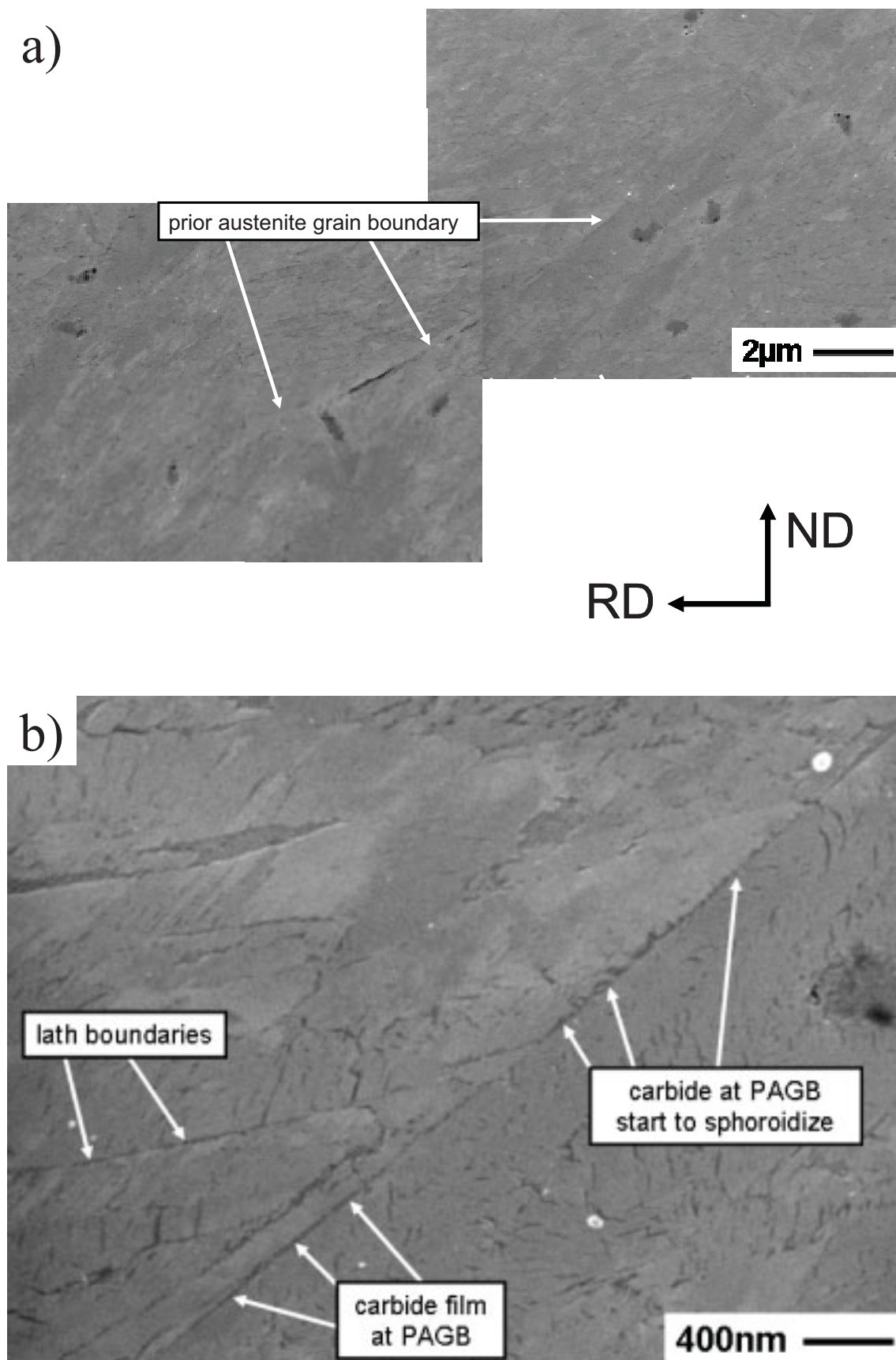


Fig. 64 Carbide morphology at prior austenite grain boundaries for conventionally heat treated samples. Melt CuSn4 , austenitization 5 minutes at 900°C , tempered at 400°C . Etching with sodium picric acid. b) higher magnification of a).

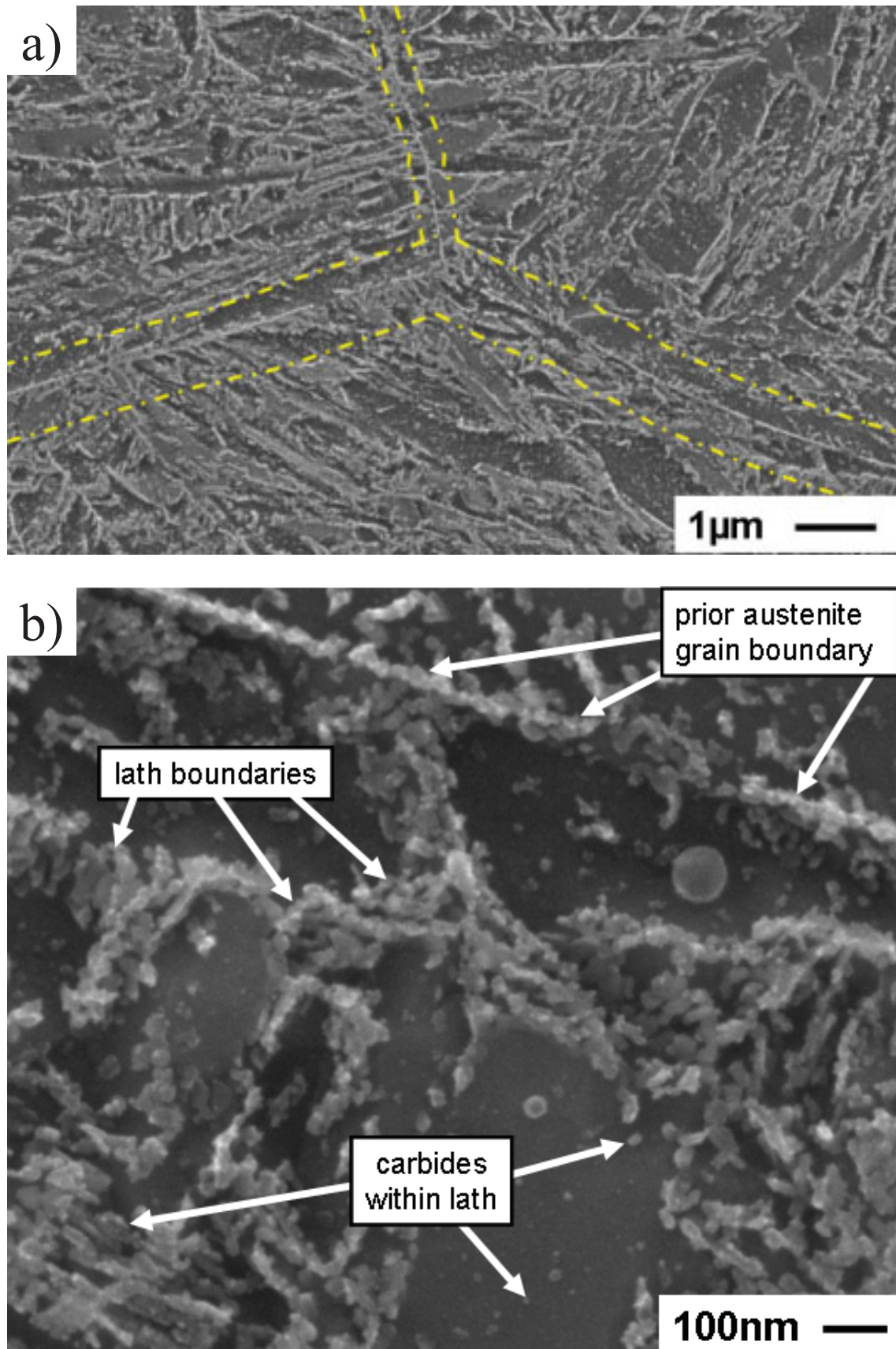


Fig. 65 Carbide morphology at prior austenite grain boundaries for conventionally heat treated samples. Melt CuSn4, austenitization 5 minutes at 900°C, tempered at 450°C. Etching with alcoholic solution of HNO₃ (1 %). b) higher magnification of a).

The variation of the deformation temperature leads to different austenite modifications prior to quenching (4.1.3.2). The austenite was either recrystallized or not recrystallized (sample deformed at 750°C). All the samples deformed above 800°C were recrystallized. However, the carbide morphology at the prior austenite grain boundaries in these samples was different (Fig. 66 to 69).

In the sample deformed at 900°C, flat and curved former austenite grain boundaries were observed (Fig. 66). Cementite films were observed at the flat prior austenite grain boundaries. At prior austenite grain boundaries with a curvature, no cementite films were observed. At some grain boundaries in addition to cementite films an additional thin film was observed. These areas were not severely attacked by the nital etchant, an alcoholic solution of HNO₃. Nital does not react with cementite, or carbides in general but attacks ferrite regions with low carbon concentrations. If the carbon concentration is high, as in the case of retained austenite, etching does not proceed as fast as in the case of ferrite. Therefore, regions not sensitive to nital were identified as retained austenite.

Most of the prior austenite grain boundaries within the sample deformed at 850°C are not flat, but curved (Fig. 67). After tempering at 350°C the carbide films at prior austenite grain boundaries seem to be continuous at small magnifications (Fig. 67a). At higher magnification (Fig. 67b) it becomes clear that most of these prior austenite grain boundaries (PAGB) are decorated with fine and small spherical or ellipsoidal carbides. After tempering at 400°C the carbides at PAGBs are all spherical or ellipsoidal.

Deformation at 800°C leads to curved prior austenite grain boundaries (Fig. 68). In some areas, continuous cementite films were observed, but only on flat boundaries. Additionally, cementite films were observed at martensite lath interfaces.

After ausforming ($T_D=750^\circ\text{C}$) and tempering at 400°C the decoration of the PAGBs is similar to that of samples deformed at 850°C. Tempering at 400°C produces the same grain boundary carbide morphology for both austenite variants prior to quenching, i.e. for the recrystallized and for the non-recrystallized austenite. In contrast, most prior austenite grain boundaries of ausformed samples tempered at 350°C were free of any precipitations (Fig. 69). The carbide morphology at the interfaces between laths and packets was changed too (Fig. 69 b). Compared to the other treatments no pronounced carbide precipitation could be observed after etching.

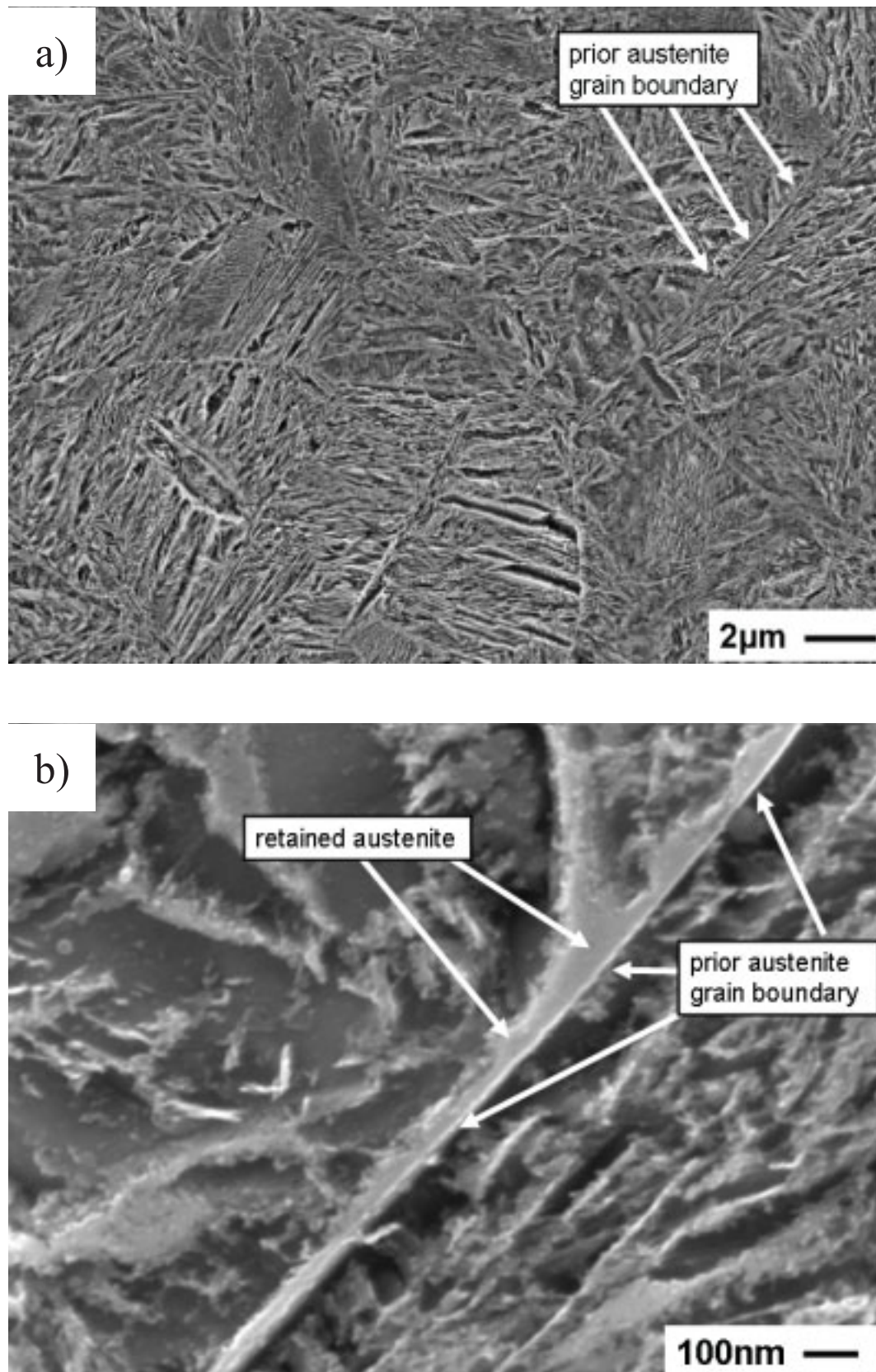


Fig. 66 Microstructure and carbide morphology at prior austenite grain boundaries (PAGB) for thermomechanically treated samples deformed at 900°C. Melt CuSn4, austenitization 5 minutes at 950°C, tempered at 350°C. Etching with alcoholic solution of HNO₃ (1%). b) is a higher magnification of PAGB shown in a).

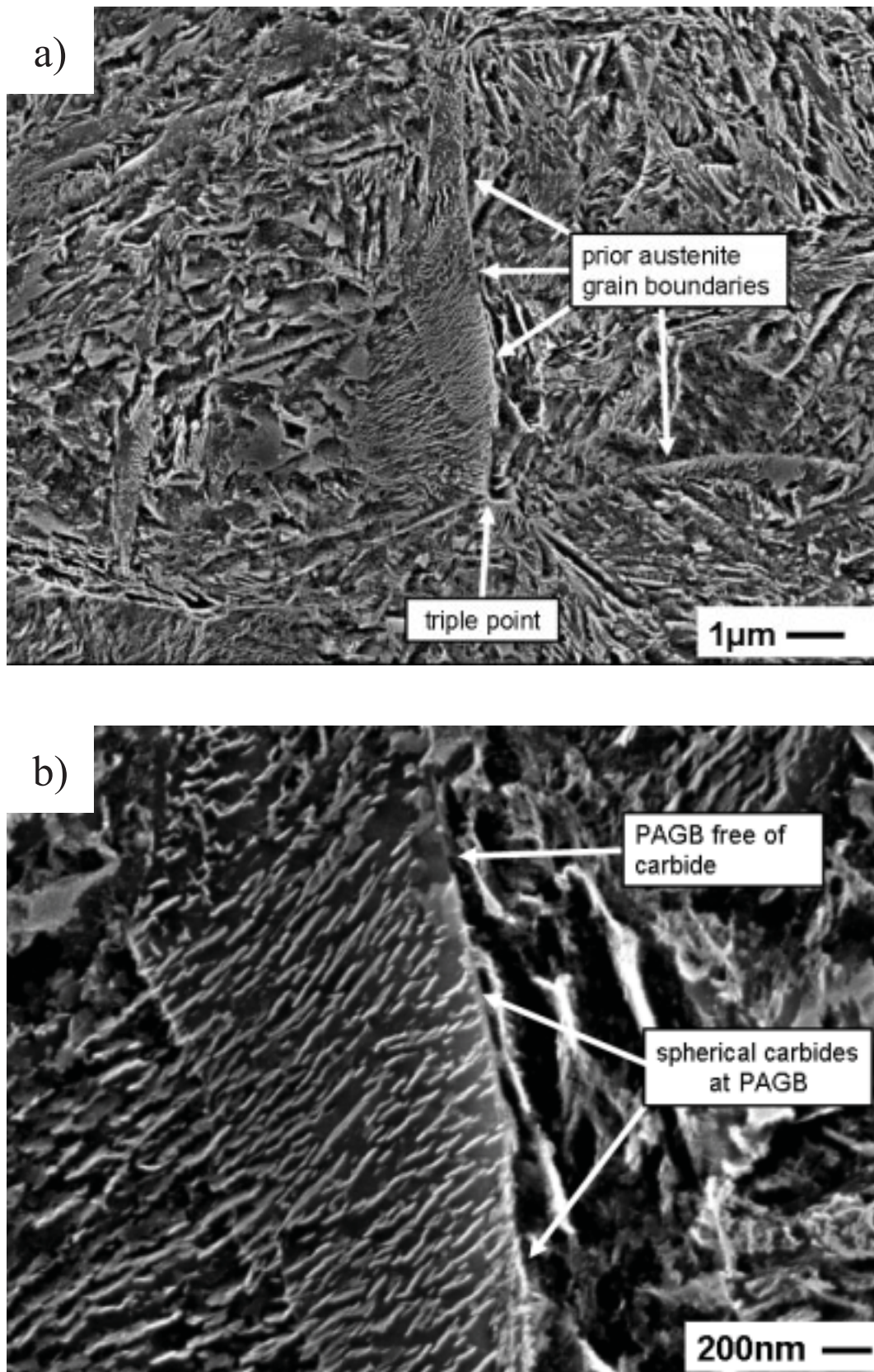


Fig. 67 Microstructure and carbide morphology at prior austenite grain boundaries (PAGB) for thermomechanically treated samples deformed at 850°C. Melt CuSn4, austenitization 5 minutes at 950°C, tempered at 350°C. Etching with alcoholic solution of HNO₃ (1%). b) is a higher magnification of PAGB shown in a).

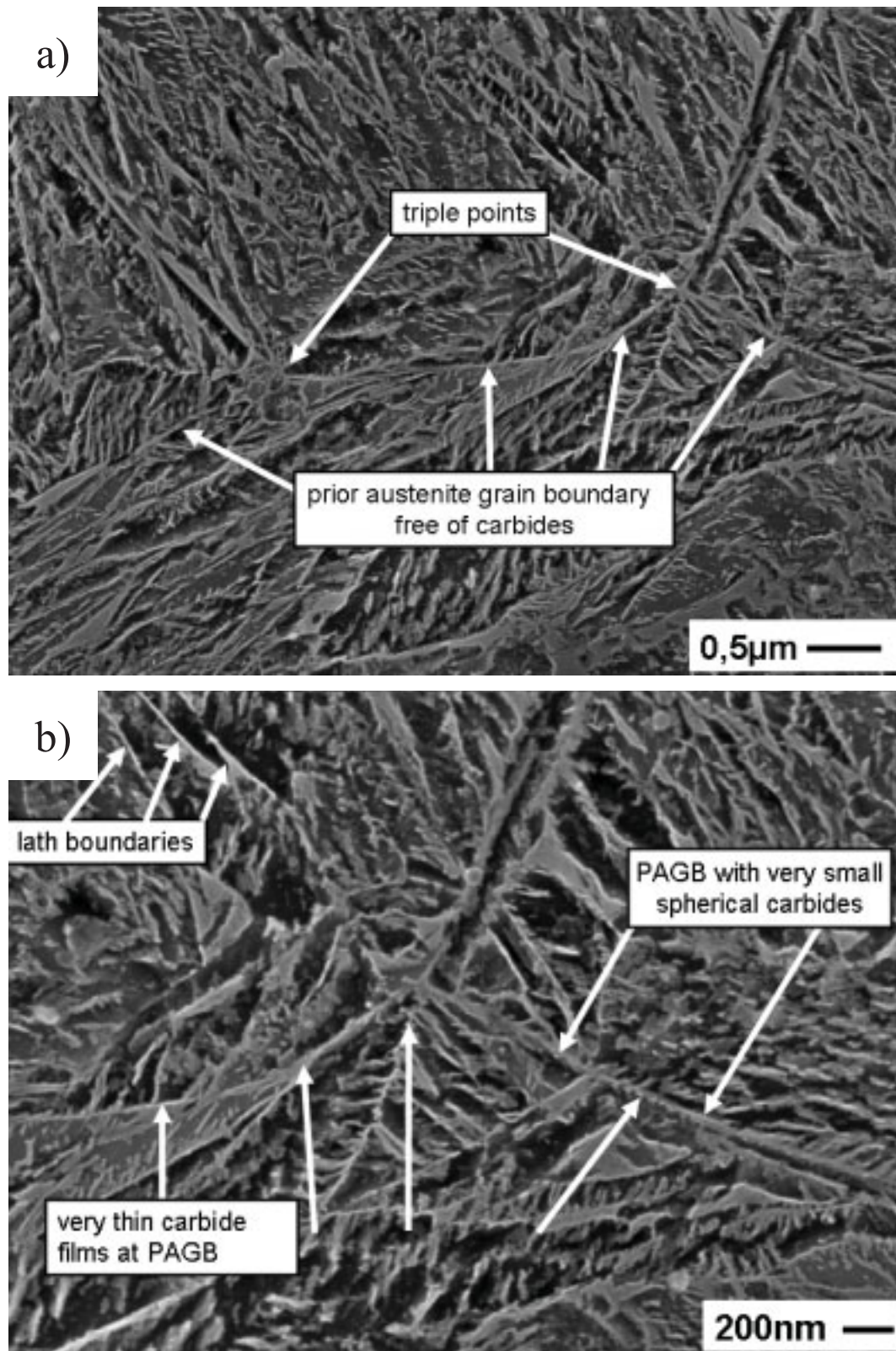


Fig. 68 Microstructure and carbide morphology at prior austenite grain boundaries (PAGB) for thermomechanically treated samples deformed at 800°C. Melt CuSn4, austenitization 5 minutes at 950°C, tempered at 350°C. Etching with alcoholic solution of HNO₃ (1%). b) is a higher magnification of PAGB shown in a).

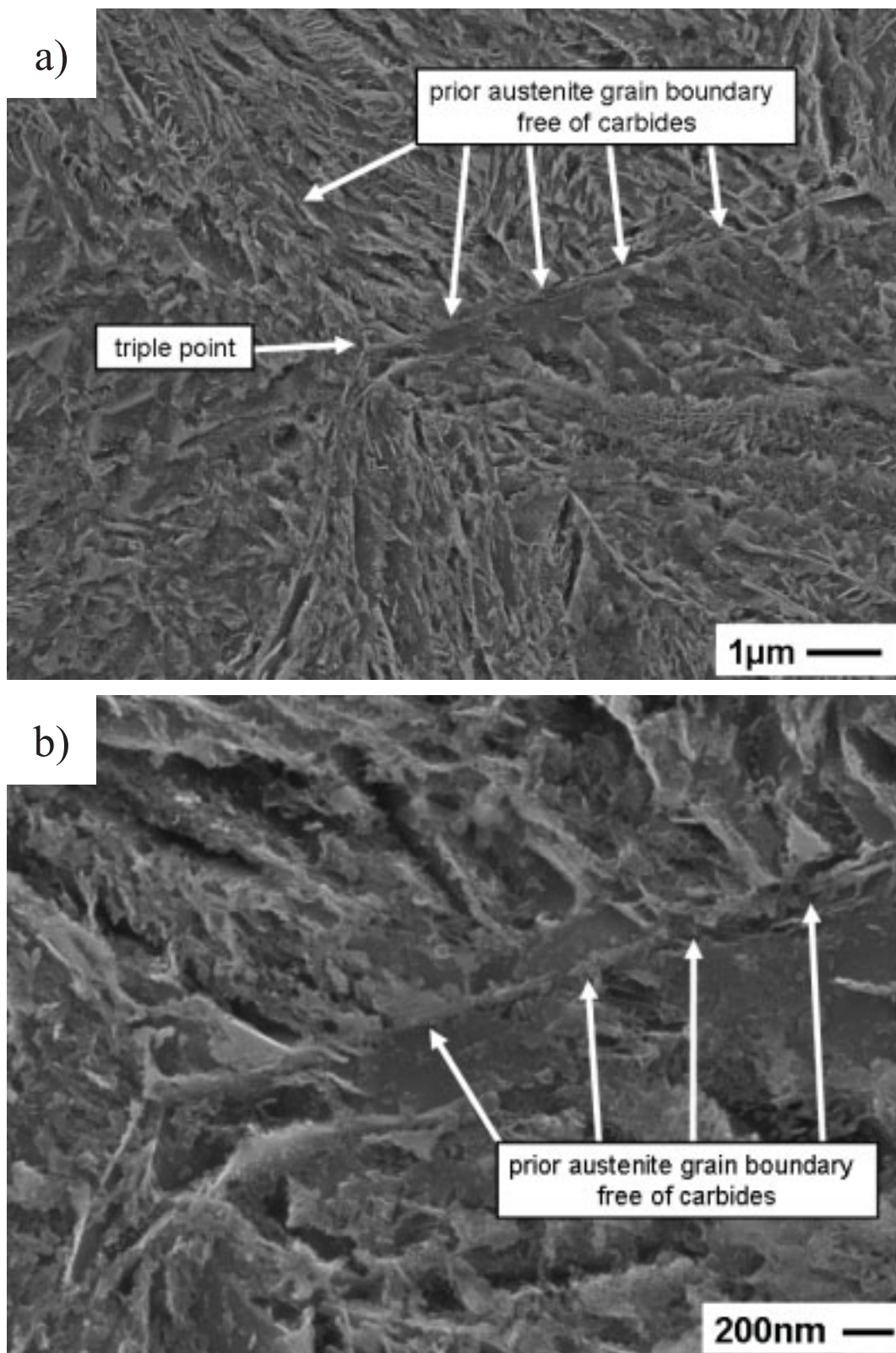


Fig. 69 Microstructure and carbide morphology at prior austenite grain boundaries (PAGB) for thermomechanically treated samples deformed at 750°C. Melt CuSn4, austenitization 5 minutes at 950°C, tempered at 350°C. Etching with alcoholic solution of HNO₃ (1%). b) is a higher magnification of PAGB shown in a).

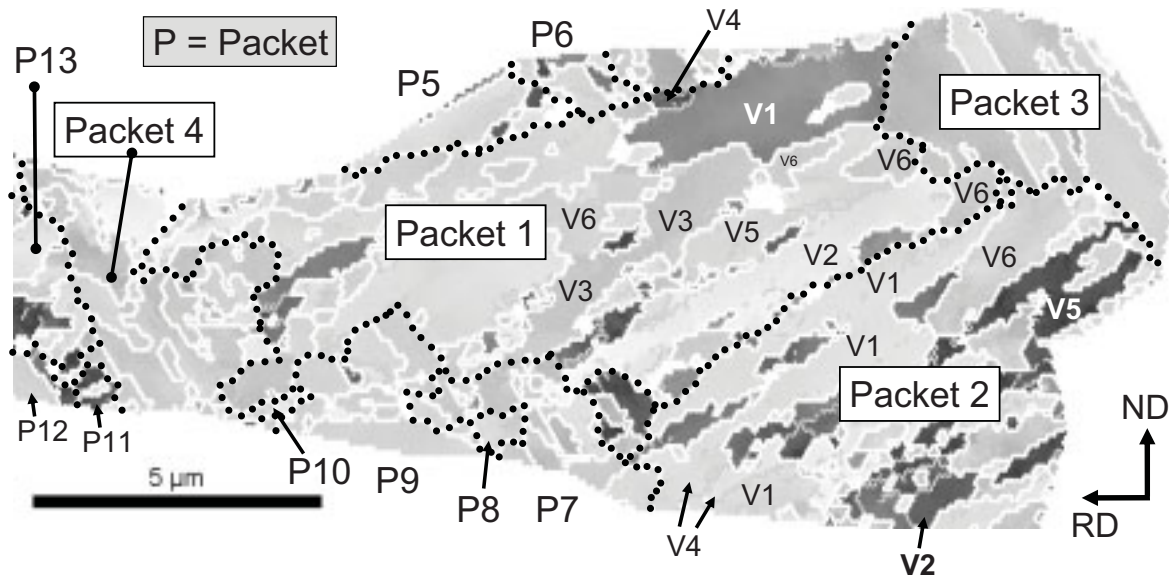


Fig. 70 Variants marked with different grey shades for an isolated prior austenite grain, sample deformed at 750°C, white lines are high angle grain boundaries and enclose individual blocks, black dotted lines mark packet boundaries.

In contrast to the flat appearance of the prior austenite grain boundaries after conventional heat treatment, the typical feature of these former boundaries after thermomechanical treatment was their pronounced curvatures in the micrographs. The occurrence of carbide films was - independent of the process - always linked with flat prior austenite grain boundaries.

In contrast to the conventionally heat treated samples without prior deformation of the austenite in the work-hardened and quenched sample deformed at 750°C most of the former austenite grains consisted mainly of one packet, i.e. in the work-hardened austenite grains one packet, built of lath with the same habit plane, is dominant. There exist as well elongated, work-hardened prior austenite grains that consist of many packets (Fig. 70). All of four possible orientation relationships between densest planes are present in the former austenite grain. Apart from large packets, there are always some small packets.

In the samples deformed above 800°C packets with all the four orientation relationships between the densest planes of parent austenite and tempered martensite according to Kurdjumov-Sachs were observed.

The effective grain size was derived from orientation imaging microscopy data. It is enclosed by high angle grain boundaries and corresponds to the average block area and is presented in Fig. 71 for all the deformation temperatures. The results show, that deformation of the austenite preceding quenching refines the average block area of the final martensite.

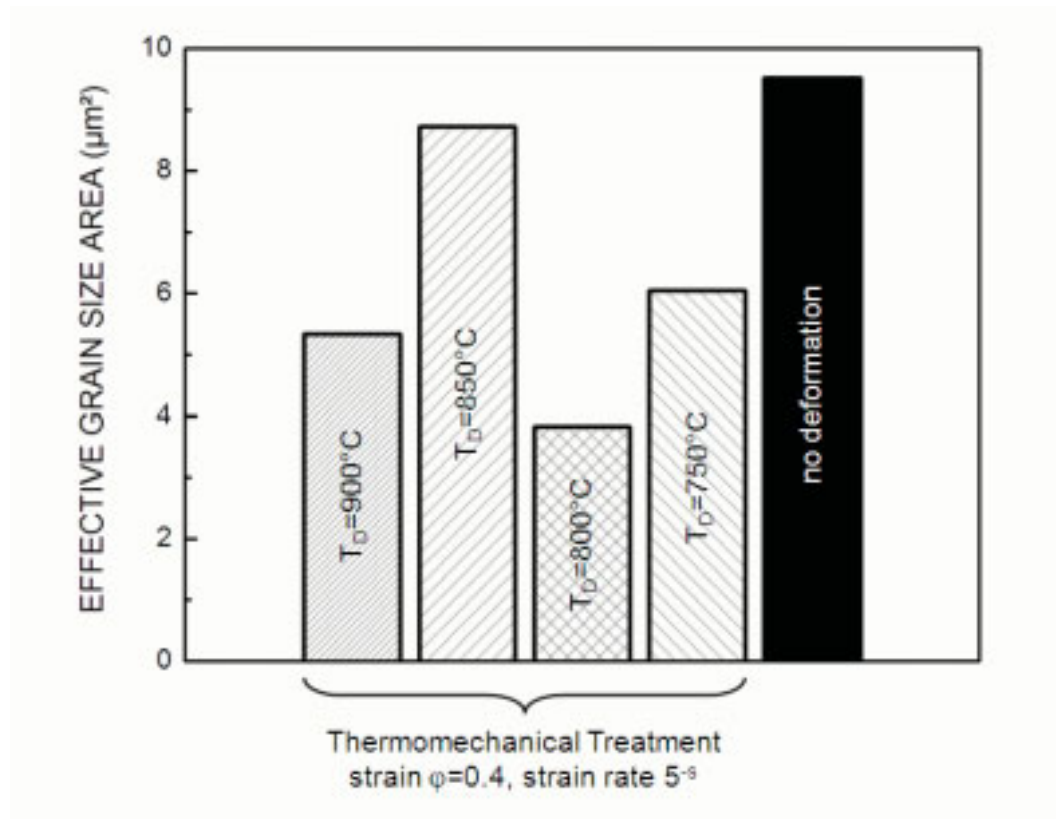


Fig. 71 Influence of austenite deformation temperature on effective grain size area defined as area enclosed by high angle grain boundaries.

4.3.2.3 Discussion

Martensite Morphology. The morphology of the tempered martensite in thermomechanically treated silicon chromium spring steel with 0.56 mass% carbon was studied. The results are presented schematically in Fig. 72. The martensite packet size within recrystallized austenite grains of the same size is not uniform and does not depend on the deformation temperature prior to quenching. If the austenite is work-hardened in some grains only one of the possible orientation relationship between densest plane of the austenite and martensite dominate.

Within a packet all possible six K-S variants for the same γ - α plane relationship exist. Blocks are made either of a single K-S variant or a combination of two specific K-S variants. The same combination of K-S variant pairs is observed for all blocks with two specific variants. This result is in contrast to the observations made for Fe-C alloys with 0.061%C. Morito et al. (2003) showed that for the latter system blocks consist of laths with a single variant and six blocks with different orientations exist in a packet. Whether the difference is due to the chemical composition or due to the deformation of the austenite has to be clarified.

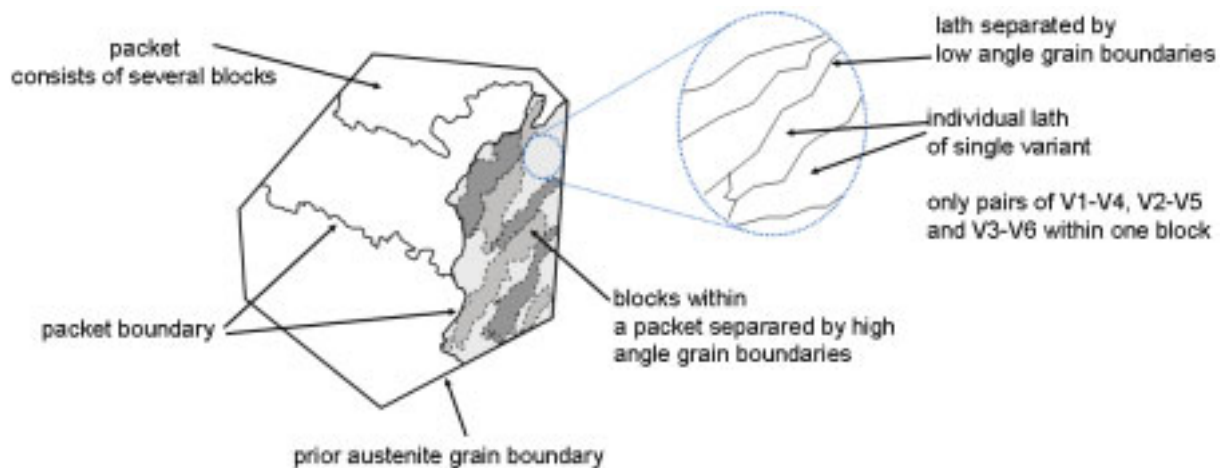


Fig. 72 Schematic drawing showing martensite morphology in Si-Cr spring steel

The refinement of the martensite microstructure is shown as a refinement of the average block area. The average block area is expressed as the average effective grain size. Thus, the refinement of the block size might be a contribution to the increased ductility observed for the thermomechanical treatment.

Precipitation. For Fe-2%Mn-0.36%C Yusa et. al. (1999) showed that grain boundary carbides can be refined by ausforming. They performed the deformation of the austenite with 80% reduction and immediate quenching after deformation. They related the carbon refinement to the serrated structure of the prior austenite grain boundaries. In Fig. 73 the carbide distribution observed in our study after tempering is shown schematically for conventionally heat treated and thermomechanically processed samples. Grain boundary carbides can be refined by high temperature thermomechanical treatment HTMT (recrystallized austenite prior to quenching) and by a low temperature thermomechanical treatment LTMT or modified ausforming (forming in metastable austenite region without recrystallization). The employed strain rate in this work was lower ($5s^{-1}$) than those used by Yusa et al. ($10s^{-1}$). Thus due to the lower strain rate no pronounced serration was observed. However, the ausforming resulted in former austenite grain boundaries free of carbides and in a higher ductility. For the same etching conditions (temperature, time, etchant used), less topology effects were developed during etching for the ausformed samples (compare Fig. 66 to 69). Less cementite was observed within the matrix at magnifications up to 100000, because etching did not produce a structure with clear, sharp edges that can be distinguished easily as a separate phase. Hence, we conclude that the resultant dislocation substructure in the austenite after the ausforming is stabilized by the diffusion of carbon atoms prior to quenching to the dislocation cores. During

transformation this dislocation substructure together with the segregated carbon atoms at the dislocation core is inherited from the parent austenite phase to the final martensite product phase. This leads to either smaller carbides after tempering at low temperatures or delays the precipitation reaction, because diffusion of carbon atoms out of the dislocation core is not favourable and increases the internal distortion energy.

Deformation at 850°C leads to equiaxed austenite grains prior to quenching. Due to this fact and the fact that the austenite grains observed were smaller than those after conventional heat treatment, it was deduced that the austenite had recrystallized prior to quenching. Observation with scanning electron microscopy revealed that the prior austenite grain boundaries were curved. Thus the observed variety in carbide morphology and size after thermomechanical treatment and deformation at $T_D=850^\circ\text{C}$ can be related to the curvature of the prior austenite grain boundaries. In addition to the grain boundary energy the activation energy for the critical nucleus formation of the precipitates depends on the orientation of the grain boundary plane (Lee and Aronson 1975 a and b). If the boundaries are flat, as was observed for conventional heat treatment, only the variant with the smallest critical nucleus energy will form. As a result several carbides will form with the same orientation relationship to the neighbouring grains and these particles will grow at the former austenite grain boundary until they touch each other and coagulate. At a curved boundary either the interface properties change or the growing carbide variant changes direction. In both cases the carbide particles do not coagulate with each other to form a continuous film at the prior austenite grain boundary. A curved boundary could therefore be the reason for the carbide refinement at the prior austenite grain boundaries of thermomechanically treated samples.

The increase in ductility can not only be attributed to the refinement of carbides. The steel in this study contains in addition to 120 ppm phosphorous a high content of copper and tin. In chapter 4.2 it is shown that for conventional heat treatment and for constant P content the ductility of samples tempered at 400°C strongly depends on the copper and tin concentration. Because in the tempering range of 350 to 400°C the diffusivity of tin is very small, and the holding time is very short, equilibrium grain boundary segregation during tempering can be neglected. According to Grabke's investigation (1989) there is a rather low tendency for grain boundary segregation of tin in alpha iron. Furthermore, as there are a limited number of vacant sites at the prior austenite grain boundary to which the atoms can segregate, and as the carbon diffusivity is much faster, the tin is replaced by carbon atoms from grain boundaries as the carbon content increases. From the observations made for conventional heat treatment, we

can state that the negative effect of copper and tin on the ductility of the tempered martensitic silicon chromium steel is eliminated by austenite deformation.

Therefore the solid phase reactions like recovery, recrystallization, diffusion and segregation taking place after the deformation and prior to quenching should not be neglected. It has been shown that recrystallization of austenite can lead to an enrichment of phosphorous at the grain boundaries (Abe et al. 1990). But depending on the deformation conditions and the temperature time evolution after deformation the grain boundaries might be cleansed as well from impurity and tramp elements. The main factor here is the actual grain boundary migration velocity during recrystallization.

From the observation made here, it can only be deduced that austenite deformation refines the grain boundary carbides. But it should be noted, that the improved ductility is not only a result of grain boundary carbide refinement, but might as well be enhanced by the redistribution of the impurity elements and refinement of the martensite structure.

Because the deformation temperatures of 850°C and 750°C lead to the most promising combination of tensile properties and because they represent two different austenite conditions, namely the recrystallized and non-recrystallized austenite, they were selected for further study of the thermomechanical treatment.

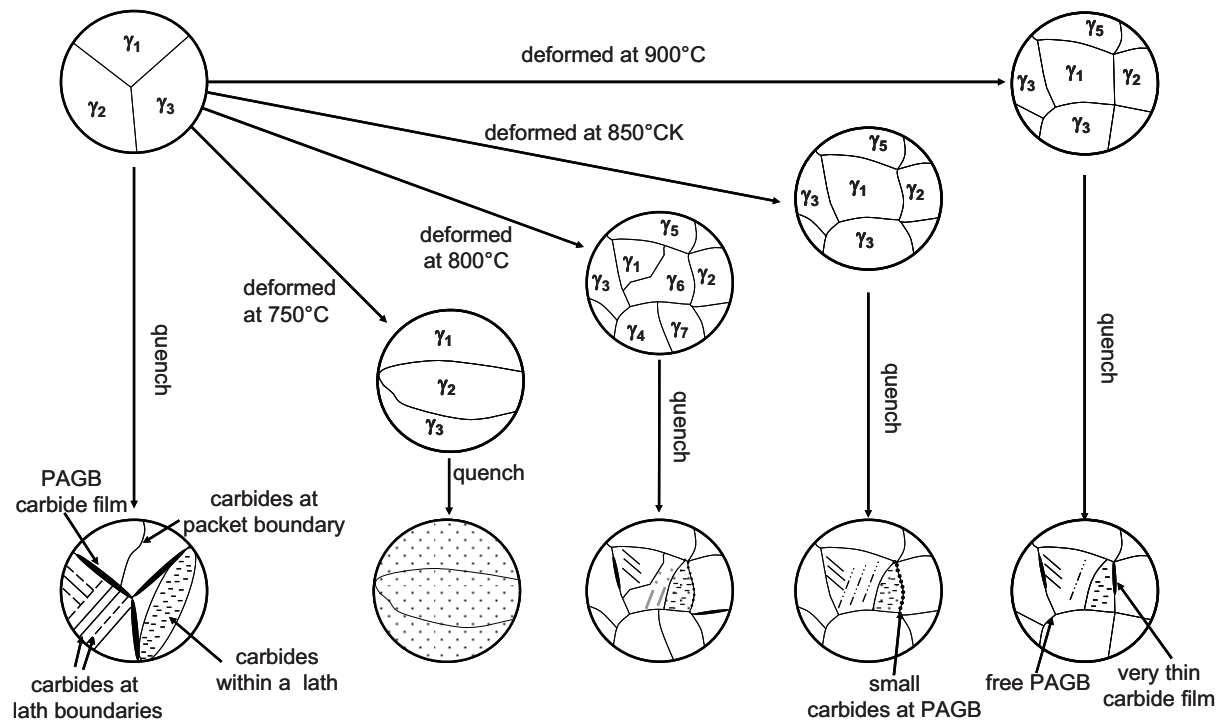


Fig. 73 Schematic illustration showing the different types of carbide morphologies and their distribution within individual lath, at lath and packet interfaces and at prior austenite grain boundaries (PAGB) observed for conventional heat treatment and thermomechanical treatment after tempering at 350°C.

4.3.3 AUSTENITIZATION TEMPERATURE AND STRATEGY FOR THERMOMECHANICAL TREATMENT

4.3.3.1 Experimental

Tests were carried out to ascertain the sensitivity of thermomechanical treatments to austenitization temperature. The variation of austenitization temperature will affect austenite grain size and impurity concentration at the austenite grain boundaries before deformation. The test parameters are presented in table 8. Thermomechanical treatment samples of the melt with the highest phosphorous content (melt P3, $c(P)=0.02213$ mass %) were heated to austenitization temperatures of 900, 950 and 1000°C. Thereafter the samples were subjected to different thermomechanical treatments. They were once deformed at 850 or at 750°C with a logarithmic strain of 0.4 or successively deformed at both temperatures. The total logarithmic strain for the two-step treatments with two deformations was either 0.4 (0.2 per deformation) or 0.8 (0.4 per each deformation). After quenching all samples were tempered for one hour at 300°C. The tensile properties of the thermomechanically treated samples were compared with those of conventionally heat treated sample of the same melt tempered at 300°C.

Table 8 Parameters for optimization of austenitization condition for thermomechanical treatment. Tempering time was one hour for all tests.

Treatment	Austenitization		Deformation				Tempering
	T _A (°C)	t _A (s)	T _{D1} (°C)	φ ₁ (-)	T _{D2} (°C)	φ ₂ (-)	
CHT	900	300	-	-	-	-	300
TMT_{RX}	900						
	950	300	850	0.4	-	-	300
	1000						
TMT_{NRX}	900						
	950	300	750	0.4	-	-	300
	1000						
TMT_{2-step}	900						
	1000	300	850	0.2	750	0.2	300
TMT_{RX+NRX}	900	300	850	0.4	750	0.4	300

4.3.3.2 Results

Independent of austenitization temperature, all deformed samples exhibited a higher ductility, i.e. a higher reduction of area (Fig. 74) or elongation to fracture, and a higher tensile strength (Fig. 75). The tensile strength was enhanced at minimum 50MPa. Among the thermomechanically treated samples the work-hardened austenite conditions have the higher strength after tempering at 300°C.

The ductility of the recrystallized austenite condition (TMT_{RX}) is almost independent from the austenitization temperature. The sample annealed at the highest austenitization temperature exhibits the largest scatter. With decreasing austenitization temperature the reduction of area of the work-hardened austenite condition (TMT_{NRX}) increases. The standard deviation reduces with decreasing austenitization temperature. The optical micrographs of the thermomechanically treated samples deformed once are shown in Fig. 76. Samples deformed at 850°C have equiaxial austenite grains. The sample austenitized at 1000°C has an average austenite grain size of ASTM 10, at 950°C an ASTM 7 and at 900°C an ASTM 9. Samples deformed at 750°C show elongated austenite grains. The average austenite grain size is smaller for lower austenitization temperatures.

Samples which were first deformed with a strain of 0.2 at 850°C and then again with the same deformation strain at 750°C exhibit a high level of reduction of area at the highest and lowest austenitization temperature. The standard deviation of these samples is very low. Optical micrography revealed that extremely large grains exist within the sample austenitized at 1000°C and deformed twice with a strain of 0.2 (Fig. 77 a). If the austenitization is carried out at 900°C the grain size is reduced (Fig. 77 b). The sample austenitized at 900°C and deformed twice with a strain of $\varphi=0.4$ (total strain of $\varphi_{tot}=0.8$) shows the highest ductility. The sample exhibited refined and elongated austenite grains with an ASTM grain size number of 9 corresponding to average austenite grain diameter of 16 μm .

In Fig. 78 the reduction of area is shown as a function of average austenite grain diameter for all thermomechanically treated samples and the conventionally heat treated sample tempered at 300°C. There is not a general dependence of reduction of area on the average austenite grain size. The reduction of area of the work-hardened austenite condition (TMT_{NRX}) decreases with increasing average austenite grain size. There is no relation for the recrystallized austenite condition and for the samples deformed twice with a strain of $\varphi=0.2$.

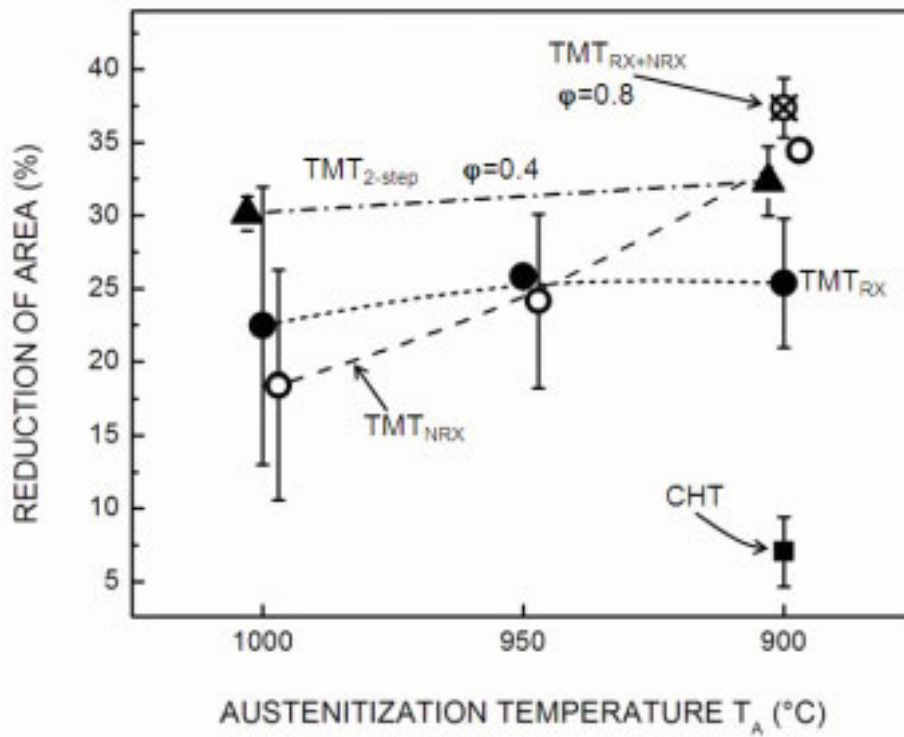


Fig. 74 Reduction of area over austenitization temperature and process. Samples austenitized at different temperatures (see table 8) directly quenched or first deformed and quenched and finally tempered.

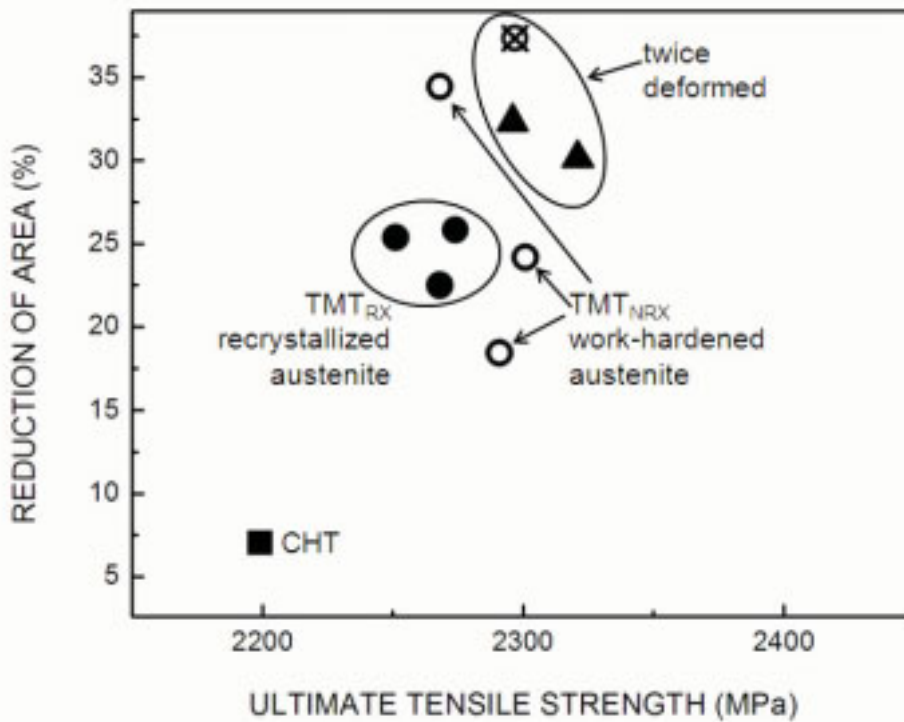


Fig. 75 Reduction of area over ultimate tensile strength for different processes within the austenitization range of 900 to 1000°C. Processing see former figure or table 8.

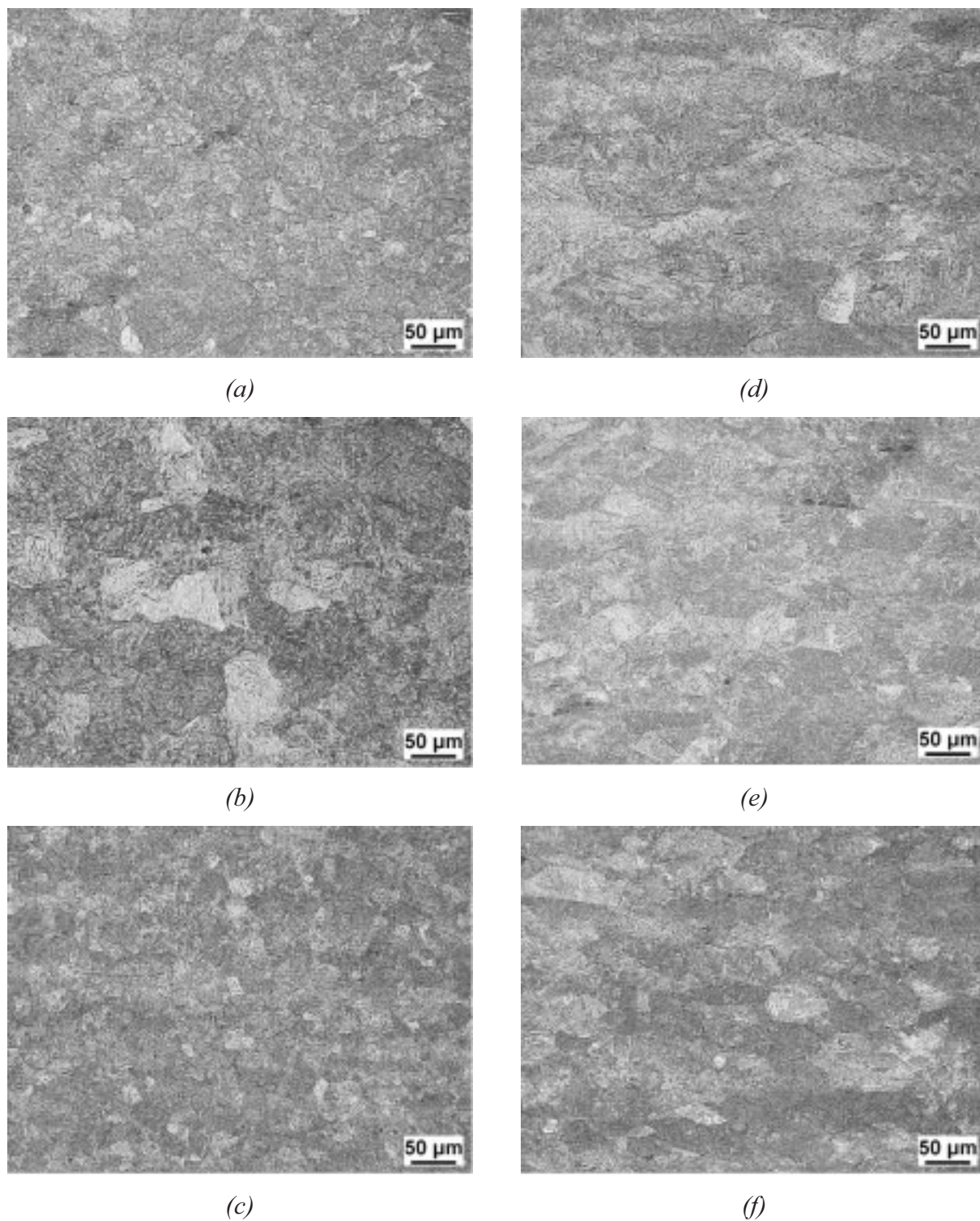


Fig. 76 Optical micrographs of thermomechanically treated samples austenitized at 1000°C (a and d), at 950°C (b and e) and at 900°C (c and f). Samples deformed at 850°C are placed at the left column, samples deformed at 750°C at the right column.

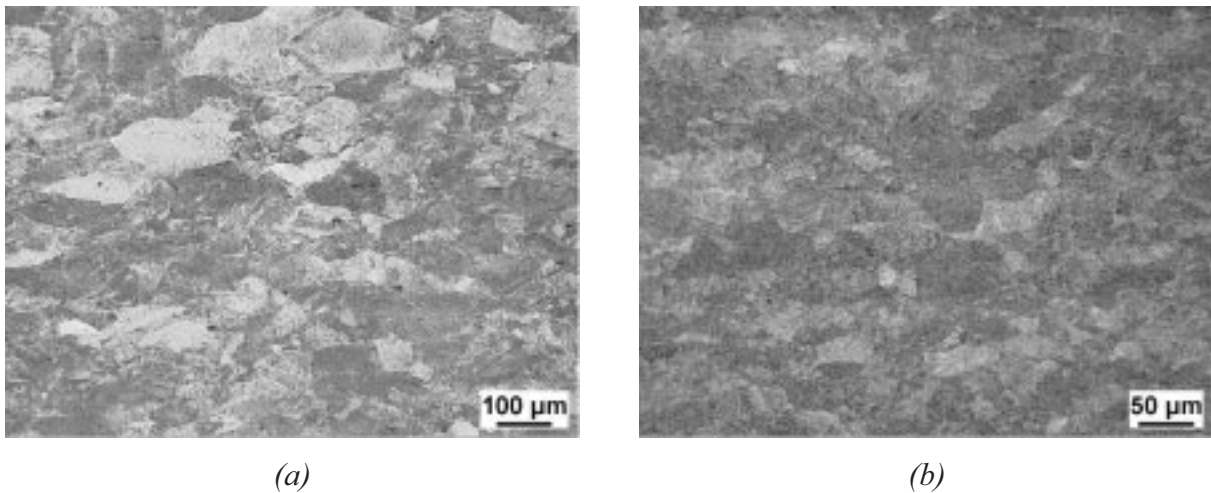


Fig. 77 Optical micrographs of thermomechanically treated samples with deformations of 0.2 at 850 and 750°C austenitized at 1000°C (left) and at 900°C (right).

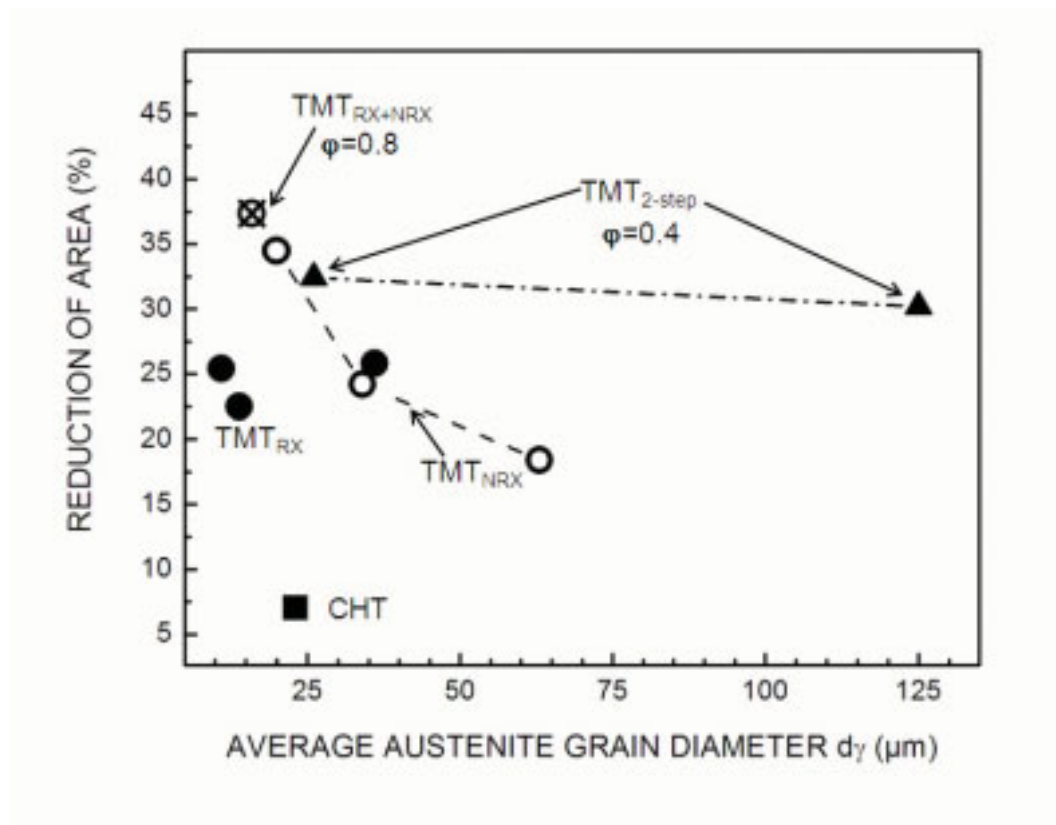


Fig. 78 Reduction of area as a function of average austenite grain size. All samples tempered at 300°C.

4.3.3.3 Discussion

The deformation of austenite results in a higher ductility. Two different austenite conditions were first tested, the recrystallized and the work-hardened. The first austenite condition

delivers ductilities insensitive to austenitization temperature. Because the recrystallization takes place after deformation and before quenching the effect of austenitization temperature and the grain size obtained by this operation is minimized by the recrystallization. It results in almost equivalent average austenite grain size. During recrystallization new grains are formed and new grain boundaries are generated. As a consequence the grain boundary concentration of impurity elements such as phosphorous has changed during this process. From the results of tensile testing we conclude that deformation at 850°C with a strain of $\varphi=0.4$ and the subsequent recrystallization preceding quenching averages out the effect of grain size and grain boundary segregation of different austenitization temperatures.

For the work-hardened austenite condition the situation is slightly different. The ductility values are dependent on the austenitization temperature. First, the deformation at 750°C does not change the austenite grain size that has been determined by austenitization temperature. Because no recrystallization follows the deformation the grains are only elongated. Secondly, no new grain boundaries are created and therefore the concentration of elements at grain boundaries remains equal before and after deformation. However, the work-hardened austenite condition results in a remarkable reduction of area or elongation to fracture after austenitization at 900°C. Thus it is concluded that the austenite subgrain structure produced with the deformation at 750°C is very effective in improving the ductility.

The two-step strategies presented were defined after evaluation of the above results for the two austenite conditions. The first deformation should equalize the effect of austenitization temperature while the second should improve the internal structure of the grains for optimized ductility. In a first trial the total deformation strain was kept constant, but the observations showed that the lower deformations lead to an abnormal grain growth. Although grains were larger than those observed for samples without deformation the ductility was significantly improved. This result shows the importance of the defect structure within the austenite grains for the final properties of martensite as was shown as well in the previous chapter.

To further optimize the thermomechanical treatment the deformation strain for each step was increased to 0.4. Recrystallization was achieved in a first step. In a second step the recrystallized austenite was work-hardened. Such a thermomechanical route combines both of the single step thermomechanical treatments. Because the lowest austenitization temperature (900°C) gives the best combination of strength and ductility for the optimized two-step thermomechanical treatment this temperature was selected.

4.3.4 TENSILE PROPERTY AFTER AUSTENITE CONDITIONING

In the previous chapters it was shown that both a recrystallized austenite and non-recrystallized austenite conditions can lead to high ductilities at high strength levels. The sensitivity of the ductility as a function of austenitization temperature was explored for both conditions and it was concluded that a two-step thermomechanical treatment could achieve optimum results. In this chapter the tensile test results for all three variants for various impurity element levels and tempering temperatures, i.e. for different strength levels, are presented.

4.3.4.1 Experimental

Samples of melts P1 to P3 and CuSn1 to CuSn4 (see table 4) were subjected to thermomechanical treatments presented in Fig. 79. The results are compared with samples that were conventionally heat treated (see 4.2). The recrystallized (TMT_{RX}) and non-recrystallized (TMT_{NRX}) austenite condition were obtained after deformation at 850°C and 750°C, respectively (Fig. 79). The third austenite condition (TMT_{RX+NRX}) was produced by a sequence of two deformations, the first at 850°C and the second at 750°C. The tempering temperature was varied between 300 and 400°C. Samples deformed twice (TMT_{RX+NRX}) were only tempered at 300°C.

Tensile testing and microstructure characterization was carried out as described in 3.

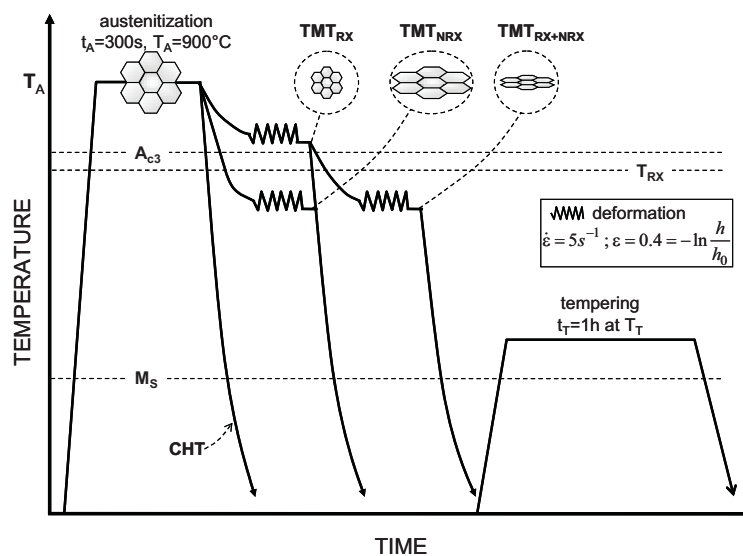


Fig. 79 Schematic representation of the tested thermomechanical procedures

4.3.3.2 Results

The 0.2% offset tensile yield strength and reduction of area of the thermomechanical treatments described above and in Fig. 79 is presented for all the phosphorous levels in Fig. 80 to 82. In all the diagrams the values for conventionally heat treated samples tempered at 300 and 450°C is presented as reference in grey (squares).

The 0.2% offset yield strength values of the recrystallized austenite tempered at 300°C are equivalent with the values obtained after conventional heat treatment. At the same time we observe that the reduction of area is equivalent to conventionally heat treated samples that were tempered at 450°C, i.e. the thermomechanically treated samples exhibit the same ductility than the latter samples with a tensile yield strength which is at least 400 MPa higher. The ductility of the thermomechanically treated samples tempered at 300°C is dependent on the phosphorous level.

Increasing the tempering temperature to 350°C increases the reduction of area at least 5 % without significant loss in tensile strength. Further increase of tempering temperature results in a slight increase of ductility but lowers the tensile strength significantly, i.e. more than 200 MPa. In contrast to samples tempered at 300°C the thermomechanically treated (TMT_{RX}) samples tempered at 400°C show no loss of ductility with increasing phosphorous content.

Work-hardening of austenite prior to quenching enhances the strength after tempering at 300°C (Fig. 81). The strength of samples tempered at 350°C is equivalent to conventionally heat treated samples tempered at 300°C. The increase in ductility for the same tempering temperatures is not as high as for the recrystallized austenite condition. However, the reduction of area shows no loss with increasing phosphorous content after tempering at 300 or 350°C. The highest ductility is observed for both tempering temperatures at the highest phosphorous level.

The integration of the two single-step thermomechanical treatment, i.e. the combination of recrystallization and work-hardening (TMT_{RX+NRX}) results in reduction of area values superior to all other processes. In Fig. 82 the 0.2% offset tensile strength and ductility are presented. The strength is equivalent to conventionally processed samples while the ductility of samples tempered at 300°C are significantly higher than conventionally heat treated samples tempered at 450°C. In other words, the strength and ductility combination is remarkably increased by the two-step thermomechanical process. No decrease of reduction of area is observed with increasing phosphorous content.

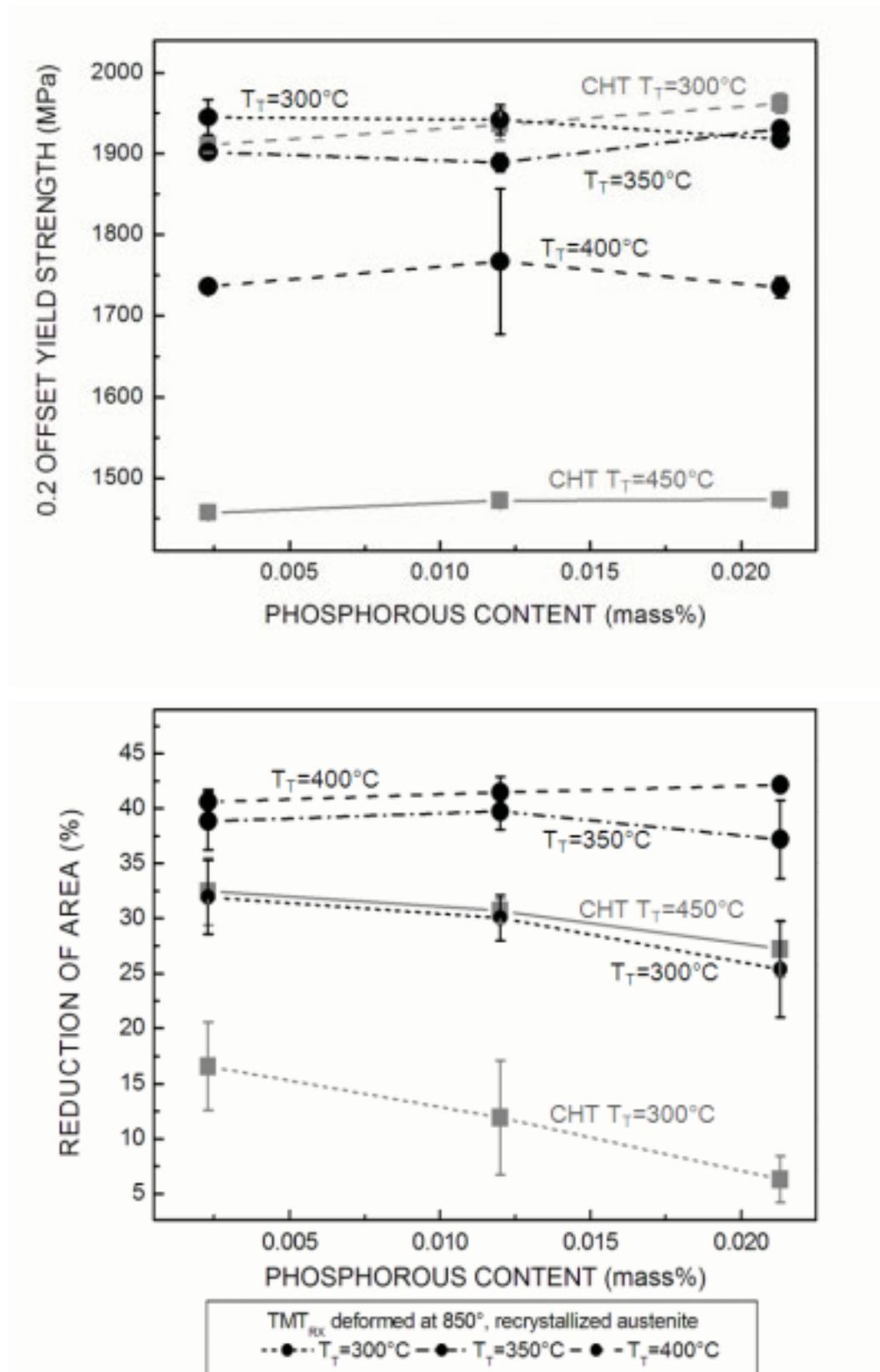


Fig. 80 0.2 offset yield strength (top) and reduction of area (bottom) of thermomechanically treated samples (TMT_{Rx}) as a function of phosphorous content for 54SiCr6. Recrystallized austenite condition produced by deformation of austenite at 850°C prior to quenching. CHT: conventionally heat treated samples.

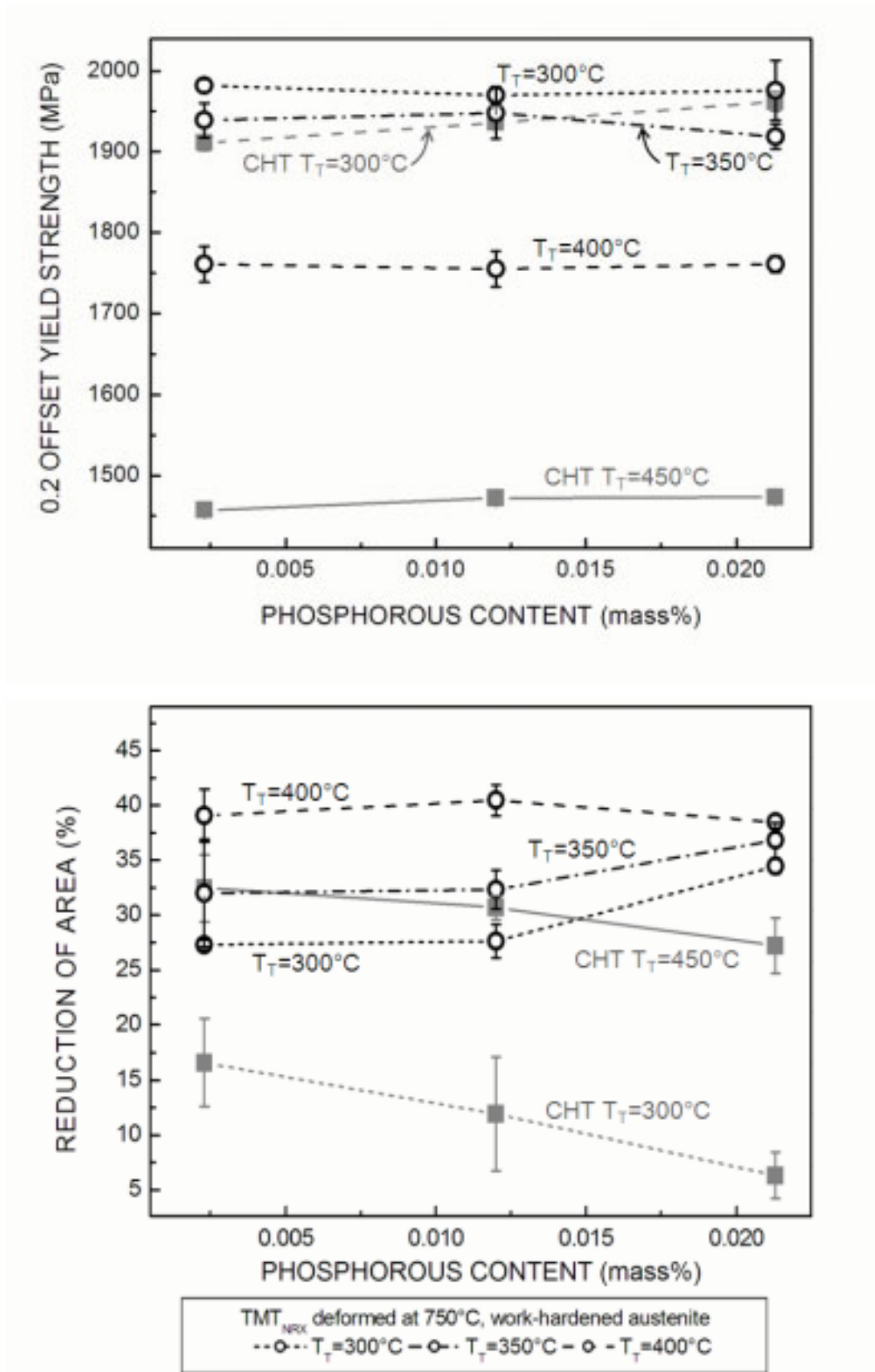


Fig. 81 0.2 offset yield strength (top) and reduction of area (bottom) of thermomechanically treated samples as a function of phosphorous content for 54SiCr6. Work-hardened austenite condition produced by deformation of austenite at 750°C. CHT: conventionally heat treated samples.

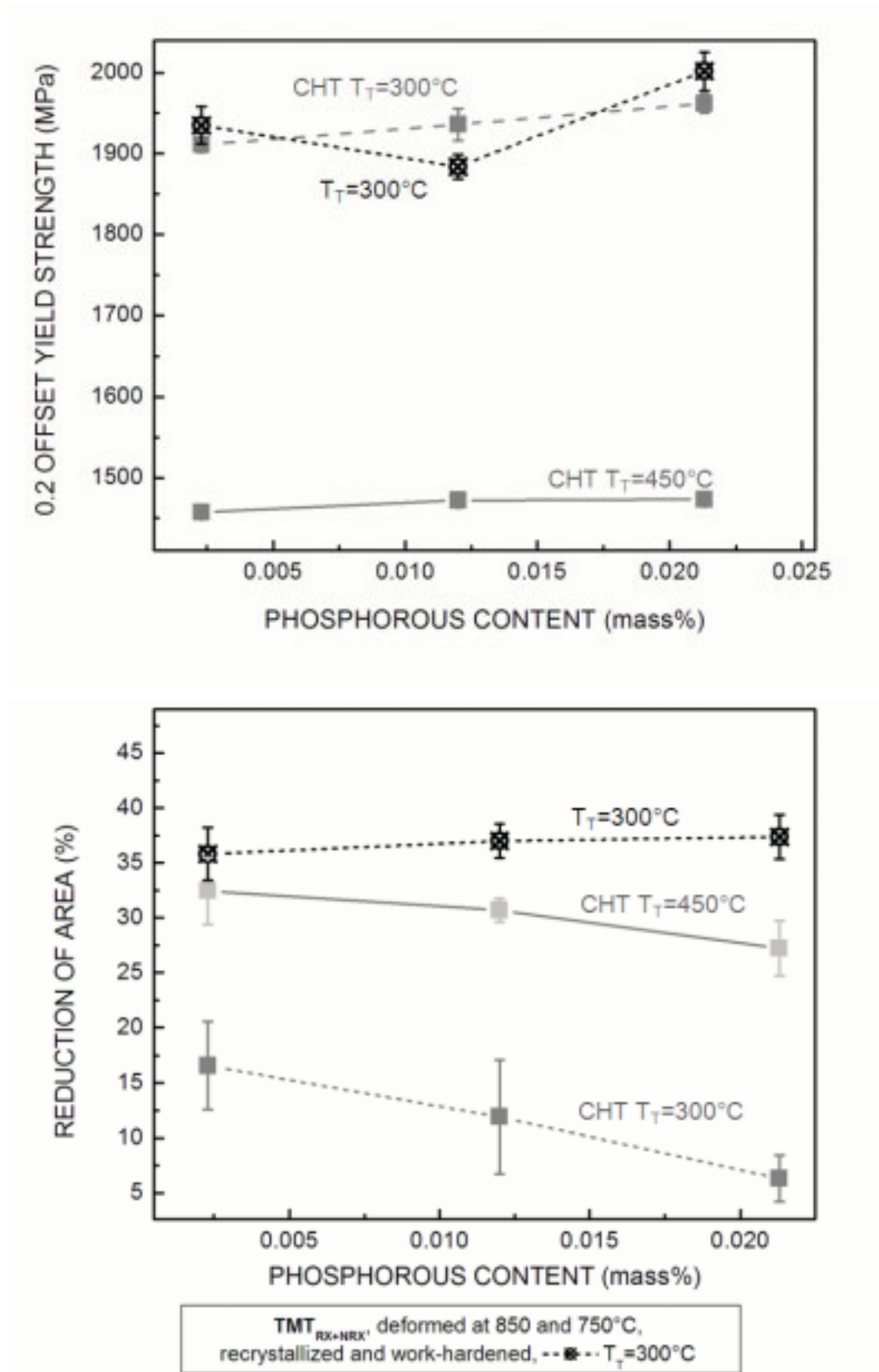


Fig. 82 0.2 offset yield strength (top) and reduction of area (bottom) of thermomechanically treated samples as a function of phosphorous content for 54SiCr6. Recrystallized and work-hardened austenite condition, produced by successive deformations of austenite at 850 and 750°C. CHT: conventionally heat treated samples.

The fraction of intergranular fracture increases for conventionally heat treated sample with increasing phosphorous content (Fig. 47, chapter 4.2). None of the thermomechanically treated samples exhibited any sign of intergranular fracture at the fractured surface observed after tensile testing. Fig. 83 shows the fractograph of a sample deformed twice prior to quenching.

Scanning electron microscopy investigations show that prior austenite grain boundaries of quenched and tempered martensite that is obtained from deformed austenite are either free from carbides or are decorated with refined spherical carbides. The work hardened sample TMT_{NRX} shows partially serrated austenite grain boundaries and almost free of any carbide (Fig. 84 a). Prior austenite grain boundaries of martensite obtained from recrystallized austenite are not continuously decorated with carbides (Fig. 84 b). In this sample curved prior austenite grain boundaries are observed indicating that the recrystallization process was not completed. In contrast to thermomechanically treated samples conventionally heat treated samples exhibit relatively straight prior austenite grain boundaries decorated partially with carbide films over one micrometer length. If the austenite is deformed a second time at 750°C after the first deformation and subsequent partial recrystallization, then prior austenite grain boundaries decorated with fine spherical carbides smaller than 10 nm (Fig. 84 c) are observed.

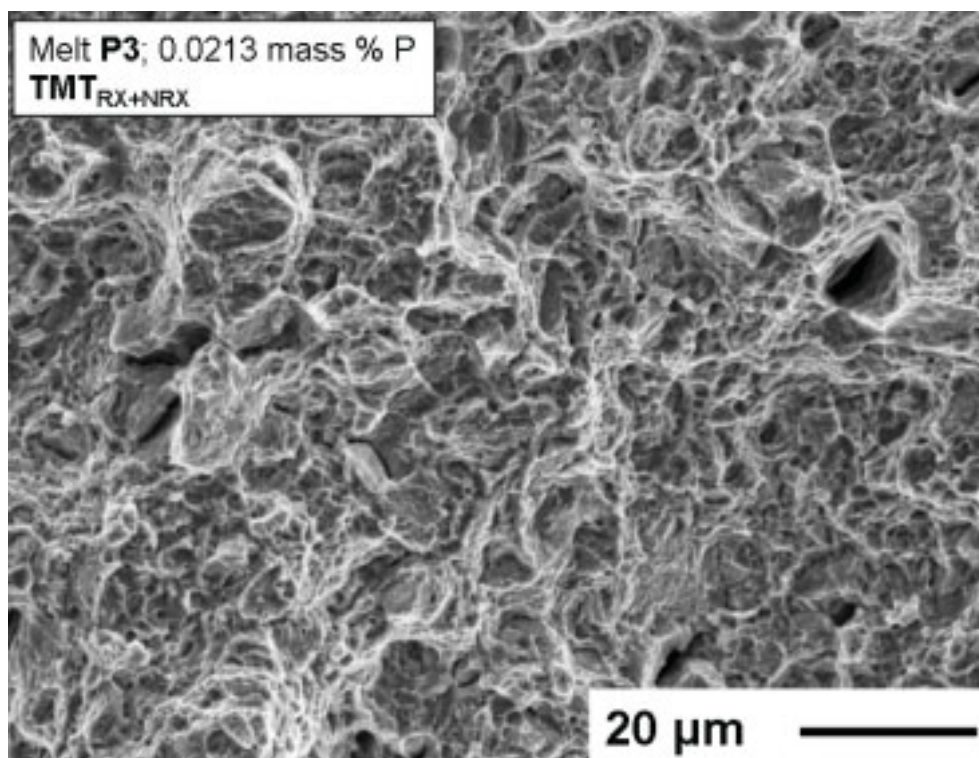


Fig. 83 Fractograph of thermomechanically treated sample deformed at 850 and 750°C prior to quenching and tempered at 300°C.

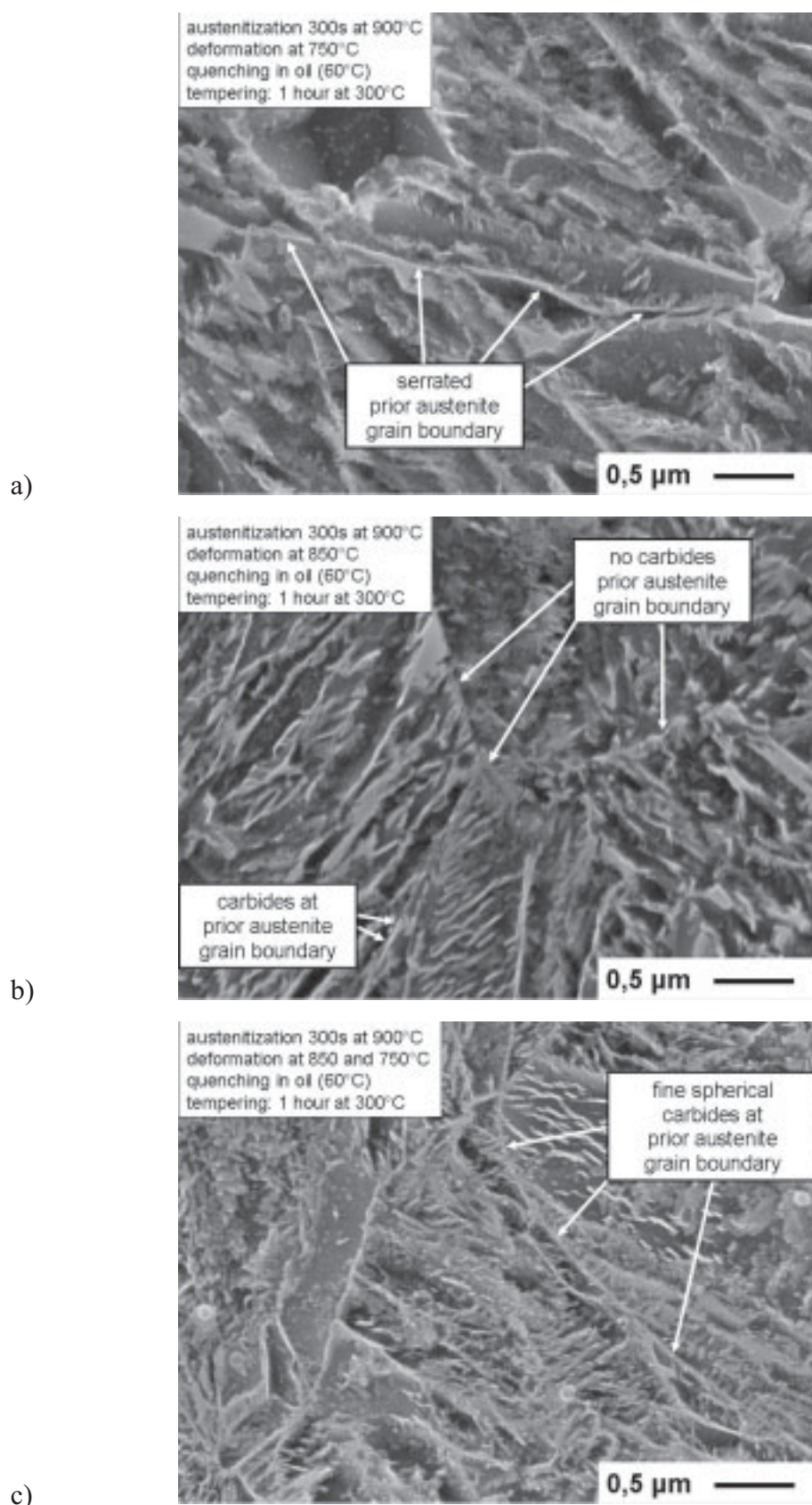


Fig. 84 SEM micrographs of thermomechanically treated sample showing prior austenite grain boundaries. Phosphorous content is 0.0213 mass %. Etching with 1% alcoholic solution of HNO_3 .

Fig. 85 presents the microstructure of the thermomechanically treated samples. The prior austenite grain boundaries are shown as black lines. Deformation at 850°C leads to a refinement of the austenite grains (Fig. 85 (a) compare with Fig. 43), at 750°C it gives elongated austenite grains (Fig. 85 (b)), and a sequence of both deformations shows refined and elongated austenite grains (Fig. 85 (c)). The effective grain size (as defined in 2.1.3) of the thermomechanically treated samples with one deformation step, i.e. of TMT_{RX} and TMT_{NRX} , is $9 \mu m^2$ and is lower than that of conventionally heat treated samples of the steel without vanadium. The combination of both deformations, i.e. successive deformations at 850 and 750°C results in martensite with an average effective grain area of $5 \mu m^2$.

Fig. 86 to 88 present the reduction of area of thermomechanically treated samples for different copper and tin contents. Thermomechanically samples deformed once at 850 or 750°C have been tempered at 300 and 350°C. The results are similar to the results obtained for different phosphorous levels. Thermomechanical treatment enhances the ductility. Among the thermomechanically treated samples the work-hardened austenite condition (TMT_{NRX}) exhibits the lowest ductility at lower copper and tin concentration, whereas the two-step thermomechanical treatment (TMT_{RX+NRX}) including recrystallization and work-hardening exhibits the highest ductility after tempering at 300°C.

The 0.2% offset yield strength of the recrystallized austenite condition is lowest at 350°C. Work-hardening shifts the 0.2% offset yield strength to higher values. An increase of 0.2% offset tensile yield strength with increasing copper and tin content ($c(Cu\&Sn) \geq 0.3$ mass %) is observed for the treatments with a work-hardened austenite condition prior to quenching, i.e. for TMT_{NRX} and for TMT_{RX+NRX} .

4.3.3.3 Discussion

The tensile test results show that the deformation of austenite is effective in achieving high ductility levels at low tempering temperatures. The reduction of area can be as high as for samples conventionally quenched and tempered at 450°C. At the same time the ductility can be equivalent or higher than those of conventionally heat treated samples tempered at 300°C. The results presented here for the three austenite conditions show that the application of thermomechanical treatment is even more beneficial for “dirty” steels that are usually prone to tempered martensite embrittlement.

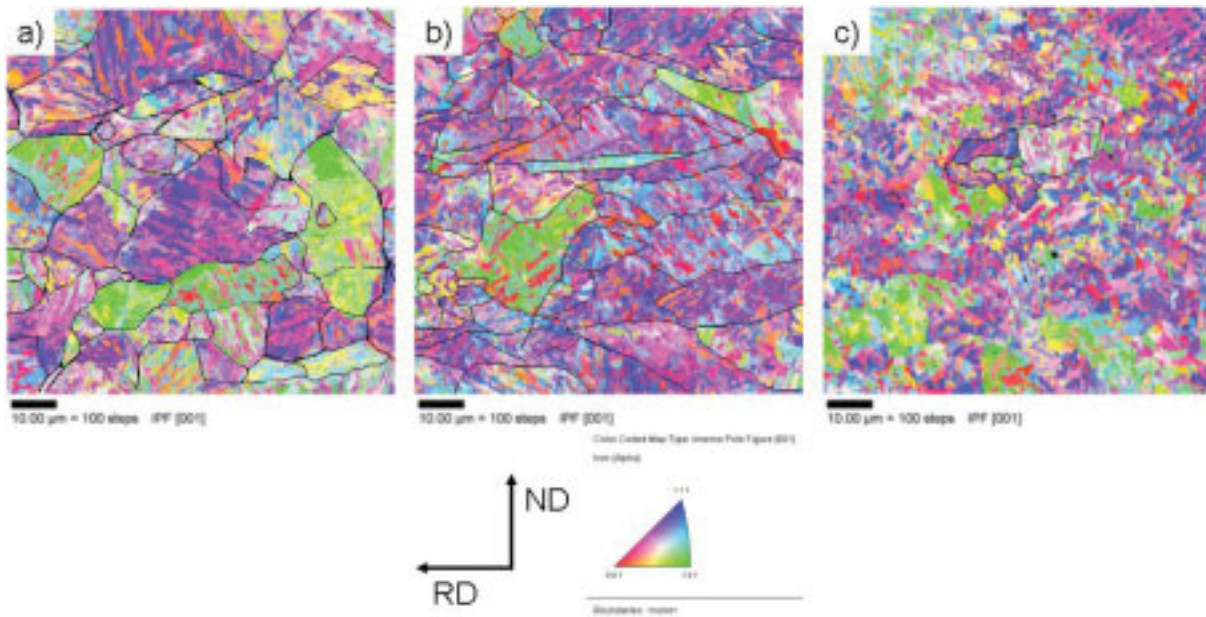


Fig. 85 Inverse pole figure maps of thermomechanically treated samples tempered at 350°C. a) deformed at 850°C; b) deformed at 750°C; c) deformed at 850°C and 750°C. Some prior austenite grain boundaries highlighted with black lines.

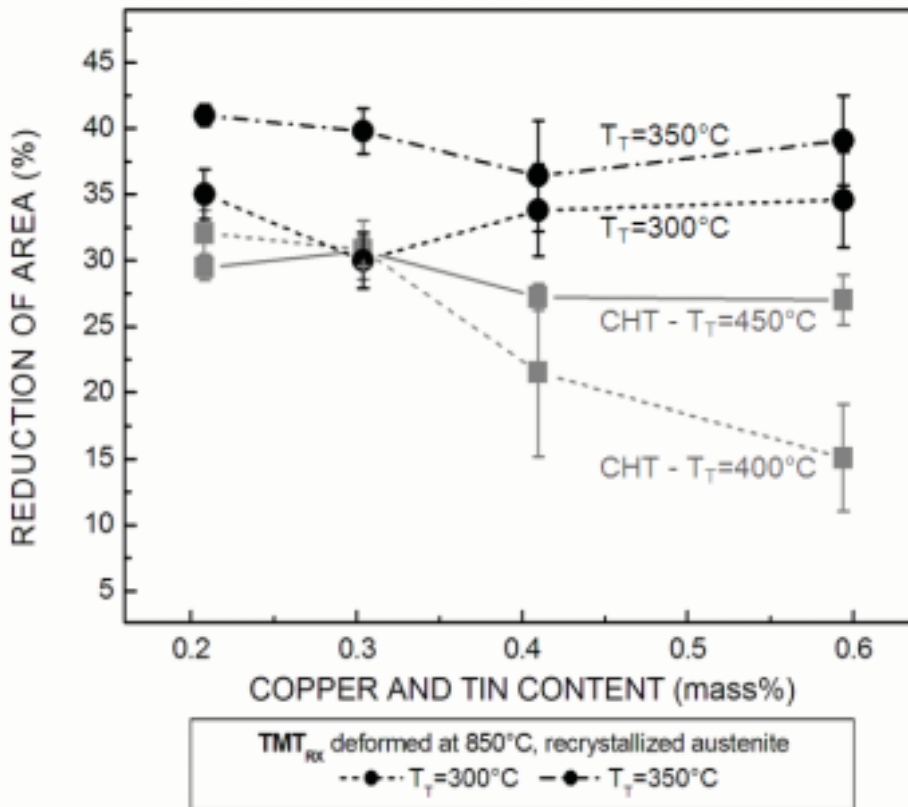


Fig. 86 Reduction of area of thermomechanically treated samples as a function of copper and tin content for 54SiCr6. Recrystallized austenite condition, i.e. deformation of austenite at 850°C.

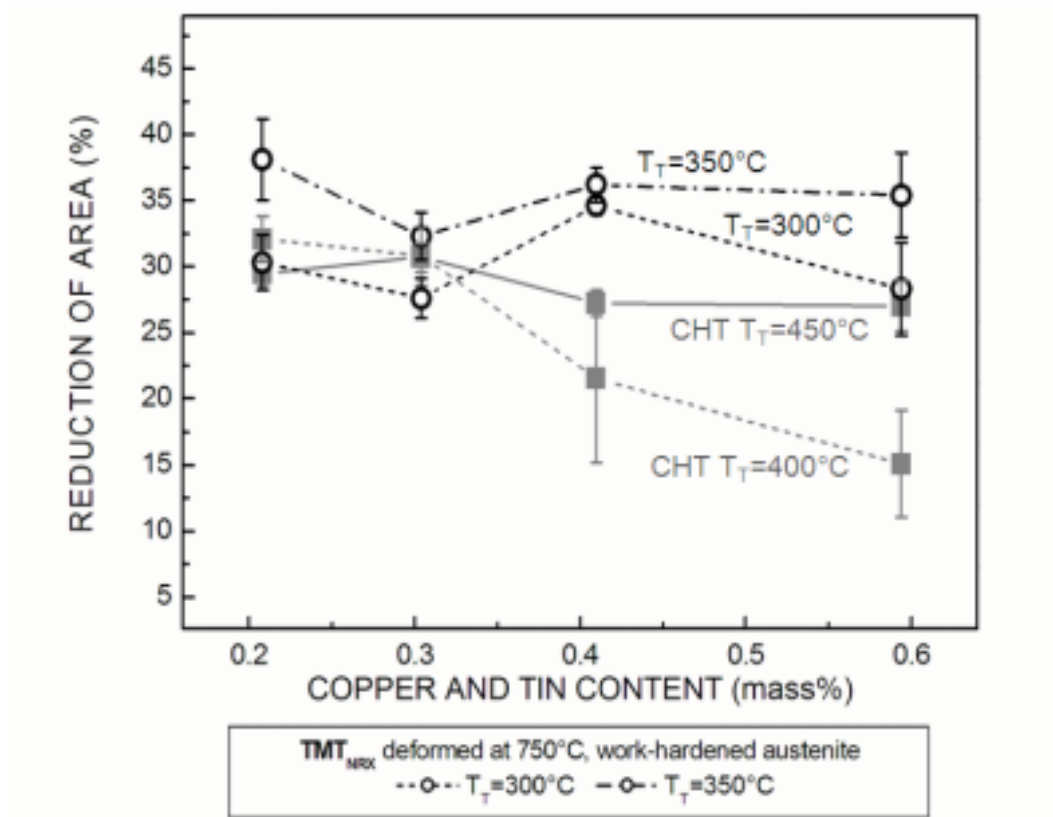


Fig. 87 Reduction of area of thermomechanically treated samples as a function of copper and tin content for 54SiCr6. Work-hardened austenite condition, i.e. deformation of austenite at 750°C .

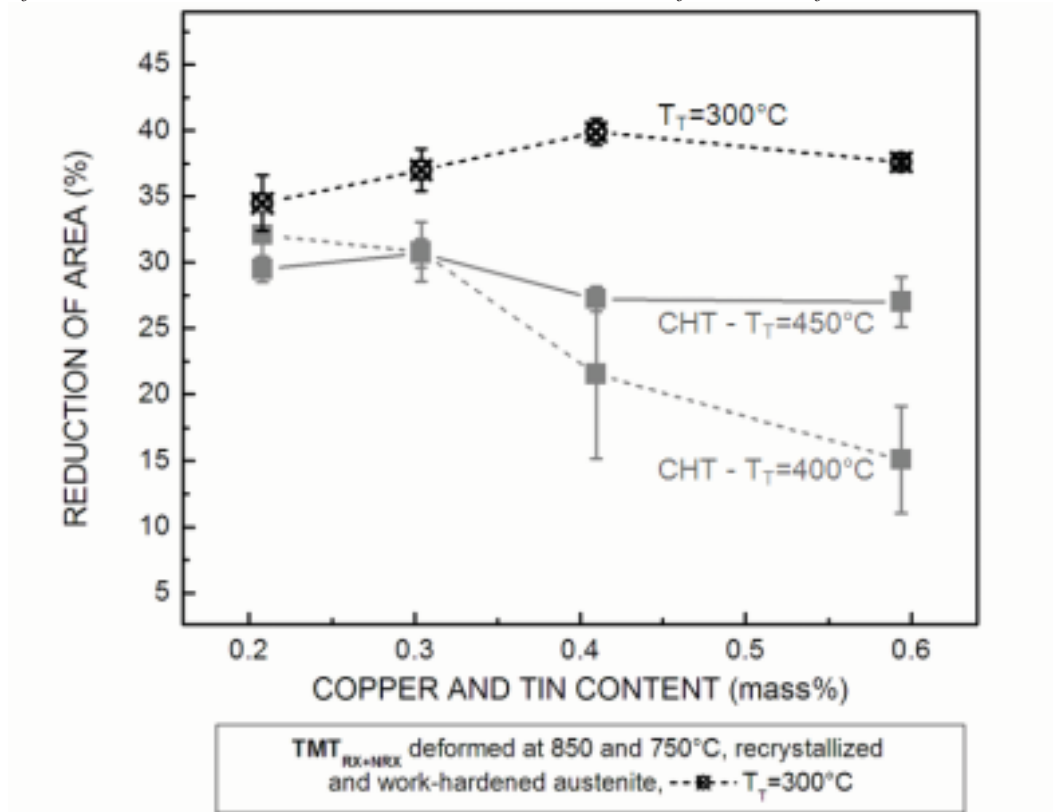


Fig. 88 Reduction of area of thermomechanically treated samples deformed twice as a function of copper and tin content for 54SiCr6.

During austenitization equilibrium grain boundary segregation of phosphorous or tin takes place. The time available during tempering, especially at low temperatures is too short for extensive enrichment of these elements at prior austenite grain boundaries as shown in for conventional heat treatment. The deformation of austenite after the austenitization can reduce the grain boundary segregation by recrystallization and thus rearrangement of atoms at the moving boundary and by increasing the specific grain boundary area by grain refinement. Work-hardening of austenite changes the substructure of austenite grains. Defects like vacancies and dislocations are generated during deformation that can be effective in minimizing the tendency for grain boundary segregation. Defects act as traps for impurity elements such as phosphorous (Grabke 1999) and minimize the tendency for grain boundary segregation. The increase in defect density might as well lead to a back-diffusion of impurity elements from the grain boundaries to the grain interior. This only occurs, when the initial grain boundary concentration of the appropriate element (e.g. phosphorous) is about the equilibrium concentration after introduction of defects through deformation. Work-hardening is effective in avoiding grain boundary carbides by deformation of grain boundaries and their serration (Maki 1993, Hensger and Bernstein 1984). The tensile properties measured for the two-step thermomechanical treatment combines the positive effect of both austenite conditions.

The increase of 0.2% offset tensile yield strength with increasing phosphorous or copper and tin concentration can have different results. To our knowledge, no precipitation reactions in steels with participation of phosphorous have been reported. Leslie (1981) has reported the effectiveness of phosphorous for solid solution strengthening in iron. However, the solid solution strengthening is only effective if phosphorous is soluble in the matrix and is not segregated to the grain boundaries. If defects such as dislocation cores or vacancies act as traps for phosphorous then the 0.2% offset yield strength can be increased.

Considering copper, it is known that copper precipitates can increase the strength of steels (Cox 1967, Miller et al. 1998, Isheim et al. 2006). If the grain substructure of the work-hardened austenite is inherited to the final martensite, then the question arises whether the dislocations or sub-boundaries act as heterogeneous nucleation sites. Cox (1967) had observed copper precipitations in a steel mainly on dislocations. Here, for the ausformed samples we observed an increase of the tensile strength values with increasing copper content and the ductility is relatively high as well. It is expected that better distribution of copper particles or copper atoms in solid solution increase the strength and because of fine dispersion the ductility is increased as well.

4.3.4 FATIGUE RESULTS

4.3.4.1 Experimental

In this chapter the results of the cyclic rotary bending test are presented for thermomechanically and for conventionally heat treated samples and compared. Only samples from the steel without vanadium have been subjected to these tests. The fatigue tests were performed to identify the effect of the impurity elements and to ascertain the potential of thermomechanical treatment.

For conventionally heat treated samples those parameters have been selected that deliver reduction of area values above 25% for all impurity levels. Samples from the phosphorous doped melts (melts P1 to P3) were tempered at 400 and 450°C. The melts with copper and tin have either been tempered at 400 or 450°C. The results of the conventionally heat treated samples have been compared with thermomechanically treated samples that were deformed at 850°C and tempered at 350°C. Here the recrystallized austenite condition (TMT_{RX}) and tempering temperature of 350°C was selected for two reasons. First, TMT_{RX} delivers a good compromise between strength and ductility, i.e. ultimate tensile strength larger than 2150 MPa and reduction of area larger than 37%. Second, because of the equiaxial grains obtained after austenite recrystallization the anisotropy of the mechanical properties should be smaller.

4.3.4.2 Results

Table 9 summarizes the results observed for different melts and processes. Plots of stress against the cycles to failure (S-N curve) were drawn in a double-logarithmic manner as shown in Fig. 89. A line was fitted to the results in the short cycle failure regime using the subsequent equation

$$\sigma = a \times N^b \quad (\text{equation 18})$$

where σ is the stress amplitude, a and b are constants and N is the cycles to failure. The fit was performed with a least square method.

Fig. 89 presents individual test results together with the fitted curve. The fracture surfaces of fatigue specimen were examined with electron microscopy to reveal the influence of phosphorous on the different stages involved in fatigue failure.

The progression of fatigue damage is usually divided into three main stages: a) crack initiation, b) crack growth and c) catastrophic failure. The crack growth can further be divided into two stages. In the first stage the initial microscopic cracks are deepened on planes of high shear stress and coalesce, while in the second stage a geometrically well-defined crack grows on planes of high tensile stress. Microscopic examinations of fracture surfaces allow distinguishing the second stage of crack growth from the cross section separated during catastrophic failure. The fractograph of three individual specimens failed at different stress levels are shown in Fig. 90. With decreasing stress amplitude the fraction of catastrophic failure decreases. At the same time the fraction of crack propagation on the life cycle of the specimen increases.

Table 9 Summary of fatigue results, T_A austenitization temperature, T_D deformation temperature, φ deformation strain, T_T tempering temperature, a and b constant from equation 18, χ^2 and R^2 the reliability of the regression, σ_B fatigue limit.

Treatment	T_A (°C)	T_D (°C)	φ (-)	T_T (°C)	Melt	a	b	χ^2	R^2	σ_B (MPa)
Conventional Heat Treatment	900	-	-	400	P1	4161	-0.13	668.7	0.97	600
					P2	3837	-0.13	7255.0	0.76	650
					P3	3171	-0.11	7690.0	0.81	650
					P1	2802	-0.10	12393.0	0.68	600
					P2	4001	-0.14	1571.0	0.96	600
					P3	3586	-0.13	995.0	0.97	550
	400	CuSn1	3342	-0.11	2907.0	0.94	600			
		CuSn2	3837	-0.13	7255.0	0.76	650			
		450	CuSn2	4001	-0.14	1571.0	0.96	600		
			CuSn3	4108	-0.14	396.0	0.99	600		
			CuSn4	4149	-0.14	572.0	0.99	550		
		Thermomechanical Treatment	900	850	0.4	350	P1	2969	-0.09	2396.00
P2	2740						-0.09	1536.00	0.93	750
P3	2781						-0.08	1977.00	0.92	750
CuSn1	3256						-0.1	3178	0.87	700
CuSn2	2740						-0.09	1536.00	0.93	750
CuSn3	3720						-0.11	6194	0.77	800
CuSn4	2650						-0.08	37202	-	800
CHT	900	-	-	350	I1	2300	-0.0672	78058	-	850
				400	I1	3928	-0.12	1100	0.97	750

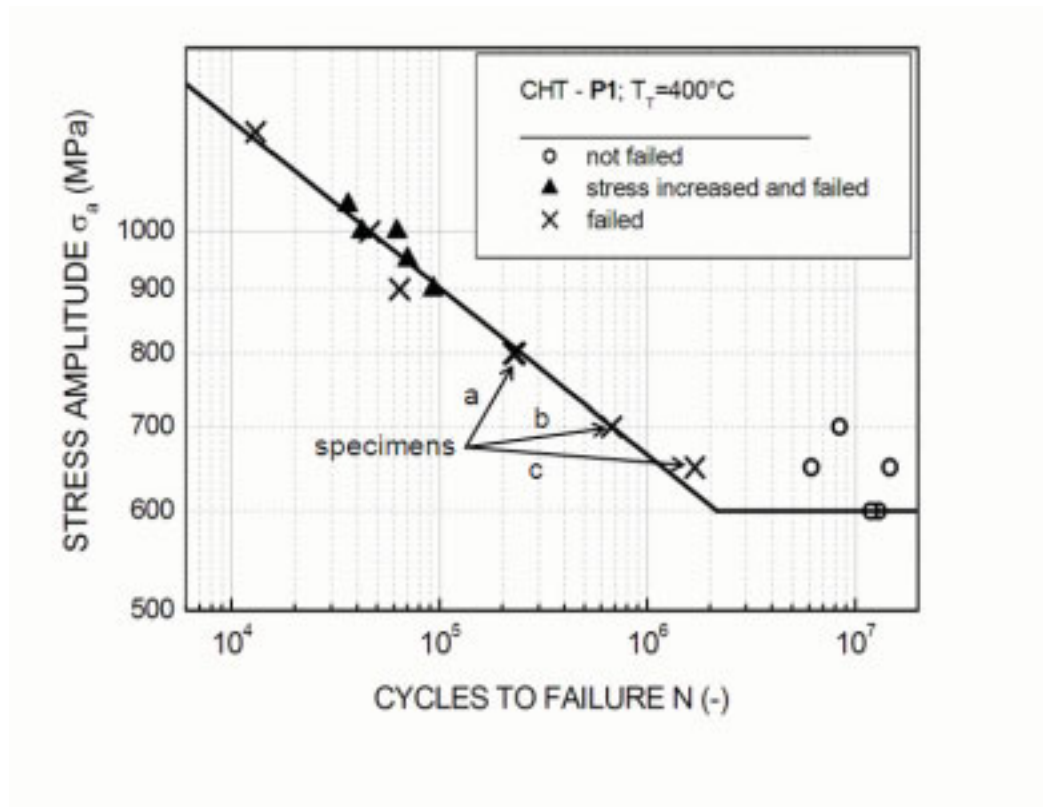


Fig. 89 Best Fit stress-cycles to failure curves for conventionally heat treated samples tempered at 400°C.

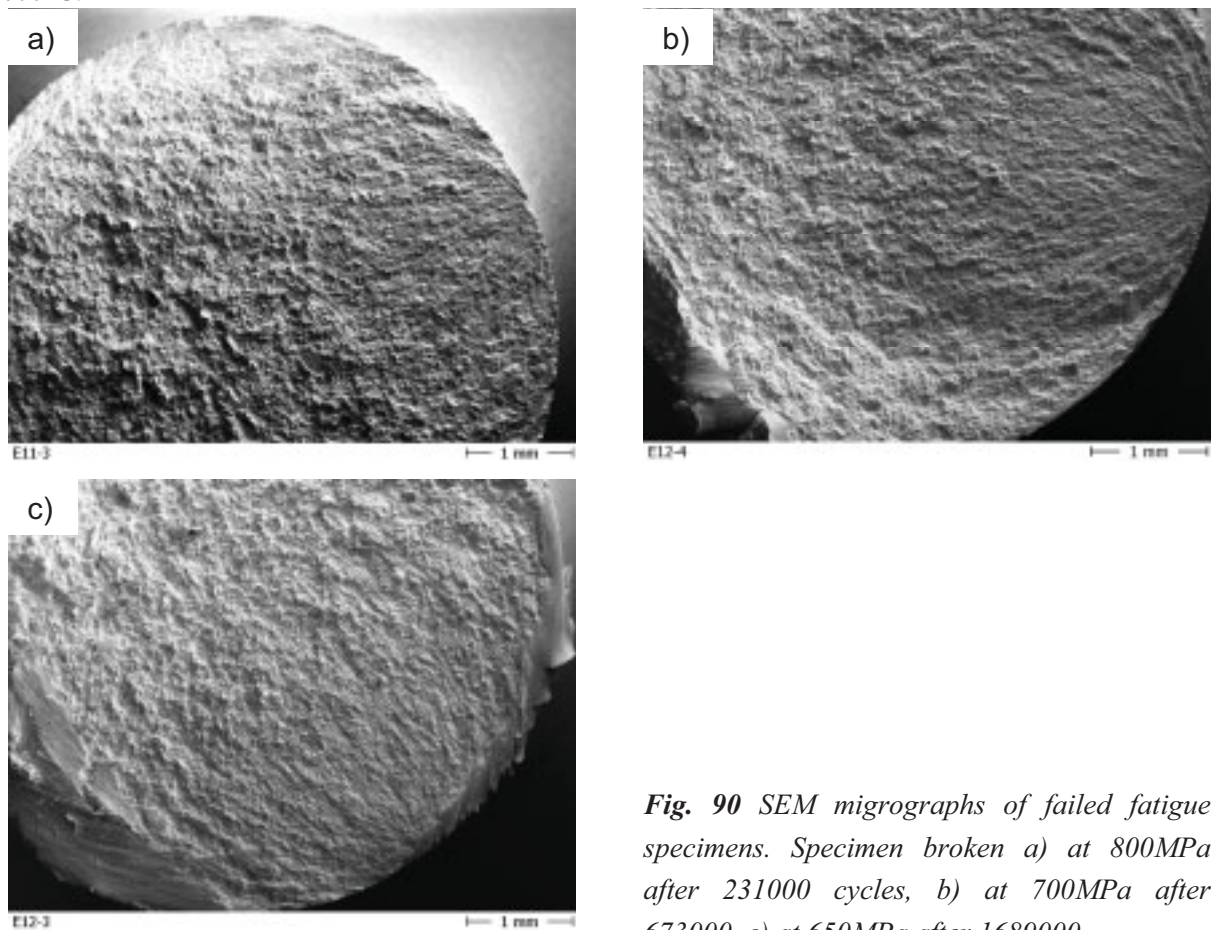


Fig. 90 SEM micrographs of failed fatigue specimens. Specimen broken a) at 800 MPa after 231000 cycles, b) at 700 MPa after 673000, c) at 650 MPa after 1689000.

With increasing phosphorous content the fatigue limit increases for samples tempered at 400°C, while it decreases for samples tempered at 450°C (Fig. 91). The conditioning of austenite and tempering at 350°C gives fatigue limits which are higher than conventionally processed sample tempered at 400 or 450°C. In the low-cycle range the thermomechanically treated samples fail at higher stresses or at higher cycles respectively. Samples with low phosphorous content exhibit a lower fatigue limit. The fatigue limit of thermomechanically treated samples increases with increasing copper and tin content Fig. 92. The values are higher than conventionally quenched and tempered samples. After tempering at 400°C the fatigue limit of conventionally heat treated samples increases slightly with increasing copper content, while it decreases after tempering at 450°C.

4.3.4.3 Discussion

Due to the lower tempering temperature the ultimate tensile strength of the thermomechanically processed samples is about 250 MPa higher than conventionally heat treated samples tempered at 400°C, and fatigue limits are frequently correlated to the ultimate tensile strength (Peters 1996, Dieter 1988). Fig. 93 summarizes the results for different phosphorous contents, processes and tempering temperatures. The fatigue limit depends on the ultimate tensile strength. The ratio of the fatigue limit over the ultimate tensile strength is around 0.34, close to the value (0.2 to 0.3) reported for notched fatigue specimen for steels (Dieter 1988). For the same tempering temperature, the melt supplied by the industry (melt I1), heat treated in a conventional manner, exhibits higher fatigue limits than thermomechanically treated samples from the laboratory melts P1 to P3. The ratio of the fatigue limit over the ultimate tensile strength is above 0.39 - higher than all the values for the laboratory melts. The industrial melt I1 with a low sulphur content exhibits higher reduction of area values than the laboratory melts. Conventionally heat treated samples of melt I1, tempered at 350°C, have the best fatigue limit but the lowest average reduction of area value ($Z=21.9\%$). The area reduction of the thermomechanically treated samples, tempered at 350°C, is higher than that of conventionally heat treated laboratory- or industrial melt tempered at 400°C.

In Fig. 91 we see that increasing the phosphorous content can result in enhancement of fatigue limit and does not lead to reduction of life cycle. Only for samples tempered at 450°C a

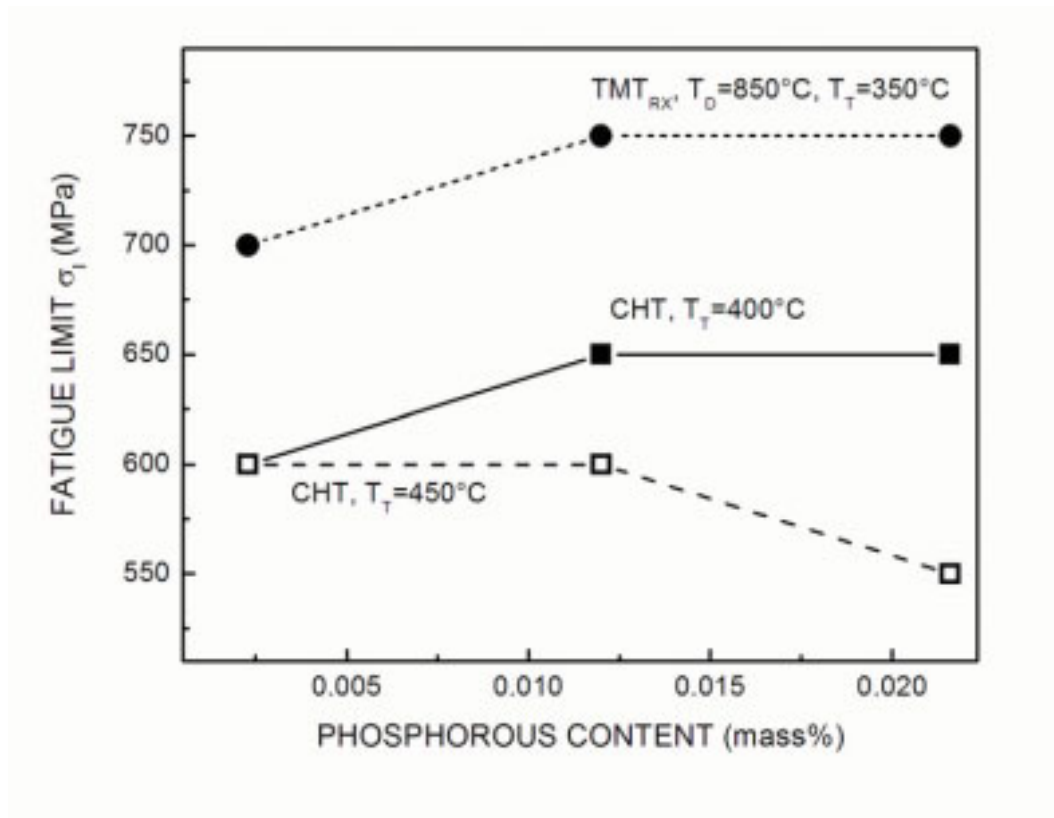


Fig. 91 Fatigue limit for conventional heat treatment and thermomechanical process as a function of phosphorous level.

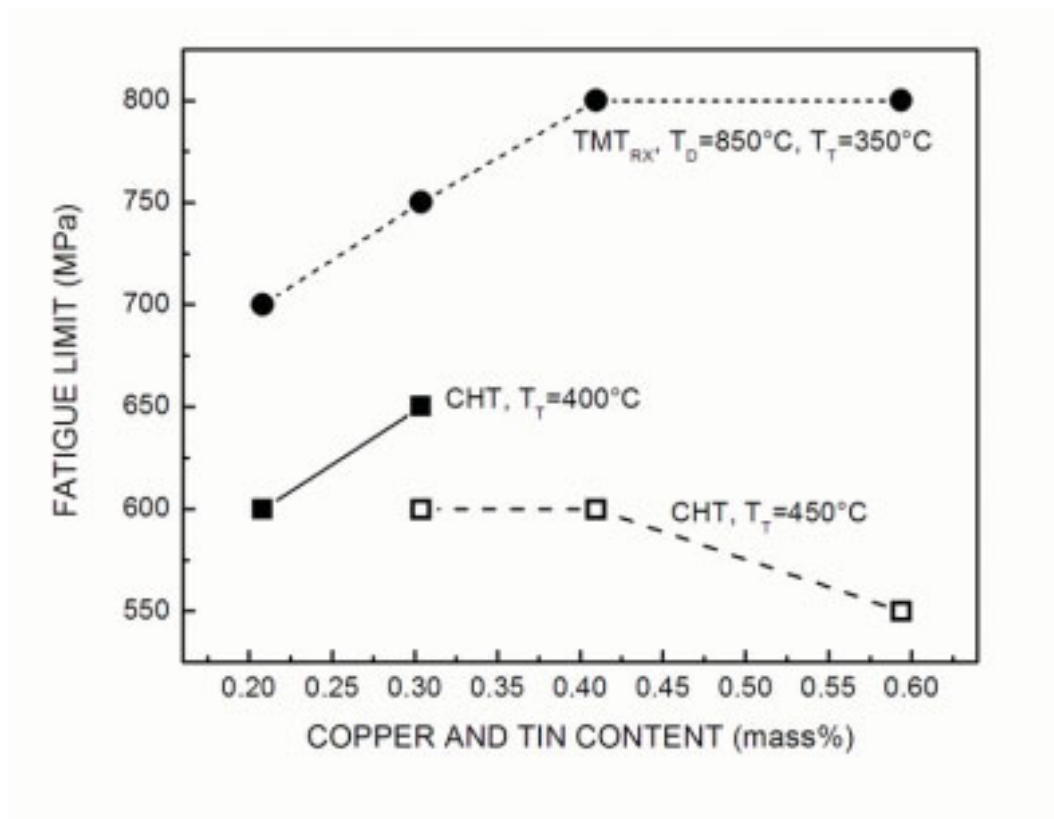


Fig. 92 Fatigue limit for conventional heat treatment and thermomechanical process as a function of copper and tin level.

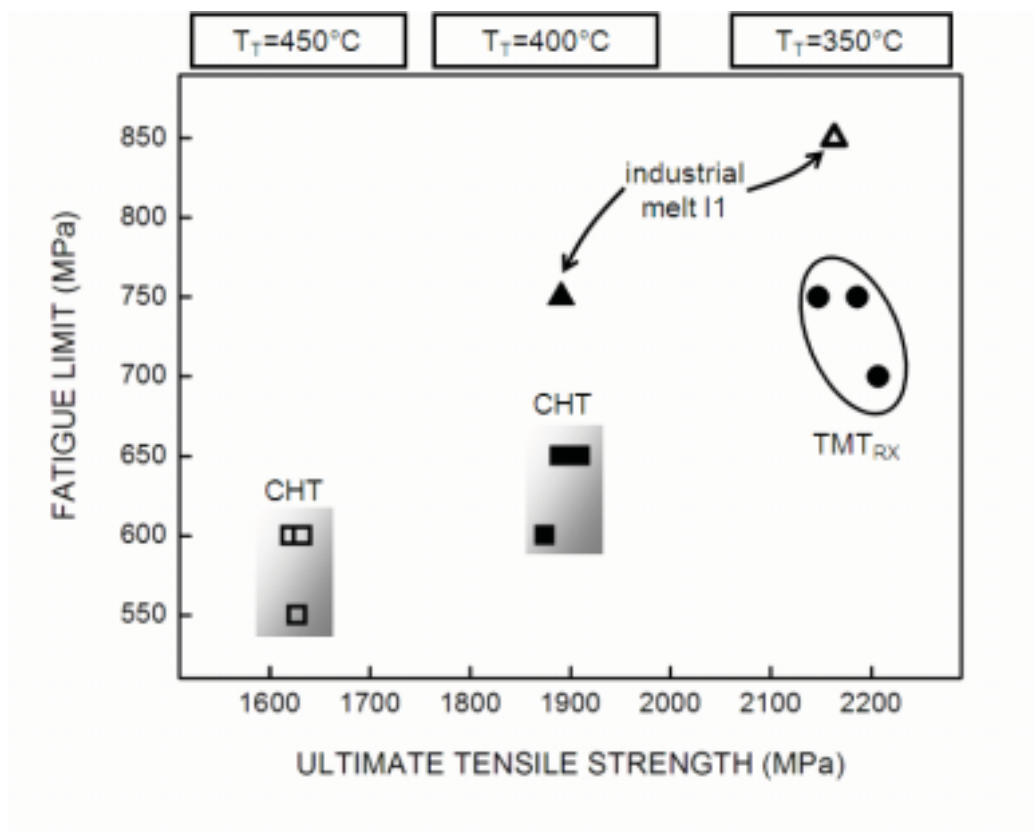


Fig. 93 Fatigue limit correlated with ultimate tensile strength for different processes and phosphorous contents. The industrial melt from was from the blast furnace.

reduction of fatigue limit with increasing phosphorous is observed. By comparing samples of the same process (e.g. CHT tempered at 400°C) broken at the same applied stress level in the low-stress fatigue range (e.g. at 700 MPa), it is observed that the proportions of the cross section involved in crack growth decrease with increasing phosphorous content (Fig. 94). This corresponds to an increase of the cross section that supports the load before final fracture occurs. At the same time, the fraction of intergranular fracture within the cross section separated during catastrophic failure increases with increasing phosphorous content. It is therefore derived, that with higher phosphorous content the crack initiation and the first stage of crack growth are slower for tempering temperatures lower than 400°C. Once micro-cracks have coalesced to form a well-defined crack, they propagate. With increasing phosphorous content however, a smaller crack length is sufficient to introduce final catastrophic fracture, because the prior austenite boundaries are weakened by segregation of phosphorous atoms. This was confirmed by scanning electron microscopy. Thus higher phosphorous content do not only reduce the ductility of the quenched and tempered martensitic steel, but as well reduce the toughness of the material. Therefore less surface damages can be tolerated during production or during operation of the parts.

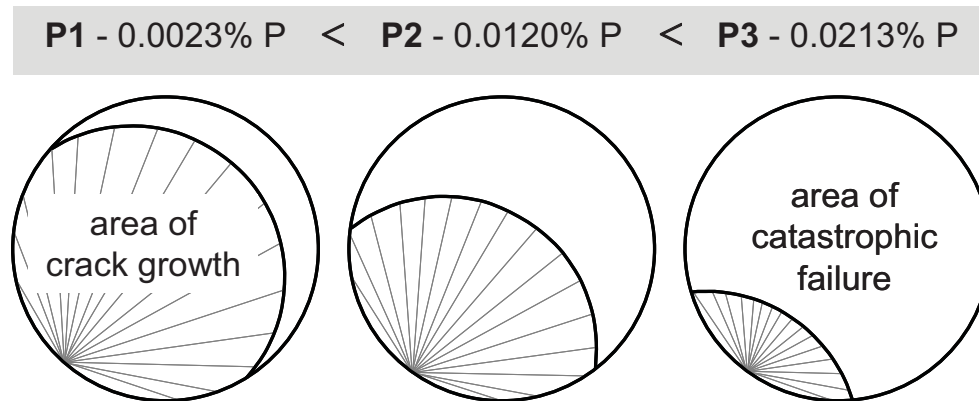


Fig. 94 Schematic representation of the fracture surface investigations of samples failed in fatigue tests. Shown area involved in crack growth and catastrophic failure for different phosphorous levels at constant applied stress.

4.3.5 MICROALLOYING AND THERMOMECHANICAL TREATMENT

In chapter 4.1.3.2, it was shown that adding vanadium to the steel retards the softening processes. In this chapter, a thermomechanical procedure for the vanadium microalloyed steel is developed and tested for different levels of impurity elements. To define the deformation temperature for the thermomechanical treatment, samples were austenitized, deformed, quenched and tempered at 300°C. The tensile properties of these samples were compared with that of conventionally heat treated specimen.

4.3.5.1 Results

In the case of the microalloyed steel single deformation of austenite does not result in a higher reduction of area (Fig. 95). The deformation reduces the standard deviation for the area reduction. The average value of all deformed samples is within the scatter range of the conventionally heat treated sample. As was observed for the steel without vanadium, the work-hardened austenite condition increases the strength of the tempered martensite. This is observed for samples deformed at 800 and 750°C.

Based on the obtained results, a two-step thermomechanical treatment was defined. The austenitization was defined to be 5 minutes at 920°C to ensure uniform fine austenite grain size. Thereafter, the samples were deformed in two successive steps at 900 and 850°C, with a strain of 0.4 at each deformation stage. In Fig. 96, the results for samples tempered at 300°C

are compared with that of samples prepared either by conventional heat treatment or by single-step thermomechanical treatment. The latter underwent only one deformation step. The two-step thermomechanical treatment exhibits the highest ductility. Relative to conventional heat treatment, the 0.2% offset yield strength is increased.

Prior to quenching, the microstructure consists of work-hardened and partially recrystallized austenite. The average effective grain size is reduced from $7.5 \mu\text{m}^2$ to $3.2 \mu\text{m}^2$ (Fig. 97). The two-step thermomechanical treatment was employed to the vanadium microalloyed steel with different levels of phosphorous or copper and tin concentrations. The results are shown in Fig. 98 and 100. The thermomechanical treatment increases the ultimate tensile strength slightly. For samples tempered at 350°C , the 0.2% offset yield strength is enhanced at least 50 MPa (Fig. 98). At the same time the area reduction is at least 10% higher. Only the samples with low phosphorous level exhibit a high ductility and a low standard deviation (Fig. 98). With increasing phosphorous content the reduction of area falls rapidly and the standard deviation increases. The prior austenite grain boundaries of thermomechanically treated samples are curved and in most cases free of carbide films. However, some carbide films were observed (Fig. 99).

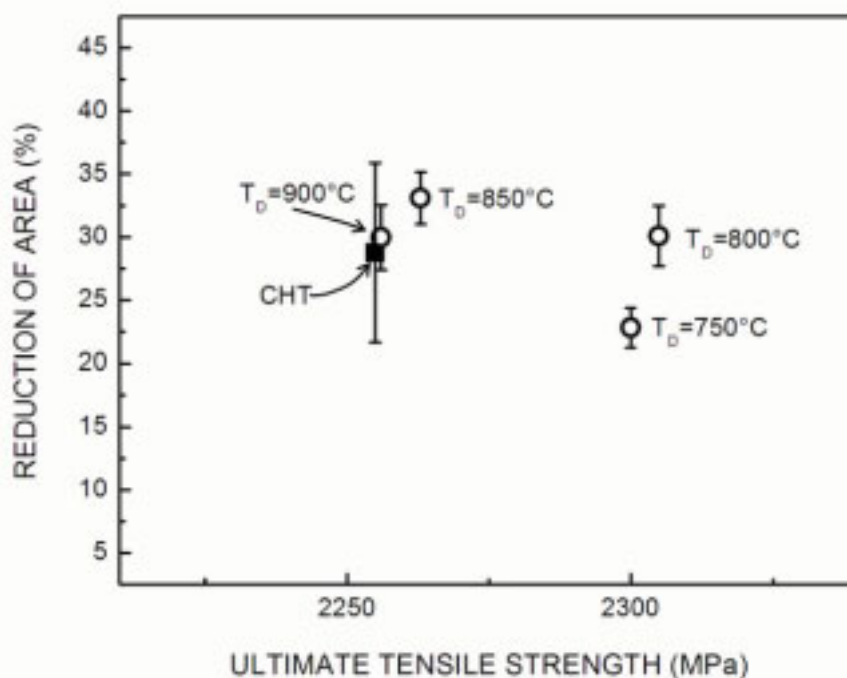


Fig. 95 Reduction of area and tensile strength of different austenite conditions. TMT samples (melt PV1) austenitized at 950°C , deformed at T_D and tempered at 300°C .

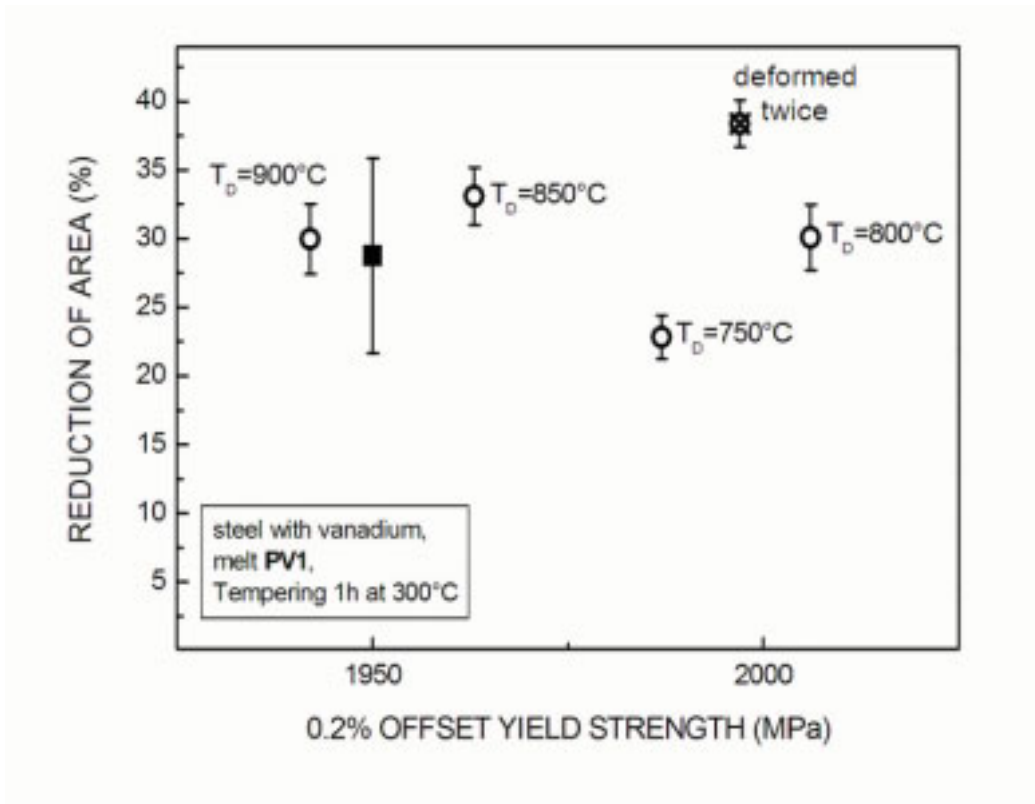


Fig. 96 Reduction of area and 0.2% offset yield strength of different austenite conditions. TMT samples (melt PV1) austenitized at 950°C, deformed at T_D and tempered at 300°C. 2-step TMT sample austenitized at 920°C, deformed at 900 and 850°C and tempered at 300°C.

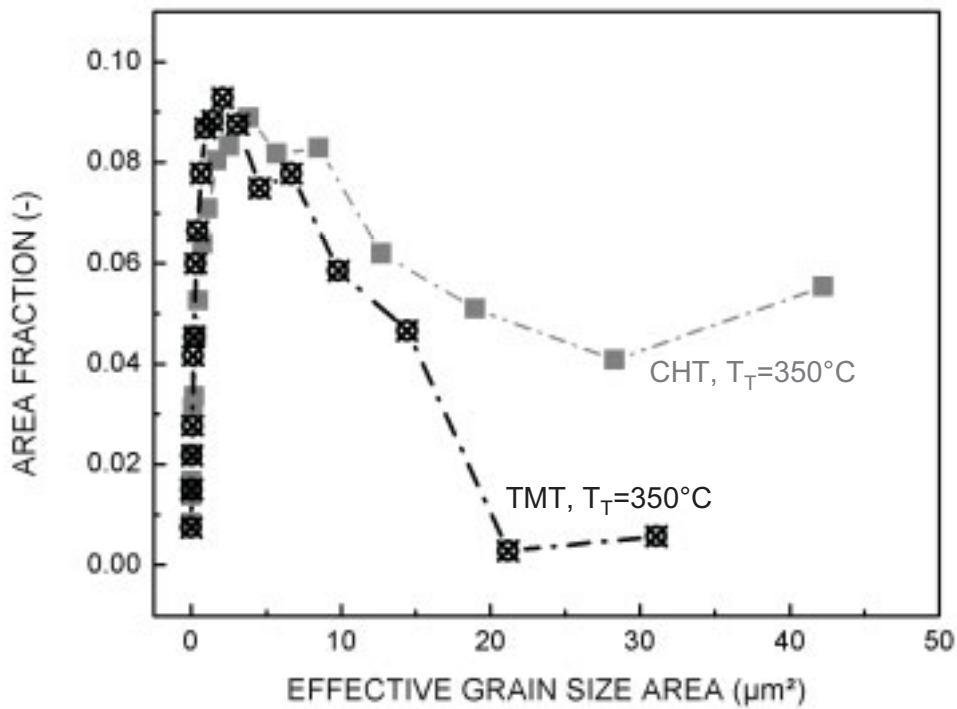


Fig. 97 Effective grain size distribution of conventionally heat treated and thermomechanically treated (deformed at 900 and 850°C) samples of microalloyed steel (PV1).

In contrast to the 0.2% offset yield strength the ultimate tensile strength of the microalloyed steel is not enhanced by the two-step thermomechanical treatment. After tempering at 350°C the average values are equivalent to those obtained after conventional heat treatment. A slow decrease of ultimate tensile strength is observed with increasing copper and tin content (Fig. 100). Thermomechanically treated samples tempered at 300°C show higher tensile strength at lower copper and tin content. A strong decay is observed from 0.3 to 0.4 mass percent copper and tin. The reduction of area is increased by thermomechanical treatment (Fig. 100). However, for some samples, the standard deviations are very large.

The fractured surfaces of the microalloyed steel exhibited parallel cracks. These cracks are planar and surrounded by low deformation areas. In all of these areas manganese sulphides were observed.

4.3.5.2 Discussion

In the present study a two-step thermomechanical treatment was defined for the microalloyed steel. Deformation of austenite slightly increases the 0.2% offset tensile yield strength. Samples processed thermomechanically possess higher reduction of area values than conventionally heat treated ones. However, only the melts with a low impurity level exhibit small standard deviations. Tempering at 300°C can result in area reductions below 25% with a large scatter. The use of the steel with vanadium is thus limited to applications with a tempering temperature above 350°C or to compositions with low phosphorous and copper and tin contents. In Fig. 101 the mechanical properties of the thermomechanically treated samples tempered at 350°C are compared with conventionally heat treated samples.

The improved properties are attributed to the elimination and refinement of carbide films at the prior austenite grain boundaries, and to the refinement of the martensite structure. Combination of microalloying and two-step thermomechanical treatment results in the smallest effective grain size distribution. Microalloying results in smaller austenite grains during austenitization (see 4.1). The first deformation at 900°C induces recrystallization and leads to an even finer austenite grain size. The second deformation step work-hardens the austenite. As described before (4.3.4) the work-hardened austenite condition refines the effective grain size in the same way as does the recrystallized austenite condition. Thus through microalloying and thermomechanical treatment martensite refinement is achieved by austenite conditioning in three steps, during austenitization, by a first deformation and recrystallization, by a second deformation and work-hardening.

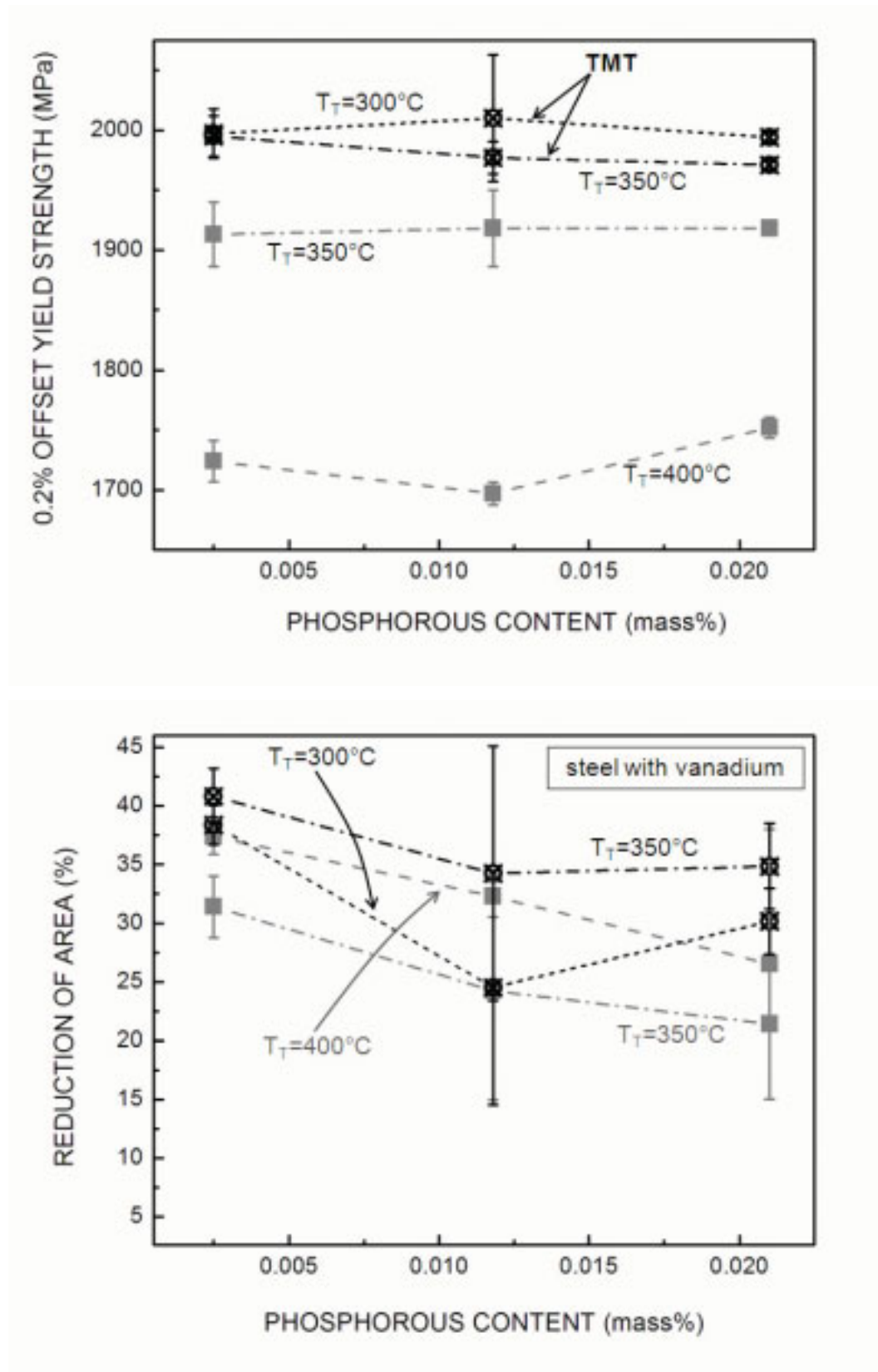


Fig. 98 0.2% offset yield strength (top) and reduction of area (bottom) of conventionally and thermomechanically processed samples over phosphorous content. Conventional heat treatment: 300s at 900°C followed by quenching and tempering at 350 or 400°C. Thermomechanical treatment: 300s at 920 followed by deformations at 900 and 850°C, quenching and tempering at 300 or 350°C.

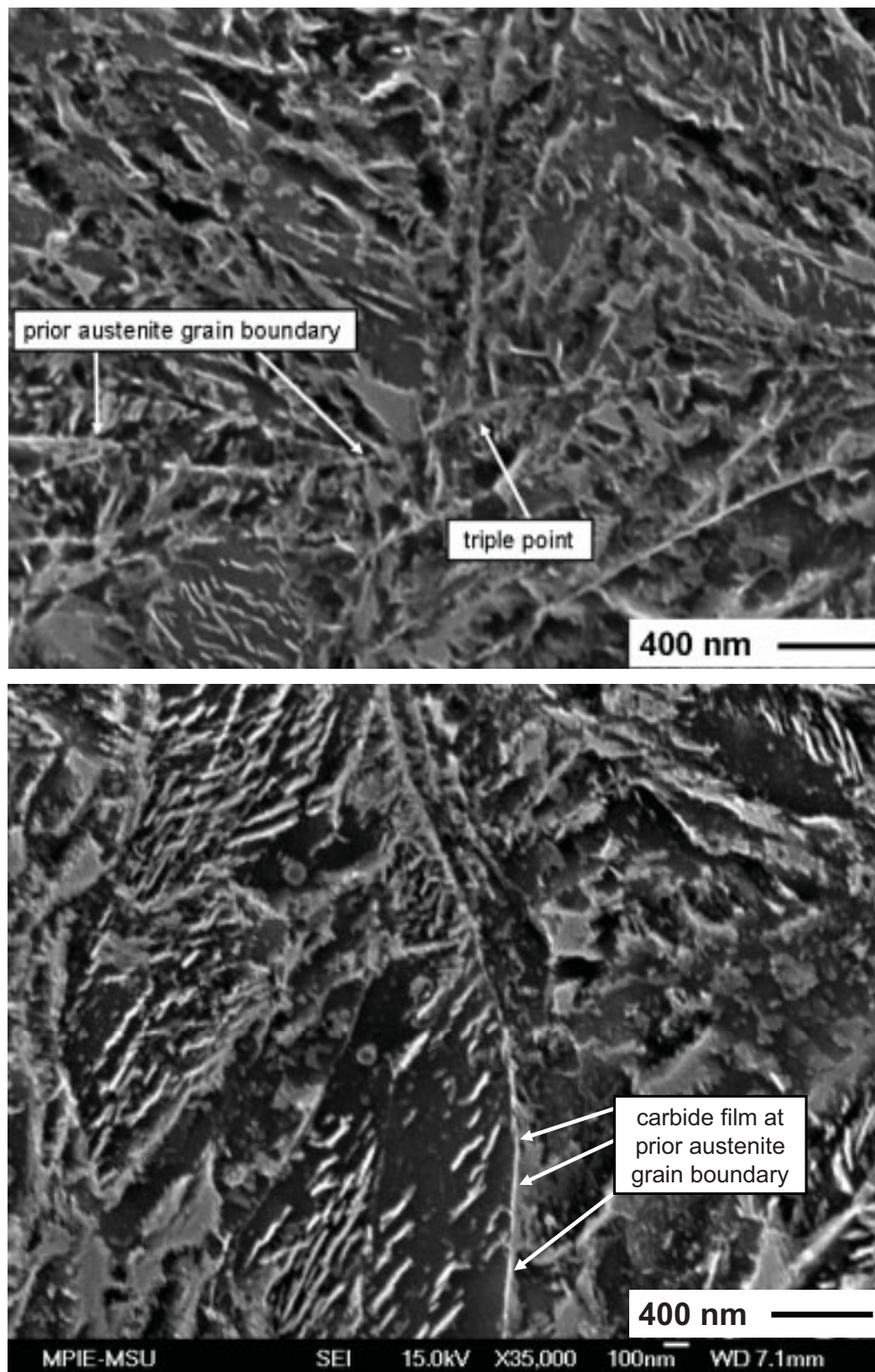


Fig. 99 SEM micrographs of thermomechanically treated sample of 54SiCrV6. Austenitization for 300s at 920°C, deformed with strain of 0.4 at 900°C and 850°C, quenched in oil and tempered at 350°C. Most prior austenite grain boundaries free of cementite (top) but small fraction of cementite films still observed.

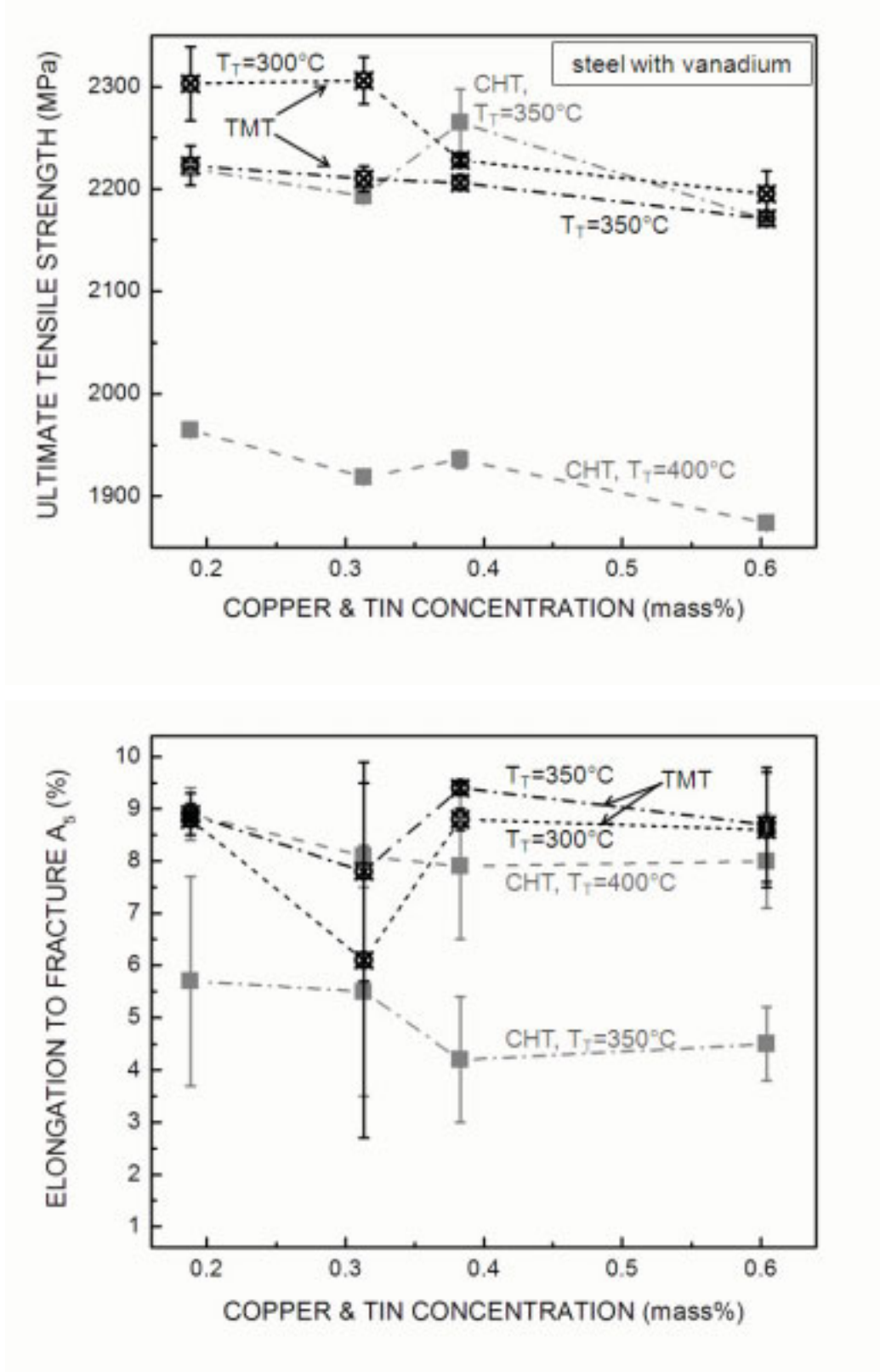


Fig. 100 0.2% offset yield strength (top) and reduction of area (bottom) of conventionally and thermomechanically processed samples over copper and tin content. Conventional heat treatment (CHT): 300s at 900°C followed by quenching and tempering at 350 or 400°C . Thermomechanical treatment (TMT): 300s at 920 followed by deformations at 900 and 850°C , quenching and tempering at 300 or 350°C .

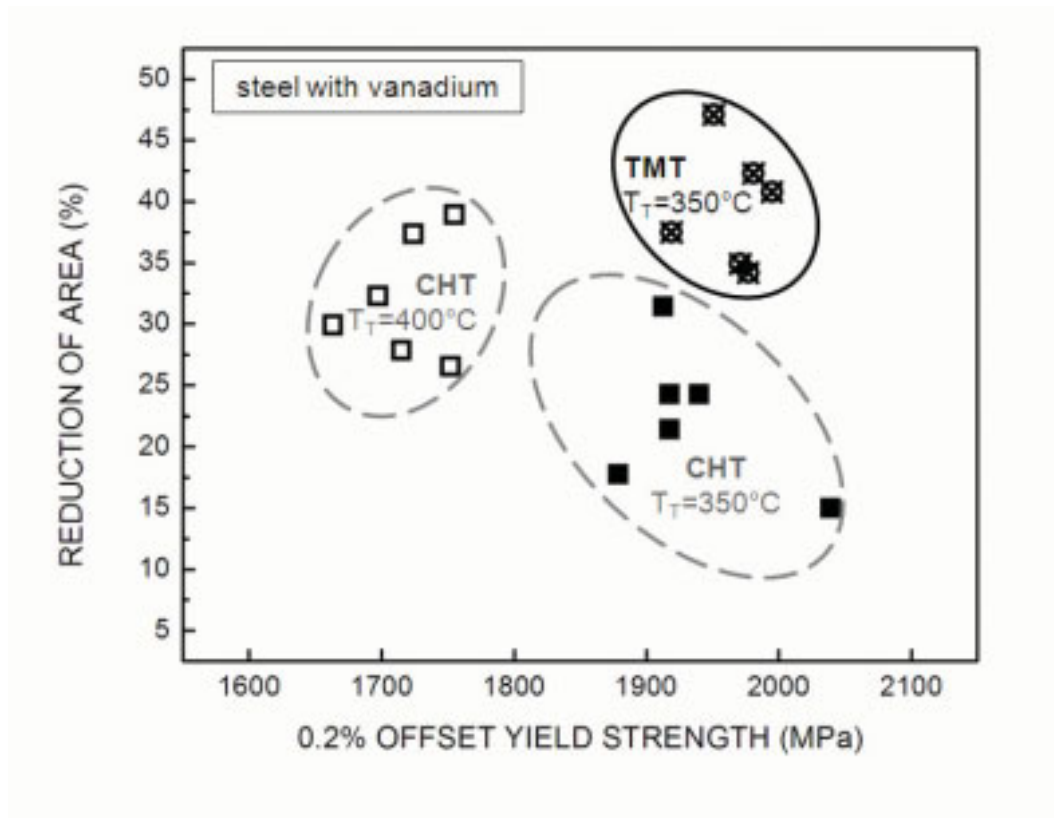


Fig. 101 Reduction of area and 0.2% offset tensile yield strength for conventionally heat treated (CHT, austenitization 5 minutes at 900°C followed by quenching and tempering) and thermomechanically treated samples (TMT, 5min@920°C, deformed at 900°C and 850°C, quenched and tempered). Microalloyed steel with different phosphorous and copper and tin concentrations.

5 FINAL DISCUSSION

Austenite deformation prior to quenching enhances the ductility. Appropriate selection of deformation parameters lead to a significant improvement of the mechanical property profile including strength, ductility and fatigue performance. Such thermomechanical parameters were developed for the silicon chromium steel 54SiCr6 with and without addition of vanadium.

For the steel without vanadium two processes with a single deformation of austenite were identified as most effective. The austenitization and tempering parameters were the same as for conventional heat treatment. In addition to conventional heat treatment a deformation prior to quenching with a logarithmic strain of 0.4 and a strain rate of 5 s^{-1} was integrated into the process. Deformation at 850°C resulting in a recrystallized austenite condition and a deformation at 750°C leading to a pan-caked austenite structure proved both effective in increasing the ductility. The best combination of strength and ductility was obtained through combination of both austenite conditions (Fig. 102). The empty squares are conventionally heat treated samples from industrial melt *II* (Table 4) with a low phosphorous, copper and tin and sulfur content. They exhibit a higher ductility than the laboratory melts (full squares). The thermomechanically treated samples of all compositions tempered at 300°C exhibit ductilities higher than all conventionally heat treated samples. Due to the lower tempering temperature employed the ultimate tensile strength could be improved by 600MPa without loss of ductility. The ductility of conventionally heat treated samples is dependent on the concentration of phosphorous or on copper and tin (chapter 4.2). Within the tested concentrations thermomechanically treated samples are not sensitive to the concentration of the aforementioned elements (Fig. 103).

The increase in ductility at high strength levels and the minimization of the negative effect of phosphorous or copper can be explained by microstructural changes that take place during and after the austenite deformation. The deformation of austenite changes the distribution of the elements, the morphology of grain boundary carbides (cementite), and the size of the structural units of martensite. These aspects are discussed in the subsequent pages.

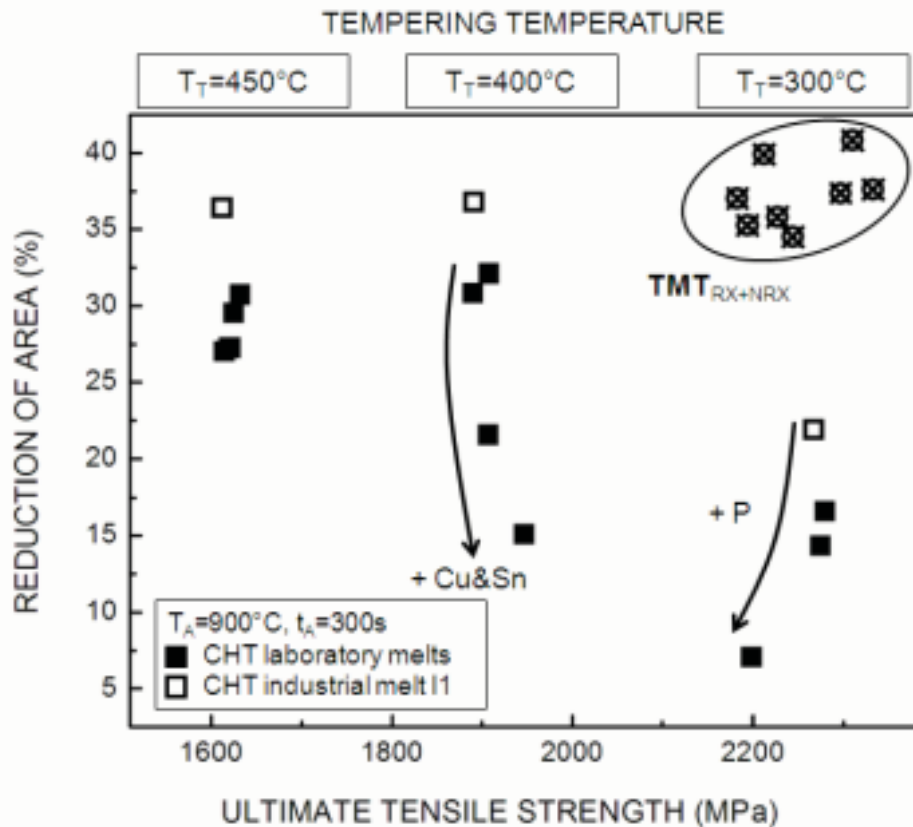
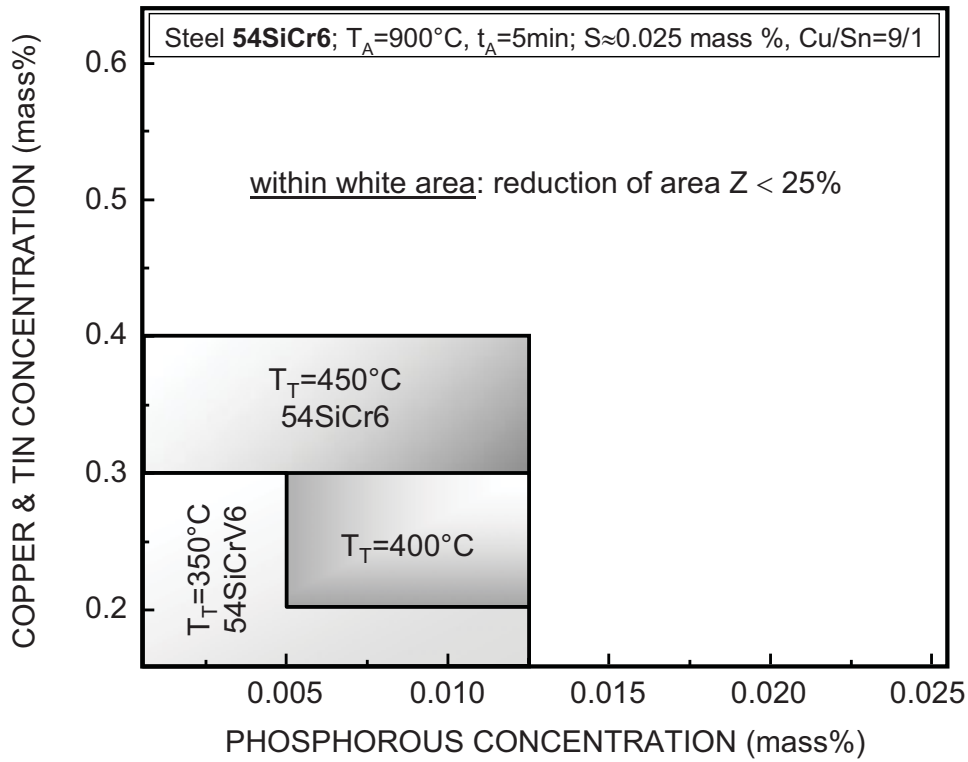


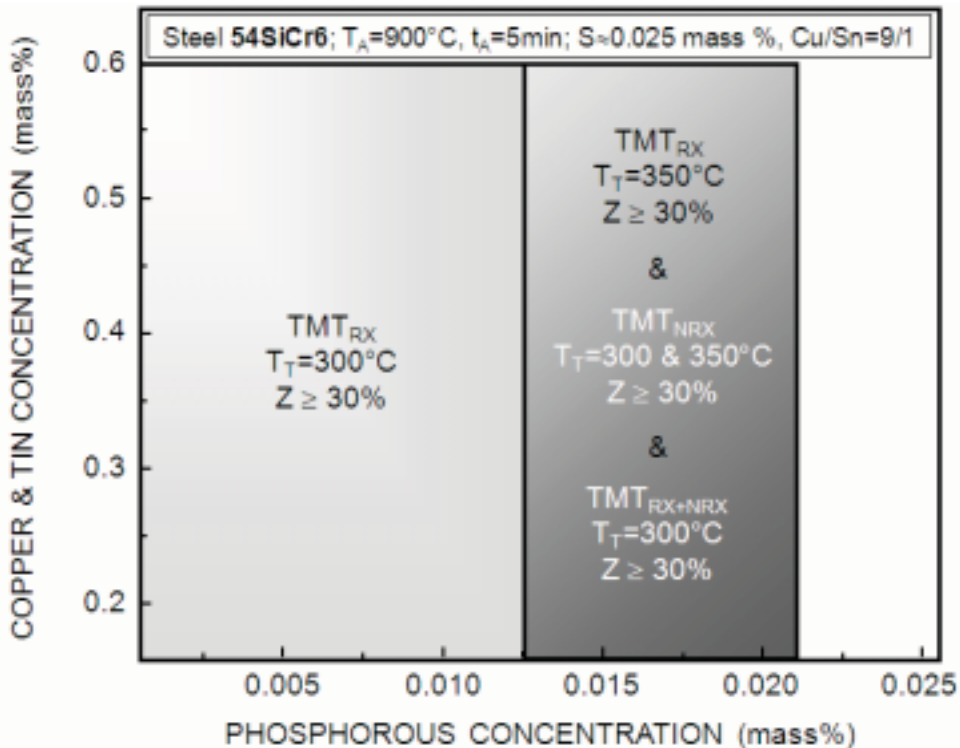
Fig. 102 Reduction of area and ultimate tensile strength for conventionally heat treated samples (austenitization at 900°C) of different phosphorous, and copper and tin levels compared with thermomechanically treated samples deformed twice. Steel 54SiCr6; T_A austenitization temperature, t_A austenitization time.

5.1 PROCESS AND IMPURITY ELEMENT EFFECT

The limits for phosphorous, copper and tin were determined in tensile tests for constant austenitization parameters (5 minutes at 900°C), but different tempering temperatures. The value of 25% was taken as minimum requirement for the reduction of area. Phosphorous, copper and tin concentrations and tempering temperatures resulting in higher values are shown in Fig. 103 for conventional heat treatment. The nominal sulfur content was 0.025 mass%, while the ratio of copper over tin was always 9:1. Today, the tempering temperature employed industrially is close to 400°C. Our results show, that reduction of tempering temperature to 350°C for higher strength level is only possible with the microalloyed steel containing very low amount of phosphorous and copper and tin. Increasing these elements will deteriorate the ductility severely.



(a) Conventional Heat Treatment



(b) Thermomechanical Treatment

Fig. 103 Limits of 54SiCr6 for phosphorous, copper and tin to obtain a required reduction of area. Top: within grey areas reduction of area is above 25% within the given compositions. Bottom: Within grey areas the reduction in area Z exceeds the values given in the boxes. Recrystallized (TMT_{RX}), not recrystallized (TMT_{NRX}) austenite condition and combination of both (TMT_{RX+NRX}).

As discussed in 4.2.4.3, phosphorous segregates during austenitization to the austenite grain boundaries and weakens the cohesion of adjacent grains. These interface areas, that are enriched with phosphorous, still exist after transformation to martensite (Fig. 104). During tempering, cementite can preferentially form as thin films at the prior austenite grain boundaries. Because cementite is a barrier for moving dislocations, dislocation pile ups built up at the prior austenite grain boundaries and microcracks are formed (Fig. 104). Due to weakening of these boundaries by phosphorous the cracks will propagate along these weak paths and increasing intergranular fracture is observed with increasing phosphorous content. This is schematically shown in Fig. 104.

If the austenite is deformed prior to quenching and recrystallized, the embrittling effect of phosphorous is minimized. The recrystallization increases the specific grain boundary area and by doing though reduces the grain boundary concentration of phosphorous. During recrystallization, the newly formed nuclei and moving grain boundaries can leave the

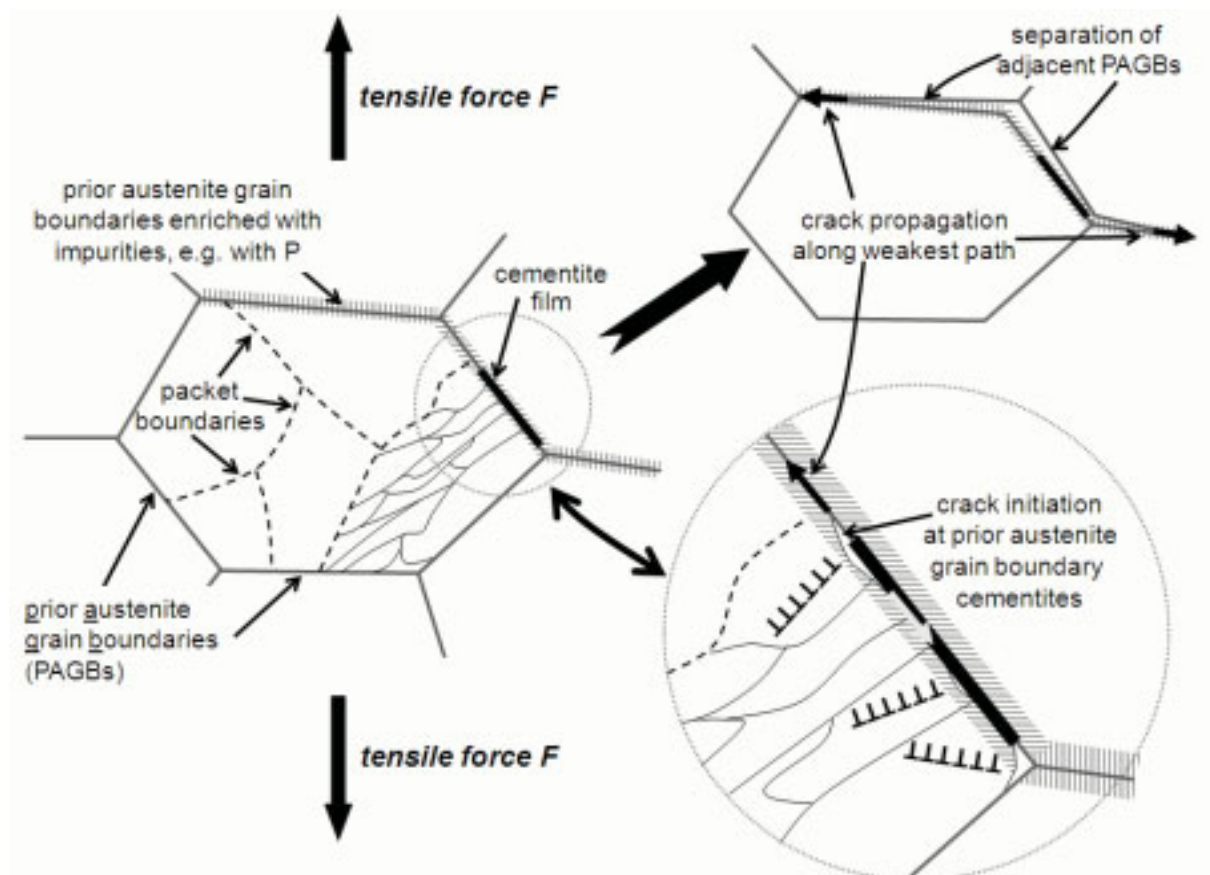


Fig. 104 Schematic representation of crack initiation at cementite films at prior austenite grain boundaries (PAGB) and their propagation along these pristine boundaries enriched with impurities like phosphorous.

phosphorous atoms behind or gather them in the migrating boundary, sweep effect (Abe 1990). The first case occurs, when the grain boundary velocity is higher than the diffusivity of phosphorous. The second occurs, when the diffusivity of phosphorous over the grain boundary thickness is smaller than a critical value of the grain boundary velocity. The results obtained within this project show, that the recrystallized austenite condition exhibits higher ductility than conventionally quenched and tempered steel. However, only one specific deformation temperature (850°C) above the recrystallization temperature (for constant deformation strain, strain rate and quench delay) provided the maximum reduction of area for the steel 54SiCr6. Austenite grain refinement was achieved as well by using the other deformation temperatures above the recrystallization temperature, but the gain in ductility was lower. It is concluded, that not only the austenite grain size is important, but how the grain refinement or recrystallization is achieved. In other words, the kinetics of the recrystallization and the mobility of the boundaries and their interaction with the impurities play a major role. For a given deformation temperature and interval time between deformation and quenching, it is important whether the recrystallization is completed or not. If recrystallization has terminated, equilibrium grain boundary segregation to the “static” boundaries starts and enriches the boundaries.

The work-hardened austenite condition resulted in enhanced ductility values. They are insensitive to the impurity content. The deformation itself generates dislocations that increase the solubility of phosphorous in the matrix. Thus the equilibrium concentration between the solutes in the matrix and solutes at grain boundaries is shifted towards the matrix. Furthermore, dislocation pile ups at grain boundaries can act as diffusion paths for elements such as phosphorous that are at grain boundaries and promote their diffusion away from the boundary. During transformation, the defects generated during austenite deformation are inherited to the final martensite and can act as trap sites for impurities like phosphorous. The work-hardened austenite conditions, TMT_{NRX} and TMT_{RX+NRX} both exhibited a slight increase of reduction of area with increasing phosphorous content. Intergranular failure was absent in all examined fracture surfaces.

Fig. 103 b) shows, how the ductility of the steel 54SiCr6 is improved by the developed thermomechanical treatments. In contrast to conventional heat treatment higher levels of phosphorous, copper and tin can be tolerated. At the same time higher ductilities are achieved by reducing the tempering temperature. Only the recrystallized austenite modification exhibits lower reduction of area values with increasing phosphorous content.

The mechanical properties obtained by the proposed thermomechanical processes are not only insensitive to the phosphorous content, but as well to copper and tin content. Thus steel or spring manufacturers could maximize the reproducibility of the mechanical values by application of the process. The influence of scrap composition, especially content of copper and tin, would then be minimized.

Fig. 105 shows the effective grain size area of conventionally heat treated samples tempered between 250 (highest tensile strength) and 450°C (lowest tensile strength). The steel with the lowest phosphorous content (melt P1 with 0.0023 mass% phosphorous) and 0.3 mass% copper and tin exhibits the largest grain size. Increasing the phosphorous content to 0.0213 mass% (melt P3) reduces the effective grain size to values between 10 to 15 μm^2 . If the copper and tin content is increased to 0.594 mass% (melt CuSn4) the effective grain size is further refined to values around and below 10 μm^2 . The refinement of the effective grain size, i.e. martensite block size, is not concurrent with improved ductility. As was shown in 4.2.3, the reduction of area falls with increasing phosphorous or copper and tin content. At the same time increased intergranular fracture is observed and is linked with grain boundary segregation of phosphorous or tin during austenitization. Nakashima et al. (2004) reported retardation of austenite grain growth in low carbon steel through addition of copper. They explained the retardation of grain growth by the dragging effect of copper atoms in solid solution. In the present work and within the copper contents investigated we could not observe a dependence of the austenite grain size on copper or tin concentration. This is in accordance with the results of Nakashima et al. for short austenitization times (300s). The investigated solute elements do not alter the austenite grain size. Thus they must alter and affect the nucleation or growth of martensite lath, which reflects itself in Fig. 105.

5.2 MORPHOLOGY OF GRAIN BOUNDARY CARBIDES

Because the martensite transformation is displacive, the austenite condition and the inherited defects have a strong influence on the precipitation behaviour during tempering. It is shown, that through deformation of austenite the grain boundary carbides are either refined or completely eliminated.

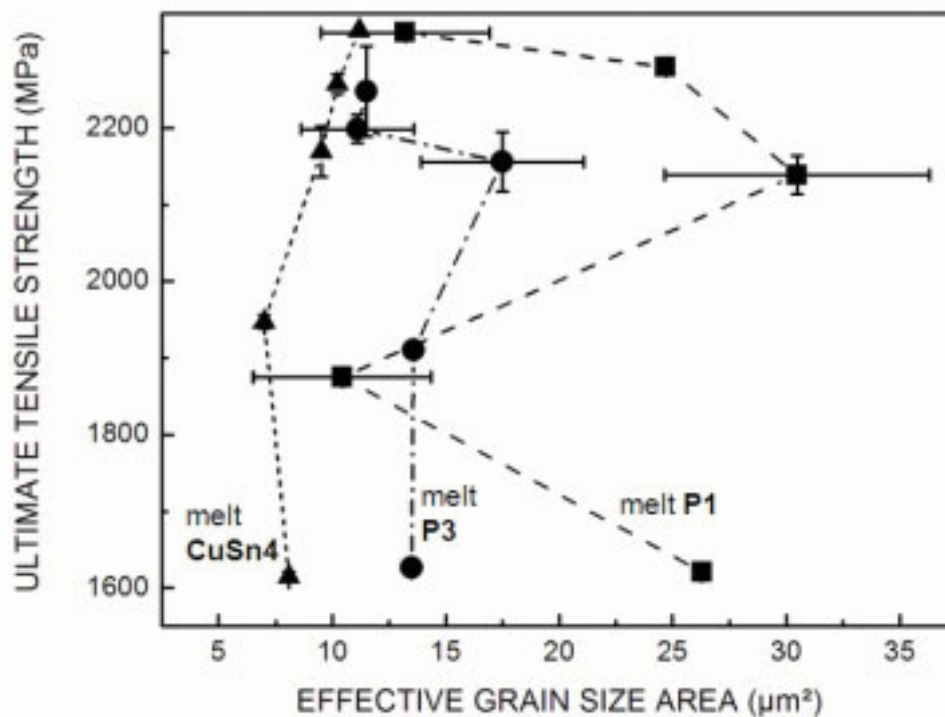


Fig. 105 Effective grain size of tempered martensite, i.e. martensite block size and ultimate tensile strength for conventionally heat treated samples tempered between 250 (highest ultimate tensile strength) and 450°C (lowest ultimate tensile strength). Steel **P1** with 0.0023P, 0.311Cu&Sn (all in mass %), **P2** with 0.0213P, 0.311Cu&Sn, and CuSn4 with 0.0115P and 0.594Cu&Sn.

The elimination of carbides was observed for the work-hardened austenite. The dislocation substructure, i.e. the dislocation pile ups at the grain boundaries of austenite lead to serration of these boundaries. Serration of these pristine boundaries avoids formation of cementite films at the grain boundary, because cementite precipitates of the same variant do not coalesce to form a film (2.1.4.2). The tendency towards segregation of carbon to the grain boundary is further decreased by the inherited dislocations from the austenite to the martensite. They not only serve as potential traps for the carbon atoms and as nucleation sites for cementite formation during tempering (Furuhara 2004, Nam 2000). Qualitatively, it is shown, that in all work-hardened samples the size of the carbides was reduced (Fig. 106).

The recrystallized austenite condition leads to refined cementite particles at the prior austenite grain boundary. The observed former austenite boundaries are in most cases curved and it seems that the recrystallization was interrupted by quenching and the transformation to martensite. Curved grain boundaries do not allow formation of cementite films as explained in 4.3.2.3.

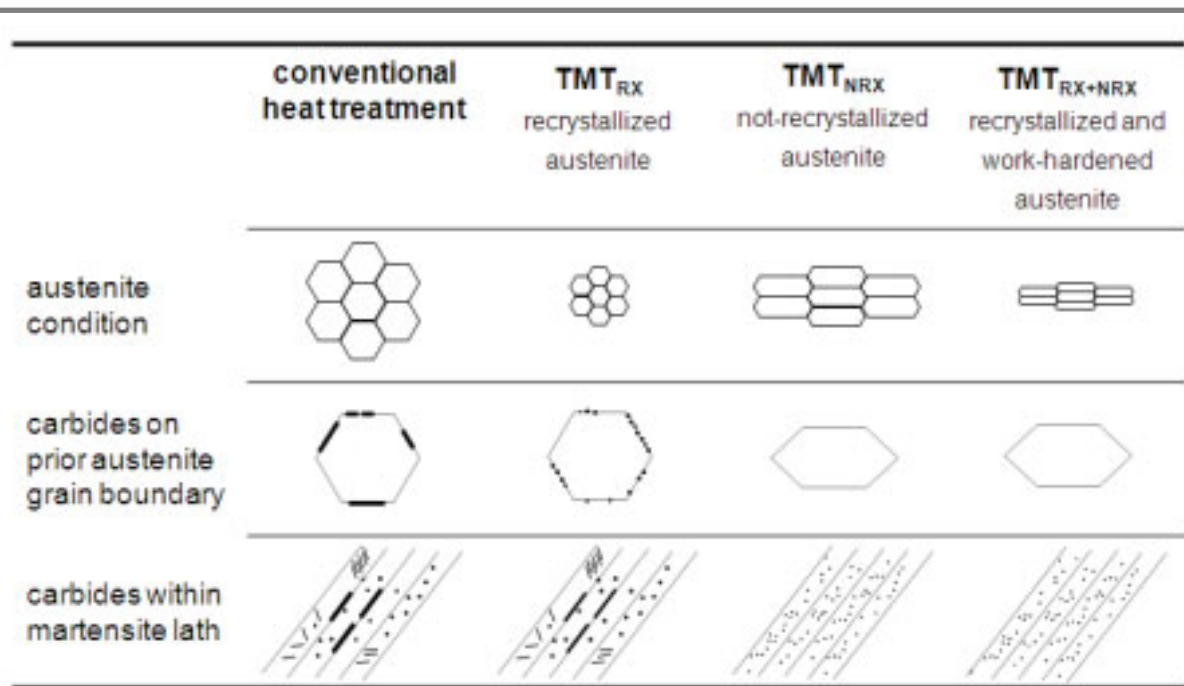


Fig. 106 Schematic presentation of the observed martensite microstructure for different austenite conditions, i.e. for different austenite conditions.

Figure 106 summarizes the observations and results. It shows the distribution of carbides at the prior austenite grain boundaries for each austenite condition investigated within the project for tempering temperatures of 350°C and below. Furthermore, the effect of various austenite conditions on the morphology and distribution of carbides within prior austenite grain boundaries is represented. Cementite films were observed at interlath boundaries of conventionally heat treated samples. The recrystallized austenite condition exhibits cementite films at prior austenite boundaries as well, whereas in the samples having a work-hardened austenite condition before quenching no cementite film was observed at interlath boundaries.

5.3 REFINEMENT OF MARTENSITE MICROSTRUCTURE

The present work shows, that austenite grain refinement is possible by microalloying or thermomechanical treatment (if recrystallization is involved) or by combination of both. It has been demonstrated, that austenite grain refinement achieved by the methods mentioned leads to the refinement of the martensite block size. The martensite blocks are enclosed by high angle grain boundaries and are defined as effective grain size, because their size influences the mechanical properties, both the strength and ductility. For the steel 54SiCr6 (melt P1)

Fig. 107 shows the distribution of the effective grain size for different processes. Relative to conventional heat treatment, the effective grain size is reduced by the austenite deformation. The recrystallized (TMT_{RX}) and the work-hardened (TMT_{NRX}) austenite condition deliver comparable effective grain size distributions and the same average grain size area ($9 \mu\text{m}^2$). Prior to quenching, the recrystallized austenite condition exhibits smaller austenite grains than conventional heat treatment. Therefore a smaller effective grain size is observed. The work-hardened austenite condition with pan-cake austenite grain structure exhibits an effective grain size comparable to that of the recrystallized austenite condition. The work-hardened condition has a higher defect density. The defects generated during deformation seem to refine the martensite. First, dislocation structures can reduce the nucleation energy barrier for martensite nucleation as reported by Petrov (1984). Second, the defect structures within the austenite grains might stop the growth of the martensite laths, because the periodicity of the lattice is disturbed or interrupted by dislocation arrangements (Schumann 1984). The maximum refinement of the martensite microstructure was achieved by the combination of thermomechanical treatment and microalloying. Through microalloying and appropriate definition of austenitization conditions (temperature and time) an austenite grain size

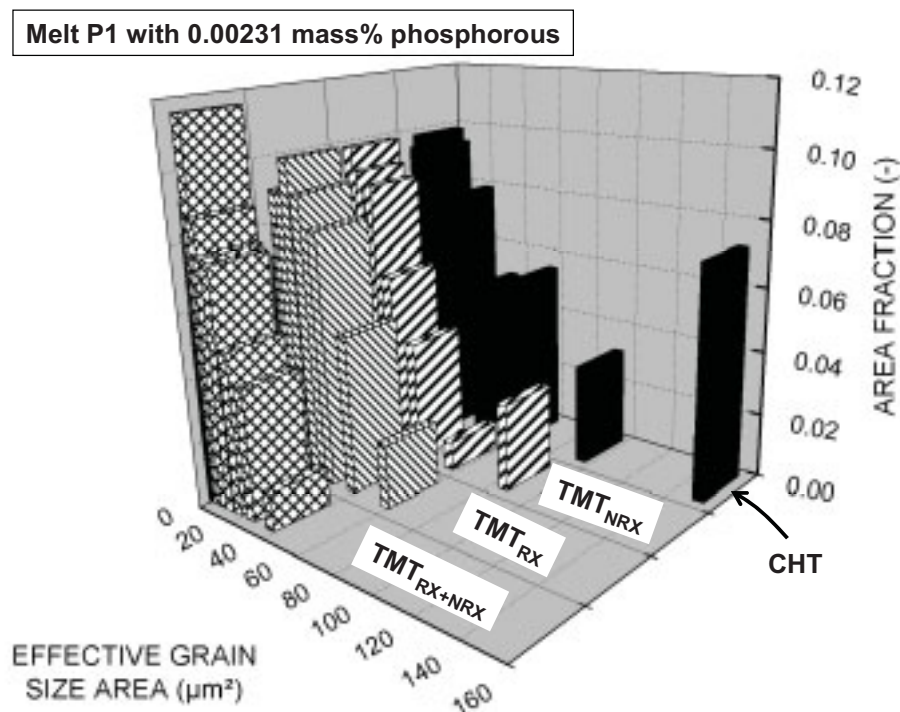


Fig. 107 Effective grain size distribution for conventional heat treatment (CHT) and thermomechanical treatment (TMT). Steel 54SiCr6, melt P1; austenitized 300 s at 900°C followed by quenching and tempering at 350°C .

significantly smaller than the steel without vanadium can be obtained. Subsequent thermomechanical treatment employing recrystallization and work-hardening leads to an effective grain size area of the order of $3 \mu\text{m}^2$.

In Fig. 108 the reduction of area is plotted as a function of the effective grain size area for the melt with low phosphorous (melt P1, 0.0023 mass% P) and high phosphorous content (melt P3, 0.0213 mass% P) and medium copper (0.280 mass% Cu) and tin content (0.0311 mass% Sn). The same level of ductility can be observed for various effective grain sizes, as it is shown for conventionally heat treated samples. This is the case, when the grain boundaries are enriched with impurities such as phosphorous and cementite films decorate at the same time the prior austenite grain boundaries. In such cases, the prior austenite grain boundaries seem to be the weakest path in the material, because intergranular fracture is observed. In other words, if these prior austenite grain boundaries are weak, the crack proceeds along these paths (Fig. 104). Then the effective grain size is not important, because then the crystallographic cohesive length for transgranular cleavage on the $\{100\}$ planes does not play a major role.

At the same time finer effective grain sizes are always observed after thermomechanical

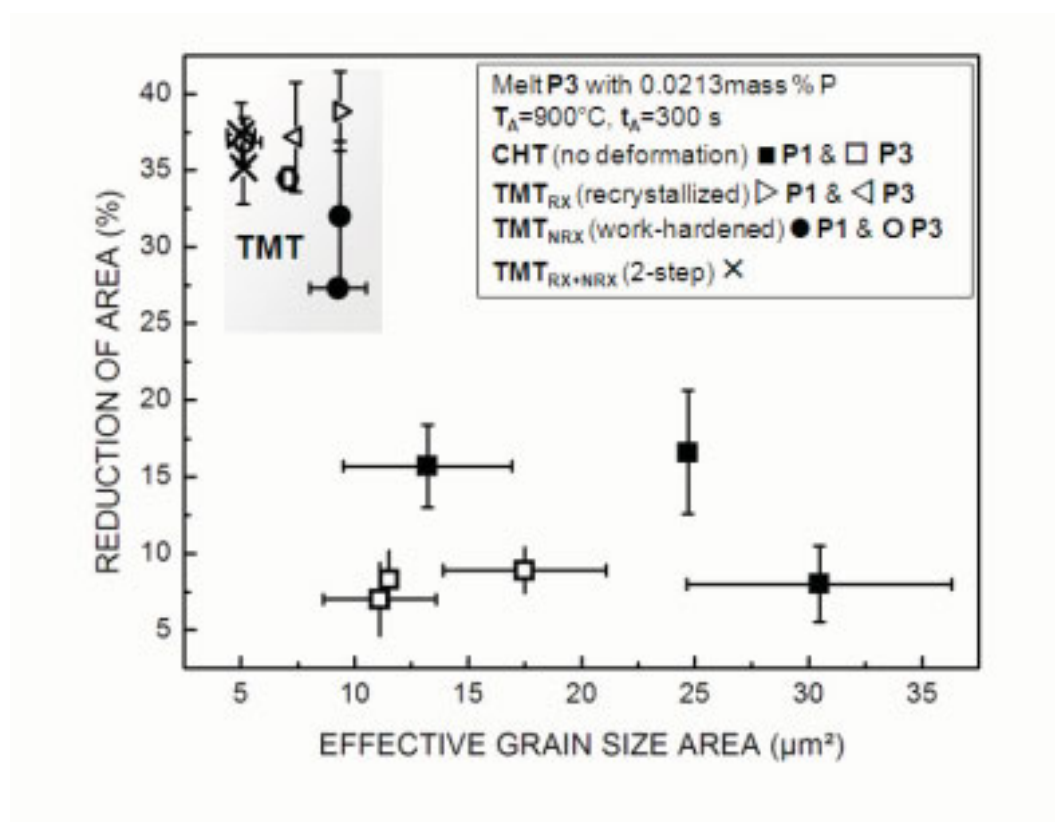


Fig. 108 Effective grain size area and reduction of area for different processes (conventional heat treatment CHT, thermomechanical treatment with recrystallized (TMT_{RX}), work-hardened (TMT_{NRX}) austenite condition and combination of the latter two (TMT_{RX+NRX}). Melts P1 and P3.

treatment and they are connected with high reduction of area values (Fig. 108). The two-step thermomechanical treatment exhibiting the finest grain size area has the highest ductility after tempering at 300°C. The grain size area of the work-hardened austenite condition depends on the phosphorous content. It is around 9 μm^2 for the melt with 0.0023 mass% phosphorous and is reduced to 7 μm^2 ($T_T=350^\circ\text{C}$) and 5 μm^2 ($T_T=300^\circ\text{C}$) if the phosphorous concentration is increased to 0.0213 mass%. The latter samples with higher phosphorous content and smaller effective grain size area exhibit higher reduction of area values than melt P1.

The effective grain size area of the recrystallized austenite condition measured after tempering at 350°C is 7.4 μm^2 for melt P3 and 9.4 for P1. From Fig. 108 and Fig. 105 we conclude that the addition of phosphorous reduces the effective grain size area. The same effect is achieved by thermomechanical treatment. All samples subjected to TMT have effective grain size areas below 10 μm^2 , while the conventionally heat treated samples can have large blocks exceeding 30 μm^2 . Only the two-step thermomechanical treatment delivers effective grain sizes independent of phosphorous content.

To determine the effect of the effective grain size, i.e. the block size on the tensile yield strength, it is inevitable to discuss, which measure should be used for the grain size. In the present work, the area was used until this stage to compare different processes or compositions with each other. To quantify the effect of the grain size on the yield strength according to the Hall-Petch equation, the shape of the grains must be considered. The Hall-Petch relation expresses the grain size dependence of yield strength. If the grains are equiaxial, then the maximum length the dislocations can glide within one grain is equal to the grain diameter and the following expression is used (Hall 1951 and Petch 1953):

$$\sigma = \sigma_0 + k_y \times \frac{1}{\sqrt{D}} \quad (\text{Equation 19})$$

σ yield strength, σ_0 stress at infinite grain size, D grain diameter, k_y slope of stress versus grain size.

In martensitic steels, where individual lath, plates or needles dominate the microstructure, the mean free path can not be a diameter, because the lath have more the shape of an ellipsoid. As was already mentioned in 2.1.3 the mean slip length in a martensite needle is rather the needle thickness rather than the needle length (Naylor 1979). In this work, the aspect ratio distribution and its mean value of the distribution were extracted from the EBSD data for conventionally and thermomechanically treated samples of melt P1. This was performed by the evaluation software by fitting first an ellipse to the points making up a grain. The aspect

ratio is defined as the length of the minor axis divided by the length of the major axis and thus ranges from 0 to 1.

The 0.2% offset yield strength was plotted over the inverse square root of the mean free path, equivalent to twice the average value of the minor axis (Fig. 109). The mean free path for the thermomechanical treatment is smaller, but the strength is not significantly higher. The data points plotted in Fig. 109 were used to calculate the Hall-Petch equation for 54SiCr6 in the tempered condition. Data of two different tempering temperatures (300 and 350°C) were used separately to fit the Hall-Petch equation to them. The two tempering temperatures used for fitting correspond to different stages of tempering. Samples tempered at the lower temperatures have mainly ϵ -carbides, while samples tempered at 350°C have cementite and ϵ -carbides. Secondly the dispersion of the carbides and the content of carbon in solid solution depend on the tempering temperature as well. These factors determining the 0.2% offset yield strength are included in the term σ_0 . Additionally, the two tempering temperatures exhibit different cementite occupation of the prior austenite grain boundaries. The equations gained after fitting are presented in table 10 and plotted in Fig. 110. They are compared with Hall-Petch relations for various metals. The term σ_0 , the base strength for a single crystal is around 1800 MPa. The very fine microstructure of the martensite contributes at maximum two 200MPa. Comparing with other material classes that are shown in Fig. 110, the increment in strength with reduction of mean free path is very small for the silicon chromium steels investigated here. The constant k_y is relatively low. Thus refinement of martensitic microstructure is beneficial mainly for the ductility, but only if the grain boundary cementite films are eliminated or refined at the same time. The refinement itself can be obtained by microalloying or by thermomechanical treatment involving recrystallization or work-hardening of the austenite.

Table 10 Hall-Petch relation for various metals (Gottstein 2004) and for 54SiCr6

Material	Lattice	σ_0 (MPa)	$k (MPa \times \sqrt{m})$	$R (-)$
Cu	fcc	25	0.11	
Ti	hex	80	0.4	
low-carbon steel	bcc	70	0.74	
Ni ₃ Al	L1 ₂	300	1.7	
54SiCr6, T _T =300°C	bcc, tetragonal	1789 ± 100	0.24 ± 0.14	0.66
54SiCr6, T _T =350°C	bcc, tetragonal	1862 ± 47	0.08 ± 0.07	0.52

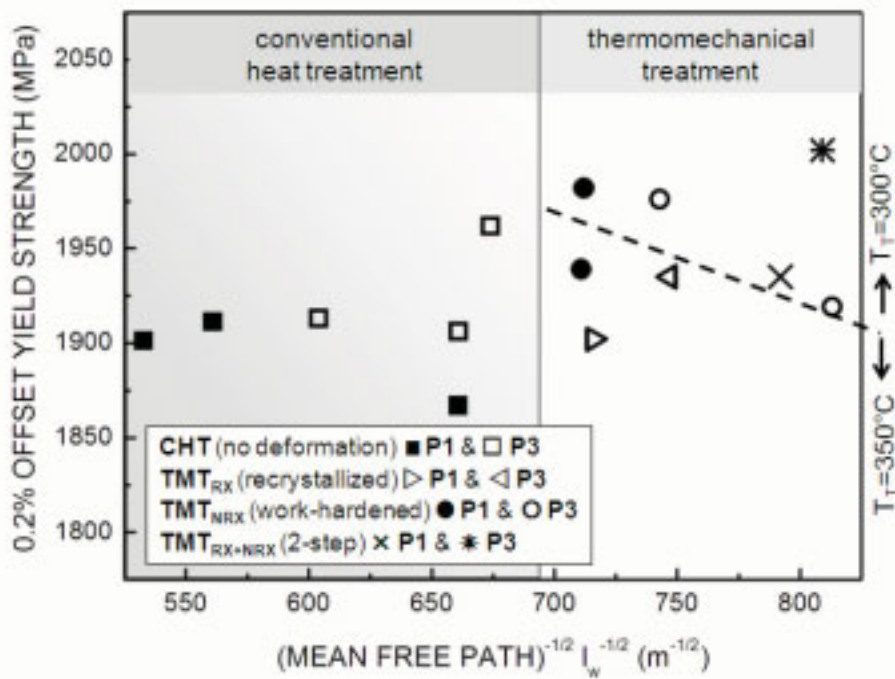


Fig. 109 0.2% offset yield strength as a function of mean free path (inverse square root of lath width) for conventional heat treatment (CHT), thermomechanical treatment with recrystallized (TMT_{RX}), work-hardened (TMT_{NRX}) austenite condition and combination of the latter two (TMT_{RX+NRX}). Melts P1 and P3. CHT samples tempered at 250, 300 or 350°C.

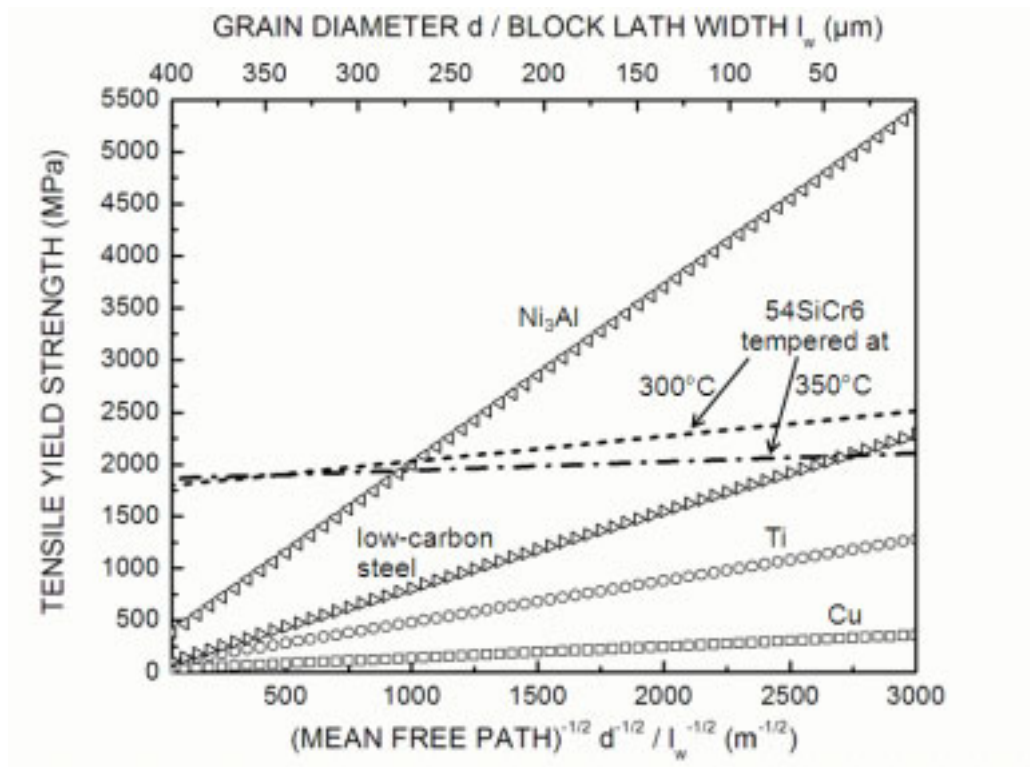


Fig. 110 Hall-Petch relation for various metals (from Gottstein 2004) and for 54SiCr6. Grain diameter is given for the metals taken from reference, while lath width is given for the martensite.

6 SUMMARY AND CONCLUSION

Based on the steels 54SiCr6 and 54SiCrV6 laboratory melts with different levels of phosphorous, copper and tin were produced. The influence of processing parameters on the microstructure and mechanical properties was investigated as a function of composition. Apart from the standard practice of quenching and tempering, various thermomechanical treatments were proposed. The processing parameters were the austenitization temperature, the tempering temperature, and various austenite deformation temperatures corresponding to different austenite conditions prior to quenching.

The microstructure characterization was concentrated on the distribution and morphology of carbides at the prior austenite grain boundary and on the characterization of the tempered martensite morphology. The grain boundary carbides are known to be detrimental for the ductility and toughness of quenched and tempered martensitic steels. The size of the structural units of lath martensite, especially that of the individual blocks surrounded with high angle grain boundaries is an important factor in determining the strength and toughness of martensitic steels. The mechanical properties were characterized by tensile testing and rotary bending tests. The influence of vanadium as a microalloying element, of the impurity element phosphorous, and the tramp elements copper and tin were analyzed separately.

The main results are:

1. The ductility of 54SiCr6 strongly depends on the tempering temperature and on the distribution and morphology of the carbides. At the beginning of the third stage of tempering the ductility is lowest. This phenomenon is related to the formation of cementite at the prior austenite grain boundaries and does not occur in steels with low concentration of phosphorous, copper and tin, or sulfur. At higher tempering temperatures the carbides spheroidize and result in high ductility. At tempering temperatures below 350° the quenched and tempered material exhibits high strength and low ductility.
2. With increasing phosphorous or copper and tin bulk concentration the ductility of conventionally quenched and tempered 54SiCr6 and 54SiCrV6 decreases for all strength levels or tempering temperature. The addition of phosphorous furthermore reduces the martensite transformation temperature. The addition of both phosphorous

or copper and tin reduces the average block size of the martensite. No effect of phosphorous on tensile strength values was observed, whereas copper and tin can increase the 0.2% offset tensile yield strength.

3. Microalloying with vanadium affects the grain growth below 950°C and by appropriate definition of austenitization parameters, i.e. time and temperature, the austenite grain size can be refined. The refinement of austenite results in improved ductility values and high strength levels, but only for low phosphorous or copper and tin concentration. No cementite films were observed in the steel with vanadium, and hence no minimum in ductility was observed at the beginning of the third stage of tempering, i.e. at 350°C. This was explained by the increase of the grain boundary area due to the finer austenite grain size prior to quenching and partial formation of pro-eutectoid ferrites at the pristine austenite boundaries.
4. Vanadium addition inhibits the static recrystallization after austenite deformation significantly. It can be used to increase the deformation temperatures to reduce the rolling forces and at the same time avoid recrystallization of the austenite or conserve the austenite grain substructure generated by deformation.
5. Austenite deformation as described in this work increases the ductility of the material at all strength levels. Three austenite conditions were tested at all phosphorous, and copper and tin contents: a recrystallized, a work-hardened non-recrystallized austenite, and the combination of both. These thermomechanical treatments results in elimination or refinement of the cementite films at prior austenite grain boundaries. As a result no intergranular failure was observed. The final martensite is refined with respect to a conventionally heat treated samples. The block size is reduced significantly and by doing though an increase in ductility is achieved. The ductility of the thermomechanically treated samples was not prone to the bulk concentration of phosphorous, or copper and tin. Beside the increase in ductility, the fatigue limit could be increased by a thermomechanical treatment with a recrystallized austenite condition prior to quenching.

The thermomechanical treatments proposed here improve the strength, ductility and fatigue at the same time. Because most industrial coil spring production is automatized, it is possible to integrate a forming step into the production, namely after austenitization and before coiling of the wire or rod to the coil spring.

The work shows that today the potential of thermomechanical treatment is not fully exploited. There are many applications to which thermomechanical treatment could be applied in order to improve mainly the mechanical properties. These are for example forgings made of quenched and tempered steels or maraging steels. Appropriate process design could enable us to tailor the desirable precipitation and grain morphology, size and distribution.

7 REFERENCES

- Abe 1990** T. Abe, K. Tsukada, H. Tagawa, I. Kozasu, *ISIJ Int.* 30 (1990) 444-450.
- Adeev 1975** V. M. Adeev, Y. N. Petrov, *Ukrainian Journal of Physics* 20 (1975) 2004-2008.
- AiF 7965** Final Report, Einfluß unteschiedlicher Anlaßbedingungen auf das Verhalten von Federstählen hoher Festigkeit bei schwingender Beanspruchung, Verband deutscher Federindustrie VdFi, Hagen, 1992.
- AiF 7966** Final Report, Einfluß unteschiedlicher Anlaßbedingungen auf die Zähigkeit hochfester Stähle, Verband deutscher Federindustrie VdFi, Hagen, 1992.
- Alten 1953** A. A. Alten, P. Payson, *Trans. ASM* 45 (1953) 498-503.
- Altstetter 1962** C. J. Altstetter, M. Cohen, B. L. Averbach, *Trans. ASM* 55 (1962) 287-300.
- Ayada 1998** M. Ayada, M. Yuga, N. Tsuji, Y. Saito, A. Yoneguti, *ISIJ Int.* 38 (1998) 1022-1031.
- Bain 1924** E. C. Bain, *Trans AIME, Steel Div.* 70 (1924) 25-46.
- Banerji 1978** S.K. Banerji, C.J. McMahon, Jr., H.C. Feng. *Met. Trans. A* 9A (1978) 237-247.
- Berns 1984** H. Berns, G. Siekmann, I. Wiesenecker, *Draht* 35 (1984) 247-252.
- Briant 1979** C.L. Briant, S.K. Banerji, *Met. Trans. A* 10A (1979) 123-126. /
- Briant 1979b** C.L. Briant, S.K. Banerji, *Met. Trans. A* 10A (1979) 1151-1155.
- Briant 1979c** C.L. Briant, S.K. Banerji, *Met. Trans. A* 10A (1979) 1729-1737.
- Briant 1999** C. L. Briant, in: C. L. Briant (Ed.), *Impurities in Engineering Materials*, Marcel Dekker, Inc., New York, USA, 1999, 1-12.
- Caballero 2004** F. G. Caballero, H. K. D. H. Bhadeshia, *Current Opinion in Solid State and Materials Science* 8 (2004) 251 - 257.
- Capus 1963** J.M. Capus, *J Iron Steel Inst.* 201 (1963) 53-54.
- Cech 1956** R. E. Cech, D. Turnbull, *Trans. AIME* 206 (1956) 124-132.
- Christien 2003** F. Christien, R. Le Gall, G. Saindrenan, *Scr. Mat.* 48 (2003) 301-303.
- Cohen 1962** M. Cohen, *Trans AIME* 224 (1962) 638- 657.
- Cohen 1963** M. Cohen, *J. Iron Steel Inst.* 201 (1963) 832 - 841.
- Cox 1967** A. R. Cox, *J. Iron Steel Inst.* 205 (1967) 51 - 57.

-
- Davies 1971** R. G. Davies, C. L. Magee, *Met. Trans.* 2 (1971) 1939 - 1947.
- Dieter 1988** G. E. Dieter, in: *Mechanical Metallurgy*, McGraw-Hill Book Company, UK, 1988.
- Dingley 2004** D. Dingley, *J Microscopy* 213 (2004) 214–224.
- Dziemballa 2005** H. Dziemballa, L. Manke, in: I. von Hagen, H.-J. Wieland (Eds.), *Steel, Future for the Automotive Industry*, Verlag Stahleisen GmbH, Düsseldorf, 2005, 341.
- Easterling 1992** K. E. Easterling, D. A. Porter, in: *Phase Transformations in Metals and Alloys*, Chapman & Hall, London, UK, 1992.
- Erhart 1980** H. Erhart, in: *Gleichgewichtssegregation von Phosphor an die Korngrenzen von Eisen, Eisenbasislegierungen und niedriglegierten Stählen*, PhD Thesis, Max-Planck-Institut für Eisenforschung, Düsseldorf, 1980.
- Fernández 1999** A. I. Fernández, B. López, J. M. Rodríguez-Ibabe, *Scr. Mat.* 40 (1999) 543-549.
- Furuhara 1996** T. Furuhashi, S. Takagi, H. Watanabe, T. Maki, *Metall. Mater. Trans.* 27A (1996) 1635-1646.
- Furuhara 2004** T. Furuhashi, K. Kobayashi, T. Maki, *ISIJ Int.* 44 (2004) 1937-1944.
- Gottstein 2004** G. Gottstein, *Physical Foundations of Material Science*, SpringerVerlag, Germany, 2004.
- Grabke 1989** H.J. Grabke, *ISIJ Int.* 29 (1989) 529-538.
- Grabke 1999** H. J. Grabke, in: C. L. Briant (Ed.), *Impurities in Engineering Materials*, Marcel Dekker, Inc., New York, USA, 1999, 143-192.
- Grange 1973** R. A. Grange, *Met. Trans.* 4 (1973) 2231-2244.
- Greninger 1941** A. B. Greninger, A. R. Troiano, *Trans. AIME* 140 (1940) 307-336.
- Grujicic 1992** M. Grujicic, H. C. Ling, D. M. Hazenbrouck, W. S. Owen, in: G.B. Olson, W.S. Owen (Eds.), *Martensite*, ASM International, USA, 1992, 175-196.
- Guo 2004** Z. Guo, C. S. Lee, J. W. Morris Jr., *Acta Mat.* 52 (2004) 5511 - 5518.
- Guttmann 1982** M. Guttmann, PH. Dumoulin, M. Wayman, *Met. Trans. A* 13 (1982) 1693.
- Hall 1951** E. O. Hall, *Proc. Phys. Soc.* B64 (1951) 747-753.
- Hensger 1984** K.-E. Hensger, M. L. Bernstein, *Thermomechanische Veredelung von Stahl*, VEB, Deutscher Verlag für Grundstoffindustrie, Leipzig, 1984.
- Hensger 1985** K.-E. Hensger, P. Klimanek, D. Böhme, *Neue Hütte* 28 (1985) 15-20.
- Hondros 1977** E. D. Hondros, M. P. Seah, *Met. Trans. A* (1977) 1363-1371.

-
- Honeycombe 1995** R.W.K. Honeycombe, H. K. d. H. Bhadeshia, *Steels – Microstructure and Properties*, second ed., Butterworth-Heinemann, Oxford, 1995.
- Horn 1978** R.M. Horn, R.O. Ritchie, *Met. Trans. A* 9A (1978) 1039-1053.
- Houdremont 1956** E. Houdremont, in: *Handbuch der Sonderstahlkunde*, Springer Verlag, Germany, 1956.
- Hougardy 2003** H. P. Hougardy, in: *Umwandlung und Gefüge von Stählen*, Stahleisen Verlag, Düsseldorf, Germany, 2003.
- Imai 1997** N. Ima, N. Komatsubara, K. Kunishige, *ISIJ Int.* 37 (1997) 224-231.
- Isheim 2006** D. Isheim, R. P. Kolli, M. E. Fine, D. N. Seidman, *Scr. Mat.* 55 (2006) 35-40.
- Kaspar 1994** R. Kaspar, U. Lottner, Ch. Biegus, *steel research* 65 (1994) 242-247.
- Kaufmann 1958** L. Kaufman, M. Cohen, *Prog. Met. Phys.* 7 (1958) 165.
- Kozasu 1992** I. Kozasu, in: R. W. Cahn, P. Haasen, E. J. Kramer, *Materials Science and Technology - A Comprehensive Treatment, Volume 7 - Constitution and Properties of Steels*, Volume Editor: F. B. Pickering, VCH, Weinheim, Germany, 1992, 184-217.
- Krauss 1971** G. Krauss, A. R. Marder, *Met. Trans.* 2 (1971) 2343-2357.
- Krauss 1984** G. Krauss, in: A. R. Marder, J. I. Goldstein (Eds.), *Phase Transformations in Ferrous Alloys*, Metallurgical Society of AIME, Philadelphia, 1984, 101-123.
- Krauss 1990** G. Krauss, *Steels - Heat treatment and processing principles*, ASM International, Ohio, USA, 1990.
- Krauss 1992** G. Krauss, C.J. McMahon, Jr., in: G.B. Olson, W.S. Owen (Eds.), *Martensite*, ASM International, USA, 1992, 295-321.
- Krauss 1995** G. Krauss, *ISIJ Int.* 35 (1995) 349-359.
- Krauss 2001** G. Krauss, *Met. Mat. Trans.* 32A (2001) 861-877.
- Kubaschewski 1982** O. Kubaschewski, *Iron-binary phase diagrams*, Springer, Berlin, Germany, 1982.
- Kurdjumov 1930** G. V. Kurdjumov, G. Sachs, *Z. Phys.* 64 (1930) 325-343.
- Lagneborg 1999** R. Lagneborg, T. Siwecki, S. Zajac, B. Hutchinson, *Scand. J. Met.* 28 (1999) 186-241.
- Leslie 1981** W. C. Leslie, *The Physical Metallurgy of Steels*, McGraw-Hill Book Company, New York, USA, 1981.
- Lee 1975a** J.K. Lee, H.I. Aaronson, *Acta. Metall.* 23 (1975) 799-808.
- Lee 1975b** J.K. Lee, H.I. Aaronson, *Acta. Metall.* 23 (1975) 809-820.
- Li 2006** F. Li, A. Ardehali Barani, D. Ponge, D. Raabe, *steel research int.* 77 (2006) 590-594.

-
- Li 2006b** F. Li, A. Ardehali Barani, D. Ponge, D. Raabe, submitted to JMPT.
- Maki 1990** T. Maki, *Materials Science Forum* 56-58 (1990) 157-168.
- Maki 1993** T. Maki, in: K. A. Taylor, S. W. Thompson, F. B. Fletcher, *Physical Metallurgy of Direct-Quenched Steels*, The Minerals, Metals & Materials Society, USA, (1993) 3-16.
- Maki 1999** T. Maki, S. Morito, T. Furuhashi, in: *Proc. of the 19th ASM Heat Treating Society Conference Including Steel Heat Treating in the New Millennium*, Ohio, (1999) 631-637.
- Manohar 1996** P. A. Manohar, D. P. Dunne, T. Chandra, C. R. Killmore, *ISIJ Int.* 36 (1996) 194-200.
- Marder 1970** A. R. Marder, G. Krauss, in: *Proc. of 2nd Int. Conf. on the Strength of Metals and Alloys*, Vol. III, American Society for Metals, Metals Park, Ohio, 1970, 822-823.
- McFarland 1965** W. H. McFarland, *Trans AIME* 233 (1965) 2028 - 2035.
- McLean 1957** D. McLean, in: *Grain Boundaries in Metals*, At the Clarendon Press, Oxford, 1957.
- McMahon 1980** C. J. McMahon, Jr., *Met. Trans.* 11 A (1980) 531-535.
- Miller 1998** M. K. Miller, K. F. Russell, P. Pareige, M. J. Starink and R. C. Thomson, *Mat. Sci. Eng. A* 250 (1998) 49-54.
- Miyamoto 2005** G. Miyamoto, T. Furuhashi, T. Maki, J.C. Oh, K. Hono, in: James M. Howe, D. E. Laughlin, J. K. Lee, U. Dahmen, and W. A. Soffa, *Solid-to-Solid Phase Transformations in Inorganic Materials 2005*, Vol. 1, The Minerals, Metals & Materials Society, USA, 2005, 363-369.
- Mohamed 2002** Z. Mohamed, *Mat. Sci. Eng.* 326A (2002) 255-260.
- Morito 2003a** S. Morito, H. Tanaka, R. Konishi, T. Furuhashi, T. Maki, *Acta Materialia* 51 (2003) 1789-1799.
- Morito 2003b** S. Morito, J. Nishikawa, T. Maki, *ISIJ International* 43 (2003) 1475-1477.
- Morito 2005** S. Morito, H. Saito, T. Ogawa, T. Furuhashi, T. Maki, *ISIJ International* 45 (2005) 91-94.
- Morris 2001** J. W. Morris, Jr., Z. Guo, R. Kenn, Y.-H. Kim, *ISIJ International* 41 (2001) 599-611.
- Nakashima 2004** K. Nakashima, K. Imakawa, Y. Futamura, T. Tsuchiyama, S. Takaki, *Mat. Sci. Forum* Vols. 467-470 (2004) 905-910.
- Nam 2000** W.J. Nam, Ch.S. Lee, D.Y. Ban, *Mat. Sci. & Eng A* 289 (2000) 8-17.
- Naylor 1979** J. P. Naylor, *Met. Trans.* 10A (2000) 861-873.
- Nolze 2004** G. Nolze, *Z. Metallkd.* 95 (2004) 744-755.

-
- Nishiyama 1978** Z. Nishiyama, in: M. E. Fine, M. Meshii, C. M. Wayman (Eds), *Martensitic Transformation*, Academic Press, New York, USA, 1978.
- Ohtani 1972** H. Ohtani, F. Terasaki, T. Kunitake, *Trans. ISIJ* 12 (1972) 118-127.
- Ohtani 1992** H. Ohtani, in: R. W. Cahn, P. Haasen, E. J. Kramer (Eds.), *Materials Science and Technology, Volume 7, Constitution and Properties of Steels*, VCH, Weinheim, Germany, 1992, 147-181.
- Ollilainen 2003** V. Ollilainen, W. Kasprzak, L. Holappa, *Mat. Proc. Tech.* 134 (2003) 405-412.
- Olson 1975** G. B. Olson, M. Cohen, *Scr. Met.* 9 (1975) 1247-1254.
- Olson 1992** G. B. Olson, A. L. Roitburd, in: G.B. Olson, W.S. Owen (Eds.), *Martensite*, ASM International, USA, 1992, 149-174.
- Owen 1992** W. S. Owen, in: G.B. Olson, W.S. Owen (Eds.), *Martensite*, ASM International, USA, 1992, 276-293.
- Pawelski 1978** O. Pawelski, U. Rüdiger, R. Kaspar, *Stahl und Eisen* 98 (1978) 181-189.
- Perhacova 2000** J. Perhácová, A. Výrostková, P. Sevc, J. Janovec, H. J. Grabke, *Surf. Sci.* 454-456 (2000) 642-646.
- Petch 1953** N. J. Petch, *J. Iron Steel Inst.* 174 (1953) 25-28.
- Peters 1996** A. Peters, PhD. Thesis, Shaker Verlag, Aachen, Germany, 1996.
- Peters 1997** A. Peters, R. Kaspar, *La Revue de Métallurgie-CIT* (1997), 939-947.
- Petkovic-Djaic 1972** R. A. Petkovic-Djaic, J. J. Jonas, *J. Iron. Steel Inst.* 210 (1972) 256-261.
- Petkovic-Djaic 1973** R. A. Petkovic-Djaic, J. J. Jonas, *Met. Trans.* 4 (1973) 621-624.
- Pickering 1976** F. B. Pickering, *Int. Met. Rev.*, Review no. 211 (1976) 227.
- Pickering 1978** F. B. Pickering, *Physical metallurgy and the design of steels*, Applied Science Publishers LTD, Essex, England, 1978.
- Pickering 1980** F. B. Pickering, *TISCO* 27 (1980)105-132.
- Petrov 1984** J. N. Petrov, *Deutscher Verlag für Grundstoffindustrie* 244 (1984) 48-59.
- Poliak 2003** E. I. Poliak, J. J. Jonas, *ISIJ International* 43 (2003) 692-700.
- Ray 1990** R. K. Ray, J. J. Jonas, *Int. Mat. Rev.* 35 (1990) 1-36.
- Reguly 2004** A. Reguly, T.R. Strohaecker, G. Krauss, D.K. Matlock, *Met. Mat. Trans. A* 35A (2004) 153-162.
- Rez 1999** P. Rez, J. R. Alvarez, *Acta Mat.* 47 (1999) 4069-4075.

-
- Roberts 1970** M. J. Roberts, *Met. Trans.* 1 (1970) 3287-3294.
- Saburi 1986** T. Saburi, S. Nenno, *Proc. ICOMAT 86*, Japan Inst. Metals, 1986, 671-678.
- Schumann 1984** H. Schumann, *Deutscher Verlag für Grundstoffindustrie* 244 (1984) 17-35.
- Schwartz 2000** A. J. Schwartz, M. Kumar, B. L. Adams, *Electron Backscatter Diffraction in Material Science*, Kluwer Academic/Plenum Publisher, USA, 2000.
- Schwerdtfeger 1974** K. Schwerdtfeger, H. Jacobi, *Stahl & Eisen* 94 (1974) 868- 869.
- Seah 1977** M. P. Seah, *Acta Met.* 25 (1977) 345.
- Seo 1997** S.-J. Seo, K. Asakura, K. Shibata, *ISIJ Int.* 37 (1997) 232-239.
- Shewmon 1998** P. G. Shewmon, *Met. Mat. Trans.* 29B (1998) 509-518.
- Smith 1971** D. W. Smith, R. F. Hehemann, *J. Iron Steel Inst.* 209 (1971) 476-452.
- Stephenson 1961** E. T. Stephenson, M. Cohen, *Trans. ASM* 54 (1961) 73-83.
- Streißberger 1984** A. Streißberger, PhD. Thesis, Aachen, Germany, 1984.
- Sutton 1995** A. P. Sutton, R. W. Balluffi, in: *Interfaces in Crystalline Materials*, Monographs on The Physics and Chemistry of Materials, Vol. 51, Oxford University Press, Oxford, UK, 1996.
- Suzuki 1981** S. Suzuki, K. Abiko, H. Kimura, *Scr. metall.* 15 (1981) 1139.
- Suzuki 1983** S. Suzuki, M. Obata, K. Abiko, H. Kimura, *Scr. metall.* 17 (1983) 1325.
- Suzuki 1997** H. G. Suzuki, *ISIJ Int.* 37 (1997) 250-254.
- Swarr 1976** Th. Swarr, G. Krauss, *Met. Trans. A* 7A (1976) 41-48.
- Tamura 1982** I. Tamura, K. Tsuzaki, T. Maki, *Int. Conference on Martensitic Transformations (ICOMAT-82)*, Belgium, 1982, 51-56.
- Thomas 1971** G. Thomas, *Met. Trans.* 2 (1971) 2373-2385.
- Tsuzaki 1995** K. Tsuzaki, N- Harada, T. Maki, *Journal der Physique IV Colloque C8*, supplément au journal de Physique III, Volume 5 (1995) 167-172.
- Umemoto 1983** M. Umemoto, E. Yoshitake, I. Tamura, *J. Mat. Sci.* 18 (1983) 2893.
- Wang 1995** Y.M. Wang, M.Y. Li, *Controlled Rolling and Controlled Cooling in Steel*, Beijing, 1995.
- Wettlaufer 2000** M. Wettlaufer, PhD. Thesis, Shaker Verlag, Aachen, Germany, 2000.
- Wettlaufer 2000b** M. Wettlaufer, R. Kaspar, *Steel Research* 71 no. 9 (2000) 362-365.
- Winchell 1962** P. G. Winchell, M. Cohen, *Trans ASM* 55 (1962) 347-361.

-
- Winchell 1963** P. G. Winchell, M. Cohen, in: G. Thomas and J. Washburn (Eds.), *Electron Microscopy and the strength of metals*, Interscience, 1962, 995.
- Yusa 1999** S. Yusa, T. Hara, K. Tsuzaki, T. Takahashi, *Mat. Sci. Eng. A273-275* (1999) 462-465.
- Zaefferer 2004** S. Zaefferer, *JEOL news* 39 (2004) 10-15.
- Zouhar 1984** G. Zouhar, *Deutscher Verlag für Grundstoffindustrie* 244 (1984) 48-59.
- Zouhar 1984** G. Zouhar, J. Kunath, R. Stahlberg, B. Winderlich, *Arch. Eisenhüttenwes.* 55 (1984) 285-290.

ZUSAMMENFASSUNG

In dieser Arbeit wurde der Einfluss der Begleitelemente Phosphor, Kupfer und Zinn einerseits und der Verfahrensparameter andererseits auf die Mikrostruktur und die mechanischen Eigenschaften eines Silizium-Chrom-Stahls mit oder ohne Vanadium untersucht. Hierzu wurden Laborschmelzen der Legierungen 54SiCr6 und 54SiCrV6 mit systematischer Abstufung des Phosphorgehaltes und des Kupfer-Zinngehaltes hergestellt.

Neben der konventionellen Wärmebehandlung, die aus dem Erwärmen im Austenitgebiet, dem Abschrecken und dem Anlassen besteht, wurden auch verschiedene thermomechanische Behandlungen entwickelt, um sowohl die Dehngrenze bzw. die Zugfestigkeit als auch die Duktilität des Werkstoffs zu optimieren. Dieses Ziel wurde durch Umformung des Austenits und seine Konditionierung vor dem Abschrecken realisiert. Die untersuchten Einflussgrößen sind die Austenitisierungstemperatur – und zeit, die Anlasstemperatur, und unterschiedliche Umformtemperaturen des Austenits für eine thermomechanische Behandlungen. Gezielt wurde eine vor dem Abschrecken rekristallisierte Austenitsvariante einem nicht-rekristallisierten Austenitzustand gegenübergestellt, um Einflüsse der Austenitmikrostruktur auf die Martensitstruktur nach dem Anlassen und auf die mechanischen Eigenschaften zu untersuchen.

Die Mikrostrukturcharakterisierung war erstens auf die Verteilung und der Morphologie der Karbide an den ehemaligen Austenitkorngrenzen und zweitens auf die Martensitmorphologie nach dem Anlassen fokussiert. Korngrenzenkarbide beeinträchtigen bekanntlich die Duktilität und die Zähigkeit vergüteter martensitischer Stähle. Die Größe der Struktureinheiten des Lanzettmartensits, besonders die der von Großwinkelkorngrenzen umgebenen Blöcke innerhalb der Martensitpakete ist ein bestimmender Faktor für die Festigkeit und der Zähigkeit martensitischer Stähle. Die mechanischen Eigenschaften wurden durch Zugversuche und Umlaufbiegeversuche geprüft.

Die Hauptresultate sind:

- 1) Die Duktilität von 54SiCr6 wird in starkem Maße von der Anlasstemperatur und der Verteilung und der Morphologie der Karbide an den ehemaligen Austenitkorngrenzen beeinflusst. Am unteren Temperaturbereich der dritten Anlasstufe ist die Duktilität am

niedrigsten. Diese Beobachtung wird durch die Bildung von Zementit an den ehemaligen Austenitkorn Grenzen erklärt und ist bei Analysen mit sehr niedrigem Gehalt an Phosphor, Schwefel, Kupfer und Zinn nicht beobachtet worden. Bei höheren Temperaturen spheroidisieren die Karbide an den ehemaligen Austenitkorn Grenzen und die Duktilität steigt. Unterhalb von 350°C weist der untersuchte Martensitstahl hohe Festigkeiten und eine niedrige Duktilität auf.

2) Mit steigendem Phosphor- oder Kupfer-Zinn-Konzentration sinkt die Duktilität der konventionell vergüteten (wärmebehandelten) Stähle für alle Festigkeitsniveaus bzw. Anlasstemperaturen. Phosphorzugabe sinkt zudem die Martensitstarttemperatur. Die Zugabe von Phosphor oder Kupfer und Zinn reduziert die mittlere Blockgröße des Martensits. Kein Einfluss des Phosphors auf die Zugfestigkeit war erkennbar. Im Gegensatz kann die Zugabe von Kupfer und Zinn die 0,2%-Dehngrenze erhöhen.

3) Durch die Mikrolegierung mit Vanadium kann eine kleinere Austenitkorngröße bei gleichen Austenitbedingungen unterhalb von 950°C erzielt werden. Die feineren Austenitkörner resultieren für die Stähle mit geringem Anteil an Verunreinigungs- oder Begleitelemente in verbesserten Duktilitäts- und Festigkeitswerte. Bei den Vanadiumvarianten wurde kein Zementitfilm und kein Minimum der Duktilität zu Beginn der dritten Anlassenstufe (bei 350°C) beobachtet. Diese Beobachtung wurde durch die größere spezifische Grenzfläche aufgrund der feineren Austenitkörner und der Bildung von proeutektoidem Ferrit an den ehemaligen Austenitkorn Grenzen erklärt.

4) Vanadiumzusatz behindert die statische Rekristallisation nach einer Austenitumformung signifikant. Daher kann Vanadium eingesetzt werden, um die Umformtemperaturen zu erhöhen, die Walzkräfte zu senken und gleichzeitig eine Rekristallisation des Austenits zu verhindern, damit die durch die Umformung erzielte Austenitmikrostruktur erhalten bleibt.

5) Die Austenitumformung wie sie in der vorliegenden Arbeit beschrieben wurde, erhöht die Duktilität des untersuchten Werkstoffs für alle Festigkeitsniveaus. Drei Austenitzustände wurden für alle Analysen untersucht: ein rekristallisierter Austenitzustand, ein verfestigter und nicht-rekristallisierter Zustand und die Kombination aus beiden. Durch die thermomechanischen Behandlungen verschwinden die Karbidfilme an den ehemaligen Austenitkorn Grenzen nach dem Anlassen oder werden feiner. Folglich wird kein interkristallines Versagen beobachtet. Der aus dem umgeformten Austenit entstandene Martensit ist im Vergleich zum konventionell wärmebehandelten Martensit feiner. Die Blockgröße ist signifikant reduziert und dadurch steigt die Duktilität. Die Duktilität der

thermomechanisch behandelten Stähle war unabhängig vom Gehalt der Verunreinigungs- und Begleitelemente sehr hoch. Neben der Verbesserung der Duktilität konnte die Dauerfestigkeit durch die thermomechanische Behandlung mit einer rekristallisierten Austenitvariante vor dem Abschrecken gesteigert werden.

LEBENS LAUF

Persönliche Daten

Name: Ardehali Barani
Vorname: Araz
Geburtsort: Teheran, Iran
Geburtsdatum: 29. August 1972
Adresse: Am Wichelhausberg 1, Wuppertal
Staatsangehörigkeit: deutsch & iranisch

Schulbildung

1978-1979 Grundschole Afrand, Teheran, Iran
1979-1981 Grundschole Bijan-Mehdad, Teheran, Iran
1981-1982 Grundschole Molla Sadra
1982-1983 Grundscholeabschluss in Beytusch, Kurdistan, Iran
1983-1984 6. Klasse in Kurdistan, Irak
März 1985 - Juni 1985 Hauptschole Manderscheid
1985-1990 Gutenberg Gymnasiums in Mainz
1990-1993 Carl-von-Ossietyky Schole Wiesbaden
16. Juni 1993 Abitur

Studium

Oktober 1993 bis 1999 Studium der Materialwissenschaft, TU Darmstadt
Okt. 1996 bis Juni '97 Auslandsstudium im Rahmen des ERASMUS-Programms;
School of Material Science, University of Bath, England
23. Februar 1999 Diplom-Ingenieur Materialwissenschaft, TU Darmstadt

Beruf

15. Februar 1999 Entwicklungsingenieur Metallische Werkstoffe - Struktur,
Fairchild-Dornier GmbH, Oberpfaffenhofen
1. September 2002 Max-Planck-Institut für Eisenforschung GmbH, Düsseldorf
Seit 1. August 2006 ThyssenKrupp Nirosta GmbH, Krefeld

